Cryospheric Carbon Cycling at an Icelandic Glacier

Rebecca Kate Burns

Lancaster University

Lancaster

LA1 4YQ

UK

Submitted December 2016

This thesis is submitted in partial fulfilment of the requirements for the degree

Doctor of Philosophy

Centre for Global Eco-Innovation

EUROPEAN UNION
Investing in Your Future
European Regional
Development Fund 2007-13

www.cgeinnovation.org

Abstract:

Glaciers and ice caps are recognised as an important component of the global carbon cycle. Carbon within glacial systems exists in organic and inorganic forms, across supraglacial, englacial and subglacial realms. It is often difficult to detach cryospheric carbon cycling from hydrology, with the transfer of carbon between glacial inventories relying upon meltwater flows. Classical glacial hydrology consists of distributed drainage delivering delayed flow meltwaters, throughout the accumulation season, superseded by quick flow, aerated channelized drainage during increased ablation. It is upon this template that most existing studies have addressed the dynamics of carbon within glaciated catchments. However, Icelandic glacial systems provide an opportunity to investigate the role of subglacial volcanism in driving carbon dynamics. Hydrochemical properties of Sólheimajökull bulk meltwaters indicate untraditional redox conditions, with discharge of reduced, anoxic meltwaters in Summer, when expansion of subglacial drainage intersects the Katla geothermal zone. This unique hydrological regime generates profound effects upon the solute flux from the glacier, particularly with regard to the carbon budget. Dissolved inorganic carbon dynamics are dominated by weathering of basaltic bedrocks and accessory hydrothermal calcites, fuelled by subglacial geothermal proton supply. Widespread basal anoxia during summer facilitates methanogenesis resulting in large quantities of methane being discharged from beneath the glacier (flux range between 9,179 to 22,551 tonnes per year). Evidence suggests subglacial microbial acetoclastic methanogenesis is responsible with δ^{13}C and δD CH$_4$ values of ~60‰ and -320‰ respectively, supported by laboratory identification of methanogenesis in Sólheimajökull subglacial sediments. The organic counterpart to the carbon cycle is invoked to serve as the energy source for microbial metabolism. Such direct measurements of subglacial methane have rarely been achieved at contemporary ice margins. This study therefore provides an exciting opportunity to identify methane sources and carbon cycling in areas subjected to subglacial volcanism and to consider these within the broader context of global carbon dynamics.

Declaration

"I hereby declare that the work presented in this thesis is my own, except where acknowledged, and has not been submitted for the award of a higher degree or other qualification at this or any other institution."

Signed _____   Date _____

Name _____

Acknowledgements

support through the hardest parts of my undergraduate and postgraduate studies, for all the exciting adventures we have had and for being a top class field assistant in Iceland when it rained for 9 days straight. Thank you.

Finally I would like to dedicate this thesis to my Aunt, Ann Threlfall, who suddenly passed away during my final stages of writing up- I hope I've made you proud.

Preface

This project was undertaken as a joint collaboration between Isoprime UK Ltd and the Centre for Global Eco-Innovation (CGE), supported by the European Regional Development Fund (ERDF). In addition to academic investigation, industrial research was a key component of study, focussing on beta testing of scientific instrumentation on behalf of Isoprime UK Ltd.

Pre market beta testing of the visION isotope ratio mass spectrometer and accompanying ionOS software coupled with method development has been an integral part of this project, alongside extensive training in mass spectrometry techniques and production of technical notes. Beta testing of the visION and ionOS software on behalf of Isoprime took place at Lancaster University from May 2013 and is still ongoing in September 2016. A wide range of Environmental samples have been analysed as part of method development, including glacial sediments used in this project. Issues with both hardware and software were continuously reported back to Isoprime throughout the testing period to help aid product development.

Numerous presentations on product development and instrument specification have been given at Isoprime Ltd. hosted events within Europe, drawing form the work undertaken on this CGE project.

The visION and ionOS software have now been developed to market release. These now form a key part of the Isoprime Ltd portfolio of analytical instrumentation.

Table of Contents

List of Figures

List of Tables

1. Introduction

1.1. Justification of study

Glaciers constitute a distinctive component of the terrestrial carbon cycle, demonstrating an influence upon carbon budgets across a range of spatial and temporal scales. Within glacial research there is a notable distinction between the inorganic carbon system dominated by hydrochemical weathering processes (Tranter et al., 1993; Wadham et al., 2010) and an organic cryospheric biome supporting microbial life (Skidmore et al., 2000; Anesio et al., 2009; Hamilton et al., 2013). It is the mutual functioning of these two components across the supraglacial, englacial and subglacial locales, underpinned by knowledge of glacial thermal regime and hydraulics which provides thorough understanding of the role of glaciers within the carbon cycle. Temperate glaciers offer the most favourable conditions for cryospheric carbon cycling linked to water at the base. The accompanying short term seasonal evolution of subglacial hydrological regime determines the drivers of inorganic weathering reactions, microbiological activity, and ultimately dictates redox status (Wynn et al., 2015). Cryospheric carbon dynamics have important ramifications for wider global carbon cycling with the potential for glaciers to provide an important role in regulating climate on short term and longer term (glacial-interglacial) timescales (Smith et al., 2015). On longer timescales, glacier advance and retreat results in the burial and exposure of subglacially stored organic carbon (Zeng, 2003), microbial populations can be incubated and product carbon gases trapped beneath the cryospheric cap (Wadham et al., 2012) and long term

weathering dynamics can generate a carbon sink via drawdown of carbon dioxide (Jacobson et al., 2015; Daval et al., 2009).

However, despite this highlighted importance of glaciers in regulating carbon dynamics, two fundamental processes have yet to be awarded significant attention in glaciology. These are the importance of redox conditions on carbon cycling (methane cycling directly relies on anoxia; carbonation reactions directly rely on connectivity to the atmosphere) and the importance of subglacial volcanism on regulating carbon output to the surface of the Earth. Glaciers which overlie regions of active volcanism, as found in Iceland, act as surface caps which regulate the volcanic 'valve' of carbon release from the deep Earth system. This can fundamentally alter the way in which glaciers are currently recognised to regulate carbon dynamics with subglacial anoxia linked to sub-ice geothermal degassing, additional CO_2 sources, and the limited connectivity with the atmosphere. The prevalence of regions of active volcanism which are currently glaciated approximates 60% of the Icelandic glacial area (Björnsson and Pálsson, 2008). On a global scale, interaction between snow/ ice and volcanism during eruptions has been documented at 40 volcanoes (Tuffen, 2010). Understanding carbon dynamics from glaciers which overlie regions of active volcanism thereby forms a research topic which has been little addressed, yet holds potentially large implications for understanding the contribution of glaciers and ice sheets to global carbon dynamics.

Here, this thesis addresses the carbon dynamics from an Icelandic glacier, Sólheimajökull, which forms part of the Mýrdalsjökull ice cap overlying the notorious Katla volcanic system. Meltwater discharge through Sólheimajökull supports unique redox conditions of Summer season anoxia associated with heightened geothermal activity beneath the ice cap (Wynn et al., 2015). This unique model of seasonal redox status is investigated for its ability to drive the weathering of basalt and the release of carbon from a deep Earth source, whilst also promoting the export of biogenic methane from beneath the ice sheet-glacier system.

1.2. Research aims, objectives and hypotheses

The main research aim of this project can be defined as follows:

To explore carbon cycling at an Icelandic glacier which overlies an active volcanic system.

This will be undertaken at Sólheimajökull, an outlet glacier of the Mýrdalsjökull Ice cap which straddles the Katla Volcanic system. The following research objectives define how this aim will be addressed:

1. Bulk meltwater chemistry will be used to identify seasonal changes in hydraulic configuration and provide a background of hydrochemistry for understanding carbon cycling dynamics (Chapter 4).

2. The impact of subglacial volcanic activity upon carbon geochemistry will be addressed through identification of inorganic weathering mechanisms, with a

particular focus on the role of basaltic bedrock, hydrothermal calcite and $p\mathrm{CO_2}$ (Chapter 5).

3. Identification of subglacial organic carbon sources will be achieved through analysis of aqueous DOC concentrations and isotopic characteristics (Chapter 6).

4. Aqueous methane generation and delivery to the proglacial zone will be traced using stable isotopes and interpreted with reference to seasonal hydrology and redox status (Chapter 7).

5. Further investigation of the role of subglacial microbial activity in driving methane dynamics will be addressed via incubations of Sólheimajökull subglacial sediments under differing redox states (Chapter 8).

These objectives will enable the hypotheses to be answered:

Hypothesis 1: Subglacial volcanic activity will have a profound impact on total dissolved inorganic carbon (TDIC) dynamics through inorganic weathering reactions involving volcanic bedrocks and $\mathrm{CO_2}$ supply and demand.

Hypothesis 2: The redox status of the Sólheimajökull subglacial waters (which is known to vary on a seasonal basis according to geothermal activity) and hydrological connectivity will influence dissolved carbon speciation in bulk outflow.

Hypothesis 3: Dissolved carbon export will include a detectable organic component with distinctive provenance characteristics which plays a fundamental role in supporting the biological component of the carbon cycle.

1.3. Outline of thesis structure

To address the outlined aims, objectives and hypotheses, this thesis is made up of 9 chapters which provide an overview of the general research themes, present findings from fieldwork and laboratory investigations and ultimately provides a holistic account of carbon cycling at an Icelandic glacier in light of seasonal hydraulic configuration and geothermal inputs. Chapter 2 presents a summary of existing literature, further highlighting the importance and relevance of this study. The methods used in both the field and the laboratory are detailed in chapter 3. Chapter 4 summarises the bulk meltwater characteristics and meteorological conditions at Sólheimajökull, establishing annual drainage features and building the template upon which carbon cycling takes place. Inorganic and organic carbon dynamics are presented in chapters 5 and 6. Methane related components of carbon cycling are presented in chapters 7 and 8, addressing both field based evidence for methane sources, and laboratory based incubation experiments respectively. Finally, conclusions and suggestions for further work are presented in chapter 9.

2. Literature Review: Understanding the significance of carbon in the global cycle and in glacial environments

2.1. The Global Carbon Cycle

The global carbon cycle is an on-going exchange of carbon between four main reservoirs: the atmosphere; terrestrial biosphere, oceans and the deep geologic store. Cycling between reservoirs occurs over both long (endogenic) and short (exogenic) timescales.
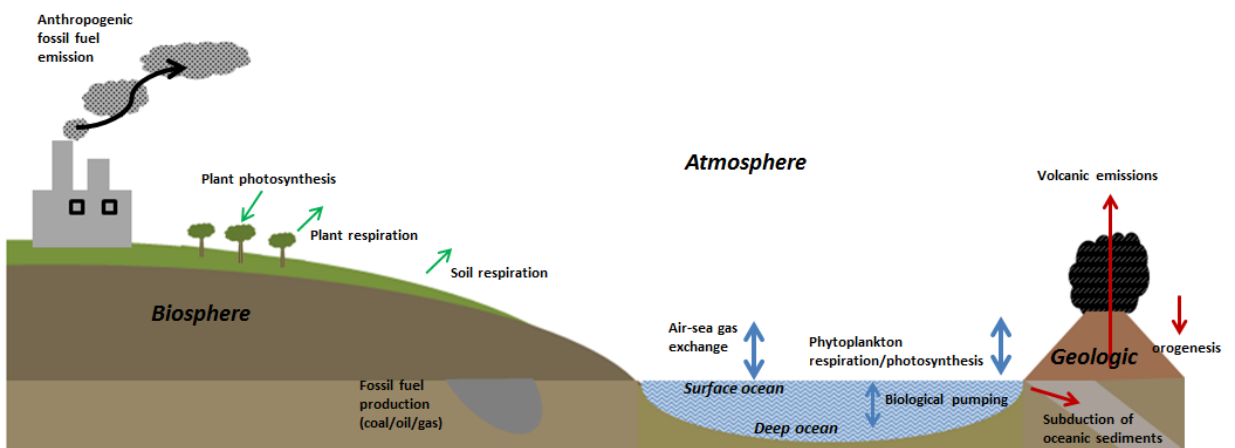
Figure 2:1: diagram depicting the global carbon cycle, including major sources, sinks and transfers

2.1.1. The Atmospheric component of the Global Carbon Cycle

As a biogeochemical compartment, the atmosphere has a capacity of 805 Gt C (~0.001% of the total carbon in the global carbon cycle) stored in the inorganic forms of carbon dioxide, methane and carbon monoxide (Archer, 2010; Post et al. 1990). The extent of atmospheric carbon has been monitored since 1958 at the Mauna Loa Observatory (Archer, 2010). Carbon dioxide (CO_2) accounts for 0.039% of all the gas

molecules in this reservoir, with ~20% of atmospheric CO_2 in active annual exchange with the ocean and terrestrial components. Methane (CH_4) is prevalent in smaller amounts, with current atmospheric concentrations of ~1800ppb. Organic carbon is not contained naturally within this compartment, instead volatile organic compounds are added to the atmosphere by anthropogenic pollutants (Macias and Arbestain, 2010; Falkowski et al., 2000; Hansen et al., 2008).

2.1.2. The Greenhouse Effect

At present, there is an identifiable split between the Natural Greenhouse Effect and the Enhanced Anthropogenic Greenhouse Effect. A Natural Greenhouse Effect is vital to maintain the stable Earth temperatures necessary for life. About 98% of the natural greenhouse effect is caused by water vapour and stratiform clouds. Perturbations caused by anthropogenic carbon release accelerates natural warming into unnatural bounds. The atmospheric content of CO_2 has gradually increased since 1750, from about 280 to 400 ppmv (IPCC, 2007; NOAA, 2015). Similarly methane concentrations have also seen a marked increase from pre industrial values of 722ppb to present day concentrations of 1800ppb- the highest value in the last 800,000 years (IPCC, 2013).

Physical evidence has found pollutants such as ozone, CO_2, N_2O, CH_4 and Chlorofluorocarbons do not condense and precipitate from the atmosphere like water vapour. Instead these gases persist in the atmosphere enhancing warming via a series of positive feedbacks. Attention has generally been directed towards CO_2 levels, which in 2015 reached record Holocene values, however CH_4 (albeit in lower concentrations) provides a largely overlooked greenhouse constituent. Atmospheric methane is the most reactive trace gas in the atmosphere, with molecule to molecule comparison shown to be 40 times more powerful than CO_2 (Archer, 2010; Nisbet, 2002). Whilst methane has a short residence time in the atmosphere (around 10 years) it has the ability to deliver a rapid perturbation in the greenhouse effect (Archer, 2010).

2.1.3. Long and short term sources of CO_2 and CH_4 to the atmosphere

Present day increase of carbon in the atmosphere represents natural fluxes and anthropogenic activity. A differentiation can be made between short term 'exogenic' and longer term 'endogenic' carbon cycling. In the short term, carbon transfer to the atmosphere involves a rapid turnover in the terrestrial and oceanic components of the carbon cycle. Superimposed on this natural exogenic cycle is anthropogenic activity. Direct releases of CO_2 and CH_4 from combustion of fossil fuels, industrial process and agriculture alongside indirect alteration of the wider carbon cycle through land clearance, modify the atmospheric inventory. On longer timescales (myr) carbon cycling is largely controlled by geological fluxes from endogenic reservoirs, with negligible inputs from orbital processes associated with climate fluctuations. Volcanic activity has been a significant source since the Earth was young; today CO_2 inputs are around 130 to 230 megatons annually (Gerlach et al., 1999).

Most natural carbon sources (both long and short term) are balanced by a natural sink. For example, carbon is added to the atmosphere by volcanic outgassing, anaerobic respiration, fermentation processes and soil heterotrophy and removed from the atmosphere via photosynthesis, rock weathering and oceanic processes. It is therefore extremely difficult to detach the atmospheric carbon cycle from the other carbon cycle components. The atmosphere is mainly a transfer mechanism for different modes of the carbon cycle to interact, leading to a large holistic carbon cycle engaging all sources and sinks.

2.1.4. The oceanic component of the global carbon cycle

The Oceanic component of the global carbon cycle contains around 38,000 Gt C, around 50 times more carbon than the atmosphere (Archer, 2010). Within this component carbon is largely accumulated in the inorganic forms of: dissolved CO_2, carbonic acid, and carbonate and bicarbonate ions, with other storage in the dissolved organic carbon and particulate organic carbon varieties (Post et al., 1990;

Archer 2010; Heinze et al., 1991). By nature, the extent of the oceanic carbon pool renders it a key player in determining atmospheric CO_2 largely through physical processes linked to air-sea-gas exchange and biogeochemical processes driven by alkalinity such as biological pumping and carbonate weathering (Sigman and Boyle, 2000).

2.1.5. The terrestrial component of the global carbon cycle

Plant biomass and soil organic carbon contain more than 2200 GtC (Cao and Woodward, 1998). Within the terrestrial portion, the carbon reservoir can be thought of as a range of carbon pools, each with individual primary production rates and turnover times (Post et al., 1990). Essentially, ecosystem carbon fluxes are dominated by autotrophic and heterotrophic transfers. Autotrophs play a major role in carbon cycling, with carbon fluxes dominated by the differences between photosynthesis and plant respiration, otherwise known as net primary productivity (NPP). In addition to this, heterotrophs cycle carbon via consumption of other organisms, meaning that the majority of carbon sequestered in the terrestrial biosphere is in organic form.

Natural carbon transfers from the terrestrial component are mostly via organic matter degradation or fluvial outwash. Organic matter which is respired rapidly transfers to the atmospheric component of the global carbon cycle, whilst carbon which is accumulated under larger pressure/temperature relationships eventually enters geological reservoirs. Additionally, rivers act as vectors of transport delivering carbon to the oceanic reservoir.

Traditionally the terrestrial biosphere is viewed as a large land carbon sink with the potential to restrain atmospheric carbon dioxide accumulation (Arneath et al., 2010). However, the biosphere is also responsible for generation of potent greenhouse gases such as methane. The organic carbon cycle generates around 90% of

atmospheric methane via biological formation facilitated by microorganisms (Boyd et al., 2010; Floodgate and Judd, 1992). Microbial formation of methane is frequent in many subsurface anaerobic settings including permafrost, deep oceans and lake sediments (Wadham et al., 2012). Whilst carbon dioxide may be regulated by processes associated with NPP, methane engages in rapid, largely unchecked natural carbon emission from the biosphere, rendering it a key output of terrestrial carbon cycling.

2.1.6. The geologic component of the global carbon cycle

In addition to considering the surficial short term exogenic exchange between oceans, the terrestrial biosphere and the atmosphere, it is vital to acknowledge contributions from rocks and geological processes operating over a much longer timescale. This long term endogenic cycle operates over millions of years and consists largely of the slow exchange between deeply buried rocks and the exogenic surficial system. Volcanic activity has been a significant carbon source since the Earth was young. Geogenic CO_2 inputs are around 130 to 230 megatons annually (Gerlach et al., 1999). In addition to CO_2 degassing, geogenic methane is generated via thermal breakdown of organic matter or abacterial mantle outgassing can also form an important carbon emission. A methane contribution from geological activity in Europe alone contributes about 4,000 to 16,000 ton/yr. (Etiope et al., 2007). On more contemporary timescales, humans act as a catalyst for this geologic carbon cycle, by burning organic carbon stored in sedimentary rocks, which would otherwise oxidise over prolonged time periods (Mackenzie and Lerman, 2006; Archer, 2010; Berner 1999; Berner 2003).

2.2. Cryospheric carbon cycling

Building on the Global Carbon Cycle featured in 2.1., glacier carbon cycling provides a unique terrestrial reservoir. This section will address the pathways of inorganic and organic carbon cycling, sources and production in a cryospheric context, plus offer insight into methane as an underappreciated component of glacial carbon dynamics.

Cryospheric carbon cycling requires an understanding of the glacial system as a functioning biome, a concept which has developed since the early millennium. Previous research up until the 1990s focussed on bulk meltwater hydrochemistry as a method to determine water routing through the glacial drainage system. Originally, solutes within bulk meltwaters were thought to originate from 4 main inorganic sources: surface deposition of sea salt, acid aerosols, dissolution of atmospheric CO_2 and crustal weathering. However, based on levels of nitrate and sulphate concentrations in subglacial meltwaters (Wynn et al., 2007, 2006; Tranter et al., 1994) and budgets of nitrate within an annual cycle (Hodson et al., 2005) microbiological activity was recognised to play a key role in determining solute export from glaciated catchments. Observation of microbes within glacial sediments (Sharp et al., 1999; Foght et al., 2004) confirmed the presence of microbial communities which held the capability of driving chemical reaction mechanisms. This marked a 'Paradigm Shift' from hydrological studies fixated by inorganic reactions and drainage pathways to discussion of organic catalysts (Wynn et al., 2006). As most microbial reactions require an organic carbon source to fuel the reaction pathway, this places glaciers firmly within the carbon biogeochemical cycle, with the need to address both organic and inorganic counterparts.

2.2.1. The sources and transfers of inorganic carbon in glacial ecosystems

Within the cryospheric carbon cycle inorganic carbon exists in dissolved form otherwise known as Total Dissolved Inorganic Carbon (TDIC). Chemical weathering is a major factor in liberation of TDIC and solutes from bedrock/mineral sources. Despite prevalence of cold conditions, rates of chemical weathering in temperate glaciated catchments are comparable, if not greater than, non-glaciated watersheds (Skidmore et al., 2004). Glaciers exhibit large chemical denudation rates, often 1.2-2.6 times higher than the continental average. This is attributed to high water flux particularly during melt seasons, high rock: water ratios and reactive freshly comminuted glacial flour (Tranter et al., 1993; Wimpenny et al., 2010). Weathering in the subglacial environment proceeds via two main forms of acid hydrolysis, including carbonation (which utilises atmospheric CO_2 to weather both carbonates and

silicates), and acid dissolution (which utilises protons liberated from sulphide oxidation). Both of these reactions are largely dependent upon drainage system and redox status.

Acid dissolution represents one of the most important chemical rock weathering processes in glacial catchments, resulting in large quantities of Ca^{2+} and HCO_3^- (Hubbard and Nienow, 1997; Hodgkins, 1997; Raiswell 1984). This is the direct action of H^+ protons to weather rock surfaces. Acid dissolution of carbonates is shown in equation 1a:

$$CaCO_{3\,(s)} + H^+_{(aq)} + H_2O \leftrightarrow Ca^{2+}_{(aq)} + 2HCO^-_{3\,(aq)}$$
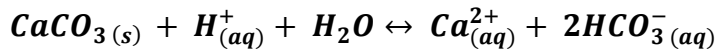
(Equation 1a taken from Raiswell, 1984)

Carbonation is the process whereby CO_2 dissolved in water (promoted through the enhanced solubility of CO_2 in the near freezing temperatures of subglacial waters (Reynolds and Johnson, 1972)) produces carbonic acid. This allows acid dissolution of carbonate and silicate rocks (as outlined in equations 1b and 1c) which liberates dissolved inorganic carbon. The exact DIC species created via this pathway is dependent upon pH.

$$CaAl_2SiO_{8\,(aq)} + 2CO_{2\,(aq)} + 2H_2O \leftrightarrow Ca^{2+}_{(aq)} + 2HCO^-_{3\,(aq)} + H_2Al_2SiO_{8\,(s)}$$
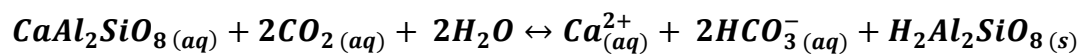
(Equation 1b: carbonation of silicates (Raiswell, 1984))

$$CaCO_{3\,(s)} + CO_{2\,(aq)} + H_2O \leftrightarrow Ca^{2+}_{(aq)} + 2HCO^-_{3\,(aq)}$$
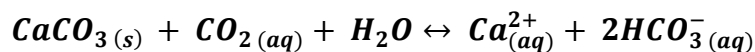
(Equation 1c carbonation of carbonates (Raiswell, 1984))

An additional weathering mechanism responsible for the liberation of TDIC in glacial environments is coupled Sulphide Oxidation-Carbonate Dissolution (SO-CD). This is a two stage reaction whereby H^+ ions gained from sulphide oxidation are used to dissolve calcium carbonate (equation 2).

$$4FeS_{2\,(s)} + 16CaCO_{3\,(s)} + 15O_{2\,(aq)} + 14H_2O_{(l)}$$
$$\leftrightarrow 16Ca^{2+}_{(aq)} + 16HCO^-_{3\,(aq)} + 8SO^{2-}_{4\,(aq)} + 4Fe(OH)_{3(s)}$$

(Equation 2 (Raiswell 1984))
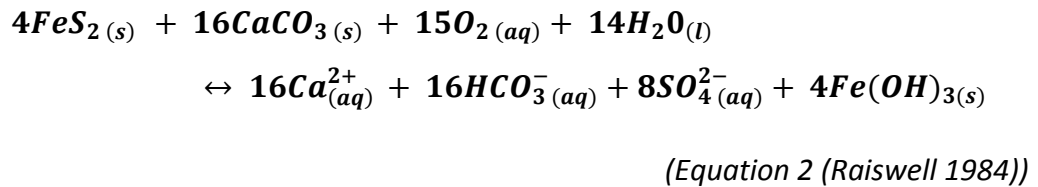
Both carbonation reactions (equations 1b/1c) and sulphide oxidation (equation 2) rely upon the ingress of atmospheric gases. However, production of sulphuric acid via oxidation of subglacial sulphides can proceed without atmospheric oxygen, using Fe (III) as demonstrated in equation 3 below:

$$FeS_{2\,(s)} + 14Fe(OH)_{3\,(s)} + 4CaCO_{3\,(s)}$$
$$\leftrightarrow 15Fe(OH)_{2\,(s)} + 4Ca^{2+}_{(aq)} + 2SO^{2-}_{4(aq)} + 4HCO^-_{3\,(aq)} + H_2O_{(l)}$$

(Equation 3 (Tranter et al., 2002))
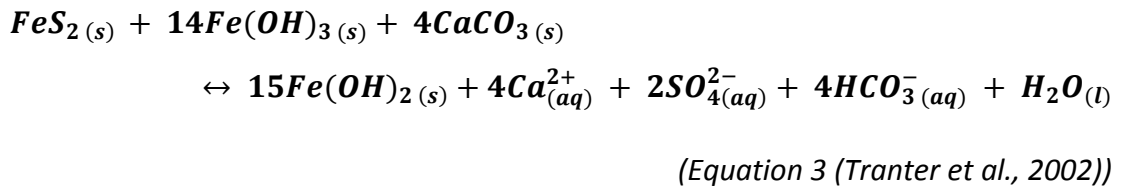
In this instance consideration of the redox scale is essential in determining solute acquisition and therefore TDIC supply pathway. Redox refers to the reduction or oxidation potential of a chemical species to gain or lose electrons (Archer, 2010). The redox status (Eh) of the subglacial system is largely determined by hydrology and has been observed to fluctuate in line with seasonality (Tranter et al., 2002; Wynn et al., 2015). In most glacial systems with limited geothermal/volcanic influence Eh is determined by the relative removal of O_2 by weathering versus supply due to connectivity between glacier surface and bed. Typically, high Eh conditions are

associated with full oxygenation, likely in main channels during periods of high summer discharge. Conversely, low Eh is usually found in areas of drainage isolated from direct ingress of atmospheric gases (Tranter et al., 2002; Wynn et al., 2015). Where glaciers have an alternative supply of CO_2, eg. from subglacial geothermal/volcanic activity or microbial respiration, connectivity to the atmosphere and Eh do not affect the viability of carbonation weathering. Microbially mediated chemical weathering reactions such as sulphide oxidation demonstrated in equation 2 utilise oxygen and where this is not replenished, the drainage system is driven towards sub oxic conditions (Tranter et al., 2002). In this environment sulphides can be oxidised by Fe(III) as outlined in eqution 3.Full anoxia is achieved where sources of organic matter force further microbial action and methanogenesis proceeds.

Once a suitable mechanism for TDIC and solute acquisition is established, pH then determines the speciation of inorganic carbon produced (as indicated in figure 2.2.). At lower pH values CO_2 dominates TDIC speciation. As pH increases HCO_3^- becomes more prevalent and under alkaline conditions CO_3^{2-} prevails.
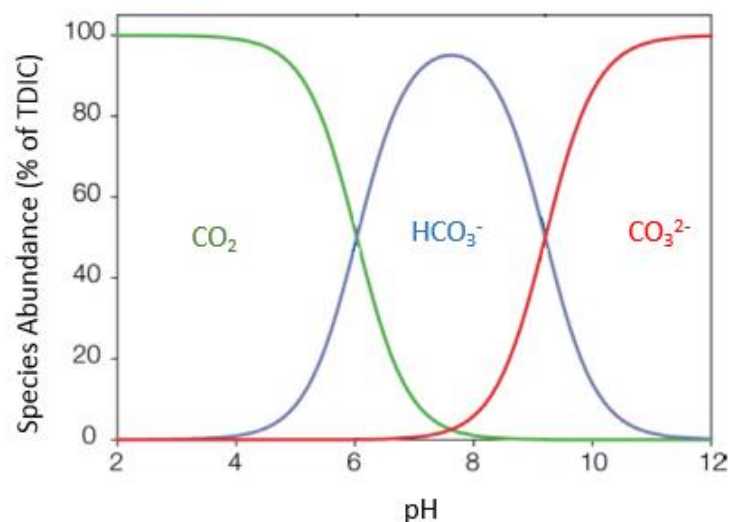
Figure 2.2: Bjerrum plot depicting changing TDIC speciation as a function of pH

pCO₂ can also be used as an indication of the extent and mechanism of weathering occurring within the subglacial system. The amount of TDIC present as carbon dioxide within glacial meltwater is expressed as the partial pressure of CO_2 (*pCO₂*). This is defined as the gaseous pressure of CO_2 dissolved within a given volume of water, in accordance with Dalton's Law of Partial Pressure and calculated using the following equation:

$$log_{10}pCO_2 = log_{10}(HCO_3^-) - pH + pKCO_2 + pK_1$$

(Equation 4 (Hodgkins et al., 1998)

Where $pKCO_2$= 1.12 and pK_1= 6.58 (outlined by Ford and Williams in Hodgkins et al., 1998).

Where values exceed $10^{-3.5}$ atmospheres, pressures are likely to be greater than atmospheric and therefore CO_2 will diffuse out of the water column, into the atmosphere. Where values are less than $10^{-3.5}$, pressures are lower than atmospheric and therefore CO_2 will diffuse into the water column from the atmosphere. In most glacial systems, the amount of CO_2 found within a glacial meltwater is controlled by the amount of weathering which occurs within the system and the ambient pH which determines carbon speciation.

Where abundant proton supply is used to drive carbonate weathering via acid hydrolysis and pH is relatively acidic, levels of CO_2 in the water can become high, exceeding those in the atmosphere and thus causing outgassing of CO_2 from the system. Where carbonation reactions dominate, utilising CO_2 from the atmosphere to fuel weathering, and pH is high, levels of CO_2 in the water are lower than those in the atmosphere, causing 'drawdown' of atmospheric CO_2. Ultimately, this is a vital component of the global carbon cycle regulating exchange at the atmosphere-hydrosphere interface.

Weathering and solute acquisition as described above may be further complicated by secondary mineral precipitation, which can play an important role in influencing chemical fluxes of bulk meltwaters. Weathering processes largely assume a congruent weathering pathway, with no secondary precipitation, therefore solutes in bulkmelters reflect the chemical composition of the parent rock from which they were weathered (Thomas and Raiswell, 1984). However, where bulk meltwaters are subject to prolonged rock: water contact times, there is a possibility that mineral saturation may occur (Crompton et al., 2015). Depletion of ions such as Ca or Si may reflect secondary subglacial precipitation (Thomas and Raiswell, 1984; Crompton et al., 2015). In terms of Ca, this may be in the form of $CaCO_3$ precipitation (Thomas and Raiswell, 1984), whilst Si concentrations can be modified by non stoichiometric dissolution rates or adsorption of cations onto mineral/clay surfaces (Crompton et al., 2015). As with dissolution processes these are influenced by hydraulic pathway and pH (particularly adsorption). Care needs to be taken when assuming solute is representative of dissolution processes, particularly where waters flowing through silicate environments display a deficiency in Si.

2.2.2. The sources and cycling of organic carbon in glacial environments

Alongside the paradigm shift towards an organic influence on hydrochemistry, is recognition of glaciers as a functioning glacial biome. Within this biome active ecosystems exist on both the glacier surface and at the glacier base. Carbon is cycled within and between these ecosystems, influencing ionic and isotopic signatures of proglacial waters.

2.2.2.1. The supraglacial ecosystem and organic carbon sources

The physical and chemical properties of the cryosphere allows ecosystems to exist on the surface of glaciers and ice sheets. Carbon inputs to these communities are mainly from surface deposition of organic and inorganic matter. Large quantities of debris are thought to be provided from adjacent ice marginal environments via aeolian transport, whilst aerosols are often scavenged from the atmosphere by the

snowpack itself. Organic carbon then interacts with surficial ecosystems contributing to biogeochemical cycling. Organic matter on the surface may then enter the glacial hydrological system where glacier drainage pathways act as a vector for carbon transport into the englacial and subglacial environment. Matter that is not entrained into the supraglacial channel network remains on the surface and decays in situ becoming less labile.

2.2.2.2. Cryoconite holes

Surficial cryoconite holes, common to the ablation zone of most glaciers have an important role in supraglacial hydrology and biology. Impacts are two fold: 1) they are a hub for surficial microbial carbon and nutrient cycling and 2) cryoconite holes also have an important influence on supraglacial run off. Cryoconite microbial activity is high, and communities occupying these ecosystems are responsible for significant carbon fixation and nutrient cycling, despite the dominance of low temperatures (Anesio et al., 2009; Sawstrom et al., 2002). During the summer, in situ primary production and respiration can be comparable with that found in nutrient rich soil ecosystems of warmer regions (Anesio et al., 2009). Processes of photosynthesis and respiration are dominant, with biogeochemical cycling producing large quantities of Dissolved Organic Carbon (DOC) and Nitrogen. During the ablation season when water supply and nutrient recharge is plentiful, photosynthesis is a major process. Production fixes inorganic carbon (CO_2) from the atmosphere into organic matter. During winter when sunlight is at a minimum and freezing causes stresses to photosynthetic organisms net respiration dominates, returning Total Dissolved Inorganic Carbon (TDIC) to solution along with some Dissolved Organic Carbon (DOC). Winter freezing also produces secondary carbonates which thaw the following ablation season (Bagshaw et al., 2007).

Meltwater generated by the formation of cryoconite holes contributes to run off, particularly in areas such as the McMurdo Dry Valleys where sediment is a necessary agent of surface melt. In the absence of cryoconite holes meltwater generation

would be reduced (Fountain et al., 2004). The hydrological connectivity or isolation of cryoconite holes adds to the importance of biogeochemical cycling in these ecosystems. Well-connected cryoconite holes allow transfer of water and solutes such as chlorine through the system. Where holes containing biological material become isolated, photosynthesis alters the chemical composition of the waters. If these isolated holes become reconnected to the system, sudden transfer of biological material to surface streams occurs (Fountain et al., 2004).

2.2.2.3. Snow algae

Over 110 species of specialized snow algae exist within the snow itself exist. These survive in extreme conditions such as nutrient depletion, acidity, large osmotic changes caused by melting, sub-zero temperatures and high levels of UV irradiation due to the albedo of ice. Optimum growth of snow algae is below 10°C, with assemblages able to survive up to -35°C owing to thick cells walls, 0.2 to 0.3µm thick (Müller et al., 1998). Species distribution is dependent upon the preferred conditions of each alga, with 4 main habitat types: snow environmental specialists found only in snow; ice environmental specialists found only in ice; generalists adapted to both; and opportunists which exploit special conditions within snow/ice (Yoshimura et al., 1997; Takeuchi et al., 2001). In terms of biogeochemical processing snow algae have the ability to assimilate atmospheric CO_2 into cell biomass during photosynthesis. Presence of snow algae also supports carbon and energy transfers through local food webs. Himalayan Snow Algae has been found to support communities of midges and copepods, whilst North American snow algae sustain ice worms and collembolas (Takeuchi et al., 2001).

2.2.2.4. The subglacial ecosystem and organic carbon sources

It is now widely accepted that communities of viable microorganisms exist across a range of subglacial settings (Foght et al., 2004; Skidmore et al., 2005). The functioning and distribution of these microbial communities is ultimately determined by a range of physical and chemical factors. Physical factors include the prevailing

properties of the subglacial environment such as lack of light and constant cold temperatures. Contrastingly, chemical factors such as, solute composition, carbon sources, electron acceptors and bedrock lithology, constrain microbial populations to exclusive areas of the glacier bed. Unfrozen subglacial sediments are assumed to harbour significant and diverse ecosystems, with high rates of biological activity (Tranter et al., 2005; Kaštovská et al., 2007). In order to support the subglacial ecosystem, liquid water and carbon substrates are essential. Carbon in a subglacial setting can result from the following key sources: 1) in situ microbial production; 2) surface in wash from the supraglacial environment; 3) bedrock comminution and weathering and 4) buried organic carbon.

2.2.2.5. In situ microbial production of organic carbon

In situ microbial production creates organic matter otherwise known as 'Necromass' (Hodson et al., 2008). In dark subglacial conditions chemoautotrophic and/or chemolithoautotrophic bacteria play an important role in the provision of organic carbon substrates at the bed. These species fix CO_2 generated by respiration of other microbes and chemical reactions into their biomass (Hodson et al., 2008). Viruses also play an important role in DOC cycling in dark environments. It was found that in the Vestfold Hills, Eastern Antarctica ~60% of the carbon supplied to the winter DOC pool originated from disintegration of bacterial cells by viruses (Hodson et al., 2008).

2.2.2.6. Surface in-wash

Surface in-wash represents an important transient source of young labile carbon and nutrients to the subglacial environment. Cyanobacteria, algae and cryoconite debris represent potentially easily biodegradable carbon sources for microbial functioning. Additionally, whilst chemoautotrophic species dominate in dark subglacial environments, photosynthetic microbes are also present in the system, washed in from surface surroundings. These are in a constant state of anabiosis, respiring CO_2 and acting as an organic carbon source for local heterotrophic microbial populations. Once the glacier recedes and the subglacial ecosystem is re-exposed to the

atmosphere, these photosynthetic microbes recolonize the proglacial area (Kaštovská et al., 2007).

2.2.2.7. Burial of organic carbon

The sequential retreat/advance of glaciers over time has resulted in 'The Glacial Burial Hypothesis' (Zeng, 2003). Advancement of continental ice sheets and contemporary valley glaciers buries vegetation and soil carbon accumulated during the preceding interglacial. These overridden sediments provide allochthonous organic carbon and act as a carbon/energy source for microbial life (Skidmore et al., 2000). The type and quality of organic carbon depends upon the surface the glacier has encroached upon. For example, high numbers of cyanobacteria and algae present in basal sediments of the Lower Wright Glacier, Antarctica suggests advancement over a delta surface within the last 200-300 years. Furthermore, subglacial discharge from the Greenland Ice Sheet contains dissolved organic matter from overridden Holocene soils and vegetation alongside organic carbon produced by in situ metabolism (Stibal et al., 2012, Ryu and Jacobson, 2012).

Overidden carbon is then insulated from contact with the atmosphere and stored beneath the ice. Known estimates state that around 500Gt of carbon was stored via this mechanism during the Last Glacial Maximum and the subglacial organic carbon pool during Quaternary glacials was considerably higher than today (Zeng, 2003; Wadham et al., 2008). Upon deglaciation the buried carbon is exposed and subjected to decomposition processes resulting in a net flux from the biospheric sink into the atmosphere.

2.2.2.8. Organic matter interaction with volcanism

Geothermal breakdown of organic matter can act as a source of methane (an inorganic carbon form) to the subglacial realm (Wadham et al., 2012). Carbon sources of this kind rely upon a very unique situation whereby glaciers overlie active volcanic systems.

2.2.2.9. Bedrock comminution and weathering

Subglacial weathering is an agent of modification of carbon within the subglacial system. Weathering of freshly comminuted bedrock, organic matter and sulphides provides both organic and inorganic sources of carbon (Wadham et al., 2004). Chemical weathering processes are critical for microbial survival through liberation of organic carbon alongside Nitrogen and Phosphorus from the bedrock, further influencing organic carbon cycling (Wadham et al., 2010).

2.3. Methane

Methane dynamics are the result of interactions between organic and inorganic carbon cycling. Methane can be formed microbially or geologically and upon release to the atmosphere engages rapidly in inorganic carbon cycling, rendering it an extremely volatile greenhouse gas. In terms of a molecule to molecule comparison methane is about 40 times more powerful than carbon dioxide (Archer, 2010; Nisbet, 2002). It is therefore essential to understand the methane component of the global carbon cycle.

2.3.1. Microbial influence on terrestrial methane cycling

Anaerobic methane production under sedimentary conditions relies on the synergistic activities of different microbial communities and favourable physical and chemical conditions such as anoxia, nutrient recharge and suitable carbon substrates (Wadham et al., 2012; Macdonald, 1990, Archer 2010). Conrad (1989) identifies this variety as 1) hydrolytic and fermenting bacteria 2) hydrogen reducing bacteria 3) homoacetogenic bacteria 4) methanogenic bacteria. The variable metabolic actions of these communities results in two main terrestrial pathways of microbial methane formation: CO_2 Reduction and Acetate fermentation. Whilst both are thought to have the capacity to operate over a range of environments, selectivity of microbes and differing optimal conditions usually leads to a dominance of CO_2 reduction in marine settings whilst acetate fermentation is more common in freshwater

environments (Archer, 2010). For terrestrial environments where both CO_2 reduction and acetate fermentation pathways exist, methanogenic pathways are seasonally controlled. In summer time and during warmer sediment temperatures acetate fermentation is the predominant pathway and in winter where sediments are colder CO_2 reduction is the main formation process (Schoell, 1988).

2.3.1.1. Acetate fermentation pathway

Within organic matter are complex compounds of carbohydrates, proteins and lipids. Methanogenesis begins with the reduction of organic compounds by fermentative bacteria to form simpler molecules such as acetate, fatty acids, carbon dioxide and hydrogen gas. Volatile fatty acids provide acetogenic bacteria with the energy to produce acetate with CO_2 and H_2 as by-products (Clark and Fritz, 1997). Methanogens then convert acetate to CH_4 and CO_2 (as outlined in equation 5). This is accomplished by the reduction of stable methyl carbon to methane and the oxidation of carboxyl carbon to carbon dioxide, essentially 'splitting' CO_2 and CH_4 during fermentation (Archer, 2010; Floodgate and Judd, 1992).

$$CH_3COOH = CH_4 + CO_2$$
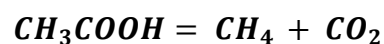
(equation 5)

2.3.1.2. CO$_2$ reduction pathway

Alternatively, many species utilise the hydrogen produced during conversion of complex compounds to simpler molecules to reduce CO_2. Dissolved inorganic carbon as CO_2 will dissociate to form bicarbonate where pH ranges from 6 to 8. Methanogenic bacteria combine this with hydrogen ions to form methane, water and hydroxide. The following equations demonstrate this (Clark and Fritz, 1997):

$$CO_2 + 4H_2 = CH_4 + 2H_2O$$

<div align="right">(equation 6a)</div>

$$HCO_3 + 4H_2 = CH_4 + 2H_2O + OH$$
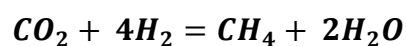
<div align="right">(equation 6b)</div>

Formate can also be used as a substrate to facilitate CO_2 reduction. In this instance formate is oxidised by methanogens to create carbon dioxide and hydrogen as follows:

$$HCOOH = H_2{}^+CO_2$$
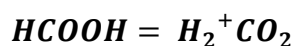
<div align="right">(equation 7)</div>

The CO_2 created is then reduced to methane as per equation 6a.

2.3.1.3. Oxidation of methane

In addition to methane production, bacteria present within sediments also offer mechanisms by which methane consumption or methanotrophy can occur facilitated by methanotrophic bacteria. Once anoxic conditions are no longer sustained oxidation occurs in an aerobic setting via a 3 stage reaction process. Initially, methane is converted to methanol, then formaldehyde or formate before finally being transformed into CO_2. This is represented by the following equation from Cicerone and Oremland (1988):

$$CH_4 \rightarrow CH_3OH \rightarrow HCOOH \rightarrow CO_2$$
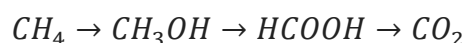
<div align="right">(equation 8)</div>

Methane flux to the atmosphere is governed by differences in the processes of methanogenesis and methanotrophy, which can occur simultaneously in terrestrial ecosystems (Chan and Parkin, 2001). Annually, oxic soils consume between 20 to

60Tg of methane, providing the only terrestrial biospheric sink for atmospheric methane (Holmes et al., 1999; King, 1997).

2.3.2. Geogenic methane production

Methane dynamics are further complicated by geogenic contributions. Geogenic methane production is important for commercial gas production, with ~80% of natural gas being of geogenic origin (Rice and Claypool, 1981). Geogenesis encompasses methane from geological stores of the endogenic carbon cycle. This includes methane formed from organic matter degradation at increased depths (typically >1km) and temperatures (between 157 and 221°C) and inorganic synthesis in volcanic and hydrothermal locations (Floodgate and Judd, 1992; Judd et al., 2002; Stopler et al., 2014).

In terms of organic matter degradation, large amounts of high quality organic matter are required for production (Kvenvolden, 1993). Methane production is associated with organic matter from higher land plants such as trees and leafy vegetation. This undergoes processes of compaction, burial and diagenetic transformation followed by thermal dissociation of kerogens where the necessary temperature-pressure-depth relationships prevail to form methane. Temperature is a sensitive factor, as once the temperature becomes too great the methane produced is destroyed (Sephton and Hanzen, 2013; Floodgate and Judd, 1992).

Once formed, methane can migrate to the surface where it is either degasses or becomes trapped as methane hydrates. This is facilitated by the light molecular structure of methane which provides the greatest buoyancy force compared to other hydrocarbons. As the most mobile hydrocarbon methane is readily supplied to the surface where it interacts with the short term carbon cycle.

In some instances geogenesis also encompasses methane from inorganic substances often in volcanic or hydrothermal locations, with no living intervention (Floodgate and Judd, 1992). This includes: high temperature (>100°C) magmatic processes in

volcanic/geothermal areas and low temperature (<100°C) gas-water rock reactions. With the latter having the ability to function at shallow depths (Etiope and Sherwood Lollar, 2013). High temperature magmatic methane can originate from 'deep earth' primordial gases of cosmic origin which have been preserved in the mantle. Additionally high temperature reactions such as hydrolysis of carbon based minerals (carbides) and release of C-O-H fluids during magma cooling also act as potential volcanic inputs. In terms of low temperature sources autonomous inorganic synthesis occurs (Etiope and Sherwood Lollar, 2013). This can be represented as follows:

$$CO_2 + \ 4H_2 = \ CH_4 + \ 2H_2O$$
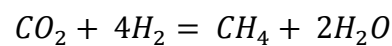
(Equation 9 (Etiope and Klusman, 2002)).

These primitive gases then exploit crustal weaknesses such as faults and plate boundaries to migrate to the surface, and are either released directly to the atmosphere or stored as methane hydrate dependent upon ambient pressure-temperature relationships.

2.4. Cryospheric methane dynamics

Since subglacial settings offer the anaerobic and favourable conditions conducive to bacterial methane production (as outlined in chapter 2.3.1), it is logical to consider these to be an important location (albeit largely overlooked) for methanogenesis. In addition, where the glacier covers areas of volcanic activity, geogenic methane is another potential input of carbon. Methane generated subglacially is then constrained beneath the ice mass which acts as a cryospheric cap. Current climate change is reducing the stability of this cap, leading to potential evasion of subglacial methane. Modelling based on the Antarctic Ice Sheet estimates potential annual release of 0.15 PgC. However this is based on assumptions that 15PgC is present as methane hydrate beneath 10% of the Western Antarctic Ice Sheet with a retreat rate

of 1,000km per year. If movement of methane was rapid with no oxidation this would exceed annual atmospheric turnover rates of 0.13PgC (Wadham et al., 2012). Clearly, these cryospheric sources of methane are an underappreciated source of inorganic carbon, with the potential to rapidly engage with atmospheric cycling and contribute to the greenhouse effect. Therefore, further parameterisation of cryospheric methane dynamics is essential.

2.4.1. Microbial methane dynamics in glacial settings

Viable microbes exist in sediments beneath all contemporary types of ice mass, ranging from small valley glaciers to the Greenland and Antarctic Ice Sheets. Such bacterial assemblages include aerobic heterotrophs, nitrate reducers, iron reducers, methanogens and sulphate reducers. These species have been found at temperatures as low as -18°c and up to pressures of 80mpa (Wadham et al., 2008; Wietemeyer and Buffett, 2006). Alongside this the presence of suitable organic carbon substrates, redox conditions and liquid water also influence methane production and consumption.

2.4.1.1. Cryospheric methanogenesis

It is now widely accepted that glaciers are favourable sites for bacterial methanogenesis (Wadham et al., 2012) providing the three fundamental conditions for methane production: 1) anoxia 2) liquid water and 3) a suitable carbon substrate (Stibal et al., 2012; Wadham et al., 2012; Wadham et al., 2008). In subglacial environments, anoxia results from a combination of exclusive factors. Firstly, subglacial environments are largely out of contact with the atmosphere; secondly, poor hydrologic connectivity and prolonged residence times of distributed drainage system leads to stagnant water dwelling in saturated sediments; and finally, oxidation of organic carbon and sulphide minerals which is common in these settings consumes any dissolved oxygen to force conditions towards a low redox status (Wadham et al., 2008; Stibal et al., 2012). Favourable physical conditions are linked

to the availability of water and nutrients at the glacier sole. Basal sediments also proffer organic carbon sources as either surface in wash, overridden soils, or in-situ microbial production.

The presence of microbes (in particular methanogens) appears to be indiscriminate of thermal regime and location with observations made from cold based glaciers such as Lower Wright Glacier, Antarctica; temperate glaciers such as Russell Glacier, Alaska and Polythermal glaciers documented by research at John Evans Glacier, Canada (Stibal et al., 2012; Wadham et al., 2008; Skidmore et al., 2000). It is conceivable that temperate and the 'warm' areas of polythermal glaciers are conducive to microbial life and methanogenesis, due to hydrological configuration providing necessary liquid water nutrient recharge (Tranter et al., 2005).

2.4.1.2. Cryospheric methanotrophy

Microbial consumption of methane also influences the overall flux of cryospheric methane to the atmosphere. Methanotrophy has the potential to occur in both the subglacial and proglacial realm. Subglacial channel margin habitats where oxic conditions prevail, provide favourable conditions for methanotrophs (Dieser, et al., 2014). In this instance subglacially produced methane would be regulated before entering the proglacial environment, limiting cryospheric methane flux to the atmosphere. In addition, the retreat of glaciers worldwide is providing a new, and under explored potential methane sink, as large areas of previously glaciated terrain are exposed to the atmosphere. Recently de-glaciated forefields have the potential to act as habitats for microbes. The initial stages of deglaciation are dominated by heterotrophic communities, which decompose allocthonous organic carbon deposits previously overridden by periods of advance (Yde et al., 2011; Bardgett et al., 2007). As time since deglaciation increases, glacier forefields become locations of net methanotrophy, with atmospherically sourced methane as the substrate to provide energy for growth. This in effect allows areas inhabited by these methane consuming

microbes to act as methane sinks, facilitating methane drawdown and removal from the atmosphere (Barcena et al., 2010).

2.4.2. Cryospheric geogenesis of methane

Geogenic methane formation and linkages to glaciology are less widely researched, possibly due to the limited locations possessing surface ice masses alongside geothermal basal activity. Antarctica is one area where large expanses of ice overlie active geothermal areas. Direct evidence of methane sourced from geogenic origins is shown through the composition of the Larsen B seep, where the hydrocarbon composition contains considerable amounts of ethane (Niemann et al., 2009). Additionally Wadham et al. (2012) consider the potential for geogenic methanogenesis in this region. It is noted that large areas of the West Antarctic Ice Sheet comprise of sediments reaching several km thickness and a combination of volcanism and geothermal heat flow. This provides suitable temperature, pressure and depth dynamics to facilitate geogenic methanogenesis. In addition, absence of sedimentation beneath the Ice Sheet reduces the downward transfer of pore waters and sediments thus allowing a potential net upward fluid flow induced by geothermal heating. Computer modelling of scenarios surrounding this found that hydrate is produced in this manner throughout the entire gas hydrate stability zone beneath the ice. If 10% of the West Antarctic Ice Sheet was covering geothermal hotspots, theoretically 90Pg C of methane hydrate could be produced over 1 million years (Wadham et al., 2012).

Similarly, geogenesis is conceivable in Iceland due to the extensive history of Volcanism related to the position of the country on the Mid Atlantic Ridge. Ice caps cover substantial parts of the active volcanic zones with ~ 60% of the glacierized area of the country underlain by operational volcanic systems (Pagli and Sigmundsson, 2008; Larsen, 2002).

2.4.3. Potential for the combination of bacterial and geogenic methane sources

Research to date demonstrates evidence for potential bacterial and geogenic sources of methane beneath ice sheets. Suggested methane dynamics can be observed in sub- Antarctic methane production. There is an evident split between the East Antarctic Ice Sheet (EAIS) and the West Antarctic Ice Sheet (WAIS) with the east displaying bacterial production in frozen bed sectors converting around 70-390 Pg C and the west demonstrating a trend towards geothermal activity providing geogenic production and some tens of Pg C (Wadham et al., 2012). The possibility for bacterial and geogenic source mixing has been greatly overlooked in many Antarctic studies. However, modelling to show the potential for combined methane sources indicates the importance of investigation into methane production in geothermal glacial areas.

Furthermore, geothermal heat potentially promotes microbial turnover. Usually lower temperatures promote slower bacterial carbon turnover (Wadham et al., 2008). Amalgamation of geothermal heat and the insulating effect of the ice causes basal temperatures reach the pressure melting point promoting the presence of liquid water and enhancing bacterial conversion of organic matter to methane (Weitemeyer and Buffett, 2006).

In areas devoid of subglacial geothermal activity, any evidence of methane can be confidently attributed to microbial processes, however in locations such as Iceland and Antarctica where subglacial volcanism is present, methane dynamics may be more complicated. In this situation the best way to decipher methane source is through isotopic analysis.

2.4.4. Detecting methanogenesis, geogenesis and oxidation using stable isotopes of Carbon and Hydrogen.

Stable isotopes of Hydrogen and Carbon offer a unique fingerprinting tool to determine methane production mechanism and the influence of microbial oxidation.

Due to differences in production conditions, bacterial and geogenic methane have contrasting isotopic signatures. Microbially produced gases are shown to be enriched in ^{12}C and ^{1}H compared to methane produced via thermal breakdown of organic matter. Typically geogenic methane generally (but not exclusively) has values of δ^{13}C = around -50 to -20 ‰ and δD= around -275 to -100‰ whilst bacterial CH_4 has values of δ^{13}C = around -50 to -60 ‰ and δD= around -250 to -380‰. Such discrepancies in the isotopic values are attributed to the higher temperatures associated with hydrocarbon production in geogenic generation and differing pathways linked to substrate and archaea type in bacterial CH_4 production (Whiticar, 1999; Cicerone and Oremland, 1988; Prinzhofer and Pernaton, 1999; Sowers, 2006; Nisbet 2002). Isotopes can also distinguish between bacterial production pathways, with differing signatures for CO_2 reduction and acetate fermentation. This is linked to Kinetic Isotope Effects (KIEs). In terms of the CO_2 reduction pathway, attributed Kinetic Isotope Fractionation discriminates against ^{13}C, resulting in separation between CO_2 and CH_4 resulting in extremely negative values around -110‰. In contrast, Kinetic Isotope Fractionation associated with acetate fermentation is lower resulting in δ^{13}C values of -50 to -60‰. The reverse applies when considering the Kinetic fractionation of deuterium, with large fractionation for acetate fermentation (δD ≈ -531‰ vs. SMOW) and smaller fractionation for CO_2 reduction (δD= -170 to-250‰). These deuterium differences are due to transfer of methyl during fermentation which is depleted in deuterium (Whiticar, 1999; Whiticar et al., 1986).

Processes such as fractionation during methanotrophy and diffusion alter the initial isotopic signature of methane. Where methane-rich waters discharge into aerobic environments they can be subject to methanotrophy. Here, methanotrophs selectively oxidize the lighter isotopes of carbon and hydrogen leaving residual methane enriched in ^{13}C and ^{2}H (Barker and Fritz, 1981). This oxidized bacterial component can give the appearance of geogenically sourced methane, often making interpretation of methane source difficult (Barker and Fritz, 1981). Similarly, diffusion processes can alter isotopic signatures. Differences in gaseous concentrations across the air-water interface and associated partial pressures promote diffusion into/out of

the atmosphere (Sebacher et al., 1983). Theoretically diffusion from methane rich waters could result in residual aqueous methane enriched in heavier isotopes. However, this is not a stable process with influences from air velocity, temperature and two way diffusivity. These complications can often cause confusion when only using $\delta^{13}C$ values as an origin tracker; however using δD values alongside carbon stable isotopes provides the most robust fingerprinting method available.

2.5. Summary of glacial carbon and linkages to hydrology

Carbon within glacial systems exists in both organic and inorganic forms, across supraglacial, englacial and subglacial realms. It is often difficult to detach cryospheric carbon cycling from hydrology, with the transfer of carbon between glacial inventories relying upon meltwater. Ultimately, glacial meltwater provides three important roles linked to glacial carbon dynamics. Firstly, meltwater acts as a vector of dissolved carbon transport, with most carbon exisiting in dissolved or particulate form. Supraglacial hydrology is responsible for the inwash of surficial carbon to the subglacial system, whilst subglacial hydrology is an important component facilitating chemical reactions which liberate inorganic carbon and mechanims by which organic carbon is degraded. Secondly, in terms of methane dynamics, redox status is often driven by hydraulic configuration and is a key factor influencing the prevalence of bacterial methanogenesis or methanotrophy in subglacial settings. Finally, it is glacial hydrology which ultimately determines the timing and rate that carbon generated within glacial catchments is transferred to the proglacial environment where it can engage in subaerial terrestrial carbon cycling. With this is mind it is essential to understand the basics of glacial hydrology alongside the unique nature of Icelandic meltwater outputs in order to fully constrain cryospheric carbon cycling.

2.5.1. Traditional glacial hydrology

Glacial hydrology is widely recognised to operate according to water flow dynamics in supra glacial, englacial, subglacial and pro-glacial zones. Limited mutual exclusivity between components of the hydrological system leads to variability in drainage

configuration across glacier types. Generalised models of glacial drainage applicable to temperate glaciers suggest highest bulk meltwater flows during summer accompanied by near cessation during winter, forming a reverse hydrograph. Bulk meltwater run off is comprised of 'quick flow' and 'delayed flow' components and it is the relative influence of these which determine many potential variations in glacial hydro-geochemistry (Fountain and Walder, 2010).

Quick flow comprises relatively dilute meltwaters mainly from the supraglacial environment. These route efficiently through moulins and crevasses (Stenborg, 1973) and rapidly exit the glacier via englacial or subglacial channels (Fountain and Walder, 2010; Röthlisberger, 1972). Delayed flow consists of waters conveyed slowly through the subglacial system, via cavity drainage (in autonomous or interconnected cavities) (Fountain and Walder, 1998; Lliboutry, 1976) or flow in saturated subglacial sediments. The slow velocities lead to increased rock: water contact times promoting enhanced weathering. This results in a chemically enriched meltwater constituent.

Spatial and temporal variations of quick and delayed meltwater flows contribute to classical drainage theory (Shreve, 1972). This largely hinges upon the prevalence of delayed flow drainage during periods of reduced melt and a transition to rapid channelized drainage during the ablation season. Once established, the channelized system expands head ward alongside the retreat of the snow line, forming an arborescent quick drainage system beneath large areas of the glacier. This dominates the ablation season until reduced flows and ice creep closure of channels forces a transition back to the linked cavity system. Increases in dilute quick flow components during summer typically result in an inverse relationship between chemistry and discharge due to dilution effects.

Glacier hydrology is dominated by classical drainage theories applicable to Alpine and Arctic Environments. However, the Icelandic glacial drainage system has been little studied. Year-round low level ablation, caused by the dominance of maritime

conditions and large fluxes of geothermal heat, result in net ablation in every season of the year and continuous subglacial drainage (Pagli and Sigmundsson, 2008). Given the unique hydrological configuration at Icelandic glaciers such as Sólheimajökull, hydrological investigation beyond established norms is necessary.

2.5.2. Icelandic glacial hydrology

Icelandic glacial hydrology is characterised by year round drainage attributed to subglacial geothermal heat sources and continual low elevation (>100m above sea level) melting of the glacier snout in a maritime setting. This results in the persistence of subglacial drainage throughout the winter season, with the likelihood of channelized quick flow drainage prevailing beneath the lower ice extent. Superimposed upon this are periodic rapid release events associated with the build-up and sudden release of meltwater generated by geothermal heat transfer. These can be large scale Jökulhlaups (for example in Grimsvotn (1996) and Sólheimajökull (1999)), or smaller scale periodic floods such as those frequently appearing at Kötlujöjull or Sólheimajökull throughout the late Spring and Summer drainage seasons (Björnsson, 1988; Lawler et al., 1996).

The hydrochemistry of the associated meltwater release may also carry a unique signature dependent upon the prevalence of any geothermal activity beneath the ice mass. This is particularly notable at Sólheimajökull where H_2S discharges from the glacier, particularly during the summer season. Furthermore, dual isotopic analysis of $\delta^{34}S$ and $\delta^{18}O$ of sulphate dissolved within meltwaters (Wynn et al., 2015) indicate reverse redox conditions with discharge of reduced, anoxic meltwaters in summer, rather than winter, a process which Lawler et al. (1996) referred to as a cyclical 'sweeping out' of the geothermal zone. Prevalence of this process during summer months is linked to expansion of the subglacial drainage system head wards, where meltwaters likely intersect the Katla geothermal zone at the time of year when seismic activity and geothermal processes are at their peak. Two areas of seismic activity have been identified beneath the Mýrdalsjökull ice cap: one in the South East

and another in the South West not far from Sólheimajökull (Lawler et al., 1996). Seismic activity is highly seasonal in South West Mýrdalsjökull, with activity peaking during July-October (Lawler et al., 1996; Gudmundsson et al., 1994; Einarsson and Brandsdóttir, 2000), frequently associated with surface melt and seasonal unloading of the snowpack. Low summertime overburden pressures from snowpack unloading (3-9m of snowpack melting lead to an estimated seasonal unloading of 0.003MPa (Einarrsson and Brandsdóttir, 2000) have been deemed sufficient to trigger seismic and geothermal activity (Pagli and Sigmundssen, 2008), coinciding with drainage system expansion.

The effects of this unique hydrological regime generate profound effects upon the solute flux from the glacier, particularly with regard to the carbon budget. Most notably, this has the potential to exert a powerful influence over subglacial methane dynamics, forcing widespread seasonal anoxia ideal for methanogenesis and inhibiting methanotrophy. Furthermore, contributions from subglacial geogenesis are possible. This potentially allows large volumes of meltwater discharging from the subglacial realm to deliver high quantities of reduced methane to the proglacial zone, where it can rapidly engage in atmospheric cycling. Due to the potency of methane as a greenhouse gas, it is essential to constrain potential reservoirs beneath ice masses and assess the influence microbial activity has on methane flux to the atmosphere (Dieser et al., 2014). In order to fully achieve this, it is essential to step away from traditional drainage regimes of Alpine glaciers and consider the quirks of carbon cycling in areas subjected to subglacial volcanism.

2.6. Synthesis

Cryospheric carbon cycling is a unique (and under estimated) terrestrial addition to the global carbon cycle. This occurs in both inorganic and organic form, acknowledged by a paradigm shift from hydrochemistry to biogeochemistry. Where inorganic and organic components combine with suitable conditions, methane is formed. Hydrology is a fundamental element in determining carbon dynamics within

glacial systems. Where hydraulic configuration conforms to classical drainage theories, cryospheric carbon cycling has been explored. However, in areas where distinctive hydraulic configuration prevails, such as Iceland, the accompanying unique carbon cycling has been little studied. In light of exclusive redox conditions and subglacial geothermal processes operating at Sólheimajökull, research areas addressed in this study offer a chance for an exclusive insight into the impact these processes have upon carbon export.

3. Introduction to Field Site, Field techniques and Laboratory Methodology

3.1. Introduction

This chapter outlines how two field campaigns were designed and executed during Summer 2013 and Spring 2014 with the intent to supply information on bulk meltwater characteristics and proglacial dynamics at Sólheimajökull. Consideration of carbon cycling within the Sólheimajökull system is apportioned into aqueous components of carbon cycling determined through monitoring of proglacial bulk meltwaters and evidence of sedimentary carbon dynamics from across the proglacial forefield, supplemented by laboratory analysis.

3.2. Study site description

Iceland offers the perfect situation for glaciological investigation with accessible glacierized catchments and little human influence. Furthermore, enhanced volcanicity due to the proximity of the mid-Atlantic ridge has created a unique situation whereby the effects of geothermal, volcanic and glacial processes can interact. Located on the Southern coast of Iceland, Sólheimajökull is an 8km long non-surging, temperate glacier (Wynn et al., 2015). Sólheimajökull is situated within a 110km^2 catchment, of which approximately 71% is glacierized. Total glacier area is 78km^2 with a maximum ice thickness of 433m. Sólheimajökull descends from ~1500m a.s.l to ~100m a.s.l where a relatively mild maritime climate characterised by average annual temperatures of 5°C and annual precipitation in excess of 10,000mm (with large volumes falling as rain), results in year round ablation and continuous drainage from the glacier snout (Friis, 2011; Wynn et al., 2015).

Sólheimajökull is an outlet glacier from the Mýrdalsjökull ice cap (figure 3.1), which blankets the 100km^2 Katla volcanic caldera, one of the most active volcanoes in Iceland (Friis, 2011). The glacio-volcanic history of Katla and Mýrdalsjökull is evident

in widespread ash deposits across the Sólheimajökull surface, with inclusion of large bands of ash from the most recent Katla 1918 eruption. Interplay between the glacier and underlying geothermal areas is also evident in proglacial waters draining Sólheimajökull. The Jökulsa á Sólheimasandi is the bulk meltwater river draining the Sólheimajökull catchment (as shown in figure 3.4). Historically this has adopted the colloquial name of Fulilaekur ('stinky river') linked to the strong sulphurous odour often emitted by the river (Wynn et al., 2015). This has often been attributed to connectivity between subglacial hydrology and geothermal water flowing from the vents between Goðabunga and Háabunga (Friis, 2011). In support of this, geothermal components have previously been identified in bulk meltwaters exiting the Sólheimajökull catchment (Sigvaldason, 1963; Lawler et al., 1996; Wynn et al., 2015). Bulk meltwaters in the Jökulsa á Sólheimasandi thereby provide a rare opportunity to explore complimentary processes of glacial hydro geochemistry and subglacial volcanism.
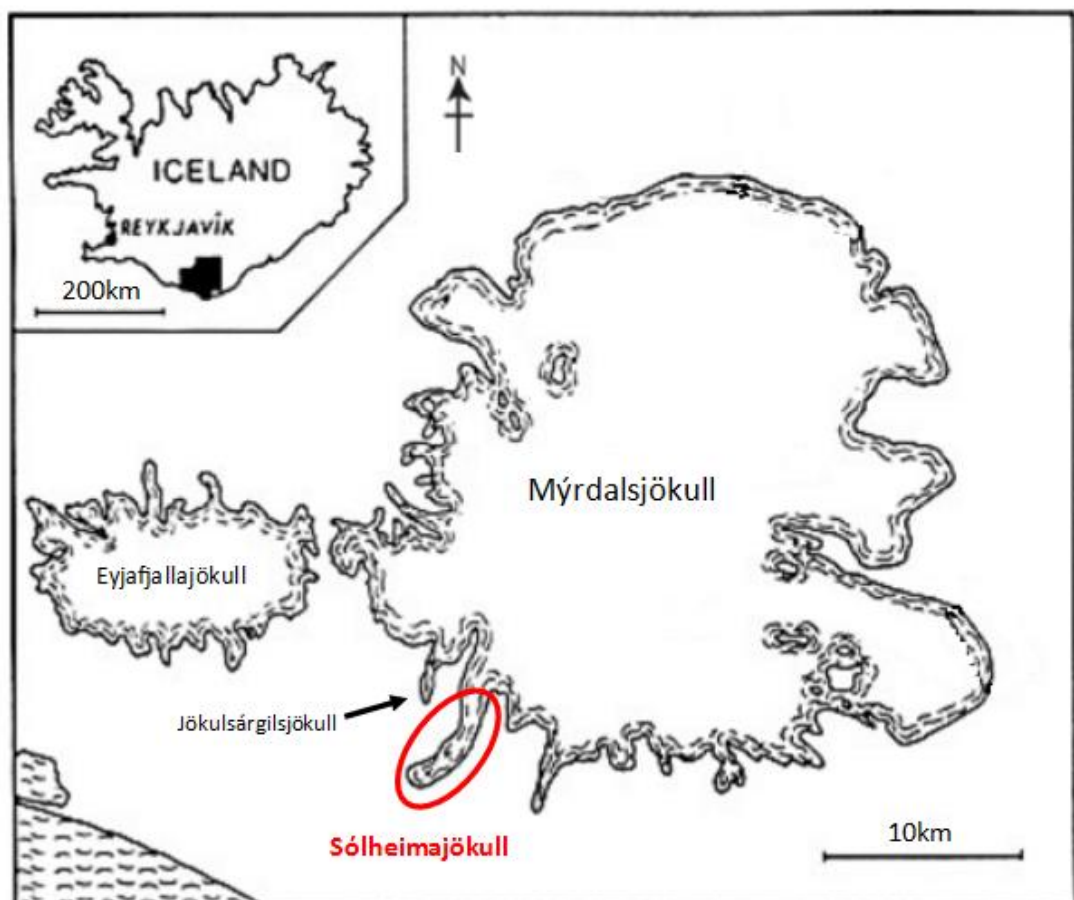
Figure 3.1: Map depicting location of Sólheimajökull adapted from Krüger (1988)

Until 2010, two proglacial channels drained meltwaters from Sólheimajökull. One to the east, primarily associated with supraglacial run off and one on the western ice margin dominated by outflow of subglacial waters (Tepe and Bau, 2014). Since 2010 a proglacial lake has developed dividing the eastern and western proglacial areas. In addition to meltwaters directly supplied from Sólheimajökull, the Jökulsa á Sólheimasandi also drains water from two additional sources. The first is Jökulsárgil, which drains Jökulsárgilsjökull, a valley glacier approximately 3km to the north of Sólheimajökull as shown in figure 3.2 (Russell et al, 2010). Secondly, Fjallgilsá (figure 3.3) joins the Jökulsa á Sólheimasandi approximately 2km downstream from the glacier snout (Guan et al., 2015). This is a non-glacial river originating from grassland to the west of Sólheimajökull. Local geology is dominated by basalts and acidic volcanic rocks (Carswell, 1983; Flaathen et al., 2007).

Figure 3.2: Photograph taken during Spring 2014 showing flow of Jökulsárgil through a gorge before joining the proglacial lake

Figure 3.3: Photograph taken during Summer 2013 showing Fjallgilsá emerging from a gorge south of the Sólheimajökull Glacier Snout

Marginal fluctuations of Sólheimajökull are influenced by climate, resulting in a well-documented history of dynamic advance and retreat cycles (Friis, 2011). From 1996 the glacier has retreated almost 800m, revealing an extensive proglacial forefield. Proglacial geomorphology is dominated by moraine assemblages and glaciofluvial outwash features resulting from the 1999 Jökulhlaup, which drained via Sólheimajökull.

3.3. Meteorological Parameters

The Sólheimajökull catchment exhibits a typical Icelandic climate characterised by relatively mild temperatures and extensive rainfall due to the close proximity to the coast. Air temperature and precipitation provide transfers of heat which influence surface melting and thus impact meltwater hydrology. Constraining the seasonal

fluctuations in climate is essential in understanding bulk meltwater characteristics. Monitoring stations set up by the Icelandic Meteorological Office (IMO) and Lancaster University currently measure the climate of the Sólheimajökull catchment.

A hydrometric gauging station operated by the Icelandic Meteorological Office (IMO) is situated where the Jökulsá á Sólheimasandi passes beneath the N1 road bridge (figure 3.4). Air temperature data (°C) is obtained from hourly intervals and used within this study to parameterise climate during sampling. Rainfall counts which were subsequently converted to mm amounts are obtained every 15 minutes from a TinyTag rainfall data logger situated on Jökulhaus, a large moraine ridge to the East of Sólheimajökull, 200m a.s.l (Carswell, 1963).

3.4. Monitoring of Proglacial waters to determine bulk meltwater characteristics

3.4.1. Sampling Locations

Meltwater sampling was carried out in Summer 2013 from the 4th July to 22nd July (Day of Year (DOY) 185-203) across the Sólheimajökull proglacial area. Monitoring of proglacial waters was undertaken across 18 sampling locations on the Eastern and Western margins of the proglacial lagoon, along the glacier snout where the ice makes contact with the lagoon and at locations along the Jökulsá á Sólheimasandi (figure 3.4). Glacier surface meltwaters were represented via sampling from transient supraglacial streams as well as water pools contained within closing crevasse depressions. In addition, external riverine inputs from Jökulsárgil and Fjallgilsá were monitored to constrain non-glacial inputs.

Principal lagoon sampling sites (where repeated monitoring took place) were established at the Upper and Middle Eastern Lagoon and the Middle Western Lagoon. In addition, two main riverine sites, namely the Mixed Zone and the Bridge, were also frequently monitored (see figure 3.4). Almost continuous (24 hour) time

series sampling took place at the Mixed Zone, a main location on the Jökulsá á Sólheimasandi downstream of the lagoon outlet, where proglacial waters have fully mixed. Samples taken here are considered to be representative of bulk outflow from the proglacial lagoon, including water from subglacial, supraglacial and external riverine (Jökulsárgil) inputs. From here, the Jökulsá á Sólheimasandi flows south of the glacier within a large channel constrained by steep sided banks consisting of moraine ridges and Jökulhlaup deposits. Eventually the main channel flows under the N1 road bridge approximately 4km from the glacier snout. Repeated monitoring of Jökulsárgil and Fjallgilsá was also undertaken to establish the characteristics of waters which do not derive from Sólheimajökull glacier. Fieldwork undertaken during Spring 2014 (28th April-17th May 2014) used the same sampling sites with the addition of subglacial upwelling samples and more extensive lagoon margin sampling to build upon findings of Summer 2013 (figure 3.5).
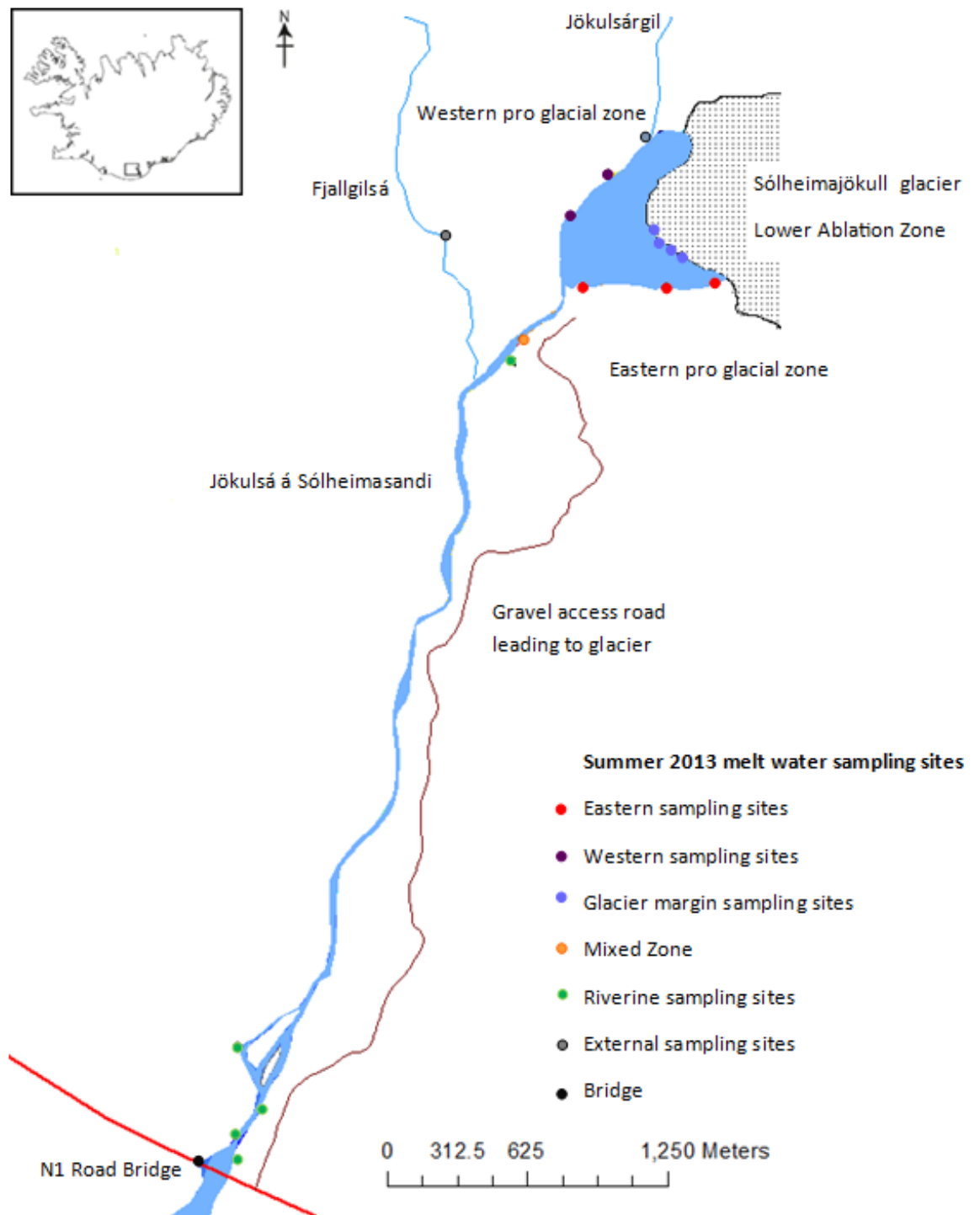
Figure 3.4: Map showing sampling sites established during Summer 2013 for

monitoring of proglacial meltwaters
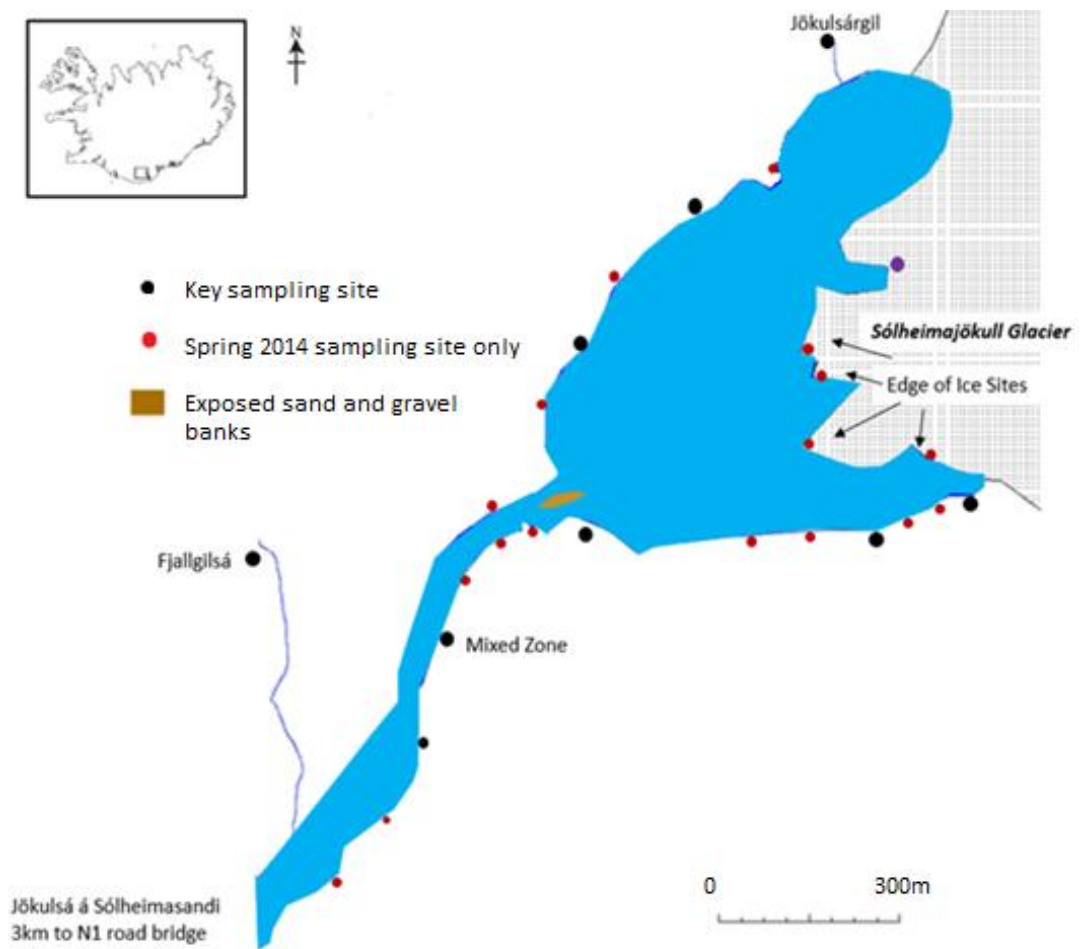
Figure 3.5: Map showing extensive sampling sites located across the proglacial lagoon during Spring 2014

3.4.2. Water stage

Water stage collected by the IMO at the N1 road bridge gauging station was used as a proxy for discharge, with variations in water stage reflecting changes in bulk meltwater output.

3.4.3. Determination of physical properties of bulk meltwaters

Electrical conductivity (EC), temperature and pH were determined in the field using a WTW 340i combination meter (Wissenschaftlich-Technische Werkstätten GmbH) compensated for temperature and calibrated daily for pH using buffers of pH 4 and 7. Secondary data from the IMO bridge hydrometric gauging site provided hourly EC measurements for the extended periods of 1st June to 31st August 2013 and 1st April to 31st May 2014.

3.4.4. Collection of Proglacial waters for chemical analysis

Water was collected from key sampling locations during Summer 2013 and Spring 2014 as outlined in figures 3.4 and 3.5. For analysis of major ions, trace metals, dissolved organic carbon and fluorescence, water was filtered upon collection to minimise further reaction with suspended sediments using 0.45 micron cellulose nitrate filters and a pre rinsed Nalgene filter unit and hand pump. Measurements of EC, pH and water temperature were recorded at the time of sampling. Waters for major ion and trace metal analysis were then transferred into 60ml pre rinsed Nalgene bottles and sealed without any air bubbles. Waters for DOC testing were placed into air tight 40ml amber borosilicate glass vials topped with foil to prevent contact with vial lids and seals. The remaining water was saved for bicarbonate titrations. Samples were then stored at cool temperature (4-8°C) (and darkness for DOC samples) before returning to the UK. Upon arrival in Lancaster these were then refrigerated at 4°C.

For testing dissolved inorganic carbon ^{13}C/^{12}C, samples of proglacial water (10ml) were directly drawn into a pre-rinsed syringe, filtered through an inline filter capsule of 0.45μm cellulose nitrate and injected into pre-evacuated and acidified (0.175 ml concentrated phosphoric acid) 12ml exetainers, leaving a 2ml headspace. Vials were then stored upside down to prevent ingress or egress of gases and transported back to the UK. Water samples to test D/H and ^{18}O/^{16}O ratios of H$_2$O were collected as unfiltered 8ml samples in Nalgene bottles pre-rinsed three times with water from the

44

sampling site. These were submerged and sealed below the water surface in order to avoid trapped air.

3.4.5. Dissolved oxygen testing in the field

Dissolved oxygen concentrations were measured in the field using a Winkler drop count titration method with reagents supplied by Hach. Water was collected in a clear 60ml glass container, rinsed 3 times with water from the sample site. Dissolved oxygen powder pillows (manganous sulphate and alkaline iodine-azide reagent) were added to the mixture and inverted several times. Sulfamic acid was added, leaving a residual brownish-yellowish hue if oxygen is present (figure 3.6). Titration with thiosulfate was used to provide dissolved oxygen concentration in mg/L.

Figure 3.6: In situ sampling for dissolved oxygen during Summer 2013. Photograph taken after addition of sulfamic acid

3.4.6. In Situ Bicarbonate analysis

Carbonate analysis was undertaken in the field by digital titration, using a Hach alkalinity test kit, model AL-DT. 25ml of pre filtered water was place into a cleaned flask and phenolphthalein indicator added. Bromcresol Green-Methyl red indicator was then added to produce a green coloured mixture. 0.16N sulphuric acid was titrated until the coloured solution changed to light pink representing the end point of the reaction. Total dissolved inorganic carbon (mg/l HCO_3^-) was calculated using the HACH digital multiplier of 0.4.

3.4.7. Collection of waters to monitor aqueous methane concentrations

Waters for aqueous methane analysis were collected in pre rinsed 1L clip lock clear plastic pots. Pots were filled with ~300ml of meltwater and sealed. A 5ml headspace sample was immediately withdrawn through a rubber septa and injected into a 3ml evacuated exetainer. Pots were then left in ambient air temperatures to allow the headspace to equilibrate with the meltwater sample. After approximately 24 hours, the headspace gas was withdrawn, comprising a 5 ml and a 20ml aliquot (stored in pre-evacuated 3ml and 12 ml exetainers) for concentration and isotopic determination respectively.

Figure 3.7: Aqueous methane sampling pots

3.5. Laboratory Analysis of Sólheimajökull proglacial waters

3.5.1. Isotopic Analysis of $\delta^{18}O$ and δD in water

Isotopic sampling of D/H and $^{18}O/\,^{16}O$ H_2O ratios was undertaken at the Stable Isotope Facility of Lancaster University using an Elementar Pyrocube elemental analyser configured to an Isoprime 100 mass spectrometer, similar to the methods of Wynn et al (2015). For D/H analyses aliquots of 0.3μL were injected and subsequently reduced to hydrogen over a chromium metal catalyst at a combustion temperature of 1050°C. For $\delta^{18}O$, analysis was undertaken in pyrolysis mode following injection of 0.4μL of sample over glassy carbon chips at a combustion temperature of 1450°C. Both D/H and $\delta^{18}O$ analyses were run in duplicate and corrected against lab calibration standards relative to V-SMOW. Analytical precisions were quoted as 0.3‰ for standards and 0.2‰ for actual samples with regards to $\delta^{18}O$ and 1‰ for both standards and samples for δD.

3.5.2. Analysis of major ion chemistry

Major anion testing was utilised to provide information on chloride, sulphate, nitrate and fluoride concentrations in Sólheimajökull proglacial meltwaters. Analysis was conducted using a Thermo Fischer Scientific Dionex ICS 2500 reagent free ion chromatography system based at Lancaster University. Data were calibrated against known lab standards where the limits of detection in mg/L (LOD) were 0.016, 0.002, 0.030 and 0.001 for fluoride, chloride, sulphate and nitrate respectively. Internal check standards and blanks were used to ensure quality control. All data are reported to within 5% of the internal standard values.

Inductively coupled plasma optical Emission spectroscopy (ICP-OES) analysis was conducted at Lancaster University using a Thermo Scientific iCAP 6000 series ICP spectrometer to test for major cations (Ca^{2+}, Mg^{2+}, K^+ and Na^+) and Silica in Sólheimajökull proglacial waters. Water samples were acidified with 0.1M HNO_3 in the original Nalgene collection bottle to desorb cations and trace metals from the

plastic sidewalls. Calibration against lab standards and internal reference materials allowed comparison between runs. Analytical precision within and between runs ranged from 0.01 to 0.05mg/L based on individual ion data. Trace metals were also analysed, however proved to be at the limit of detection and are therefore not reported in this thesis.

Major ions were not corrected for potential sea salt contribution, despite the close proximity of Sólheimajökull to the Atlantic Coastline. Na^+: Cl^- ratios for Sólheimajökull meltwaters (ranging from 1.56 (1SD=0.07) to 3.80 (1SD=0.34) in Spring 2014 and 2.45 (n=2) to 6.24 (1SD= 2.37) in Summer 2013) indicate large deviations from marine sources (ratio of 0.56 quoted by Wake, 1989). Given the unique situation of Sólheimajökull with connectivity to subglacial geothermal systems and previous evidence of injection of geothermal fluids, inappropriate marine aerosol correction could misrepresent sources of Na^+ and Cl^-. In addition, similar studies monitoring Sólheimajökull bulk meltwaters (Lawler et al., 1996) do not correct for a seasalt component. TDIC $\delta^{13}C$ values were obtained through analysis of exsolved headspace gases sampled via an Isoprime 100 isotope ratio mass spectrometer (refer to chapter 3.5.4.

3.5.3. Dissolved organic carbon analysis

Proglacial meltwater samples were collected during Summer 2013 and Spring 2014 and filtered using the methods outlined in section 3.3.4. Samples were then acidified prior to analysis to remove DIC content. Analysis of DOC in Summer 2013 proglacial waters was undertaken at the Institute for Biodiversity and Ecosystem Dynamics, based at the University of Amsterdam, Netherlands. This was achieved using a pre-market IsoTOC total organic carbon analyser adapted from the existing HTC TOC analyser VarioTOC Cube (Elementar Analysensyteme GmbH), interfaced to an Isoprime 100 IRMS, using methods outlined by Federherr et al. (2014). Proglacial waters were automatically injected into the combustion system using a 5ml syringe. Combustion was undertaken using a Platinum (Pt) catalyst on a ceramic carrier

material at a combustion temperature of 850°C with oxygen pulse. Water, hydrogen halides and halogens were removed before DOC concentration was quantified by a non-dispersive infrared detector (NDIR). Specifically designed separation of CO_2 and O_2 allowed for focussing and gas exchange ultimately resulting in determination of $\delta^{13}C_{DOC}$. Results were calibrated against lab standards and blanks. Attempts to analyse Spring proglacial waters for DOC concentration and $\delta^{13}C$ using similar methods at Isoprime House, Manchester were unsuccessful due to low DOC content.

Fluorescence of glacial waters was conducted using a Cary Eclipse Luminescence Spectrophotometer at the University of Birmingham. In line with techniques adopted by Wynn et al. (unpublished) samples were analysed at 20°C with a voltage of 900V. Results were standardised against a Raman spectra which was analysed before each batch of samples. Limited amounts of Humic and Fulvic-like substances were detected. However, in light of potential microbial degradation of fulvic-like fractions, analysis was limited to characterisation of humic-like substances from Summer 2013. This was normalised into humic-like fluorescence intensity per mgC by extracting humic like fluorescence intensity values from a window of emission and excitation wavelengths associated with humic like substances. Emission was typically between 400.75nm to 459.07nm, whilst excitation ranged from 15.77nm to 29.56nm. This was then corrected against DOC per mg C.

3.5.4. Dissolved inorganic carbon analysis

Where in field testing of inorganic carbon (TDIC) concentrations as outlined in chapter 3.4.6 was not possible, carbonate was estimated from charge balance equations. Balancing the ionic charge in equivalence units (generated via major ion analysis outlined in chapter 3.5.2) is based on the assumption that net charge of ions in a solution is 0. Therefore, providing all other major ions have been accurately measured the missing negative charge can be attributed to HCO_3^- (Hubbard and Glasser, 2005). Regression against field titrations demonstrated a line of best fit, which was used to estimate the carbonate content using the following equation:

Titration unit = gradient x calculated charge balance + intercept

<div align="right">(equation 10)</div>

This was then multiplied by the digital multiplier supplied by Hach (0.4) to give an estimated concentration of HCO_3^- in mg/L. Calculated values were found to be in keeping with known digital titrations.

For isotopic analysis of inorganic carbon exetainers containing headspace CO_2 exsolved from meltwater samples were analysed in the Lancaster University stable isotope facility for $\delta^{13}C_{DIC}$ using a multiflow prep line interfaced to an Isoprime 100 isotope ratio mass spectrometer in continuous flow mode. Results are expressed relative to VPDB following standardisation to international reference materials (LSVEC lithium carbonate and NBS 18 Calcite). Analytical precisions within runs were better than 0.14‰ and 0.10‰ and 2.16‰ and 2.23‰ between runs for LSVEC and NBS 18 respectively.

3.5.5. Analysis of aqueous methane concentrations

Methane concentrations were analysed using flame ionisation detection on a gas chromatograph situated in the Centre for Ecology and Hydrology (CEH) Lancaster. A three point calibration was obtained using standard gas mixtures of 1, 10 and 500ppm methane in air. Final aqueous concentrations were determined through Henry's Ideal Gas Law, whereby the amount of gas dissolved in a given solution is proportional to its partial pressure in the gas phase (Sander, 2015). The concentration of methane in water (C_{aq}) is related to the concentration of gas measured in the headspace (C_g) and the dimensionless Henry's Law solubility Constant (H^{CC}) through the following equation:

$$C_{aq} = C_g \times H^{CC}$$

<div align="right">*(Equation 11, taken from Sander, 2015)*</div>

For an ideal gas the dimensionless Henry's Law solubility constant (H^{CC}) is calculated using the following equation:

$$H^{CC} = H^{CP} \times RT$$

(Equation 12, taken from Sander, 2015)

Where R is Henry's gas constant (equivalent to 8.31Jmol^{-1} K^{-1}) and T is the temperature in Kelvin (K). The H^{CP} of methane at a standard temperature of 298K (25°C) is 0.000014 mol/m^3 Pa.

Solubility of gases increases with decreasing temperatures. Since glacial waters are at much lower temperatures, calculating the concentration of aqueous methane using the standard temperature of 298K would lead to significant underestimation of methane concentrations. Instead the Henry's Law solubility constants of H^{CP} and H^{CC} were recalculated for a temperature of 275.15K (0°C) based on the temperature dependence between the two, using 298K as a reference temperature. A derivative of the van 't Hoff equation was utilised taking into account the enthalpy of methane (internal energy in relation to pressure and volume, denoted by $\Delta_{sol}H$) which was quoted as 13,180J/mol (Naghibi et al., 1986). This was factored into equation 3 alongside a standard temperature (T^θ) of 298K and a desired temperature (T) of 273.15K and the Henry's gas constant (R) of 8.314 Jmol^{-1} K^{-1} as follows:

$$H\left(T\right) = H^\theta \times \exp\left(\frac{-\Delta solH}{R}\left(\frac{1}{T} - \frac{1}{T^\theta}\right)\right)$$

(Equation 13, taken from Sander, 2015)

This provided an adapted H^{CP} value which could be applied to equation 12 in order to recalculate H^{CC} for 273.15K. Aqueous methane concentrations were then calculated using equation 11 and converted to mg/L using the molar mass of methane (16.4g mol^{-1}).

3.5.6. Isotopic analysis of aqueous methane

Isotopic analysis for $\delta^{13}C_{CH4}$ was conducted at the Stable Isotope Facility based at CEH Lancaster, using a Gilson TraceGas preconcentrator linked to an Isoprime IRMS. Results were calibrated against reference gases (10, 100 and 500ppm methane in air). Due to low methane concentrations, supraglacial and external riverine samples were omitted from isotopic analysis. Precision of analysis for both samples and standards was better than 0.3‰. Isotopic analysis for δD was conducted at the UC Davies Stable Isotope Facility using a Thermo Scientific PreCon concentration system interfaced to a Thermo Scientific Delta V plus isotope ratio mass spectrometer. Reported isotopic values were calibrated against a pure reference gas standard with a known isotopic value of -157.0‰ with a standard deviation of 2.6‰. Only samples collected during the Spring 2014 field season were analysed for both $\delta^{13}C$ and δD.

3.6. Analysis of proglacial sediments at Sólheimajökull

3.6.1. Sediment collection

Extensive sediment sampling on the eastern proglacial forefield, glacier snout and a limited number of western forefield samples was undertaken during Summer 2013 to investigate soil organic carbon content and for isotopic analysis to identify potential carbon sources in proglacial sediments. In total, 50 samples were collected including 37 from a sampling grid between the proglacial forefield to the east of the lagoon and Jökulsa á Sólheimasandi, 10 from the glacier surface and 3 from the western proglacial area. The 10 on-glacier samples can be further divided into samples consisting of surficial ash (4 samples) and perceived subglacial sediments (6 samples). Glacier sampling sites were selected based on points of interest, with the

majority of sites situated on the lower glacier snout. Ashes were sampled from melt out cones, debris stripes and directly from a higher altitude band of exposed Katla 1918 ash. Clays were predominantly sampled from crevasse traces and thrust planes, where subglacial material had been squeezed up from the bed of the glacier by differential ice flow velocities as shown in image 3.9.

Figure 3.8: Debris Cone consisting of ash on the lower reaches of the Sólheimajökull glacier, Summer 2013

Figure 3.9: Subglacial sediments sampled from a crevasse during Summer 2013.

Angle is looking vertically down into the crevasse.

During spring 2014 supraglacial sediment sampling continued from crevasses and thrust planes in order to obtain additional subglacial clays. During this season larger amounts of sediment appeared to be present, likely linked to winter advance and cooler, drier conditions leading to less surface melt for eroding sediments away. These were stored in plastic 100ml bottles to better ensure preservation of moisture and ensure suitability for later incubation experiments.

Figure 3.10: Subglacial sediments sampled from a thrust plane on the Sólheimajökull glacier snout, Spring 2014

3.6.2. Static chamber methods to monitor proglacial methane flux

Static chamber methods were employed to test methane fluxes across the Sólheimajökull proglacial area during Summer 2013 and Spring 2014. Most sampling occurred on the eastern proglacial forefield due to accessibility. Two transects were studied as outlined in figure 3.12. The first a north to south transect was based on distance from the glacier in order to parameterise influence of changing sediment age on methane flux. The second was a west to east transect based on increasing distance from the proglacial lagoon aiming to parameterise the influence of changing moisture conditions on methane flux. One spot sample from the western proglacial forefield was also undertaken close to Fjallgilsá where vegetation cover was more extensive. Chambers measuring 10cm height by 15cm diameter were buried approximately 3cm into the soil leaving a headspace of 683.3cm^3 or 1.41L equivalent. Surrounding sediments were pushed against the chambers to ensure full closure from the atmosphere. Samples of 5ml were drawn off using a needle and syringe at

15 minute (for chambers operated for 45 minutes) and 45 minute (for long term 120 minute experiments) intervals through a butyl rubber septa and stored in 3ml pre-evacuated exetainers. Unless otherwise stated, three static chambers were deployed at each site (as shown in figure 3.11).

Figure 3.11: Static Chamber sampling adjacent to the proglacial lagoon Summer 2013
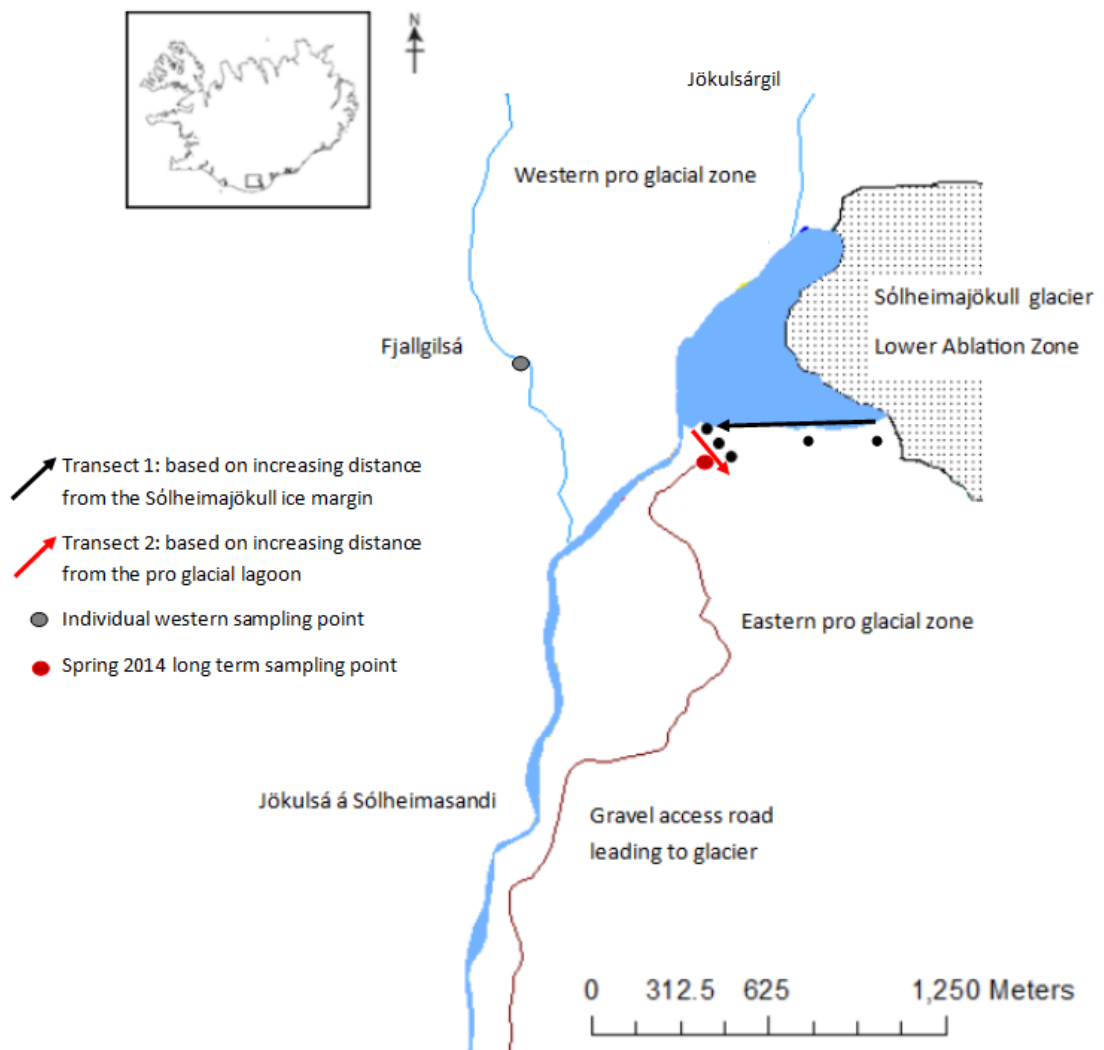
Figure 3.12: Map showing locations of static chamber sites Summer 2013.

Due to little change in the proglacial forefield, sites from transect 1 were also sampled during Spring 2014 alongside the addition of the red point which represents a long term individual sampling point. A total of 36 replicates were done during Summer 2013 whilst 10 replicates were sampled during Spring 2014

3.6.3. Laboratory analysis of proglacial sediments

Sediments collected from the proglacial area in Summer 2013 and Spring 2014 were tested for total carbon content in addition to δ^{13}C signature. Roughly 10g wet weight of sediment was placed into tin boats and air dried in a drying cabinet at approximately 30-40°C for 24 hours. These were then transferred into an agate pestle and mortar and ground to homogenise. The samples were then split into two. One portion was stored a in 1.5ml Eppendorf micro centrifuge tube awaiting weighing prior to sampling for total Carbon content. The second portion was acidified using 10% ultra-pure hydrochloric acid solution. These were subsequently rinsed, dried and stored in 1.5ml Eppendorf micro centrifuge tubes awaiting weighing for isotopic analysis.

Where field filtration of water samples yielded enough sediment on the filter papers, these were saved and processed for δ^{13}C analysis and %C content. Each filter paper was dried and the sediment removed prior to homogenisation and analysis. Filter papers were analysed as blanks to ensure no contamination occurred during sample processing.

3.6.4. Determination of total Carbon and δ^{13}C isotopic signatures of proglacial sediments

Proglacial sediments were tested on an Elementar Vario Micro Cube Elemental Analyser linked to a VisION prototype mass spectrometer at the University of Lancaster. Approximately 10mg of each sediment (Absolute mass of sediment was dependent upon percentage carbon content) was weighed into tin boats and placed into an auto sampler. Analysis was undertaken using catalytic combustion at a temperature of 1,200°C. Isotopic analysis of δ^{13}C was undertaken using a combined C/N mode with a zero dilution setting and a carbon trap set at 400. Samples were run in three batches and calibrated against known lab standards (corn and low carbon substrate) to provide consistency between runs. Internal precisions based on

calibration and reference materials was better than 0.15‰. The long term external precision (between runs) for the VisION is better than 0.19‰.

3.6.5. Sediment Incubations

3.6.5.1. Preliminary testing

Two types of sediment were visually identified during Spring 2014- light brown and grey. XRD analysis has shown almost identical chemical composition of these sediments, therefore colour was thought to represent iron oxidation state. The light grey sediment would be typically associated with Fe^{2+} under anoxic conditions and oxidized Fe^{3+} prevalent within the brown sediment.

Sediments collected from the glacier surface and proglacial forefield were incubated to test for the production/ consumption of methane. Preliminary testing of various incubation conditions (temperature, headspace, substrate, and slurry) took place prior to the main investigation to determine a suitable sampling technique, as outlined in table 3.1.

Sediments Tested	Headspace Conditions Tested	Temperatures Tested	Saturation Tested
Subglacial sediment collected Summer 2013 Fe^{2+} enriched grey subglacial sediment collected Spring 2014 Fe^{3+} enriched brown subglacial sediment collected Spring 2014 Eastern glacier forefield sediment collected Spring 2014	N_2 headspace (methanogenesis) CH_4 enriched headspace (methanotrophy) Compressed air (ambient)	4°C 15°C	Slurry Non slurry

Table 3.1: Parameters tested during preliminary incubation experiments

Field sediments were added to 100ml Wheaton bottles, slurried with de-ionised water, sealed using rubber septa caps and incubated at set temperatures. Headspace gases were added prior to sealing the incubation chambers to investigate either methanogenesis (headspace gas = N_2), or methanotrophy (headspace gas = CH_4). Sample extraction by syringe at set time intervals enabled rates of production/consumption to be monitored respectively. Initial incubations revealed limited microbial methanogenesis/ methanotrophy at 4°C, regardless of headspace composition or substrate type. At 15°C Grey Fe^{2+} slurried substrate demonstrated evidence of methanogenesis under an N_2 headspace, whilst under a methane enriched atmosphere, brown Fe^{3+} slurried sediments exhibited methanotrophy. These constitute the range finder experiments outlined in Appendix 4.

Figure 3.12: Example of slurried wheatons used for inclubation experiments

3.6.5.2. Testing for Methanogenesis

Fe^{2+} enriched grey subglacial sediment was allocated for methanogenesis testing using the laboratory facilities at CEH Lancaster. Approximately 5g wet weight of glacial sediment A was placed into a 100ml autoclaved clear glass Wheaton jar and slurried with 20ml of deionised water, which had been flushed with nitrogen.

Wheatons were then also flushed with nitrogen for 2 minutes before being immediately sealed with a butyl rubber stopper and crimp cap. An additional 20ml of nitrogen was added to each Wheaton to establish a positive pressure. A control experiment was set up under the same conditions, but without the addition of any sediment. Samples were then placed on a gyratory shaker and incubated in the dark at 15°C for 49 days. 1ml headspace concentrations were measured immediately after closure using GC analysis then at regular intervals, initially this was every 7 days for the first 21 days then every 14 days for the remainder of the sample period.

3.6.5.3. Testing for Methanotrophy

Approximately 10g wet weight of the Fe^{3+} enriched brown subglacial sediment was placed into a 100ml autoclaved clear glass Wheaton Jar and slurried with 20ml of deionised water. Wheatons were flushed with compressed air for two minutes before being immediately closed and sealed with a butyl rubber stopper and crimp cap. Additional methane was added to the headspace after closure to create a 150ppm methane enriched headspace. Alongside this a control experiment was created. This followed the same steps although no sediment was added. Samples were then placed on a gyratory shaker and incubated in the dark at 15°C for 167 hours. A 1ml sample was immediately withdrawn from each Wheaton and analysed for methane concentration by GC analysis. In addition to each sample removed for determination of methane concentration, an isotopic sample was extracted and injected into a pre evacuated 3ml exetainer. Sampling of methane concentration and $\delta^{13}C$ CH_4 isotopes then continued over regular time intervals for 7 days.

Samples for $\delta^{13}C$ CH_4 analysis were taken from Wheatons one, three and four (control) and tested at the CEH Lancaster Stable Isotope Facility using a TraceGas preconcentrator linked to an Isoprime IRMS as outlined in section 3.4.6. Measurements of $\delta^{13}C$ CH_4 proved consistent between incubation chambers, therefore the remaining samples from Wheaton two were tested for δD CH_4 at UC Davies, California. This was undertaken using a Thermo Scientific PreCon

concentration system interfaced to a Thermo Scientific Delta V plus IRMS also

discussed in chapter 3.5.6.

4. Outlining the Sólheimajökull System: Hydrology, Meterology and Run-off Characteristics

4.1. Introduction to glacial hydrology

Glacial hydrology refers to the passage of meltwater via three distinct pathways: supraglacial, englacial and subglacial, before emergence in the proglacial zone. Variability in drainage configuration is dictated by glacier type (temperate, polar or polythermal) and seasonality. Generalised models of glacial drainage applicable to temperate glaciers, suggest highest bulk meltwater flows during summer, accompanied by near cessation during winter, forming a reverse hydrograph. The majority of this bulk meltwater is comprised of 'quick flow' and 'delayed flow' components. Quick flow comprises relatively dilute supraglacial meltwaters, which route efficiently through moulins and crevasses and rapidly exit the glacier via englacial or subglacial channels. In contrast, delayed flow consists of solute rich waters sourced from supraglacial and subglacial melt, conveyed slowly through subglacial cavity drainage. Spatial and temporal variations in these modes of subglacial drainage constitute a classical drainage theory, whereby delayed cavity hydrology thought to dominate the accumulation season is superseded by rapid channelized drainage during periods of increased ablation. Due to changing rock: water contact this typically results in an inverse relationship between chemistry and discharge. From this, classical glacier hydrogeochemistry is born.

However, the Icelandic glacial drainage system exhibits differences from this classical model, due to year round low altitude ablation and the influence of subglacial geothermal activity. The Icelandic Institute of Earth Sciences have documented low level ablation from ablation stakes positioned 200m and 220m a.s.l. on the Sólheimajökull snout since Spring 2013. Over this time Summer ablation rates of 7-9m have been recorded, in addition to ~3m of ablation during the winter. This year-round ablation provides sufficient meltwater to maintain continual glacial discharge. Furthermore, previous investigation of bulk meltwater discharge and solute load

highlights a seasonal maxima in geothermal constituents coincident with summer season drainage (Lawler et al., 1996; Wynn et al., 2015). Physical and chemical characteristics of bulk meltwaters exiting the Sólheimajökull catchment are presented to develop an understanding of the hydro-geochemical dynamics at this unique location. This then serves as a platform on which subsequent chapters build an understanding of the glacial carbon cycle. Methods utilised to obtain meterological data are outlined in section 3.3, whilst collection and analysis of meltwaters can be found in section 3.4.

4.2. Results of physical and chemical analyses

4.2.1. Annual glacier run-off characteristics

Secondary data of uncalibrated relative water stage, absolute water temperature, air temperature and EC was obtained at hourly intervals from a hydrometric gauging station operated by the Icelandic Meteorological Office (IMO) where the Jökulsa á Sólheimasandi passes beneath the N1 road bridge. Here bulkmeltwaters represent a culmination of water from a variety of sources. Glacial sources from both the surface and base of the glacier and external waters from Jökulsárgil discharge into a large proglacial lake. This is drained by the Jökulsa á Sólheimasandi, with inputs from Fjallgilsá 4km downstream from Sólheimajökull (as shown in figures 3.4 and 3.5 chapter 3.3.1 (sampling site locations)). Estimation of river discharge has proved problematic due to poor results from salt dilution gauging and accessibility issues prevented using the velocity-surface area technique. The IMO Bridge gauging station uses pressure sensors to monitor water stage. This has been used as an estimate of seasonal differences in river discharge. Whilst this does not take into account deepening of the river bed during periods of high flow, or braiding of waters in multiple channels observed during summer, it can offer a best estimate of changes in discharge in the main channel and relationships to other meltwater characteristics.

Bulk meltwaters for the period September 2012 to September 2014 reflect a seasonal fluctuation between increased water stageduring summer and lower water stage observed during winter months (as shown in figure 4.1, below). A notable feature of annual hydrology at Sólheimajökull is continual discharge during the winter with no seasonal cessation of meltwater production. In keeping with this, greater water stage was observed during Summer sampling with values ranging from 414.5cm to 454.14cm and an average of 433.77cm (1SD= 10.54). Spring early ablation season water stages are reduced ranging from 384.30cm to 411.59cm with an average of 394.85cm (1SD= 5.69).
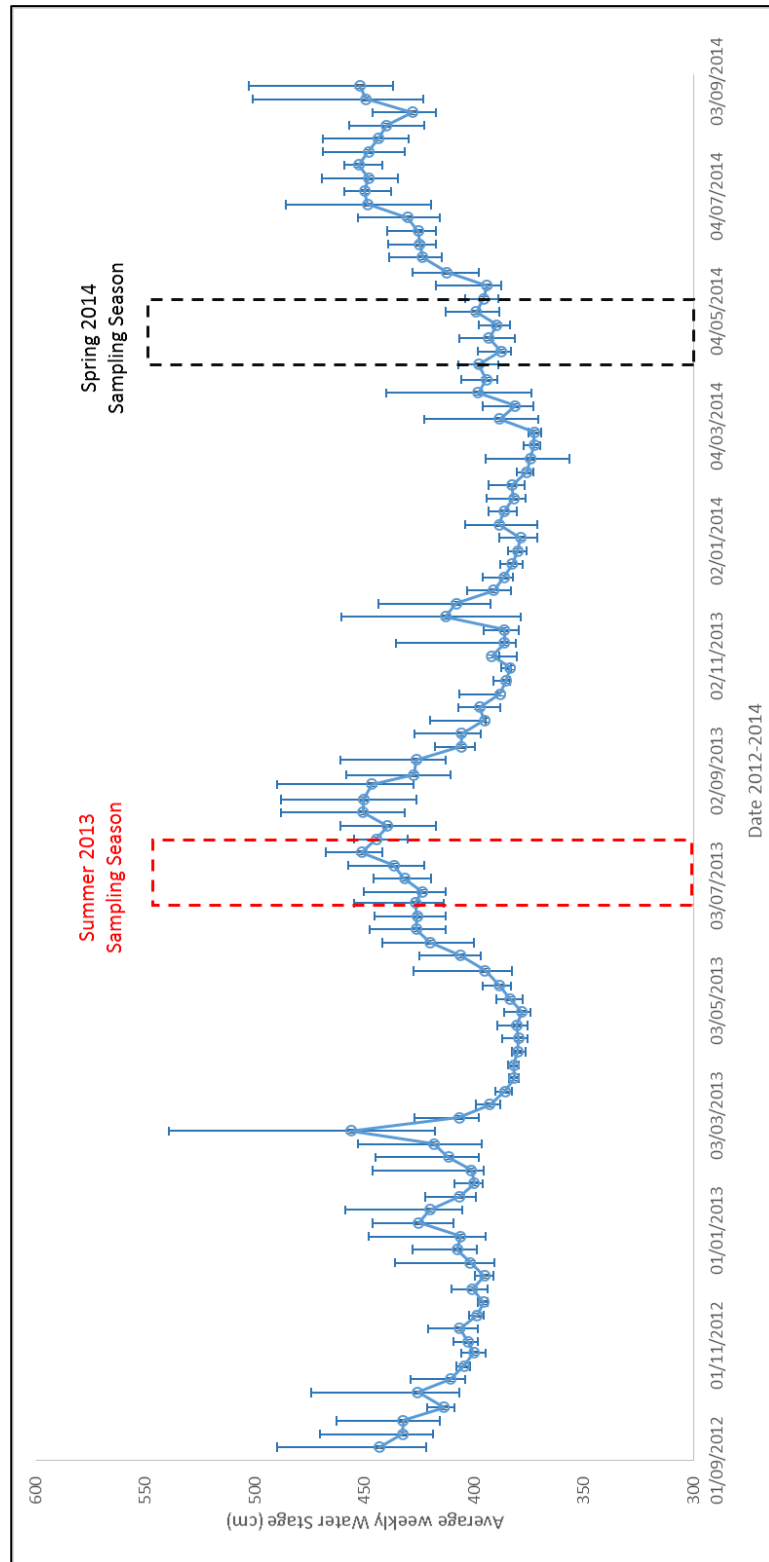
Figure 4.1: Average water stage based on weekly data collected at the Icelandic Meteorological Office Bridge Gauging Station from September 2012 to September 2014

Error bars represent weekly maximum and minimum values.

4.2.2. Meteorological Conditions

Monthly air temperatures and total rainfall at Sólheimajökull are presented in figure 4.2. Annual air temperatures based on recordings taken from the IMO bridge gauging station range from -12.19°C to 19.81°C with an average of 5.96°C (1SD= 3.41). Total precipitation over this period was 2705mm (excluding April where data was unavailable). Highest average monthly air temperatures were recorded in July with an average of 11.78°C (Minimum= 5.91°C; Maximum= 19.81°C). Rainfall exhibited a distinct peak in August with a total of 587.3mm. Lowest rainfall occured in February with 52.9mm recorded.
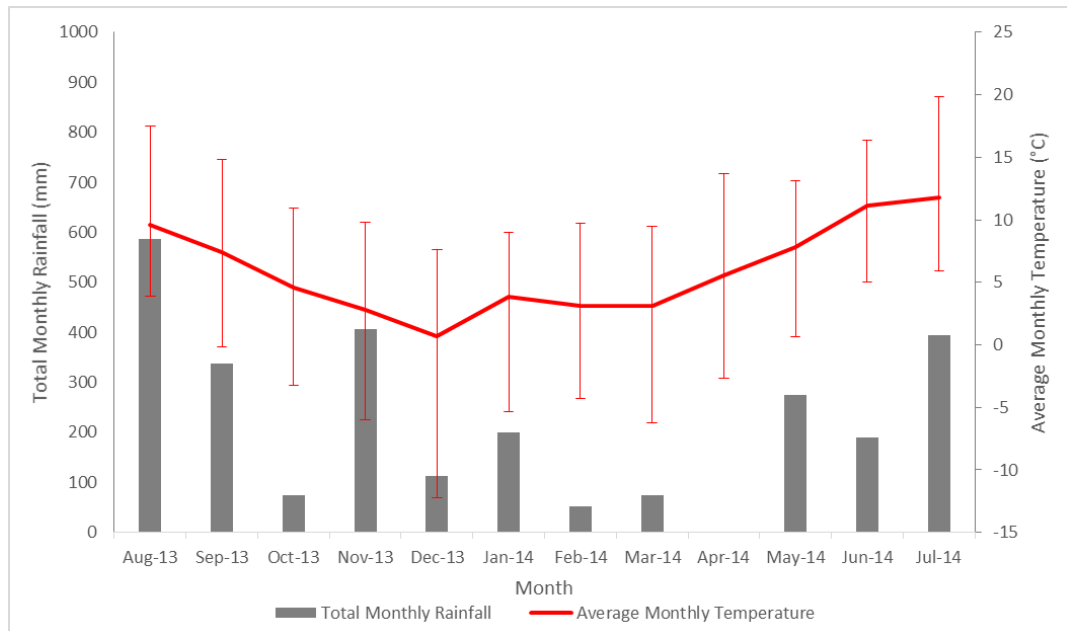
Figure 4.2: Annual monthly rainfall and average temperatures from August 2013 to July 2014 (excluding rainfall data for April 2014)

Error Bars depict maximum and minimum values

Figures 4.3 and 4.4 present temperature and rainfall data from Summer and Spring study periods respectively. Increased air temperatures and precipitation were noted during Summer with peak air temperatures of 13.39°C and precipitation up to 34.7mm over a 24 hour period. During Spring conditions were relatively cooler and

drier. Temperatures ranged from 3.32°C to 9.11°C whilst precipitation was minimal, with peak values of 18.2mm.
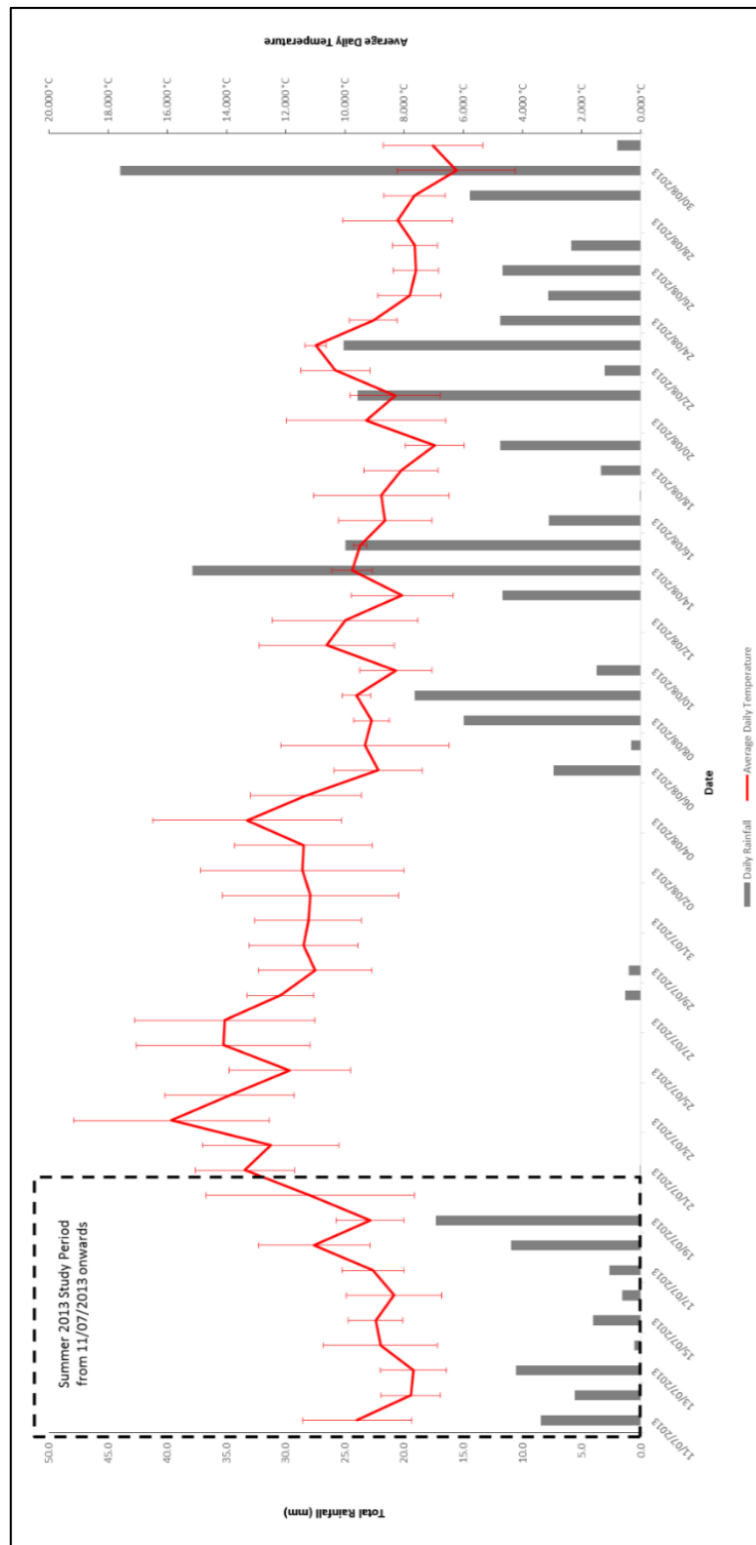
Figure 4.3: Average daily temperature and total rainfall for Summer 2013

Error bars depict daily maximum and minimum values
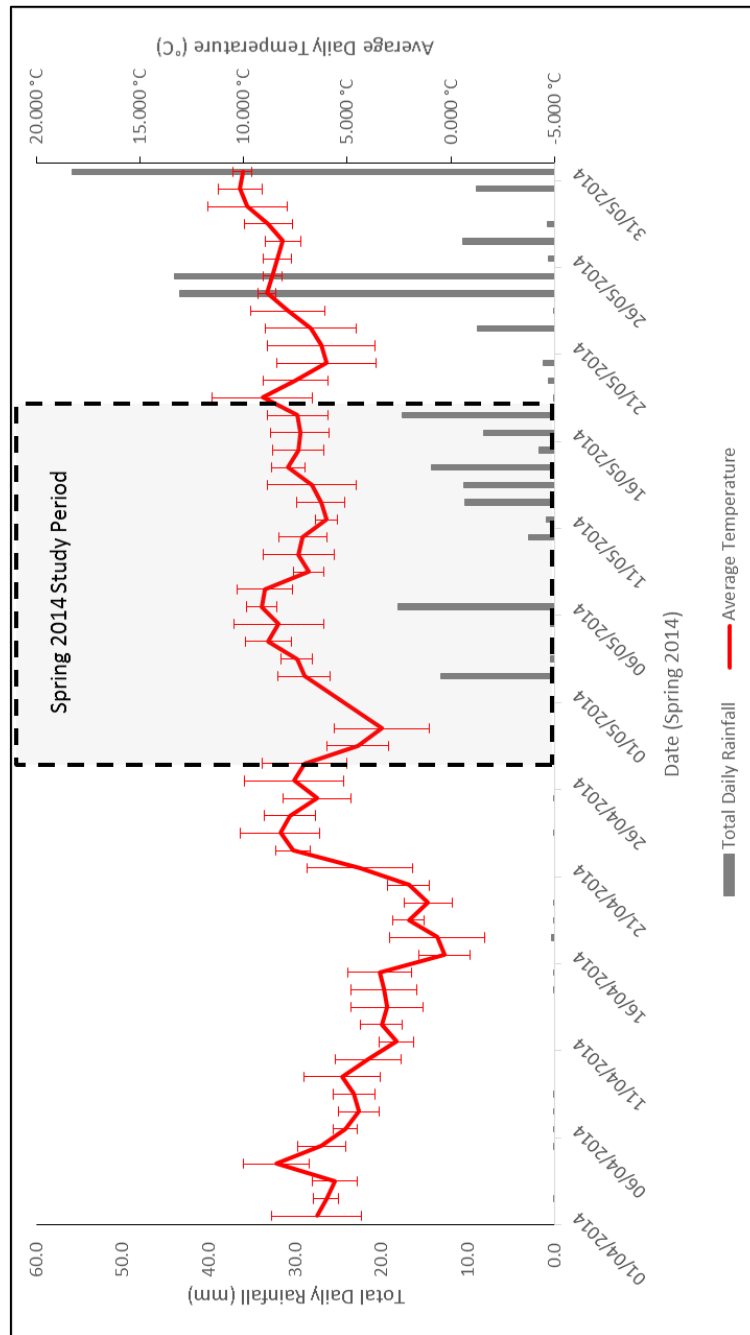
Figure 4.4: Average daily temperature and rainfall for Spring 2014

Error bars depict daily maximum and minimum values

Prevailing meteorological conditions are a driving force for proglacial discharge. Icelandic glacier melt is thought to be highly correlated to air temperature and sea surface temperature (Jóhannesson et al., 2007). Furthermore, 20% of Icelandic precipitation falls over glacial regions, meaning this could also play a role in hydro-glacial dynamics. Precipitation and temperatures are shown to be higher in the South of Iceland, therefore the southerly coastal location of Sólheimajökull provides close linkages between mass balance and climate, ultimately influencing the rate and timing of discharge exiting the catchment. Time series data from Spring 2014 revealed synchronicity between air temperature and average daily water stage, after lag of 1-2 days is accounted for (figure 4.5) as exhibited by a positive linear R^2 relationship of 0.40 (figure 4.6).
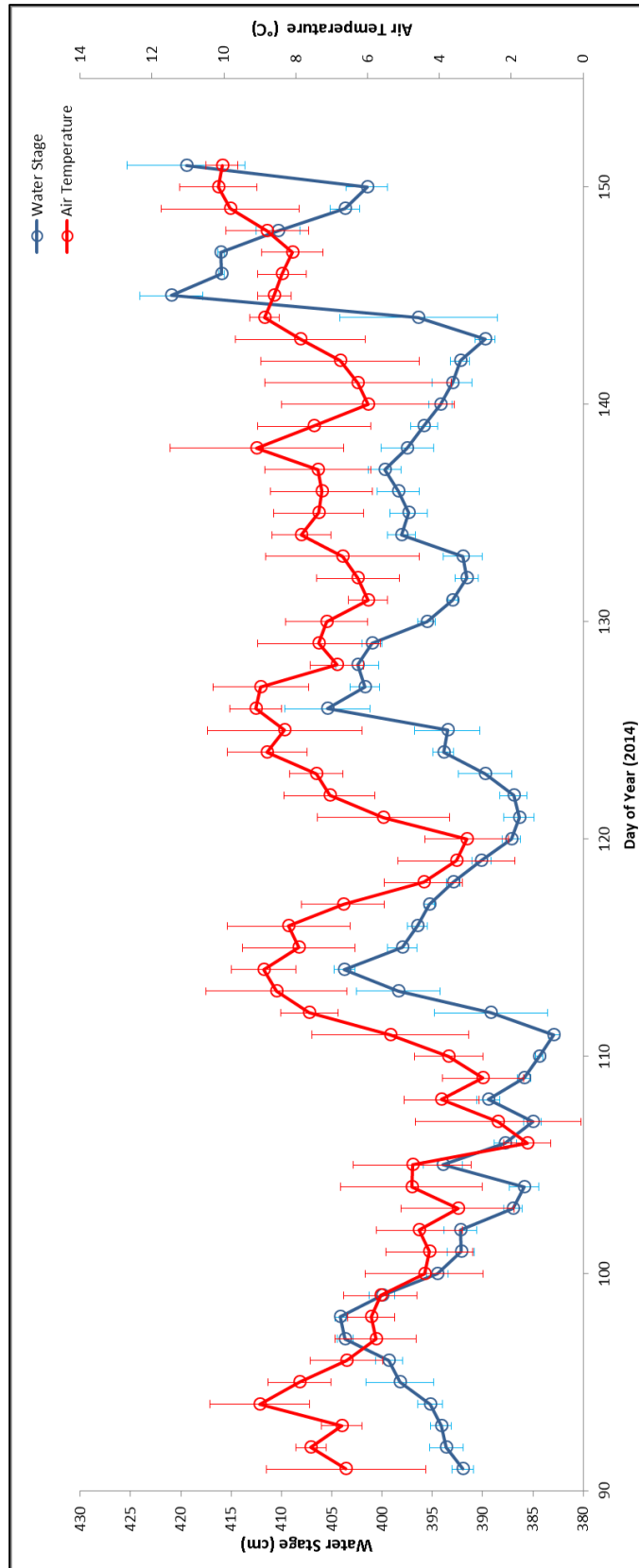
Figure 4.5: Air temperature and water stage during Spring 2014

Error bars depict daily maximum and minimum values
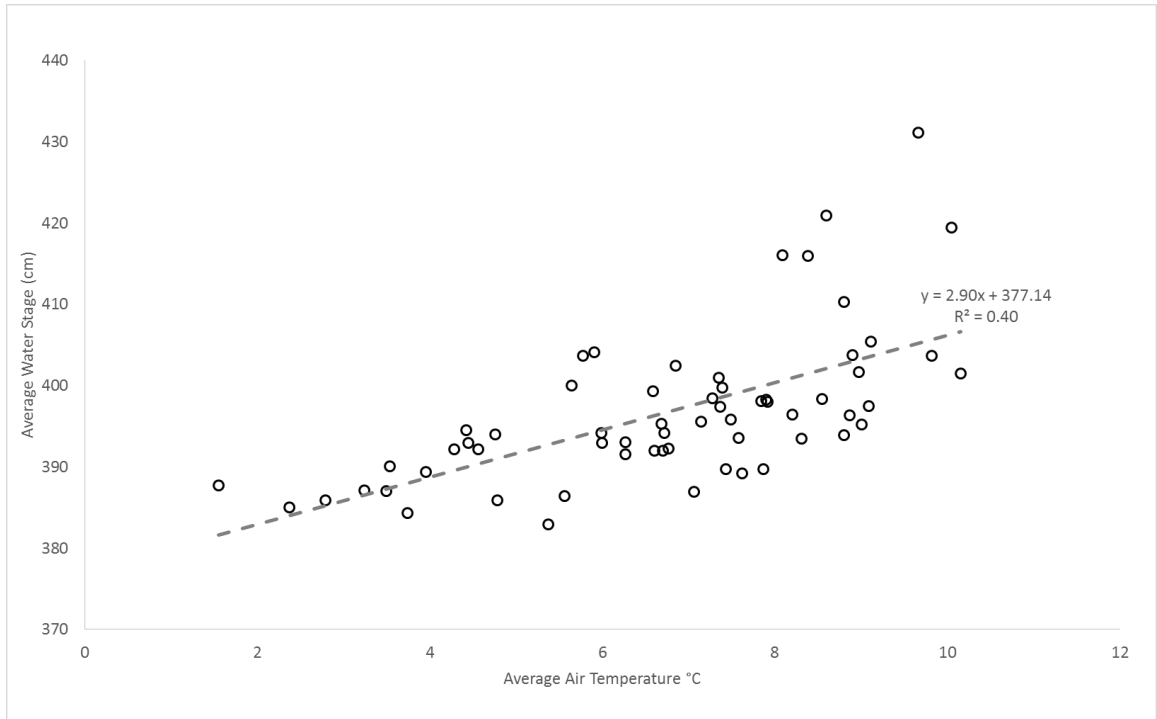
Figure 4.6: Bi-plot of air temperature and water stage during Spring 2014

During Summer, relationships between average daily temperature and water stage are not as strong as indicated in figures 4.7 and 4.8 with an R^2 value of 0.04. This is potentially indicative of other factors such as subglacial meltwater discharge influencing summer bulk meltwater output.
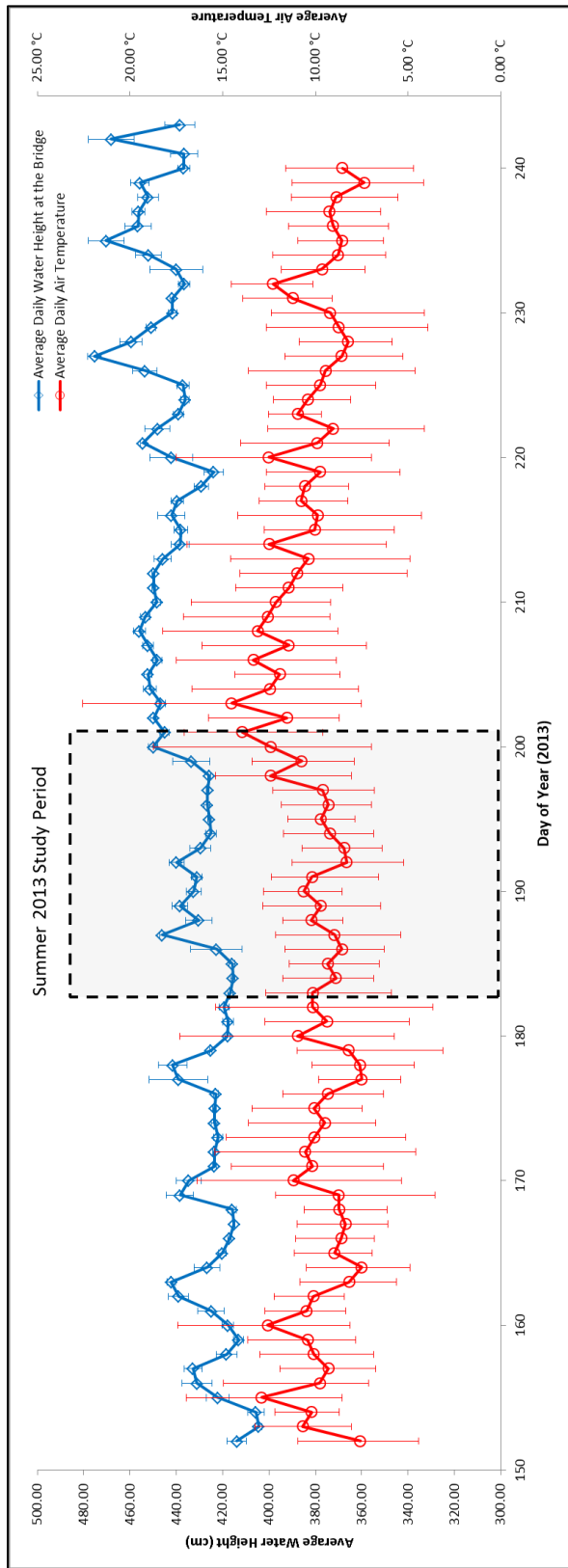
Figure 4.7: Air temperature and water stage during Summer 2013

Error bars depict daily minimum and maximum values
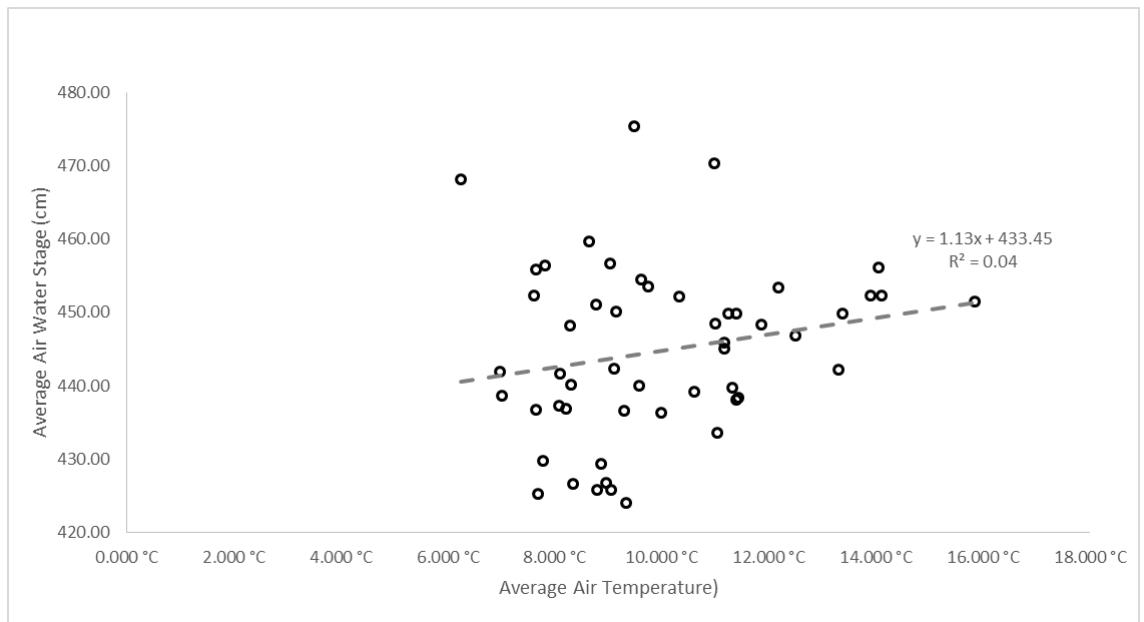
Figure 4.8: Bi-plot of air temperature and water stage during Summer 2013

Energy balance modelling at Sólheimajökull has identified incoming shortwave radiation as a key energy source, with lesser amounts attributable to turbulent fluxes and precipitation (Thompson, Unpublished Maters Thesis). A study undertaken during the balance year of 2014-2015, indicates that precipitation adds yearly averages of 2.1% and 1.9% to the overall energy balance at Sólheimajökull for elevations of 211 and 219m respectively (Thompson, Unpublished Masters Thesis). This is mostly through generation of enhanced surface ice melt linked to heat fluxes, reduction in albedo and changes to surface roughness caused by rainfall. Spring is characterised by prevalence of drier conditions, however (as indicated in figure 4.9) during Summer, increased frequency of peak rainfall events periodically influences water stage.
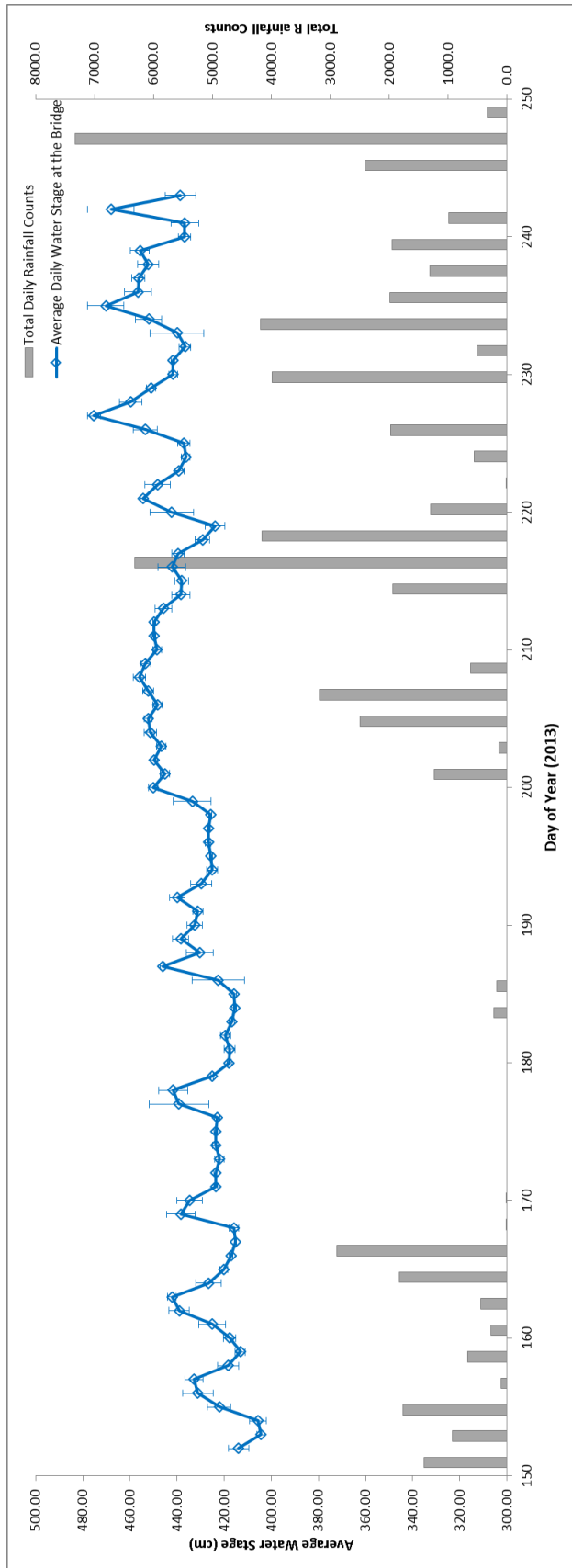
Figure 4.9: Time series of Summer 2013 total daily rainfall and average daily water stage.

Error bars depict daily maximum and minimum water stage

4.2.3. Water Temperature

Seasonal fluctuations in water temperature were linked to the variable influence of water sources and changes in air temperature. Subglacial and supraglacial waters form two main water sources from Sólheimajökull. In addition, a third source from riverine inputs of external catchment origin (Jökulsárgil and Fjallgilsá) deliver waters independent of Sólheimajökull. Each source occupied a unique temperature range with subglacial upwellings displaying the lowest average temperatures of 0.00 °C (1SD= 0.08) and extra glacial inputs being relatively warmer, reaching maximum upper values of 5.20°C in Jökulsárgil during Spring and 5.80°C in Fjallgilsá during Summer. An East/West split was evident across the proglacial lagoon, with lowest average Spring temperatures observed across the Eastern Lagoon and highest average temperatures prevailing at Western sites. During Summer, this was reversed with cooler average temperatures at Western sites. This temperature pattern within the proglacial lake likely reflected the variable influence of subglacial discharge and water from Jökulsárgil, both of which dominated the western side of the lake and which vary in importance between the summer/spring seasons.

	Average Water Temperature (°C) 1 standard deviation (1SD) in parentheses	
Site	**Spring 2014**	**Summer 2013**
Mixed Zone	**2.83** *(1.34)* Min= 1.50 Max= 5.60 *n=17*	**1.19** *(0.31)* Min= 0.70 Max= 2.00 *n=13*
Bridge	**3.43** (0.78) Min= 2.80 Max=4.3 *n=7*	**2.55** (0.56) Min= 1.90 Max= 3.20 *n=4*
Subglacial upwellings	**0.00** *(0.08)* Min= -0.10 Max= 0.10 *n=6*	**Not Sampled**
Eastern Lagoon	**1.14** (0.73) Min= 0.20 Max= 2.60 *n=20*	**2.53** (0.21) Min= 2.30 Max =2.80 *n=3*
Western Lagoon	**3.32** (1.40) Min= 1.80 Max= 6.10 *n=6*	**1.68** (1.01) Min= 0.70 Max= 4.4 *n=13*
Edge of Ice Sites	**0.75** (0.65) Min= 0.1 Max= 2.4 *n=11*	**1.42** (0.36) Min= 1.00 Max= 1.80 *n=5*
Supraglacial sites	**2.15** (...) Min= 0.10 Max= 4.20 *n=2*	**0.30** *(0.17)* Min= 0.10 Max= 0.50 *n=5*
Fjallgilsá	**3.80** *(0.85)* Min= 3.20 Max= 5.00 *n=3*	**4.95** (...) Min= 4.1 Max= 5.80 *n=2*
Jökulsárgil	**4.17** *(0.76)* Min= 3.40 Max= 5.20 *n=3*	**3.20** (...) Min= 3.20 Max= 4.30 *n=2*

Table 4.1: Average water temperatures across the Sólheimajökull catchment

4.2.4. Spatial pH distribution.

Table 4.2 reflects the average variability in pH between water sources at Sólheimajökull. Lowest springtime pH values were found in waters emanating from subglacial sources, ranging from 6.30 to 6.98, with an average of 6.66 (1SD= 0.25). In contrast, highest average pH values were found in Jökulsárgil waters, with average values of 7.91 (1SD= 0.13) and 7.75 (n=2) for spring and summer respectively. In addition, Supraglacial and external catchment waters from Fjallgilsá also exhibited

amongst the highest average pH values at Sólheimajökull, with little seasonal change. Mixed Zone values demonstrated seasonal fluctuations in pH with average values of 7.31 (1SD= 0.38) and 6.52 (1SD= 0.16) for Spring and Summer respectively. During Spring variability in pH was greater with values ranging from 6.89 to 8.51.

| Site | Average pH | |
| | 1 standard deviation (1SD) in parentheses | |
Site	Spring 2014	Summer 2013
Mixed Zone	**7.31** *(0.38)* Min= 6.89 Max= 8.51 *n=18*	**6.52** *(0.16)* Min= 6.32 Max= 6.85 *n=13*
Bridge	**7.57** (0.11) Min= 7.44 Max= 7.70 *n=7*	**6.97** (0.14) Min=6.77 Max= 7.15 *n=4*
Subglacial upwellings	**6.66** *(0.25)* Min= 6.30 Max= 6.98 *n=6*	**Not Sampled**
Eastern Lagoon	**7.55** (0.59) Min= 5.84 Max= 8.55 *n=20*	**6.76** (0.31) Min= 6.28 Max= 7.40 *n=13*
Western Lagoon	**7.18** (0.26) Min= 6.89 Max= 7.77 *n=6*	**6.75** (0.27) Min= 6.51 Max= 7.13*n=3*
Edge of Ice Sites	**7.35** (0.57) Min= 6.35 Max= 8.65 *n=12*	**6.73** (0.32) Min= 6.21 Max=7.15 *n=5*
Supraglacial sites	**7.51** *(…)* Min= 7.22Max= 7.80 *n=2*	**7.54** *(0.47)* Min= 6.87 Max= 8.32 *n=10*
Fjallgilsá	**7.26** *(0.48)* Min= 6.68 Max= 7.86 *n=3*	**7.41** *(…)* Min= 7.20 Max= 7.62 *n=2*
Jökulsárgil	**7.91** *(0.13)* Min= 7.74 Max= 8.05 *n=3*	**7.75***(…)* Min= 7.67 Max= 7.82 *n=2*

Table 4.2: pH values across the Sólheimajökull catchment

Spatial variability in meltwater pH is illustrated through figures 4.10 and 4.11. During Spring 2014 lowest pH values were associated with the influence of subglacial upwelling water, as well as localised areas along the glacier snout. In addition to this,

low pH values were also evident at the Lower Eastern Lagoon where pH values range from 5.84 to 7.18 (average of 6.67, 1SD= 0.50 n=4). Areas of higher pH values were found close to inputs from Jökulsárgil and at the Upper Eastern Lagoon linked to supraglacial run off. During Summer 2013 reduced pH values prevailed across the proglacial lagoon. Areas of lowest pH, below 6.5 were found at a localised point along the glacier margin and around the lagoon outlet. Localised increases are associated with inputs from Jökulsárgil and potential areas of surface run off along the ice margin.
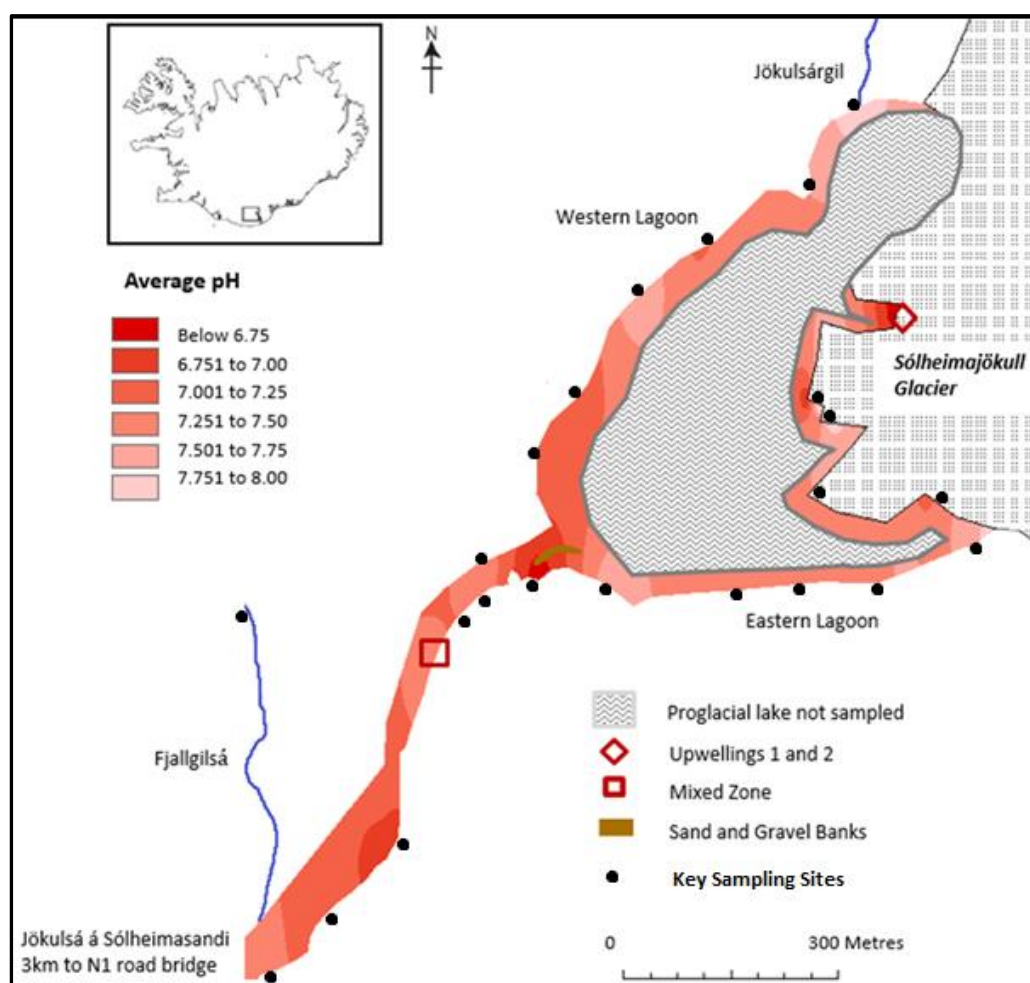
Figure 4.10: Map of pH distribution across the Sólheimajökull proglacial lagoon Spring 2014.

Lagoon and Riverine spatial distribution shown encompasses data averaged from 116 pH measurements taken across 22 sampling locations (excluding Fjallgilsá) between DOY 119-137 (2014)
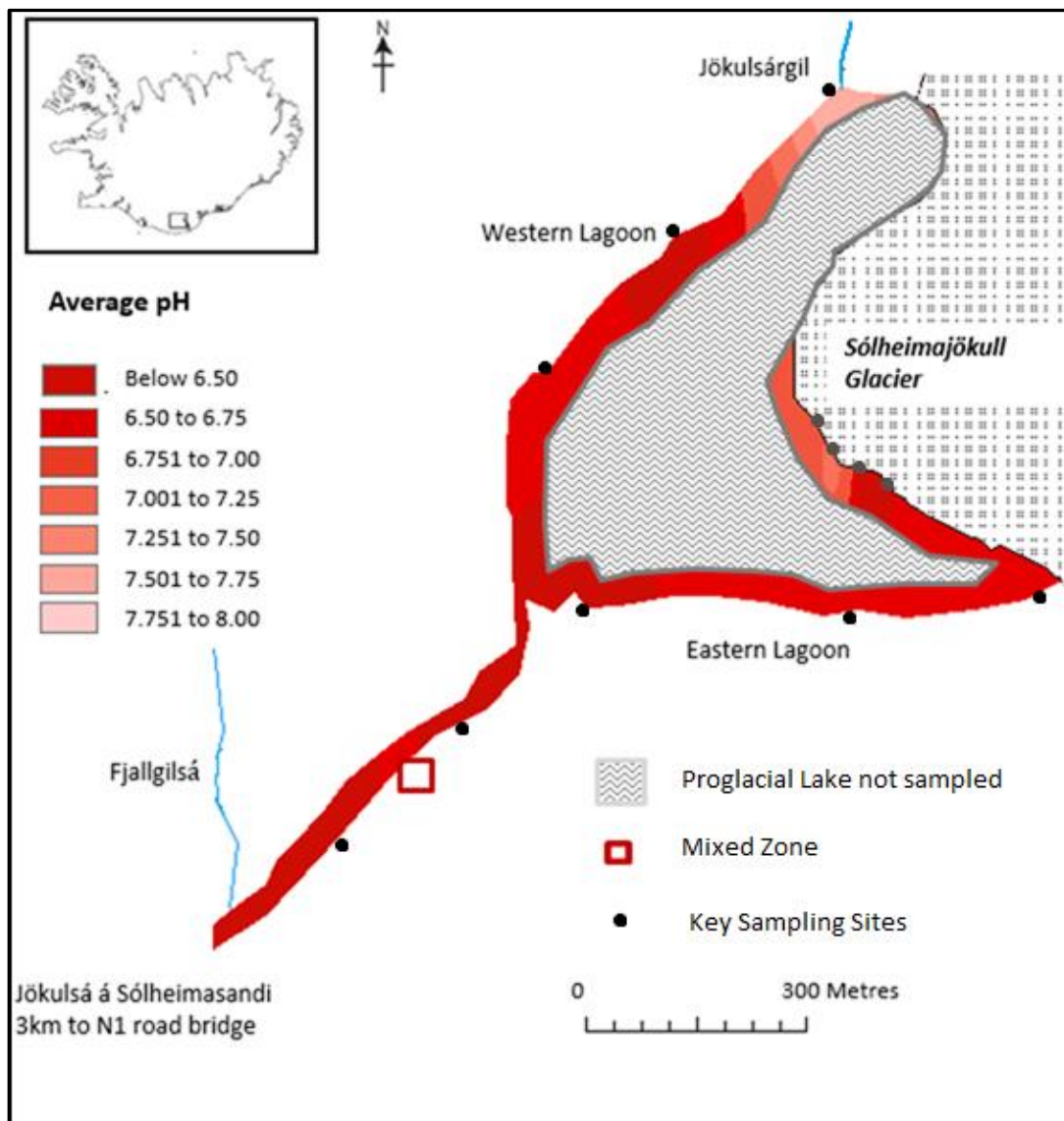
Figure 4.11: Map of pH distribution across the Sólheimajökull proglacial lagoon

Summer 2013

Lagoon and Riverine spatial distribution shown encompasses data averaged from 37

pH measurements taken across 13 sampling locations between DOY 185-203 (2013)

4.2.5. Electrical Conductivity Characteristics

Electrical Conductivity (EC) is widely used as a surrogate for Total Dissolved Solids giving a rough measure of total cations/anions. Waters emanating from subglacial upwellings exhibited the greatest EC values ranging from 122μS/cm to 166 μS/cm, with an average of 145 μS/cm (1SD=17.27). Lowest EC values for both seasons were found in supraglacial samples with averages of 8 μS/cm (n=2) and 7 μS/cm (1SD=7.17) for Spring and Summer respectively. Seasonal variation was evident at the Mixed zone, where lower EC values were associated with summer sampling. Similar trends also occured in Jökulsárgil and Fjallgilsá waters. Supraglacial waters showed consistency in EC values regardless of season.

| | Average Electrical Conductivity μS/cm | |
	1 standard deviation (1SD) in parentheses	
Site	**Spring 2014**	**Summer 2013**
Mixed Zone	**134** *(14.24)* Min= 108 Max= 153 *n=18*	**107** *(17.05)* Min= 80 Max= 135 *n=13*
Bridge	**126** *(11.46)* Min= 106 Max= 138 *n=7*	**96** *(11.28)* Min= 85 Max= 114 *n=4*
Subglacial upwellings	**145** *(17.27)* Min= 122 Max= 166 *n=6*	**Not Sampled**
Eastern Lagoon	**98** *(27.05)* Min= 53 Max= 165 *n=20*	**66** *(40.30)* Min= 14 Max= 129 *n=12*
Western Lagoon	**138** *(15.90)* Min= 110 Max= 157 *n=6*	**112** *(11.00)* Min= 97 Max= 122 *n=3*
Edge of Ice Sites	**107** *(37.08)* Min= 31 Max= 150 *n=13*	**69** *(22.50)* Min= 36 Max= 93 *n=5*
Supraglacial sites	**8** *(…)* Min= 4 Max= 11 *n=2*	**7** *(7.17)* Min= 2 Max= 22 *n=10*
Fjallgilsá	**74** *(6.68)* Min= 67 Max= 83 *n=3*	**42** *(…)* Min= 38 Max= 45 *n=2*
Jökulsárgil	**106** *(8.29)* Min= 97 Max= 117 *n=3*	**66** *(…)* Min= 52 Max= 79 *n=2*

Table 4.3: Electrical conductivity across the Sólheimajökull catchment

Figure 4.12 depicts EC distribution across the Sólheimajökull proglacial lagoon during Spring sampling. Highest EC values were associated with close proximity to subglacial water sources. This revealed an East/West split in lagoon values, whereby western lagoon sites exhibited greater EC values. Localised areas of low EC were found close to the glacier snout proximal to the discharge of supraglacial streams into the lake. As indicated in figure 4.13 EC decreased during Summer. Similarly, there was an East/

West split with highest EC values at Western Lagoon sites and prevailing low EC at the Upper Eastern Lagoon. EC was predominantly low along the glacier ice margin.
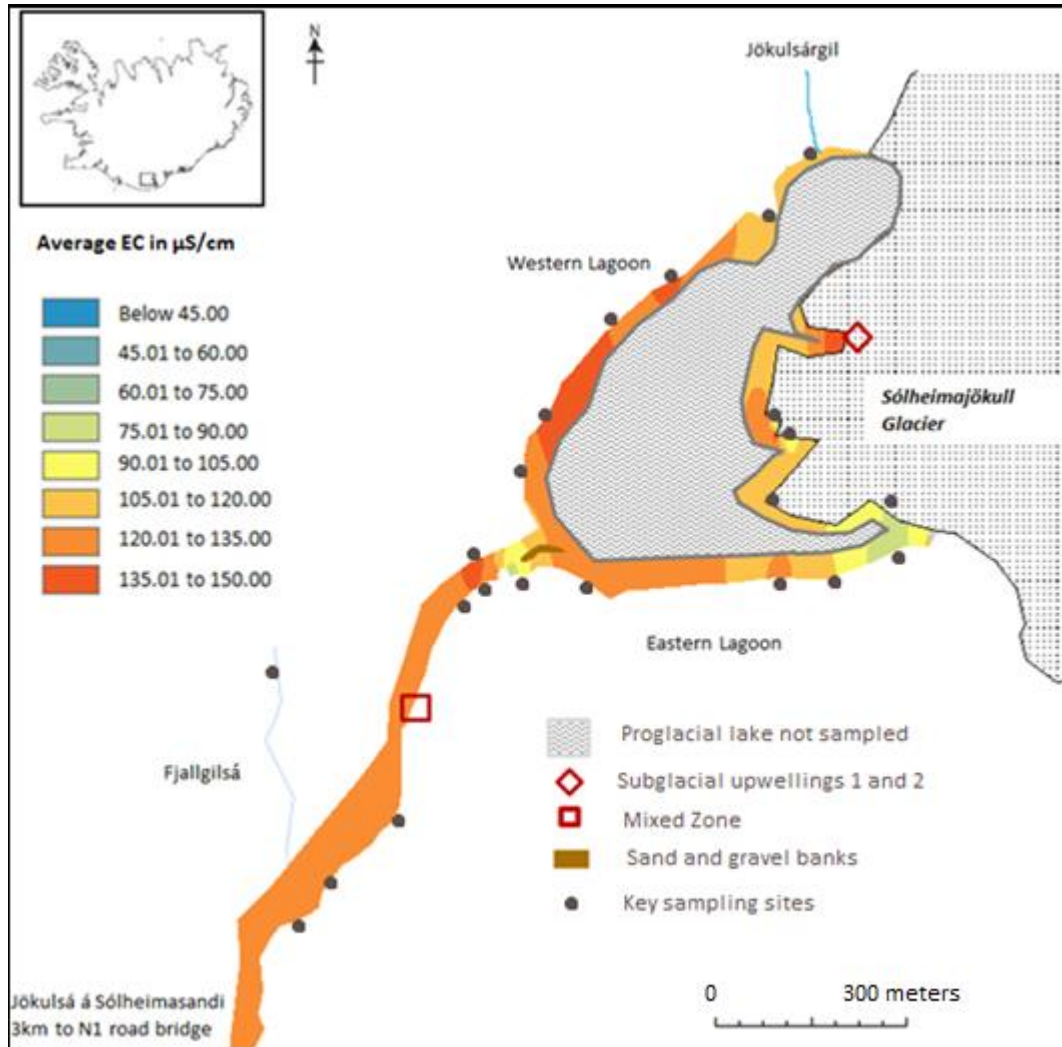
Figure 4.12: Map of EC distribution across the Sólheimajökull proglacial lagoon Spring 2014

Lagoon and Riverine spatial distribution shown encompasses data averaged from 116 EC measurements taken across 22 sampling locations (excluding Fjallgilsá) between DOY 119-137 (2014)
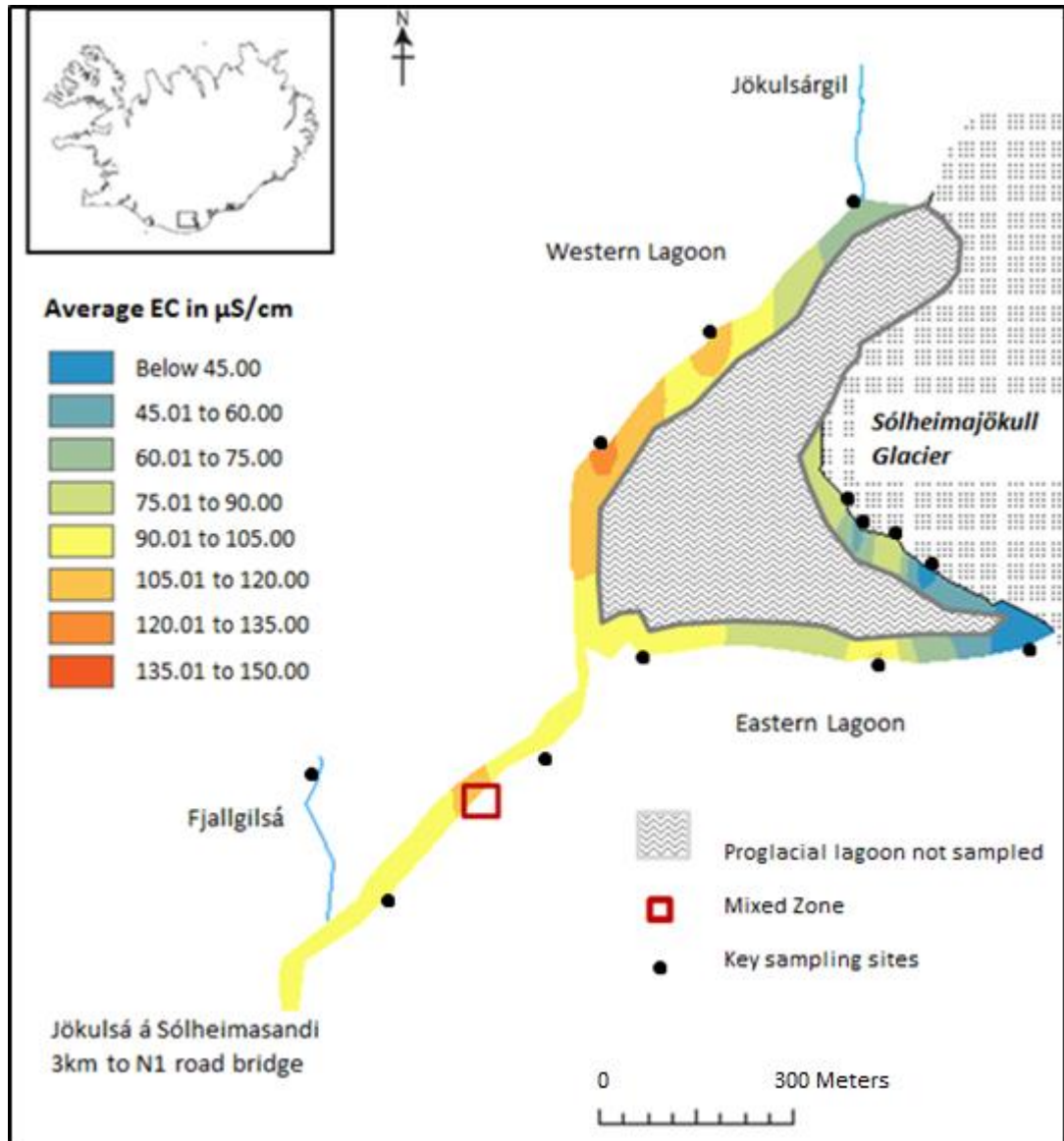
Figure 4.13: Map of EC distribution across the Sólheimajökull proglacial lagoon Summer 2013

Lagoon and riverine spatial distribution shown encompasses data averaged from 37 EC measurements taken across 13 sampling locations (excluding Fjallgilsá) between DOY 185-203 (2013)

Discharge is a potential factor influencing EC via dilution effects. Figures 4.14 and 4.15 present time series of average daily water stage from the IMO Bridge gauging station alongside EC values recorded at the Mixed zone. During Spring an inverse pattern existed with high EC concentrations corresponding to periods of relatively lower water stage. A bi-plot of average water stage and EC (figure 4.16) supports this displaying a negative non linear relationship with an R^2 value of 0.59.

This negative relationship between EC and discharge persisted throughout the summer season, albeit demonstrating a weaker relationship (R^2 = 0.43 as shown in figure 4.17) than in Spring.
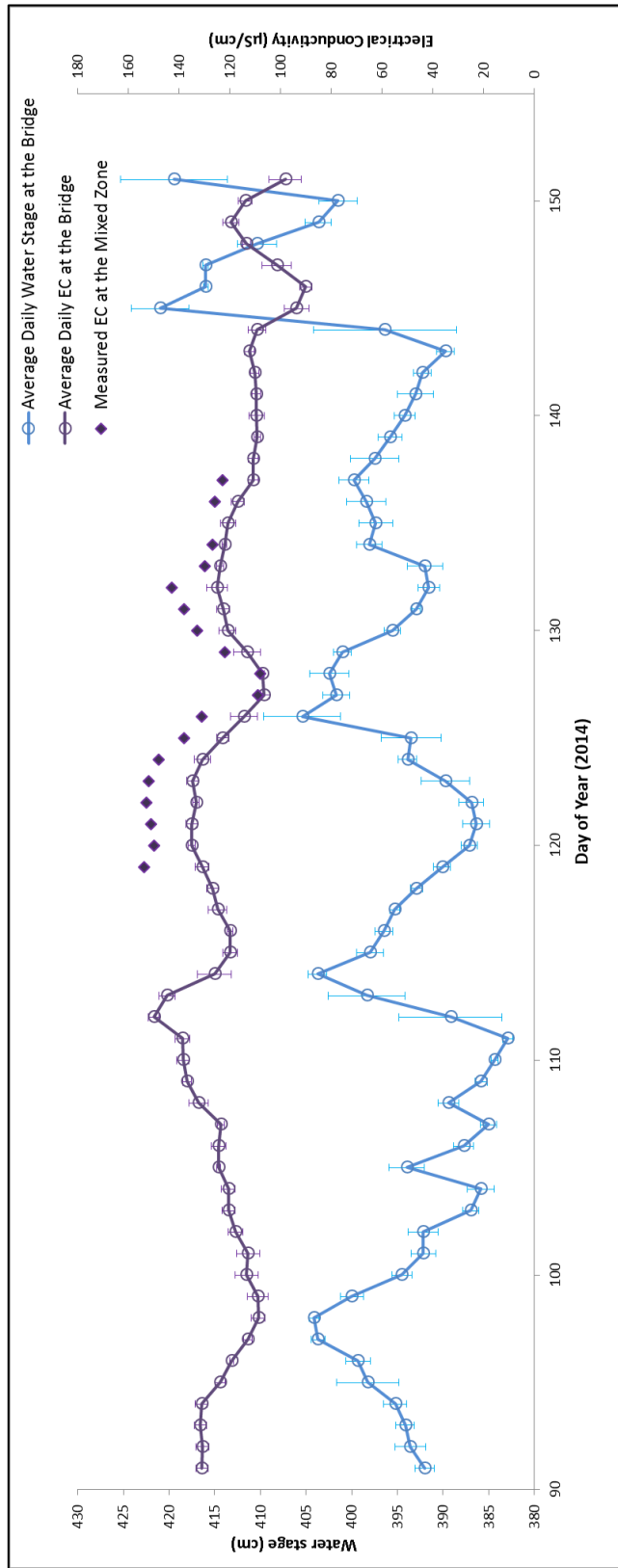
Figure 4.14: Time series of average water stage and EC during Spring 2014
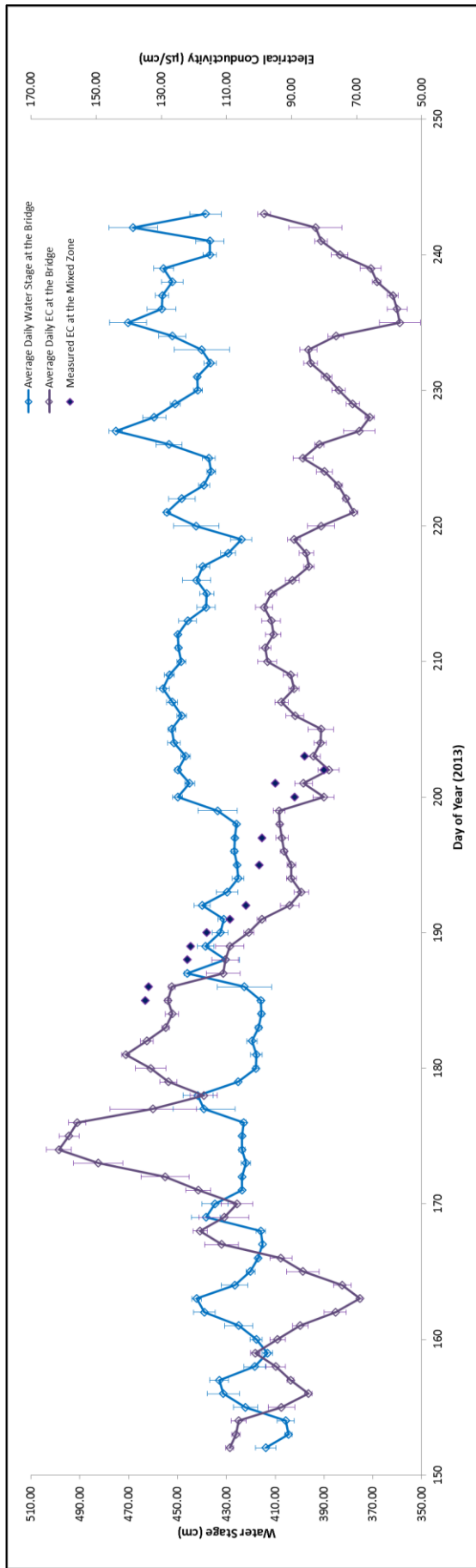
Figure 4.15: Time series of average water stage and EC during Summer 2013
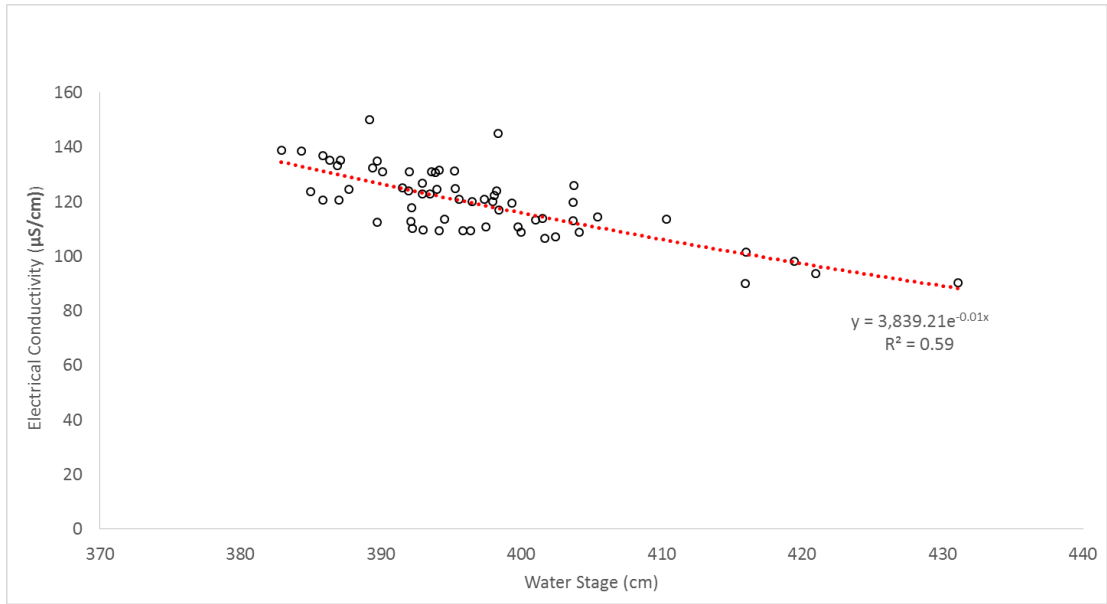
Figure 4.16: Bi-plot of average water stage and EC during Spring 2014
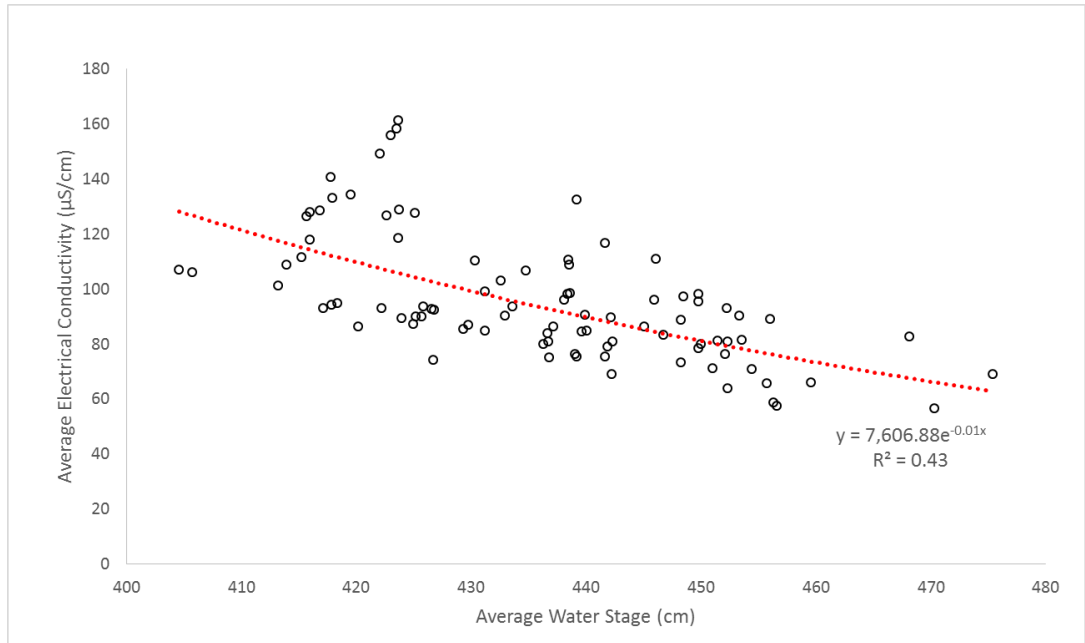
Figure 4.17: Bi-plot of average water stage and EC during Summer 2013

4.3. Geochemical Parameters

Hydro-glaciology provides physical observations of bulk meltwater characteristics from small scale daily fluctuations to seasonal and annual trends. However, physical observation is not sufficient in addressing origins of bulk meltwater run off. Classical geochemistry linked to ion abundance and isotopic analyses ($\delta^{18}O$ and δD of H_2O) can offer greater insight into contrasting water sources and their importance to bulk meltwater outflow (Fairchild et al., 1999). The measure of EC reflects a rough estimate of total dissolved solids. Rivers in glaciated catchments usually contain high concentrations of dissolved ions and suspended sediments. These are traditionally obtained from mechanical weathering at the bed, aerosol deposition at the surface and in the unique case of Sólheimajökull, dissolved into meltwater as it passes close to geothermal vents. Quick flow waters are ionically dilute whilst delayed flow and waters routed extensively through the subglacial realm are chemically enriched (refer to chapter 2.5.1). Therefore, consideration of major ion chemistry can help constrain variability of water sources at Sólheimajökull.

4.3.1. Major Ion Chemistry of Water Sources at Sólheimajökull

4.3.1.1. Subglacial waters

In line with elevated EC measurements, subglacial upwellings monitored during spring 2014 provided a concentrated, high abundance ion source (as indicated in appendix 2). Relative cation and Si abundances were as follows: $Na^+ > Ca^{2+} > Si > Mg^{2+} > K^+$, with observed concentrations ranging from 581.49 µmol (1SD= 56.04) to 30.93 µmol (1SD= 2.01) n=6 for Na^+ and K^+ respectively. This exceeded cation concentrations observed for supraglacial and external riverine waters, indicating cation acquisition from the subglacial realm. Heightened anion concentrations were also evident, with relative abundances of $HCO_3^- > Cl^- > SO_4^{2-} > F^- > NO_3^-$, ranging from 1048.89 µmol (1SD= 145.47) to 0.56 µmol (1SD= 0.72) for HCO_3^- and NO_3^- respectively. In addition to this low dissolved oxygen concentrations (5 and 6mg/L for

upwellings 1 and 2 respectively) indicated ion acquisition in a sub-oxic or potentially anoxic (low oxygen) weathering environment.

4.3.1.2. Supraglacial waters

Supraglacial waters provide a relatively dilute source component. Spring Supraglacial cation and Si concentrations were in the order: Ca^{2+} >Na^+ >Mg^{2+} >K^+>Si whilst anions demonstrated relative abundances of HCO_3^- >Cl^- >F^- > SO_4^{2-} >NO_3^-. Summer supraglacial samples were obtained from three notable sources: free flowing supraglacial streams situated at low altitudes on the glacier snout; stagnant supraglacial meltwater pools also located on the glacier snout and a larger high altitude stream flowing out from Katla 1918 ash deposits with a murky brown appearance. Highest cation concentrations during summer were associated with stagnant pooling water, whilst the lowest concentrations were found in free flowing supraglacial sites across the glacier snout. Across all supraglacial sampling sites, HCO_3^- was shown to be the dominant anion with NO_3^- and F^- demonstrating the lowest abundances. For more information refer to appendix 2.

4.3.1.3. Waters of external catchment origin

Jökulsárgil and Fjallgilsá deliver waters independent of the Sólheimajökull glacier and therefore geochemistry reflects this. Seasonal consistency of most relative cation and anion abundances prevailed in both rivers, despite reduced summer ionic concentrations.

Cation and Si concentrations for Jökulsárgil were Na^+ >Ca^{2+} >Si>Mg^{2+} >K^+ for both Spring and Summer (as outlined in appendix 2). The dominance of Na^+ in Jökulsárgil waters was particularly evident during Spring where high values (535.42 µmol) account for 66% of the total base cations. Relative anion concentrations were in the order: HCO_3^- >Cl^-> SO_4^{2-}>F^->NO_3^-. Anion concentrations were dominated by HCO_3^- and Cl- which constituted ~97% of the total bulk anion load in Spring and Summer.

SO_4^{2-} demonstrated little seasonal change with values of 10.58 µmol (1SD=2.17) and 13.66 µmol in Spring and Summer respectively.

Relative cation and Si concentrations for Fjallgilsá were: $Na^+ > Si > Mg^{2+} > Ca^{2+} > K^+$. Large Spring quantities of Na^+ compared to other ions accounted for 62% of the total base cation load in Spring and 60.76% in Summer. Relative Anion concentrations were $HCO_3^- > Cl^- > SO_4^{2-} > F^- > NO_3^-$. HCO_3^- was the dominant anion in Spring and Summer with values of 386.78µmol and 224.25µmol respectively. Cl was also present in large amounts, with average Spring values of 205.73 (1SD= 10.47) being the highest Cl concentrations across the Sólheimajökull proglacial area. Seasonality was reflected by lower summertime anion concentrations, with the exception of SO_4^{2-} which displays peak values during Summer.

4.3.1.4. Mixed Zone

Mixed Zone values represent the bulk outflow from the Sólheimajökull proglacial lagoon. This is a combination of subglacial, supraglacial and Jökulsárgil waters which are well mixed upon exiting the lagoon. Mixed Zone relative cation and Si abundances for both Spring and Summer were as follows: $Na^+ > Ca^{2+} > Si > Mg^{2+} > K^+$. Na^+ was the dominant cation with average values of 561.32 µmol (1SD= 49.49) and 424.23 µmol (1SD= 84.88) for Spring and Summer respectively. Dominance of Na^+ over both seasons aligned with high absolute Na^+ abundances found in subglacial waters, and could not be accounted for by Na^+ concentrations in supraglacial run off or inputs from Jökulsárgil. K^+ was almost continuous over both seasons with average concentrations of 29.98µmol (1SD= 2.49) and 26.48µmol (1SD= 5.06) for Spring and Summer respectively (refer to appendix 2). Relative anion abundances for both seasons are $HCO_3^- > Cl^- > SO_4^{2-} > F^- > NO_3^-$. HCO_3^- was the dominant anion for both Spring and Summer with average concentrations of 892.07 µmol (1SD= 103.18) and 642.52 µmol (1SD= 108.11). Again, higher concentrations were in line with elevated levels found in subglacial waters. Seasonality was reflected by lower summertime

concentrations of major anions, with the exception of SO_4^{2-}, which demonstrated peak values during summer almost 3 times the values observed during Spring.

4.4. Water isotopic analyses of oxygen and deuterium

Isotopic ratios of D/H and $^{18}O/^{16}O$ can offer further insight into water source. During Spring 2014 isotopic data for proglacial sampling sites were plotted alongside δD and δ^{18}O values from the Global Meteoric Water Line (GMWL) and Local Meteoric Water Line (LMWL) taken from Reykjavik. Subglacial upwellings were shown to plot at the lighter end of the isotopic spectrum displayed, with δ^{18}O values below -9.3‰ and δD values below -65‰. In contrast, supraglacial waters displayed a heavier isotopic range above -9.0‰. Proglacial waters mainly plotted between the two end members suggesting a mixing of water sources.
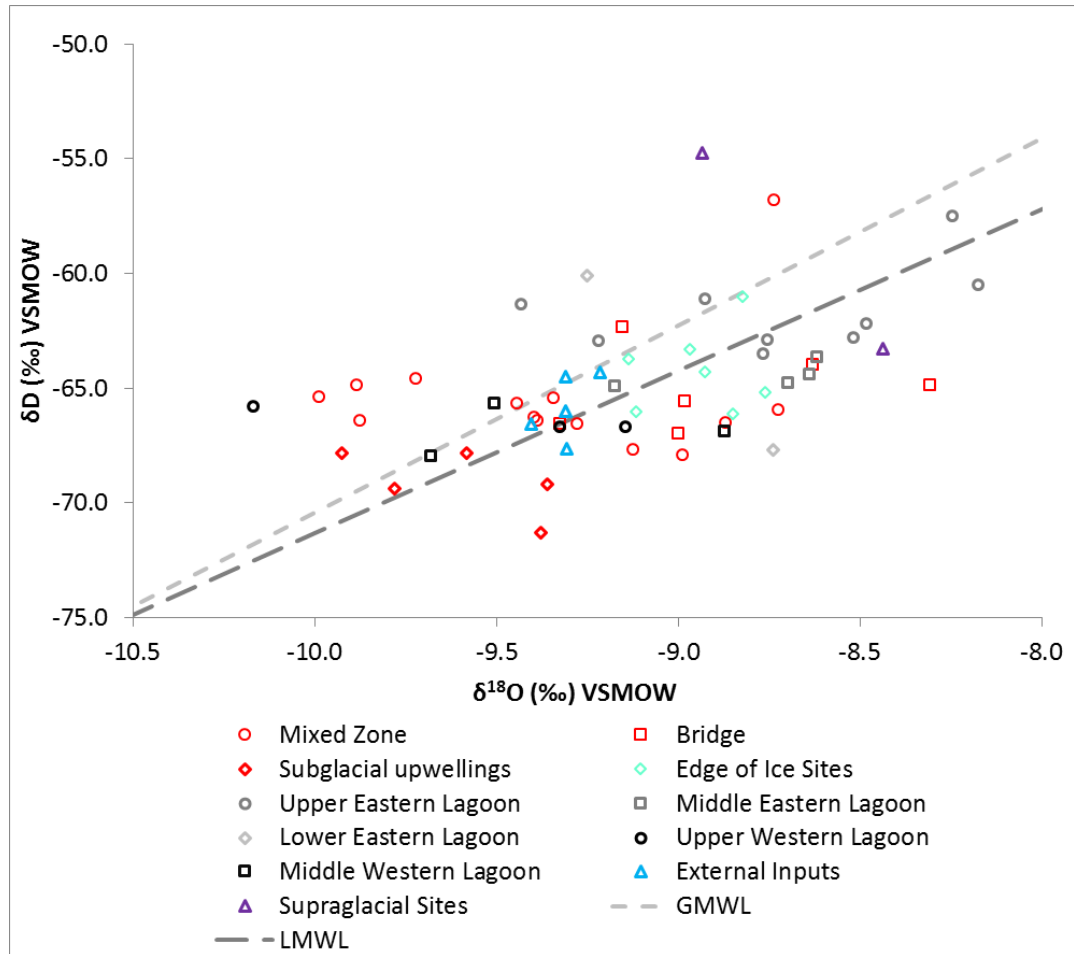
Figure 4.18: Bi-plot of δ^{18}O and δD values during Spring 2014

GMWL= Global meteoric water line

LMWL= Local meteoric water line (taken from Reykjavik)

For Summer 2013 supraglacially sourced waters displayed amongst the heaviest isotopic signatures, again above -9.0‰. In comparison, Mixed Zone and Middle Western Lagoon samples exhibited lighter isotopic signatures (summertime 2013 subglacial upwelling site not accessed directly for sampling). The majority of samples appeared to plot beneath the GMWL and LMWL suggesting a localised enrichment was likely associated with summertime evaporative processes.
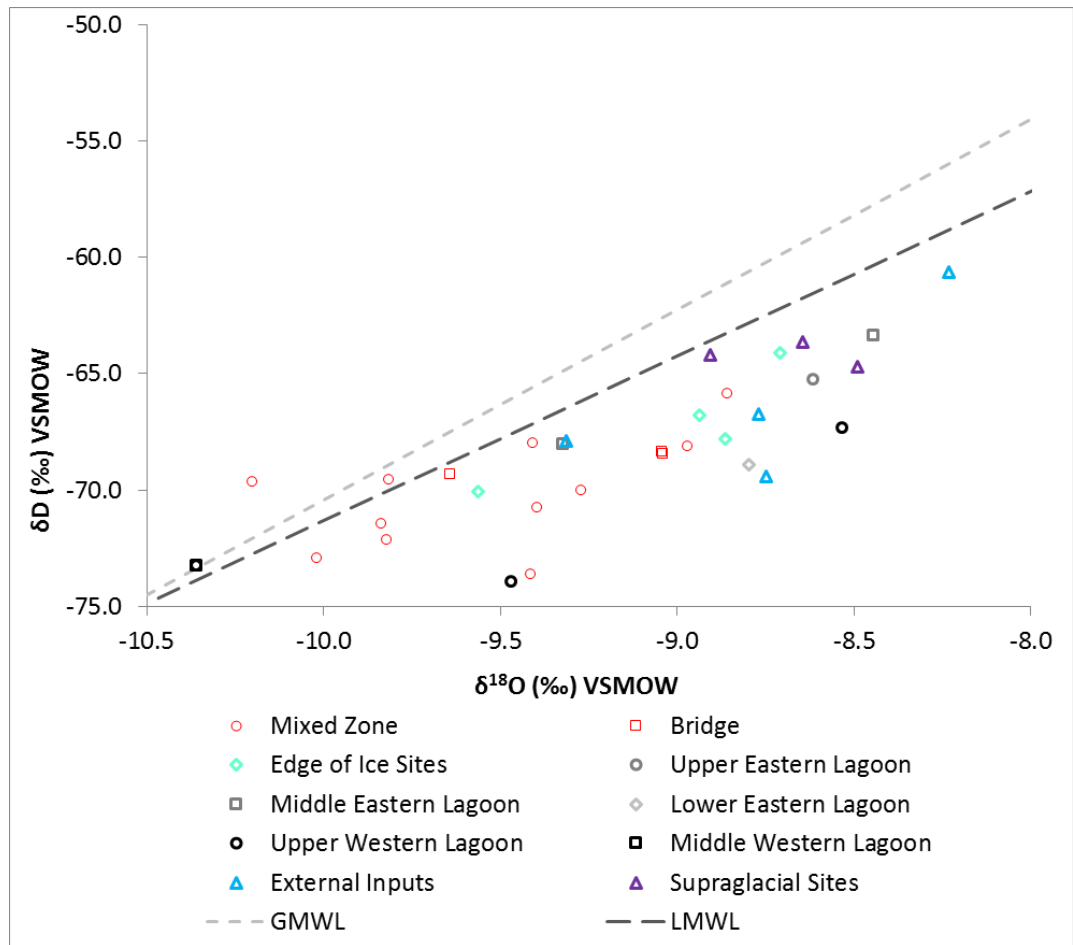
Figure 4.19: Bi-plot of δ^{18}O and δD values during Summer 2013

GMWL= Global meteoric water line

LMWL= Local meteoric water line (taken from Reykjavik)

δ^{18}O and EC data for Spring 2014 reflected a geochemical partitioning between sources at Sólheimajökull. Highest EC values and lightest δ^{18}O signatures were found in subglacial waters, whilst low EC and relatively heavier δ^{18}O values were in waters of supraglacial origin. Lagoon samples plotted between these two sources. An east-west split was evident with western lagoon waters showing comparable geochemical signatures to upwelling waters, whilst eastern lagoon samples transitioned to values

closer to those demonstrated by supraglacial waters. Proximity to source appeared key to determining Spring hydro-geochemistry.
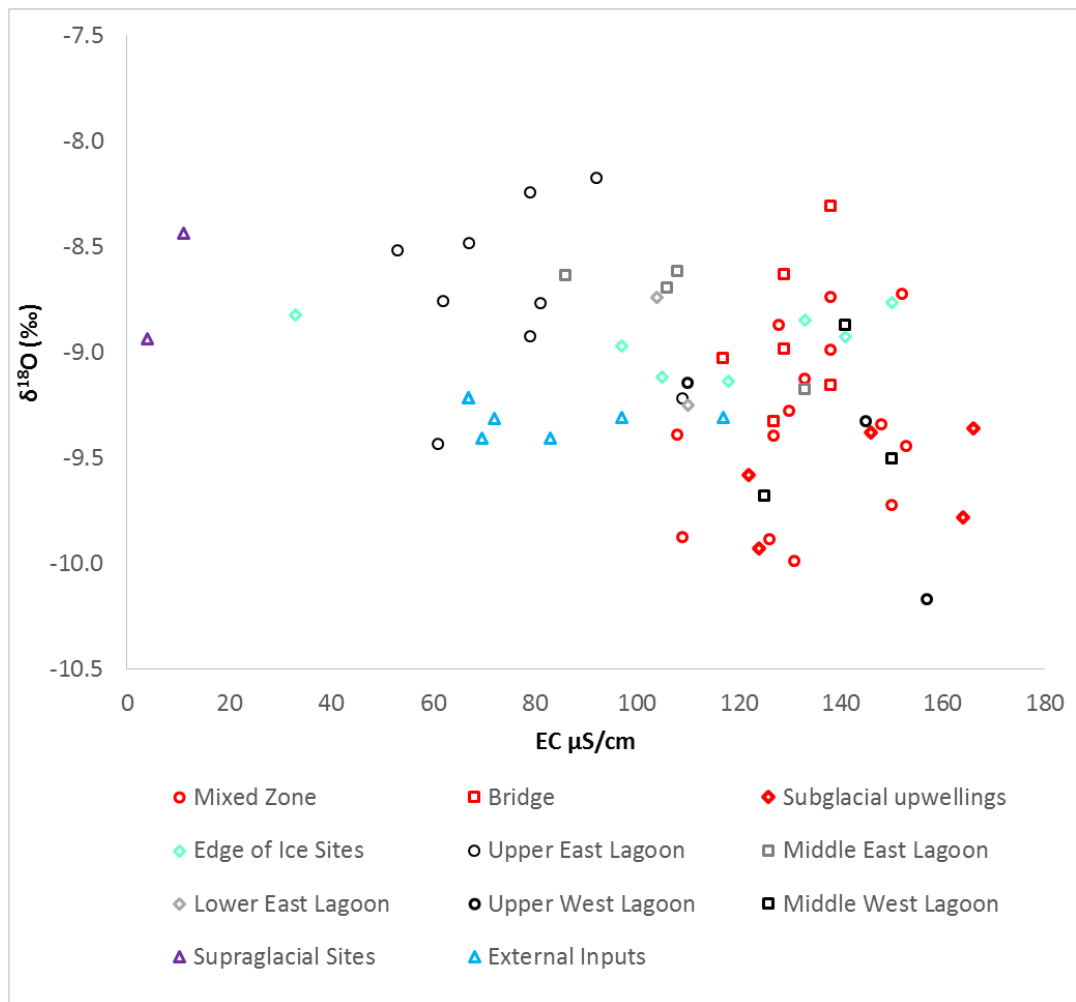
Figure 4.20: Bi-plot of $\delta^{18}O$ and EC Spring 2014

Summer $\delta^{18}O$ and EC values are presented below (Figure 4.21). Similarly to Spring, supraglacial sites represented a low EC and relatively heavier $\delta^{18}O$ source. Highest EC values were accompanied by lightest $\delta^{18}O$ signatures at the Middle Western lagoon and the Mixed Zone. Since western lagoon sites have displayed geochemical parameters similar to water of subglacial origin this could be indicative of subglacial flows directed along the western lagoon during summer.
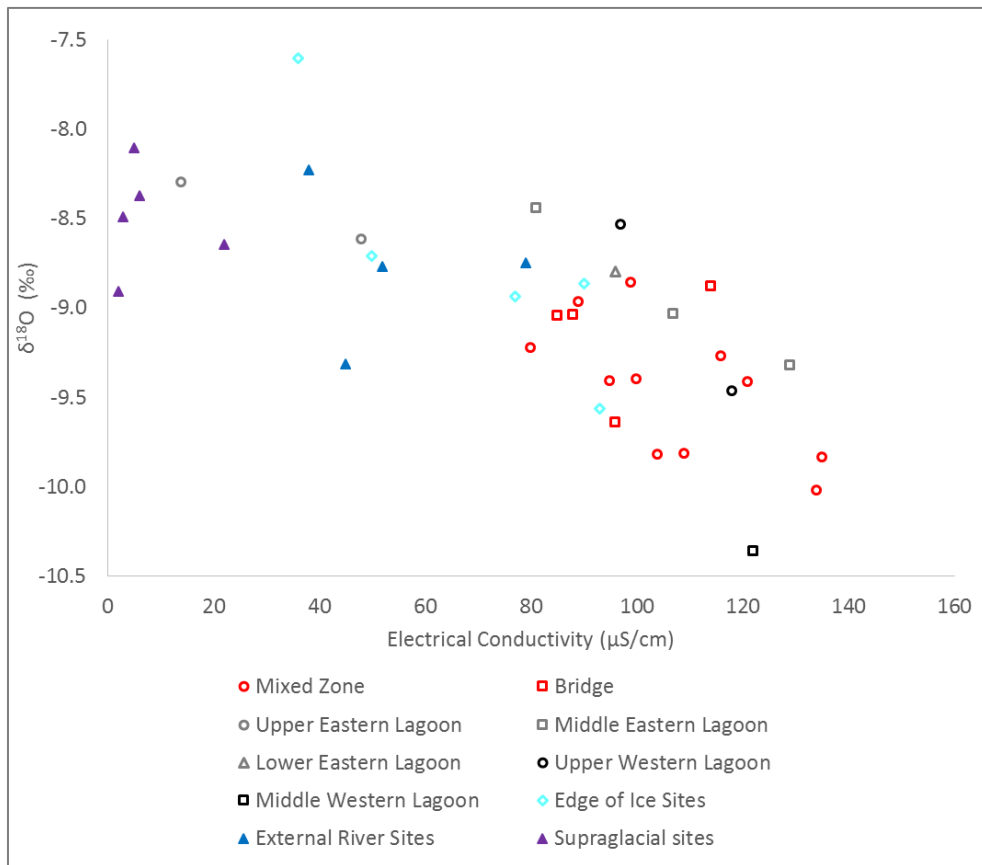
Figure 4.21: Bi-plot of $\delta^{18}O$ and EC Summer 2013

4.5. Discussion

4.5.1. Water source characteristics at Sólheimajökull

Icelandic glacial hydrology possesses a unique annual cycle linked to seasonal evolution of the glacial drainage network. During winter months (November-April) Icelandic discharge is relatively reduced, ranging from 50 to 100m^3/s, with little variation (Kristmannsdóttir et al., 1996). Cessation of winter bulk outflows commonly associated with alpine glaciers is not always evident in Iceland, with year round drainage often observed. This is likely attributed to Iceland's maritime climate and

the low elevation of each glacier snout. Observations of glacier extents below 100m a.s.l. show continuous negative mass balances, even during winter months thereby contributing to a continual supply of low elevation meltwater (Björnsson and Pálsson, 2008).

During Summer, heightened snow and ice melt causes peak flow, with up to fivefold increases in glacial river discharge (Kristmannsdóttir et al., 1996). At Sólheimajökull bank full discharge at the Bridge gauging station is estimated to be 100m^3/s with peaks occurring in late July (Lawler et al., 1996). Observations of river stage taken from Sólheimajökull during this study coincide with typical Icelandic annual glacial bulk meltwater fluctuations. Low river stage with little variation is shown to prevail during Spring (1st April-31st May 2014) with average water stage of 396.16cm (1SD= 8.48). During Summer (1st June-31st August 2013) greater average water stage of 435.96 (1SD= 15.32) are observed, accompanied by greater variability in water stage. Air temperature seems to be a major forcing factor for springtime supraglacial melt, with positive relationships between air temperature and water stage (R^2= 0.40). During Summer, increased volumes of rainfall as precipitation exert periodic influence upon water stage measured at the Bridge. Precipitation contributions to glacial melt are low (observed average summertime energy fluxes of 2.0% and 1.9% for melt at 211m and 219m respectively (Thompson, unpublished Masters Thesis) suggesting that periodic rainfall influence is associated with supraglacial runoff and overland flows. Overall this leads to a switching between increases in discharge driven by increased air temperatures and increased discharge during cooler periods driven by increased rainfall.

Bulk outflow from the Sólheimajökull catchment is a combination of subglacial, supraglacial and external riverine inputs. The contribution and relative importance of each of these sources varies seasonally. Subglacial waters are an important component of the Sólheimajökull hydro-glacial budget. Basic observations show subglacial waters had low average temperatures, low average pH and high average

EC values. In addition, geochemical analysis indicated comparatively light $\delta^{18}O$ signatures suggesting a high altitude source for these waters. This can account for large quantities of basally derived ions suggesting extensive transit through a subglacial weathering environment. Seasonal fluctuations in subglacial water delivery have the potential to influence bulk meltwater quality and quantity, inferring the essential role glaciers have on hydrological outputs in Iceland.

Supraglacial run off also provides another glacier derived source of meltwater. Supraglacial waters flowing over the glacier represented a relatively pure component with low average EC values, pH close to neutral and fluctuating average temperatures linked to seasonal air temperatures (range from 0.30°C (1SD= 0.17) in Summer to 2.15°C in Spring). During summer large volumes of surface ice melt leaded to water pooling in old crevasse traces. These stagnant supraglacial waters exhibited slightly elevated average EC levels, likely linked to in situ acquisition of ions via surface weathering. $\delta^{18}O$ analysis reflected consistent heavier values for supraglacial sites during Summer. This was consistent with a lower altitude source. In this instance the heavily crevassed nature of the Sólheimajökull glacier snout means only localised ice melt can feed surface streams, thus restricting the surface $\delta^{18}O$ signature to one of a localised isotopically heavy source.

Glacial inputs are not the only source of water to the Sólheimajökull proglacial area. The Sólheimajökull catchment up to the Bridge gauging station encompasses an area of approximately 110km^2, of which only 78km^2 (or 71%) is glacierised (Lawler et al., 1996). In addition to glacial inputs, non-glacial rivers such as Jökulsárgil and Fjallgilsá also contribute to bulk water outputs from the Sólheimajökull catchment. Jökulsárgil provided a relatively warm water source, with elevated pH levels and mid-range EC values reflecting acquisition of ions from in situ riverine and subaerial weathering within the Jökulsárgil catchment. Ions may be supplied by high altitude melting of Jökulsárgilsjökull, however given the high elevation this is a minimal source. $\delta^{18}O$ analysis shows a seasonal transition to heavier $\delta^{18}O$ signatures during Summer,

potentially reflecting low altitude seasonal overland flow inputs and heavier $\delta^{18}O$ values of summer precipitation. Jökulsárgil waters are shown to provide a physically and chemically distinct source of water to Sólheimajökull.

Fjallgilsá is another non glacial riverine component to the Sólheimajökull system. Fjallgilsá enters the Jökulsa á Sólheimasandi approximately 4km from the glacier snout, therefore does not contribute to hydro-dynamics within the proglacial lagoon or at the Mixed Zone but has the potential to influence total bulk meltwater outputs at the Bridge. Like Jökulsárgil, Fjallgilsá is also distinct from the Jökulsa á Sólheimasandi. Fjallgilsá waters were relatively warm with pH values close to neutral. EC was lower than Jökulsárgil, and low in comparison to values recorded in the proglacial lagoon and river. $\delta^{18}O$ values were similar to Jökulsárgil with evident seasonality demonstrated through lighter Spring time signatures and heavier Summer values.

Subglacial, supraglacial and external Jökulsárgil waters converge in the proglacial lagoon, which has developed from two proglacial channels in 2009 into the extensive lagoon present today (Wynn et al., 2015). Prevalence of an East/West division in EC and $\delta^{18}O/\delta D_{H2O}$ and to a lesser extent pH, particularly during Spring suggested proximity to water source is vital in shaping lagoon hydrogeochemistry. Western hydrogeochemical characteristics shared many similarities with subglacial waters. Here it is likely that inflow of cold, dense water from the subglacial portal maintained integrity as a plume and routes along western lake margins (Carrivick and Tweed, 2013). Contrastingly, Eastern sites (particularly the upper eastern lagoon) displayed resemblance to supraglacial flows, likely reflecting contributions from glacier run off. These spatial distributions emulate previous proglacial riverine morphology, where the Eastern River was dominated by waters displaying characteristics similar to supraglacial flows, whilst the Western River consisted of subglacial outflow (Tepe and Bau, 2014). The degree of mixing in the interior of the proglacial lagoon is unknown,

however, once waters enter the Jökulsa á Sólheimasandi mixing occurs, with the Mixed Zone representative of the culmination of sources to the proglacial lagoon.

4.5.2. Evolution of the Sólheimajökull drainage system over an annual balance cycle

Field evidence indicated a seasonal development of the Sólheimajökull subglacial drainage system with a restricted early Spring subglacial drainage system which developed into an extensive Summer hydraulic configuration. Initial Spring hydrology demonstrated a prevalence of increased EC, pH and water temperature across the proglacial lagoon. In contrast water emerging from subglacial upwellings exhibited characteristics associated with low velocity passage through a subglacial weathering environment: increased EC particularly linked to heightened acquisition of basally derived ions such as Ca^{2+}, Na^+ and HCO_3^- and reductions in water temperature. pH values were unusually low. In addition, $\delta^{18}O$ H_2O values of subglacial waters were amongst the lightest signatures across the Sólheimajökull proglacial area. The isotopically distinct nature of these reflects fractionation driven by altitude effects, whereby isotopically 'heavier' ^{18}O H_2O values are preferentially 'rained out' from ascending air masses leaving a $\delta^{18}O$ H_2O signature enriched in the lighter ^{16}O H_2O isotope. Isotopic distinction found in subglacial waters could have reflected a higher altitude source of water- likely melt from above the snowline. These physically distinct characteristics reflected the early season development of the drainage system; where newly established subglacial plumes did not have the sufficient meltwater volume to exert considerable influence across the entire proglacial area. Instead, proximity to subglacial sources became a definitive factor in determining water hydro-geochemistry with localised reductions in pH alongside increased EC close to areas of upwelling water. Linkages between water stage and air temperature, indicated that early Spring meltwater outflow was dominated by surficial melt. Reinforcing that at this stage subglacial upwelling water was superseded by continual localised supraglacial melt drainage beneath the lower reaches of the glacier tongue.

This was in contrast with Summer season hydrological configuration where extensive channelized subglacial drainage rapidly conveyed meltwaters with limited rock: water contact times, which reduced ion acquisition and resulted in an overall reduction in EC across the lagoon. A breakdown in the relationship between air temperature and water stage demonstrated other factors influencing meltwater generation. This can be somewhat accounted for by precipitation events, however overall energy balance modelling has shown these to have limited impact on meltwater drainage in the Jökulsa á Sólheimasandi (Thompson, Unpublished Masters Thesis). Instead, notable increases in water stage can be attributed to basal melting and release of subglacially stored water during hydraulic expansion. This supplies large volumes of subglacial meltwater to the proglacial lagoon via multiple subglacial openings beneath the lake surface.

Based upon this it could be thought that Sólheimajökull largely obeys the classical theory with respect to the drainage system of Alpine glaciers. However, Sólheimajökull proglacial meltwaters exhibited some distinctive peculiarities. Indicators of anoxia in Summer subglacial meltwaters (this study and Wynn et al., 2015) alongside reduction in pH suggested seasonal connectivity to subglacial geothermal areas, with the potential to perturb hydrogeochemistry (explored in Chapter 5). In addition previous identification of low redox status of $\delta^{18}O_{SO4}$ in summer season waters draining the Sólheimajökull subglacial realm was at odds with ideas of classical drainage theory where waters would flow at low pressures in well aerated summer channels (Wynn et al., 2015). Without invoking extensive cavity drainage throughout the duration of the summer, the only possible cause of summer season anoxia must be associated with the injection of hydrothermally altered waters. Furthermore, existing analysis of bulk meltwater components supported a leakage of geothermal fluids into subglacial drainage facilitated by hydraulic configuration during the melt season. Increases in H_2S, SO_4^- alongside decreases in pH have been linked to major geothermal fluid injections caused by seismic disturbance (Lawler et al., 1996; Wynn et al., 2015). This geothermally perturbed system contributes to the bulk meltwater characteristics observed at Sólheimajökull

and likely has an extensive impact on glacial carbon cycling via unique reversed seasonal redox conditions and exclusive glacier hydrology-volcano interactions. The remainder of this thesis will now explore carbon cycling and hydrological system behaviour in light of this adapted model of glacial drainage.

4.6. Summary

1. Meteorological conditions prevalent at Sólheimajökull were represented by colder, drier conditions during Spring and warmer, wetter conditions during Summer. This influenced discharge dynamics, with Spring runoff associated with temperature induced melt. The Summer breakdown in temperature forced meltwater generation could not fully be accounted for by periodic precipitation events, suggesting other factors influencing meltwater outflow.

2. There are three identified sources of water to the Sólheimajökull system. Subglacially conveyed waters provided a high EC source dominated by crustally derived chemical species providing evidence of subglacial chemical weathering. This was accompanied by low pH, low temperature and light isotopic signatures indicative of a higher altitude snowmelt source. Secondly, supraglacial sources provided waters with low EC, low temperatures, neutral pH and heavier isotopic signatures from localised ice melt on the glacier snout. Finally, waters of external source origins such as Fjallgilsá and Jökulsárgil delivered waters with a mid-range EC indicative of sub aerial and in channel weathering, higher temperatures and neutral pH.

3. These three sources contribute to drainage and bulk outputs from the Sólheimajökull catchment. However the relative dominance and importance of each source varied seasonally and spatially according to the development of the subglacial drainage network.

4. During early Spring, subglacial drainage was poorly developed and proglacial meltwater is dominated by continual low level melt.

5. Summertime observations of lower pH, lower temperatures and prevalence of lighter $\delta^{18}O$ H_2O signatures across the proglacial lagoon inferred great inputs of subglacial waters. This was linked to seasonal head ward expansion of the arborescent drainage system. Hydrochemical indicators such as increased SO_4^{2-} (Lawler et al., 1996) and decreased pH, alongside evidence of summer season anoxia (Wynn et al., 2015) suggested hydraulic expansion into zones of geothermal activity and subsequent release of geothermally altered waters.

6. Unique redox status and geothermal perturbations resulting from subglacial volcanism, likely exert a significant influence on carbon cycling within the Sólheimajökull catchment, dictated by the timing of subglacial drainage expansion, which will be further explored.

5. Sources, Supply and Dynamics of Total Dissolved Inorganic Carbon at Sólheimajökull

5.1. Introduction

Weathering mechanisms offer the potential to liberate large quantities of total dissolved inorganic carbon (TDIC) from bedrock, fundamentally contributing to global carbon cycling. Basalt in particular provides a major source of dissolved solute in both glacial and non-glacial rivers (Georg et al., 2007). Basalt weathering may disproportionately contribute to long term carbon cycling. Basalt contains calcium bearing silicate minerals such as calcic plagioclase feldspars, which are susceptible to rapid dissolution. Weathering of these primary silicate minerals consumes protons, usually supplied by atmospheric CO_2 and releases cations, driving increased pH and alkalinity (Daval et al., 2009). This constitutes a large carbon sink through the drawdown of atmospheric CO_2. Based upon this, it can be thought that basalts provide a key feedback loop in regulating atmospheric CO_2 (Jacobson et al., 2015; Georg et al., 2007). Basaltic terrain encompasses only around 4.6% of the continental silicate surface area, yet may constitute around 30 to 35% of the global CO_2 consumption flux (Dessert et al., 2003; Duval et al., 2009; Jacobson et al., 2015).

The nature of Icelandic basalt weathering is more complex. Icelandic basalt also contains secondary Ca-bearing minerals such as Icelandic Spar, produced during hydrothermal alteration processes (Jacobson et al., 2015). The CO_2 encapsulated during hydrothermal calcite formation originates from the mantle, which upon liberation supplies a non-atmospheric CO_2 source. Ultimately, this has the potential to perturb the perceived capability of basalt weathering as a CO_2 sink (Jacobson et al., 2015). Acidic and basaltic rocks dominate the Sólheimajökull area (Carswell, 1983). However, the chemical composition of glacial bulk meltwaters at Sólheimajökull reveals carbonate loaded meltwaters exiting the catchment (Lawler et

al., 1996). Whilst this source of TDIC at Sólheimajökull has previously been attributed to the dissolution of volcanic CO_2 beneath the glacier, (Lawler et al., 1996), more recently the geochemistry of Icelandic rivers has been found to reflect a mixing of TDIC sources from weathering of basalt silicate minerals and hydrothermal calcites, with the majority of TDIC in Icelandic rivers originating from hydrothermal calcite sources (Jacobson et al., 2015).

Recognition of a carbonate component present within the Sólheimajökull geology (Gristwood, unpublished masters thesis) now highlights the importance of hydrothermal calcite as a TDIC source to Sólheimajökull bulk meltwaters. Additional complexities of subglacial geothermal degassing and meltwater interactions can offer a unique weathering scenario whereby Sólheimajökull hydrology acts as a vector by which mantle derived CO_2 is transported to the proglacial realm, where it exchanges with the atmosphere. In order to fully explore this distinctive mode of subglacial carbon cycling, this chapter presents major ion data alongside concentrations and isotopes of carbon species within the Jökulsa á Sólheimasandi proglacial system (using the methods outlined in sections 3.4 and 3.5). Analysis will be used to provenance the source, supply and transfer of TDIC at Sólheimajökull. The role of hydrothermal calcite and subglacial geothermal activity in contributing to the carbon dynamics at Sólheimajökull will form a focus of this chapter.

5.2. Results: major ion analysis to identify potential sources of TDIC in the Sólheimajökull subglacial realm

Solute acquisition in the subglacial realm of temperate and polythermal glaciers is most commonly associated with chemical weathering of freshly comminuted rock flour supplied by basal erosion. This provides subglacial waters with a unique chemical composition dominated by crustally derived ions. The analysis of the relative abundances (ratios) of these ions can help elucidate if TDIC is of primary silicate mineral or hydrothermal calcite origin.

5.2.1. Ratios of Ca^{2+}: Si as an indicator of TDIC origin

In order to evaluate the dissolution of basalts during chemical weathering and therefore attempt to distinguish between TDIC sources, it is commonplace to begin with the relative abundances of Ca^{2+}: Si, as silica and calcium are the most abundant cations in basalt. Additionally, mobilities of silica and calcium during weathering are similar, therefore constant Ca^{2+}: Si ratios in bulk meltwaters are representative of a consistent basaltic mineral source. Any large perturbations in the Ca^{2+}: Si ratio may be indicative of periodic contributions from areas draining rocks which are not purely basaltic e.g. containing a hydrothermal calcite component, particularly if ratios increase due to Ca^{2+} enrichment of waters. Furthermore, if silicate weathering is low, then Si concentrations supplied by dissolution will be low (Yde et al., 2012).

This may be complicated by secondary mineral precipitation (Crompton et al., 2015). Precipitation of Si can be associated with adsorption of Si onto the surface of clay particles. However, this may not be applicable at Sólheimajökull. Appendix 2 indicates consistent inter-seasonal Si fluxes between subglacial, proglacial and extra-glacial waters, despite differing weathering conditions. Furthermore, adsorption of cations onto mineral surfaces is amplified by increasing pH (Crompton et al., 2015). Unusually low pH values found in subglacial waters (springtime average of 6.66, standard devition 0.25) would therefore be a limiting factor affecting mineral precipitation. Given that Icelandic basalts are known to contain disseminated calcites (Jacobson et al., 2015) and a carbonate component has been identified at Sólheimajökull, perturbations in the Ca^{2+}: Si ratios can be largely attributed to changes in Ca^{2+} and not reductions in Si due to mineral precipitation.

During Spring 2014 average Ca^{2+}: Si molar ratios for glacial meltwaters ranged from 1.69 (1SD= 0.13) at the Mixed Zone to 10.68 (n=2) in supraglacial waters. Average Ca^{2+}: Si molar ratios in Summer 2013 ranged from 1.42 (1SD= 0.18) at the Bridge to 1.93 (1SD=0.04) at Western Lagoon sites. With exception of the Mixed Zone, average Summer ratios were slightly lower, largely caused by decreases in Ca^{2+} abundance

(Appendix 2). Given that Silica and Calcium exhibit similar abundances and mobilities within basaltic minerals, ratios of 1:1 can be expected for congruent silicate mineral weathering- in line with the composition of the weathering product. Ratios greater than 1 were indicative of greater Ca^{2+} acquisition, reflecting non basaltic Ca^{2+} sources. Standard deviation values indicated seasonal overlap between Spring and Summer, reinforcing the potential for a consistent source of silica draining from a basaltic rich terrain, with additional calcium inputs.

	Average Ca^{2+}: Si Molar Ratio 1 standard deviation (1SD) is in parentheses	
Location	Spring 2014	Summer 2013
Mixed Zone	1.69 (0.13) *n=14*	1.69 (0.25) *n=12*
Bridge	2.04 (0.53) *n=6*	1.42 (0.18) *n=4*
Subglacial upwellings	2.09 (0.36) *n=6*	Not sampled
Eastern Lagoon	2.08 (0.31) *n=16*	1.75 (0.43) *n=10*
Western Lagoon	2.61 (0.17) *n=6*	1.93 (0.04) *n=3*
Edge of Ice Sites	2.05 (0.60) *n=7*	1.91 (0.47) *n=4*
Supraglacial sites	10.68 (…) *n=2*	1.61 (…) *n=4*
Jökulsárgil and Fjallgilsá	1.00 (0.28) *n=6*	0.81 (0.38) *n=4*

Table 5.1: Ca^{2+}: Si Molar ratios for Spring 2014 waters in comparison to Summer 2013.

5.2.2. Using Ca^{2+}: Mg^{2+} ratios to identify basalt mineral and hydrothermal calcite weathering

Ca^{2+}: Mg^{2+} ratios offer an indication as to whether solutes are obtained through weathering of primary basaltic minerals or trace carbonates contained within as hydrothermal calcites. Ca^{2+}: Mg^{2+} molar ratios of basaltic rocks have been found to

range from 0.9-3 (Georg et al., 2007). Highest ratios are representative of inputs from hydrothermal calcites which are enriched in Ca^{2+} relative to Mg^{2+}. Lower ratios have been associated with weathering of primary minerals such as plagioclase and olivine found within mafic basalts. These tend to be compositionally rich in Mg^{2+} and Ca^{2+} which weather congruently (Georg et al., 2007).

Sólheimajökull bulk meltwaters fall at the upper end of the Ca^{2+}: Mg^{2+} ratios outlined above, suggesting a potential hydrothermal calcite source. During Spring, average glacial meltwater Ca^{2+}: Mg^{2+} ratios ranged from 2.02 (1SD=0.06) at the Mixed Zone to 8.83 in supraglacial waters. Subglacial waters supported an average value of 2.13 (1SD= 0.13). During Summer, average Ca^{2+}: Mg^{2+} ratios were mostly higher. Average Ca^{2+}: Mg^{2+} ranged from 3.19 (1SD= 0.18) at the Bridge to 4.42 (1SD= 2.70) in supraglacial waters. Jökulsárgil and Fjallgilsá demonstrated consistently lower ratios over both seasons.

	Average Ca^{2+} : Mg^{2+} molar ratio 1 standard deviation (1SD) is in parentheses	
Location	**Spring 2014**	**Summer 2013**
Mixed Zone	2.02 (0.06) *n=14*	3.41 (0.19) *n=12*
Bridge	2.56 (0.52) *n=6*	3.19 (0.18) *n=4*
Subglacial upwellings	2.13 (0.13) *n=6*	Not sampled
Eastern Lagoon	2.98 (0.23) *n=16*	3.49 (0.83) *n=10*
Western Lagoon	2.98 (0.11) *n=6*	3.27 (0.02) *n=3*
Edge of Ice Sites	2.48 (0.55) *n=7*	3.59 (0.21) *n=4*
Supraglacial sites	8.83 (…) *n=2*	4.42 (2.70) n=4
Jökulsárgil and Fjallgilsá	1.21 (0.23) *n=6*	1.55 (0.29) *n=4*

Table 5.2: Ca^{2+}: Mg^{2+} molar ratios of bulk meltwaters in the proglacial zone

Figure 5.1 demonstrates two distinct water types when plotted as a bi-plot of Ca^{2+} and Mg^{2+} concentration. Most data plotted along a positive linear trend representing mixing between a low concentration supraglacial end member and high concentrations of Ca^{2+} and Mg^{2+} found in western proglacial lagoon waters (R^2 value of 0.96). A second cluster of data comprised waters with higher Mg^{2+} concentrations. These were subglacial water, Mixed Zone samples and some Bridge and Edge of Ice samples. These still displayed a positive linear relationship between Ca^{2+} and Mg^{2+} (R^2 value of 0.71) however average ratios of Ca^{2+}:Mg^{2+} were lower, likely indicating a slightly greater input of solutes associated with weathering of basaltic minerals.
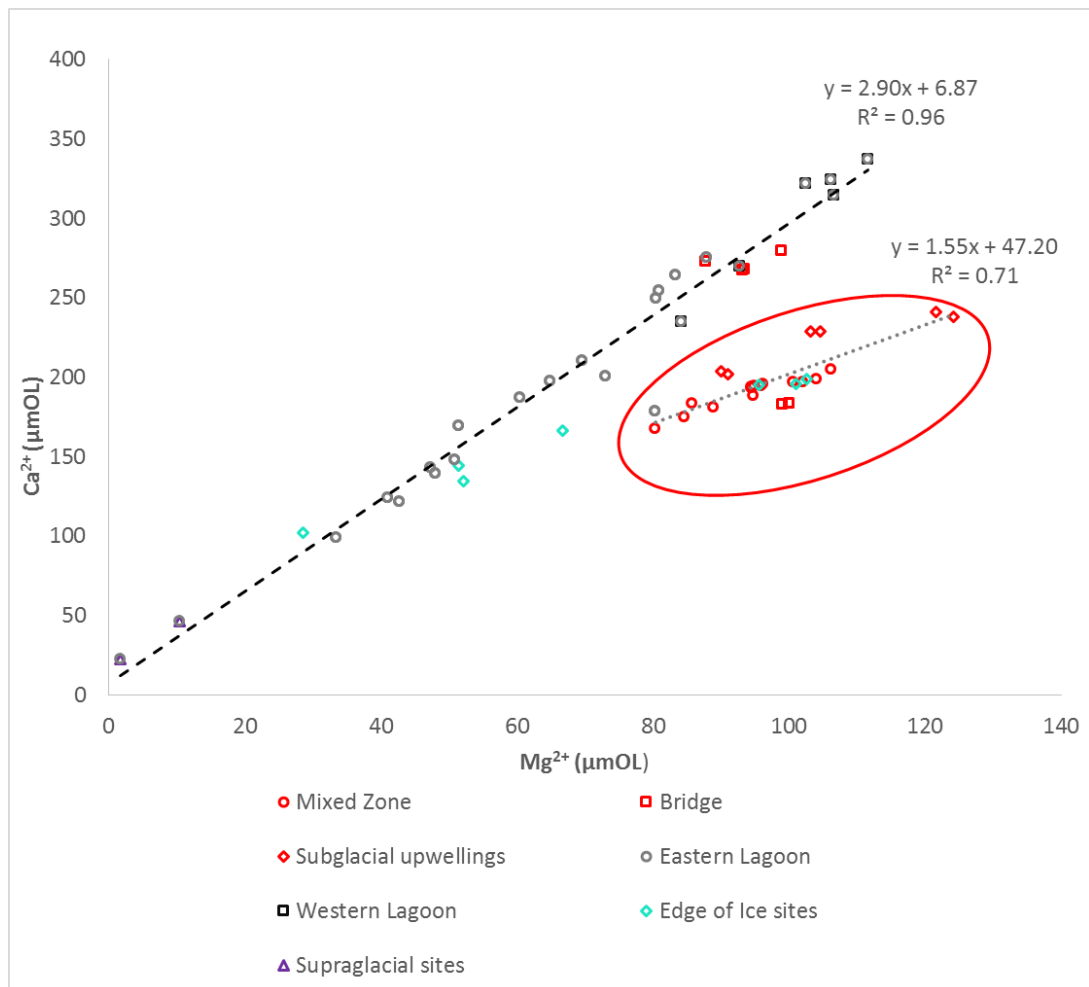
Figure 5.1: Ca^{2+} and Mg^{2+} concentrations for Spring 2014 glacial meltwaters

Figure 5.2 shows that Ca^{2+} and Mg^{2+} concentrations in Summer also demonstrated mixing between a dilute supraglacial end member and lagoon waters enriched in Ca^{2+} and Mg^{2+}. This can be expressed by a linear trend (R^2= 0.90) similar to that displayed for the main bulk of lagoon waters during Spring.
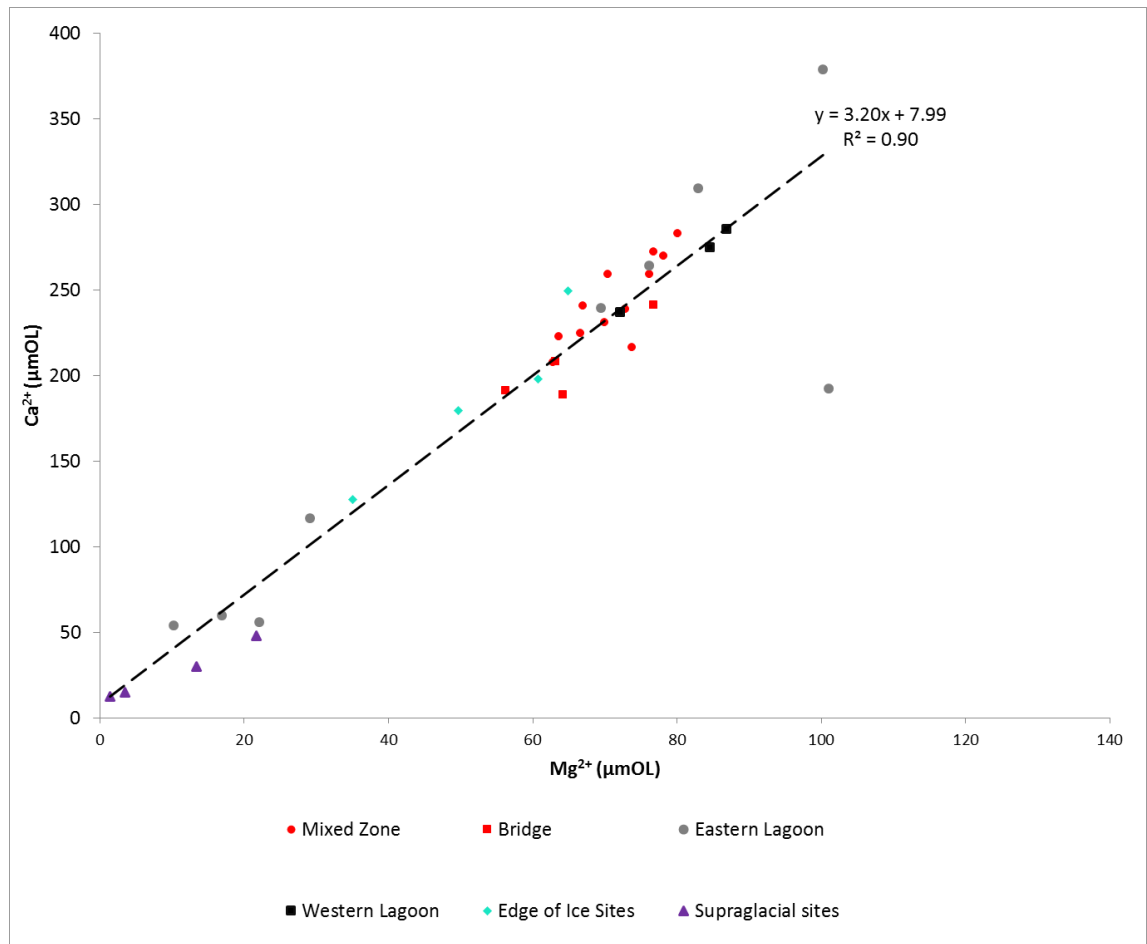
Figure 5.2: Ca^{2+} and Mg^{2+} concentrations for Summer 2013 glacial meltwaters

5.2.3 Using Ca^{2+}:Na^+ ratios to explore silicate, hydrothermal calcite and potential volcanic volatile components of TDIC

The abundance of Na^+ can offer insight into silicate weathering and potential volcanic components. Glacial and non-glacial rivers draining basaltic terrain have Ca^{2+}:Na^+ molar ratios ranging from 0.2 to 3.9, linked to the abundance and mobility of these cations within basalt (Dessert et al., 2003). In terms of a rock weathering based

source, molar Ca^{2+}:Na^+ ratios <1 are indicative of the silicate mineral end member, whilst >1 infer hydrothermal calcite dissolution (Oliva et al., 2003).

Ca^{2+}:Na^+ ratios at Sólheimajökull were at the lower end of quoted Ca^{2+}:Na^+ ratios for rivers in basaltic catchments. During Spring, glacial meltwater ratios ranged from 0.34 (1SD =0.02) at the Mixed Zone to 2.00 (n=2) at supraglacial sites. External waters from Jökulsárgil and Fjallgilsá demonstrated low ratios of 0.27 (1SD= 0.00). During Summer, glacial meltwater Ca^{2+}:Na^+ molar ratios were slightly higher, ranging from 0.50 (1SD= 0.07) at the Bridge to 2.56 (1SD=1.08) in supraglacial waters. Again consistently low ratios were observed in Jökulsárgil and Fjallgilsá. In the first instance, low Ca^{2+}:Na^+ ratios appear to be indicative of pure silicate mineral weathering from the surrounding basaltic terrain, linked to dissolution of basaltic glass and the acidic nature of basalts. However, ratios of Ca^{2+}:Si and Ca^{2+}:Mg^{2+} only supported this conclusion for the streams of external catchment origin. All other melt streams within the Sólheimajökull catchment appeared to support an additional source of Ca^{2+} (likely sourced from dissolution of hydrothermal calcite), at odds with this low Ca^{2+}:Na^+ ratio. This ratio within the Sólheimajökull melt streams must therefore represent a mixed source origin, with high concentrations of Na^+, likely obtained from geothermal activity masking the high Ca^{2+} sourced from hydrothermal calcite. In contrast, supraglacial ratios >1 demonstrate differing subaerial weathering processes, potentially with a greater input of Ca^{2+} from a hydrothermal calcite dissolution source.

	Average Ca^{2+} : Na^+ molar ratio 1 standard deviation (1SD) is in parentheses	
Location	**Spring 2014**	**Summer 2013**
Mixed Zone	0.34 (0.02) *n=14*	0.60 (0.09) *n=12*
Bridge	0.45 (0.10) *n=6*	0.50 (0.07) *n=4*
Subglacial upwellings	0.39 (0.03) *n=6*	Not sampled
Eastern Lagoon	0.42 (0.06) *n=16*	0.81 (0.29) *n=10*
Western Lagoon	0.53 (0.03) *n=6*	0.63 (0.00) *n=3*
Edge of Ice Sites	0.40 (0.09) *n=7*	0.65 (0.14) *n=4*
Supraglacial sites	2.00 (…) *n=2*	2.56 (1.08) *n=4*
Jökulsárgil and Fjallgilsá	0.27 (0.00) *n=6*	0.33 (0.04) *n=4*

Table 5.3: $Ca^{2+:}$ Na^+ molar ratios of bulk meltwaters in the proglacial zone

Concentrations of Ca^{2+} and Na^+ during Spring (figure 5.3) reflected a mixing between low concentration supraglacial samples and high concentration western lagoon samples. Water emanating from subglacial upwellings, Mixed Zone and some Edge of Ice samples plotted away from the main positive trend reflecting the lower ratios of Ca^{2+}:Na^+ in these environments.
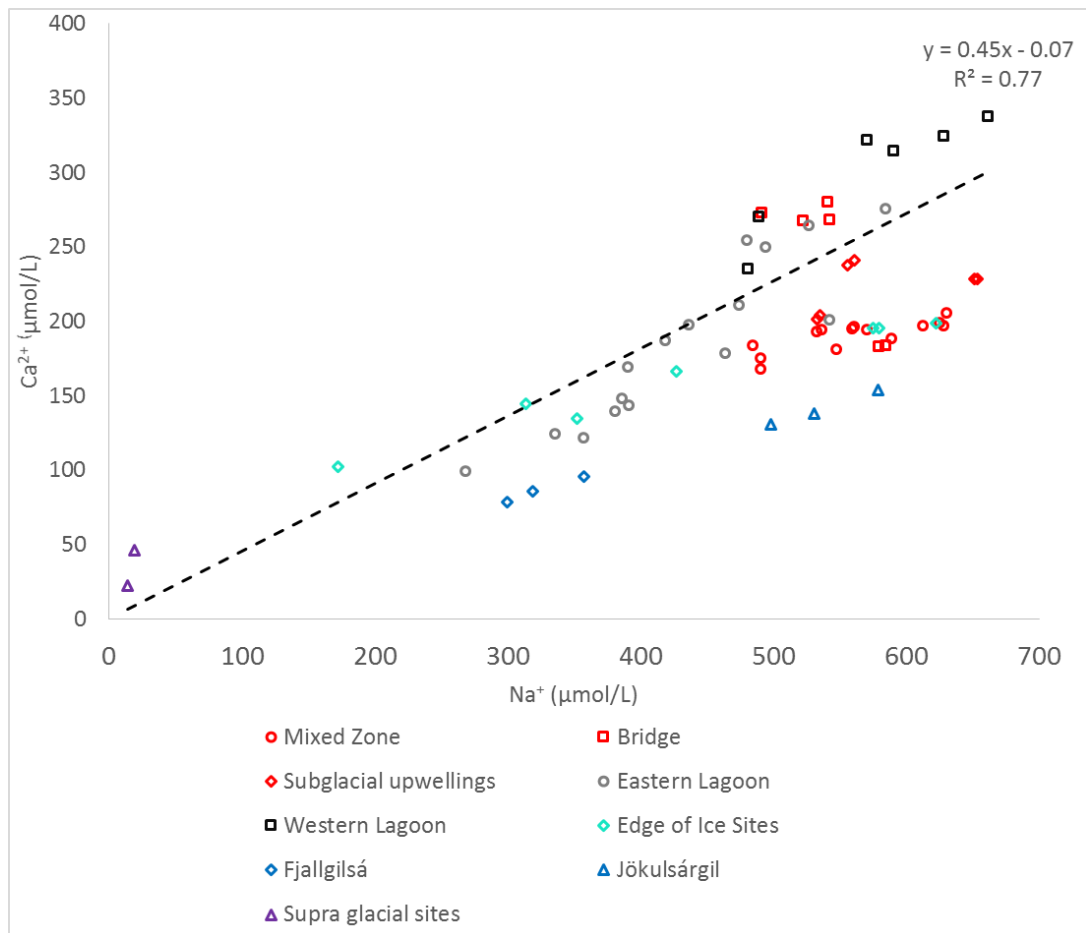
Figure 5.3: Ca^{2+} and Na$^+$ concentrations for Spring 2014 waters

Linear trend does not include rivers of external catchment origin, as these do not represent weathering in the Sólheimajökull glacial system.

Similarly during Summer, supraglacial sites once again exhibited low concentrations of Ca^{2+} and Na$^+$. Highest abundances were associated with Mixed Zone, Bridge and Middle Eastern Lagoon Samples. Upper Eastern Lagoon values showed ionic similarity to supraglacial waters, perhaps indicating localised surficial run off. This demonstrates a division between sites dominated by subglacial waters and those influenced by supraglacial flows.
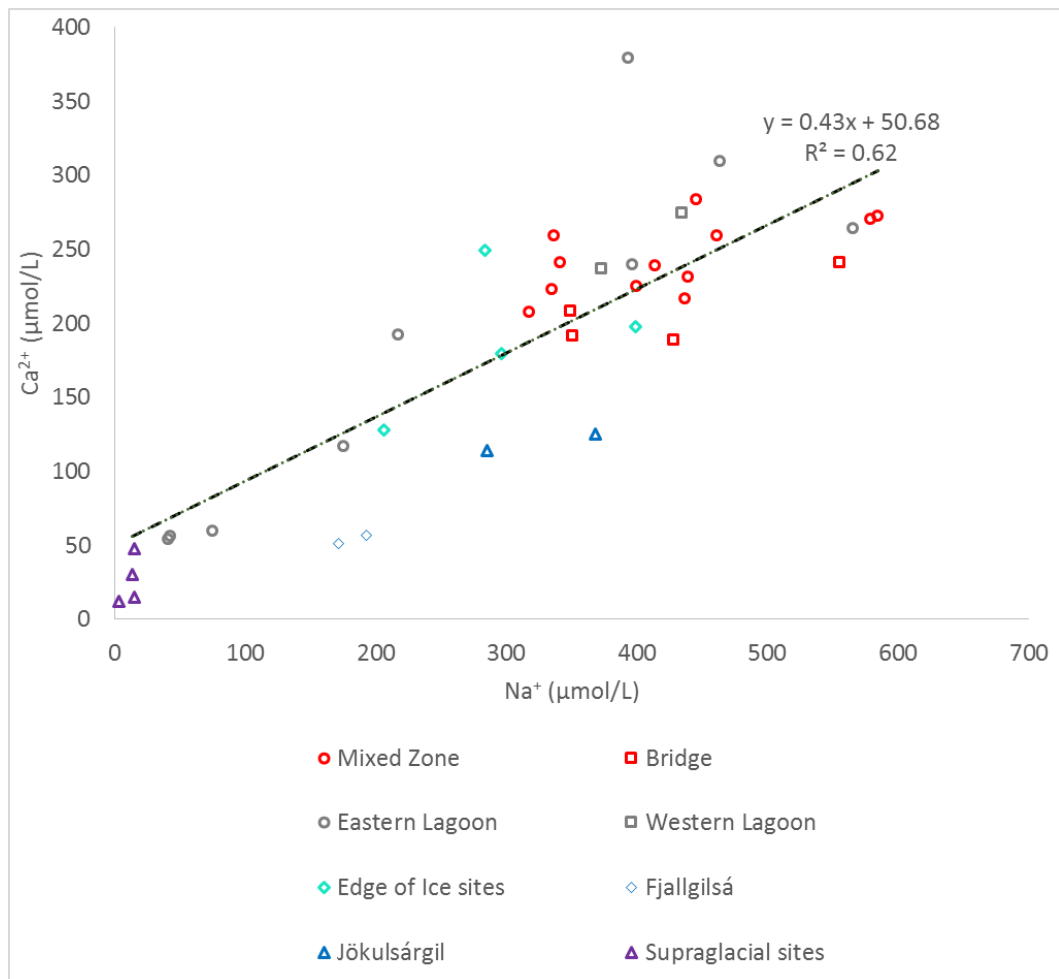
Figure 5.4: Ca^{2+} and Na^{+} concentrations for Summer 2013 waters

Linear trend does not include rivers of external catchment origin, as these do not represent weathering in the Sólheimajökull glacial system.

5.2.4. Summary of initial investigation of TDIC sources at Sólheimajökull

1. Given the basaltic volcanic geology of the Sólheimajökull region this could offer a widespread source of TDIC.

2. Ca^{2+}: Si ratios indicated acquisition of Ca^{2+} in excess of Si, suggesting an additional non-basaltic source of Ca^{2+} to glacial meltwaters.

3. Ca^{2+}: Mg^{2+} ratios plotted at the upper end of the range associated with weathering of basaltic rocks. Since Ca^{2+} and Mg^{2+} contained within primary basaltic minerals weather congruently, this relative enrichment of Ca^{2+} is

likely indicative of a hydrothermal calcite source of TDIC contained within the basalt rocks.

4.   Molar ratios of Ca^{2+}: Na^+ were at the lower end of the observed range for weathering in basaltic terrains, proposing a primary basaltic mineral source for all waters other than those of supraglacial origin.

5.3. Chemical Weathering Mechanisms of TDIC supply at Sólheimajökull

Ionic analysis has shown the potential for primary minerals within basaltic bedrock (including a hydrothermal calcite component) to act as sources of TDIC to the Sólheimajökull system. Bi-plots of major ions has shown a division between dilute supraglacial waters and more ionically enriched waters conveyed via subglacial drainage. This suggests that large scale TDIC acquisition occurs in the subglacial realm, facilitated by widespread subglacial weathering. Here, ratios of cations to TDIC acquired during weathering will be used to offer an insight into dominant weathering mechanisms, supporting the pathways of TDIC acquisition defined above.

5.3.1. Investigating the presence of hydrothermal calcite weathering in the catchment

In environments dominated by a carbonate bedrock component, the relationship between $Ca^{2+}+Mg^{2+}$ and TDIC should be present as a 1:1 ratio. This is based on the assumption of Sharp et al. (1995) that weathering of carbonate minerals supplies all crustally sourced $Ca^{2+}+Mg^{2+}$ and all crustally derived TDIC, as expressed in the following equation taken from Wynn et al. (2006):

$$DIC_{(hydrolysis/acid\ dissolution)} = Ca^{2+}_{crustal} + Mg^{2+}_{crustal}$$

Data presented in figure 5.5 demonstrated a linear relationship between $Ca^{2+}+Mg^{2+}$ to TDIC ($R^2 = 0.57$). Supraglacial sites demonstrated lowest $Ca^{2+}+Mg^{2+}$ and TDIC values, and subglacial upwellings, Mixed Zone and Bridge sites exhibited the highest $Ca^{2+}+Mg^{2+}$ and TDIC concentrations. Evidently, sites which conveyed meltwater of

subglacial origin evidenced the greatest degree of rock: water contact with weathering components. The linear 1:1 trend between $Ca^{2+}+Mg^{2+}$ and TDIC represents pure carbonate weathering, however the strong deviation of Sólheimajökull waters from this indicated greater amounts of TDIC are acquired than carbonate weathering can account for. Therefore, the additional TDIC source cannot be of a pure carbonate (hydrothermal calcite) origin, supporting additional sources, potentially basaltic minerals, volcanic fluids or oxidation of organic matter where redox conditions allow.
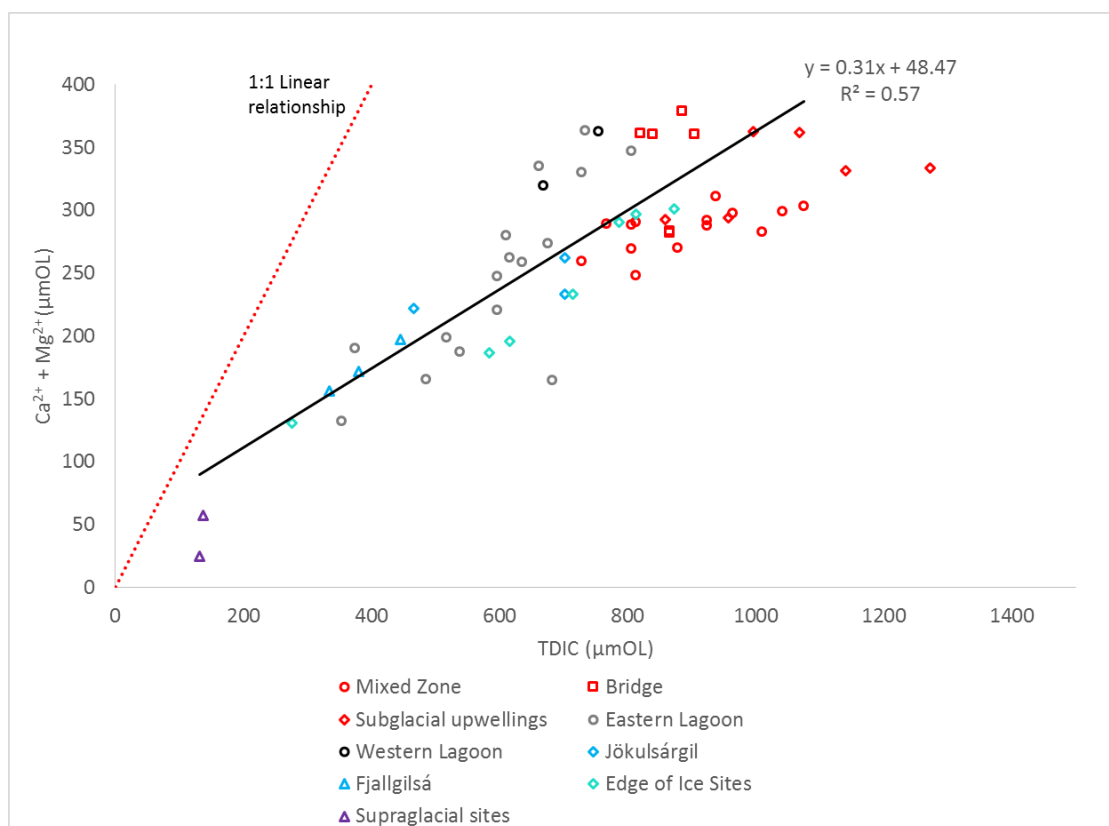
Figure 5.5: Bi-plot of TDIC and combined Ca^{2+} + Mg^{2+} concentrations for Spring 2014

Linear trend does not include rivers of external catchment origin, as these do not represent weathering in the Sólheimajökull glacial system.

Summertime Ca^{2+} + Mg^{2+} and TDIC values also represented a linear positive relationship (R^2 value of 0.82). Again supraglacial waters had the lowest $Ca^{2+}+Mg^{2+}$ and TDIC values. Waters which have been conveyed subglacially had higher

$Ca^{2+}+Mg^{2+}$ and TDIC concentrations. A linear intercept of 23.69, accompanied by an evident deviance from the 1:1 trend line, indicated that TDIC is acquired in excess of Ca^{2+} and Mg^{2+}.
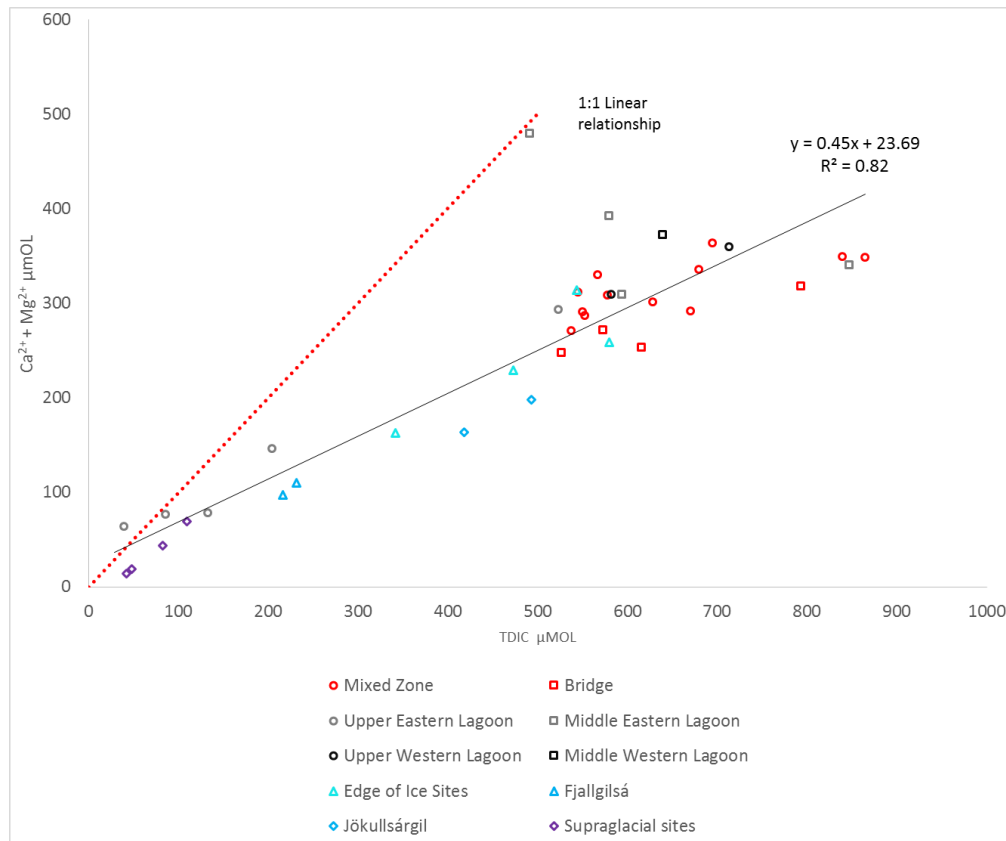
Figure 5.6: Bi-plot of TDIC and combined $Ca^{2+} + Mg^{2+}$ concentrations for Summer 2013

Linear trend does not include rivers of external catchment origin, as these do not represent weathering in the Sólheimajökull glacial system.

Additional basaltic TDIC components can be estimated using provenance calculations outlined in Hodson et al (2000) whereby 1.58 times the amount of Si in meltwaters can offer an estimate of the relative percentage of TDIC supplied from weathering of Silicates (Basalt). However, this is on the basis that weathering here was the same as the global average and all solute is representative of dissolution and not subject to secondary precipitation. The remaining percentage TDIC (calculated by difference) could be sourced from weathering of hydrothermal calcites within the catchment.

Calculation of TDIC sourced from hydrothermal calcites can be undertaken based on the assumption that $Ca^{2+}+Mg^{2+}$: TDIC = 1. This allowed budget closure in slight excess of measured TDIC concentrations and likely reflected the additional source of Ca^{2+} and Mg^{2+} released during basalt silicate weathering. Percentage contributions indicated that TDIC in Sólheimajökull meltwaters was largely supplied by weathering of hydrothermal calcite (approximately 70 % of TDIC load), with approximately 30 % obtained from weathering of basalt minerals (as shown in table 5.4). The percentages from each TDIC source did vary depending upon the environment through which the waters had been routed, apart from Fjallgilsá and Jökulsárgil waters which consistently displayed the lowest contribution from a carbonate weathering component.

Site	Spring 2014		Summer 2013	
	%TDIC from Silicate Weathering (Basalt)	%TDIC from Carbonate Weathering	%TDIC from Silicate Weathering (Basalt)	%TDIC from Carbonate Weathering
Mixed Zone	**23.92** (1.24) Min= 21.62 Max= 25.21 *n=13*	**76.08** (1.24) Min= 74.79 Max= 78.38 *n=13*	**26.79** (2.69) Min= 21.88 Max= 30.70 *n=12*	**73.21** (2.69) Min= 69.30 Max= 78.12 *n=12*
Bridge	**22.43** (3.76) Min= 17.43 Max= 27.45 *n=6*	**77.57** (3.76) Min=72.55 Max= 82.57 *n=6*	**29.93** (2.36) Min= 26.85 Max= 32.50 *n=4*	**70.07** (2.36) Min= 67.51 Max= 73.15 *n=4*
Subglacial Upwellings	**20.80** (2.83) Min= 16.20 Max= 22.87 *n=6*	**79.20** (2.83) Min= 77.13 Max= 83.80 *n=6*	Not Sampled	
Edge of Ice Sites	**22.13** (3.15) Min= 15.36 Max= 24.95 *n=7*	**77.87** (3.15) Min= 75.04 Max= 84.64 *n=7*	**25.15** (4.00) Min= 18.94 Max= 29.87 *n=4*	**74.85** (3.96) Min= 70.13 Max= 81.06 *n=4*
Eastern Lagoon	**22.37** (2.33) Min= 18.28 Max= 26.41 *n=16*	**77.63** (2.33) Min= 73.59 Max= 81.72 *n=16*	**26.49** (3.88) Min= 19.96 Max= 33.00 *n=10*	**73.51** (3.88) Min= 67.00 Max= 80.04 *n=10*
Western Lagoon	**18.51** (0.87) Min= 16.89 Max= 19.40 *n=6*	**81.49** (0.87) Min= 80.60 Max= 83.11 *n=6*	**23.86** (0.40) Min= 23.30 Max= 24.24 *n=3*	**76.14** (0.40) Min= 75.76 Max= 76.70 *n=3*
Fjallgilsá	**35.16** (0.24) Min= 34.82 Max= 35.36 n=3	**64.84** (0.24) Min= 64.64 Max= 65.17 *n=3*	**48.29** (-) Min= 47.80 Max= 48.80 *n=2*	**51.71** (-) Min= 52.20 Max= 51.20 *n=2*

Jökulsárgil	26.75 (0.34) Min= 26.27 Max= 27.03 *n=3*	73. 25 (0.34) Min= 72.97 Max= 73.73 *n=3*	32.80 (-) Min= 29.50 Max= 31.13 *n=2*	68.87 (-) Min= 67.2 Max= 70.5 n=2
Supraglacial Sites	1.46 (-) Min= 0 Max= 2.93 *n=2*	98.53 (-) Min= 97.07 Max= 100 *n=2*	28.38 (4.32) Min= 2.22 Max= 34.38 *n=4*	71.62 (4.32) Min= 65.63 Max= 77.78 *n=4*

Table 5.4: Spring 2014 and Summer 2013 percentage contributions from silicate and carbonate weathering

A detailed outline of the data generating these percentages (in equivalent units) and the adaptation of equations from Hodson et al (2000) can be found in Appendix 3.

5.3.2. The relative importance of weathering via sulphide oxidation and carbonation

Relationships between TDIC and SO_4^- offer insight into weathering mechanisms supplying TDIC to Sólheimajökull meltwaters. Given the pH range at Sólheimajökull (pH = 6.4-10.3), most TDIC will exist as HCO_3^- and potentially some as CO_3^{2-}. The C Ratio of Brown et al. (1996) investigates weathering pathway via the following relationship between HCO_3^- and SO_4^{2-} where units of concentration are in equivalents:

$$HCO_3^- \ / (HCO_3^- + SO_4^{2-}) \hspace{3cm} (equation\ 14)$$

A ratio of 1 signifies weathering by carbonation reactions (understood more widely to represent a source of protons from any source other than sulphide oxidation), whilst a ratio of 0.5 indicates SO-CD weathering processes (Brown, 2002; Brown et al., 1996).

The S Ratio (also known as Sulphate Mass Fraction or SMF) used by Tranter et al. (1997) is indicative of weathering via SO-CD through the following relationship:

$$SO_4^2 / (SO_4^{2-} + HCO_3^-) \hspace{3cm} (equation\ 15)$$

A ratio of 0.5 (where units of concentration are in equivalents) indicates weathering proceeds via SO-CD whilst a ratio of 0 is associated with protons from alternate sources (potentially carbonation of carbonates and silicates).

S ratios for Spring and Summer are close to 0, demonstrating TDIC acquisition cannot be accounted for solely through SO-CD, but infers acquisition of TDIC via alternative proton sources. Inter seasonal differences highlight a slight summertime increase in S ratios, particularly in proglacial Waters. Supraglacial and external sources demonstrate consistency between seasons.

	S Ratio (Tranter et al, 1997) *also known as SMF* 0.5= SO-CD 0=Carbonation		
Site	**Spring**	**Summer**
Proglacial Waters	0.02 (1SD=0.01) *n=42*	0.08 (1SD= 0.06) *n=29*
Subglacial Waters	0.02 (1SD=0.00) *n=6*	Not Sampled
External Riverine Inputs	0.02 (1SD=0.00) *n=6*	0.03 (1SD= 0.00) *n=4*
Supraglacial Inputs	0.01 (-) *n=2*	0.01 (1SD= 0.00) *n=4*

Table 5.5: S ratios for Spring and Summer (units of concentration are equivalents)

These low S ratio values support the assertion that the majority of TDIC is acquired by processes other than SO-CD. Whilst traditionally assumed to represent 'carbonation' reactions (the drawdown and dissolution of atmospheric CO_2 as a source of protons for rock weathering), in Iceland, the source of protons to drive weathering could be associated with drawdown of atmospheric CO_2, subglacial emission of volcanic CO_2, or protons supplied through dissolution of acidic gases

from subglacial geothermal fields. When displayed as a bi-plot of TDIC and SO_4^- concentration this limited role of SO-CD as a proton source for TDIC production manifests itself as a positive linear relationship, with a large positive intercept. During Spring, R^2 values of 0.60 reflect a transition from low TDIC and SO_4^- concentration supraglacially sourced waters to relatively higher acquisition at the Mixed Zone. Waters emanating from subglacial sources plot slightly off this trend, with highest TDIC values but not the highest SO_4^- concentrations.
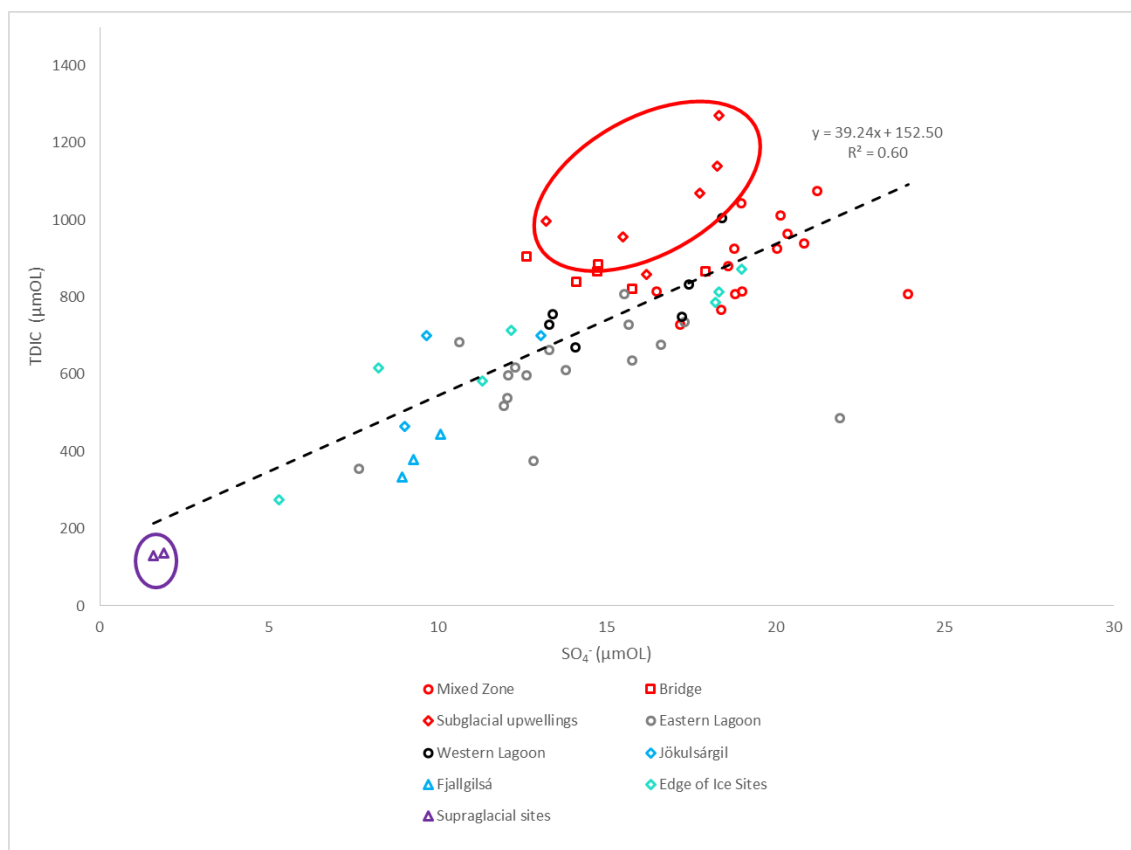
Figure 5.7: Bi-plot of TDIC and SO_4^{2-} concentrations for Spring 2014

The red oval outlines subglacial waters, whilst the purple oval represents supraglacial waters

Large increases in SO_4^- during summer are the main driver of increased S ratios in proglacial waters. Differences in SO_4^- concentration result in two main clusters of data, outlined by black and red ovals (Figure 5.8). The majority of data has SO_4^-

values sub 80µmol, placing it within the black cluster. Here, lowest concentrations of TDIC and SO_4^- are found in supraglacial sources whilst highest TDIC and elevated SO_4^- concentrations are present in proglacial lagoon and river samples. A weak correlation exists between these waters represented by an R^2 value of 0.48, consistent with a mixing trend between high rock: water contact and low rock: water contact sources. A large positive intercept of 237.24 represents a source/supply of TDIC independent of SO_4^-. Samples within the red cluster also exhibit a positive relationship between TDIC and SO_4^- (R^2 value of 0.88). However, a lower intercept and greater SO_4^{2-} concentrations indicate a periodic influence of sulphide oxidation.
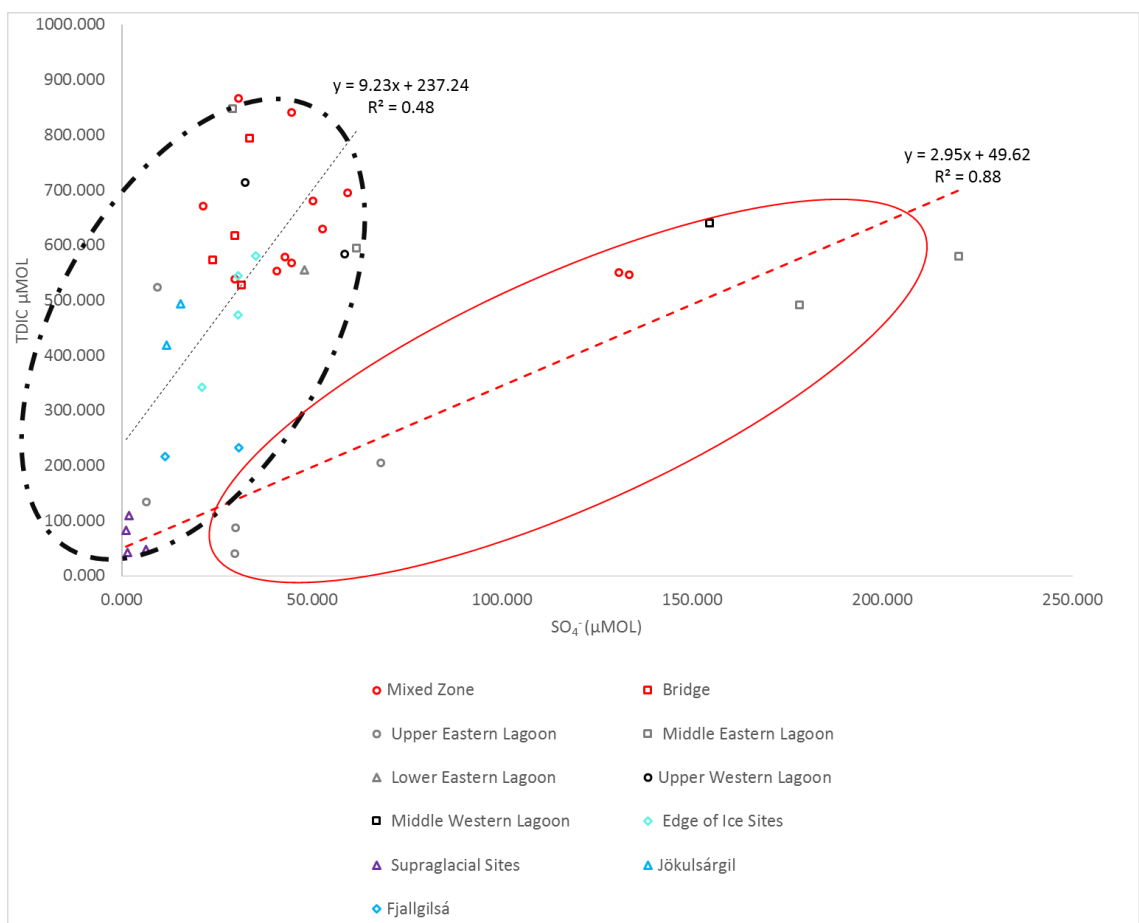
Figure 5.8: Bi-plot of TDIC and SO_4^{2-} concentrations for Summer 2013

Supraglacial samples are incorporated in both linear trend lines

5.3.3. Summary of weathering mechanisms in the Sólheimajökull subglacial system

1. Relationships between TDIC and Ca^{2+} + Mg^{2+} indicate that hydrothermal calcite dissolution cannot solely account for all the TDIC in Sólheimajökull proglacial waters.

2. Low S ratios and solute partitioning indicates that large quantities of TDIC are supplied from hydrothermal calcite weathering with an additional 20-30% from silicate sources.

3. Low S ratios suggest SO-CD plays a minimal role in the supply of protons for weathering. Alternative proton sources utilise the drawdown of atmospheric CO_2, volcanic CO_2 injected subglacially, or the dissolution of acidic gases effusing from subglacial geothermal zones.

4. Based on findings so far TDIC is supplied from basaltic bedrock containing both silicate and hydrothermal calcite minerals. The contribution of both minerals to the TDIC pool is approximately: 70 % hydrothermal calcite and 30 % silicate weathering. It is weathered in the subglacial realm utilising protons supplied from sources other than SO-CD. The remainder of this chapter will attempt to reconcile the potential proton sources and use stable isotopes to support these preliminary findings.

5.4. pCO_2 as an indicator of subglacial weathering at Sólheimajökull

Previous evidence (sections 5.21 to 5.3.3) has suggested production of dissolved inorganic carbon from basaltic bedrock or accessory hydrothermal calcite by mechanisms other than SO-CD. This could be due to carbonation reactions, with CO_2 obtained from atmospheric, geothermal or even microbial origin, or direct acid hydrolysis utilising a proton source obtained from low pH geothermal waters.

The partial pressure of meltwater CO_2 (pCO_2) reflects the rate at which CO_2 diffuses in/out of a solution in relation to the chemical weathering environment. When

compared to atmospheric equilibrium ($10^{-3.5}$ atmospheres) pCO_2 can offer insight into weathering dynamics. Deviation from atmospheric pCO_2 values indicates disequilibrium between weathering rates, gas exchange and proton supply. pCO_2 conditions above atmospheric equilibrium values indicates that proton supply exceeds the rate of consumption and CO_2 diffuses out of solution, making the river a net source of CO_2. Where pCO_2 values are lower than atmospheric the demand for protons exceeds CO_2 diffusion and meltwaters become a net sink of CO_2 (Singh et al., 2012).

pCO_2 values at Sólheimajökull were mostly above atmospheric equilibrium indicating the potential for CO_2 release from meltwaters in the proglacial zone. Spring subglacial waters exhibited highest pCO_2 values with an average of $10^{-1.94}$ (1SD= 0.23) accompanied by large TDIC concentrations. Little connectivity to the atmosphere can be expected during early Spring subglacial drainage, inferring a subglacial proton source. Supraglacially sourced waters varied in pCO_2 despite having consistent TDIC concentrations.
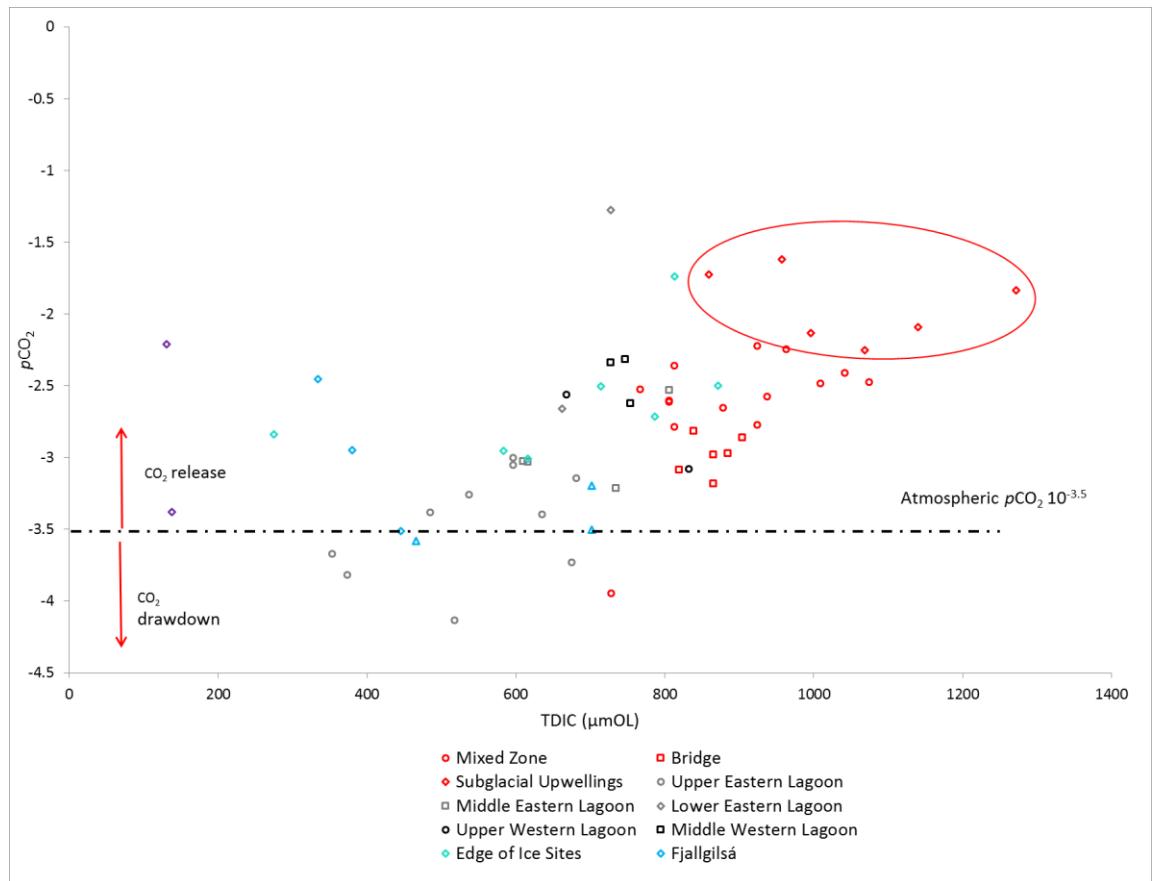
Figure 5.9: Relationship between pCO_2 and TDIC concentrations during Spring.

The dashed line represents atmospheric pCO_2

Summertime pCO_2 values were greater than those observed in Spring, likely due to the lower pH of summer discharge. Highest values above 10^{-2} atmospheres were in keeping with pCO_2 values observed in Spring subglacial upwelling waters. Supraglacial sites and waters of external catchment origin exhibited near atmospheric or sub atmospheric pCO_2 values. Where TDIC concentrations increased, indicative of subglacial drainage, pCO_2 values increasde and meltwaters became a net source of CO_2.
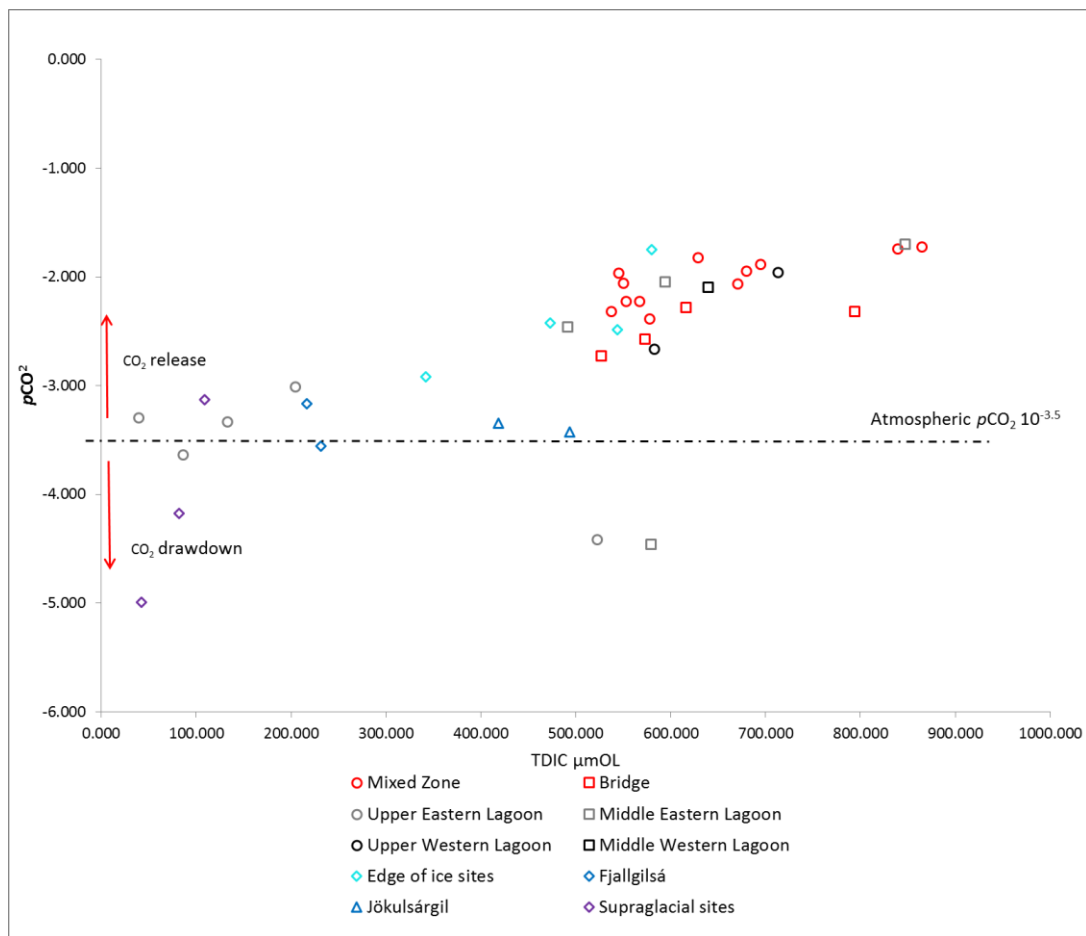
Figure 5.10: Relationship between pCO_2 and TDIC concentrations during Summer.

The dashed line represents atmospheric pCO_2

5.4.2. Summary of investigation of *pCO_2* values in Sólheimajökull proglacial waters

1. *pCO_2* values of waters conveyed subglacially are above $10^{-3.5}$ atmospheres suggesting proton supply exceeded proton consumption during subglacial weathering, hence the low pH values observed in subglacial waters.

2. This disequilibrium prevailed in waters with high TDIC concentrations. Since ionic analysis also indicated high solute concentrations (Chapter 4) and therefore high weathering rates in the subglacial realm, excess protons must originate from a subglacial source.

5.5. Isotopic analysis of TDIC at Sólheimajökull

5.5.1. Isotopes as Confirmation of TDIC Source and Supply Processes at Sólheimajökull

Investigation of TDIC sources and supply mechanisms has suggested a hydrothermal calcite source alongside contributions from basaltic minerals weathered via carbonation (or proton sources other than SO-CD) in the subglacial realm. Confirmation of these sources and processes can be investigated using isotopic methods. Environmental isotopes offer a unique tracer of TDIC source and can be used to distinguish between TDIC end members within the Sólheimajökull proglacial system.

$CaCO_3$ of accessory hydrothermal carbonates can offer a TDIC source, however investigation at Sólheimajökull is limited. Carswell (1963) found calcite present in discrete Pleistocene lava units within the Sólheimajökull valley but makes no reference to potential accessory calcite. Furthermore, carbonate charged waters have previously been identified at Sólheimajökull, which has been assumed to be linked to geothermal degassing (Lawler et al., 1996). However constant background carbonate has been overlooked. Rocks containing carbonate inclusions are abundant across the Sólheimajökull proglacial area and range in isotopic value from $\delta^{13}C_{calcite} =$ -7.61‰ to +3.35‰ with an average of -0.90‰ (1SD=2.53, n=27). Carbonate inclusions have been proven to be in the form of calcite, based on Thermo Gravimetric Analysis (TGA) analysis (Gristwood, unpublished MSc dissertation).

$\delta^{13}C_{TDIC}$ values across the Sólheimajökull proglacial area showed values ranging from -6.85 to -0.45‰ with supraglacial waters extending beyond this to lighter values. Comparison of Sólheimajökull $\delta^{13}C_{TDIC}$ values to other known environmental isotopic signatures is presented in figure 5.11. Lightest $\delta^{13}C_{TDIC}$ signatures at Sólheimajökull were associated with supraglacial water sources, with seasonal averages of -5.76‰ and -6.85‰ (1SD= 2.15) for Spring and Summer respectively. This closely aligned

with TDIC from atmospheric CO_2 origins and known calcite values. Waters emanating from subglacial sources and proglacial lagoon and river waters had $\delta^{13}C_{TDIC}$ values which closely align with signatures found within hydrothermal calcites from the Sólheimajökull forefield. In addition, these also fell within the isotopic range of Icelandic rift basalts, further supporting a basaltic source containing accessory hydrothermal calcites. From isotopic analysis, geothermal supply of TDIC from Icelandic geothermal fluids cannot be ruled out, however analysis of TDIC percentage contributions (Chapter 5.3.1) indicated TDIC can be accounted for by rock weathering.
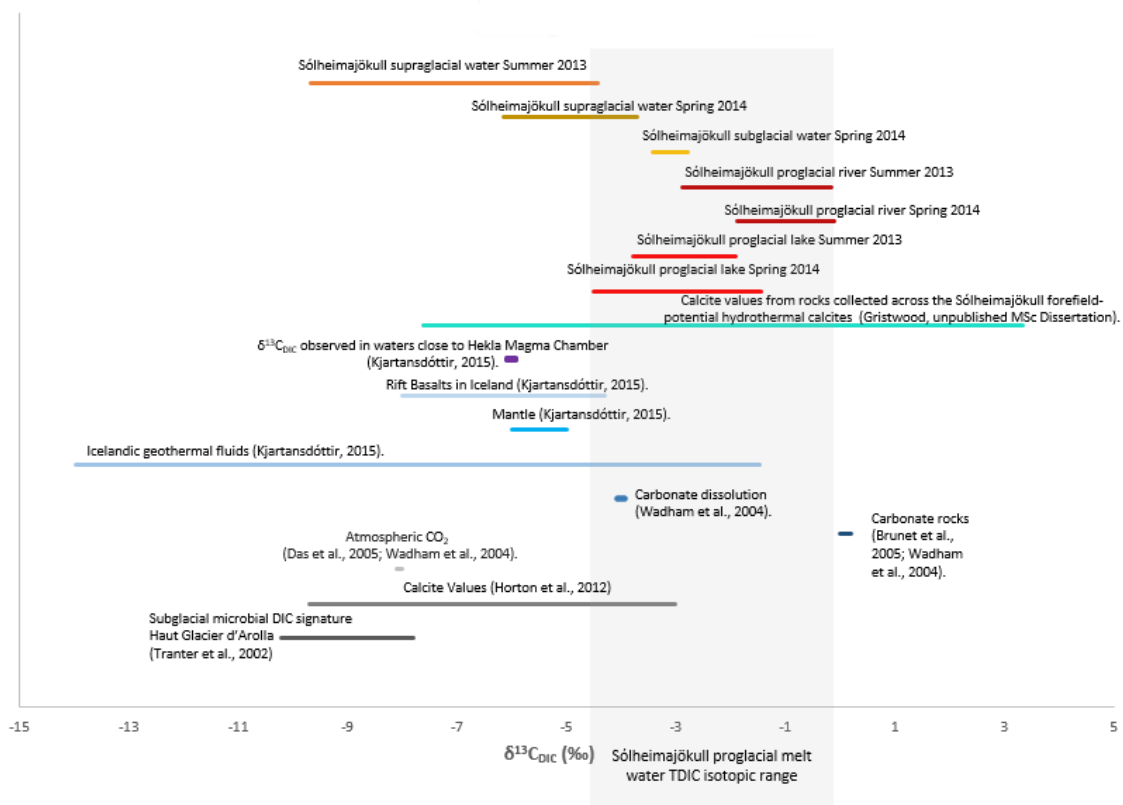
Figure 5.11: comparisons of Sólheimajökull $\delta^{13}C$ range to known isotopic values from glacial studies

There are three main inputs of water to the Sólheimajökull catchment: subglacial, supraglacial and waters of external origin. Each displays a distinctive isotopic

signature and varying TDIC concentrations. Supraglacial waters had the lowest TDIC concentrations and the lightest average isotopic signatures of -5.76‰ in Spring and -6.85‰ (1SD=2.15) in Summer. In comparison subglacial inputs to the system had the highest TDIC concentrations and also displayed mid-range $\delta^{13}C_{TDIC}$ average values of -3.22‰ (1SD= 0.22). External inputs varied in TDIC concentration and $\delta^{13}C$ value. Jökulsárgil which has headwater origins from Jökulsárgilsjökull displayed isotopically light $\delta^{13}C_{TDIC}$ values of -4.07‰ in Spring and -6.70‰ in Summer. Fjallgilsá, which is of a high grassland origin also had relatively low TDIC concentrations and heavier $\delta^{13}C_{TDIC}$ values of -2.56‰ in Spring and +2.12‰ in Summer.

TDIC values within the proglacial lagoon demonstrated an East/West split with higher TDIC concentrations at western sampling sites. Average $\delta^{13}C_{TDIC}$ values did not follow such a clear split, with variability between sites and seasons. Lagoon outputs measured at the Mixed Zone indicated increases in TDIC concentrations and enrichment in $\delta^{13}C_{TDIC}$ in comparison to lagoon values. Further enrichment was evident as water exits the catchment via the Jökulsa á Sólheimasandi, with heaviest $\delta^{13}C_{TDIC}$ values recorded at the Bridge site. In contrast, TDIC concentrations did not exhibit significant downstream changes.

Site	Season	TDIC (μMOL)	$\delta^{13}C_{DIC}$ ‰
Mixed Zone	Spring 2014	892.07 (107.08) *n=14*	-1.22 (0.33) *n= 10*
	Summer 2013	642.52 (108.11) *n=12*	-2.54 (0.21) *n= 7*
Bridge	Spring 2014	863.15 (30.66) *n=6*	-0.5 (...) n=2
	Summer 2013	627.47 (101.05) *n=4*	-0.45 (...) n=2
Subglacial upwellings	Spring 2014	1048.89 (145.47) *n=6*	-3.22 (0.22) *n=6*
	Summer 2013	Not Sampled	
Edge of Ice Sites	Spring 2014	665.86 (201.16) *n=7*	-2.99 (0.54) *n=6*
	Summer 2013	484.64 (90.94) *n=4*	-3.96 (0.17) *n=4*
Upper Eastern Lagoon	Spring 2014	545.42 (115.21) *n=10*	-3.68 (0.52) *n=5*
	Summer 2013	197.30 (171.73) *n=5*	-3.33 (0.33) *n=3*
Middle Eastern Lagoon	Spring 2014	691.61 (95.53) *n=4*	-2.22 (0.53) *n=4*
	Summer 2013	627.94 (132.49) *n=4*	-2.97 (...) n=2
Lower Eastern Lagoon	Spring 2014	694.89 (46.35) *n=2*	-2.76 (...) n=2
	Summer 2013	555.6 (...) n=1	Not Sampled
Upper Western Lagoon	Spring 2014	834.74 (167.18) *n=3*	-3.73 (...) n=2
	Summer 2013	648.05 (...) n=2	-1.9 (...) n=1
Middle Western Lagoon	Spring 2014	742.96 (13.65) *n=3*	-2.22 (0.50) *n=3*
	Summer 2013	639.76 (...) n=1	-2.6 (...) n=1
Fjallgilsá	Spring 2014	386.78 (56.01) *n=3*	-2.56 (...) n=2
	Summer 2013	224.25 (...) n=2	-2.12 (...) n=2
Jökullsárgil	Spring 2014	622.78 (136.25) *n=3*	-4.07 (...) n=2
	Summer 2013	455.95 (...) n=2	-6.7 (...) n=2
Supraglacial Sites	Spring 2014	134.39 (...) n=2	-5.76 (...) n=2
	Summer 2013	70.42 (27.14) *n=4*	-6.85 (2.15) *n=3*

Table 5.5: TDIC and $\delta^{13}C_{TDIC}$ isotopes across the Sólheimajökull proglacial area Spring 2014 and Summer 2013

Bi-plots of $\delta^{13}C_{TDIC}$ and TDIC concentration reflected a transition from supraglacial waters with low TDIC values and lighter isotopic signatures close to atmospheric, to highest TDIC concentrations and more enriched $\delta^{13}C$ isotopes in waters across the proglacial lagoon and river. Subglacial waters demonstrated a slight deviation from this trend with lighter $\delta^{13}C_{TDIC}$ signatures accompanied by high TDIC values. These two end members are pivotal in the characteristics of TDIC. Enriched $\delta^{13}C_{TDIC}$ signatures evident at the Mixed Zone and Bridge were likely a product of fractionation. Laboratory experiments demonstrate a kinetic fractionation during the initial stages of calcite dissolution, albeit limited to a 2 per mille enrichment in ^{12}C

over 24 hours (Gristwood, unpublished MSc Dissertation). Similarly Skidmore et al. (2004) note that carbon fractionation results in an initial enrichment of ^{12}C until equilibrium is achieved. Comparatively lighter isotopic signatures observed in subglacial waters, alongside above atmospheric pCO_2 values, may suggest early stage carbonate dissolution, where all protons are not utilised and equilibrium is not achieved. The greatest enrichment at the Bridge could be representative of the completion of in stream carbonate reactions and isotopic equilibrium.
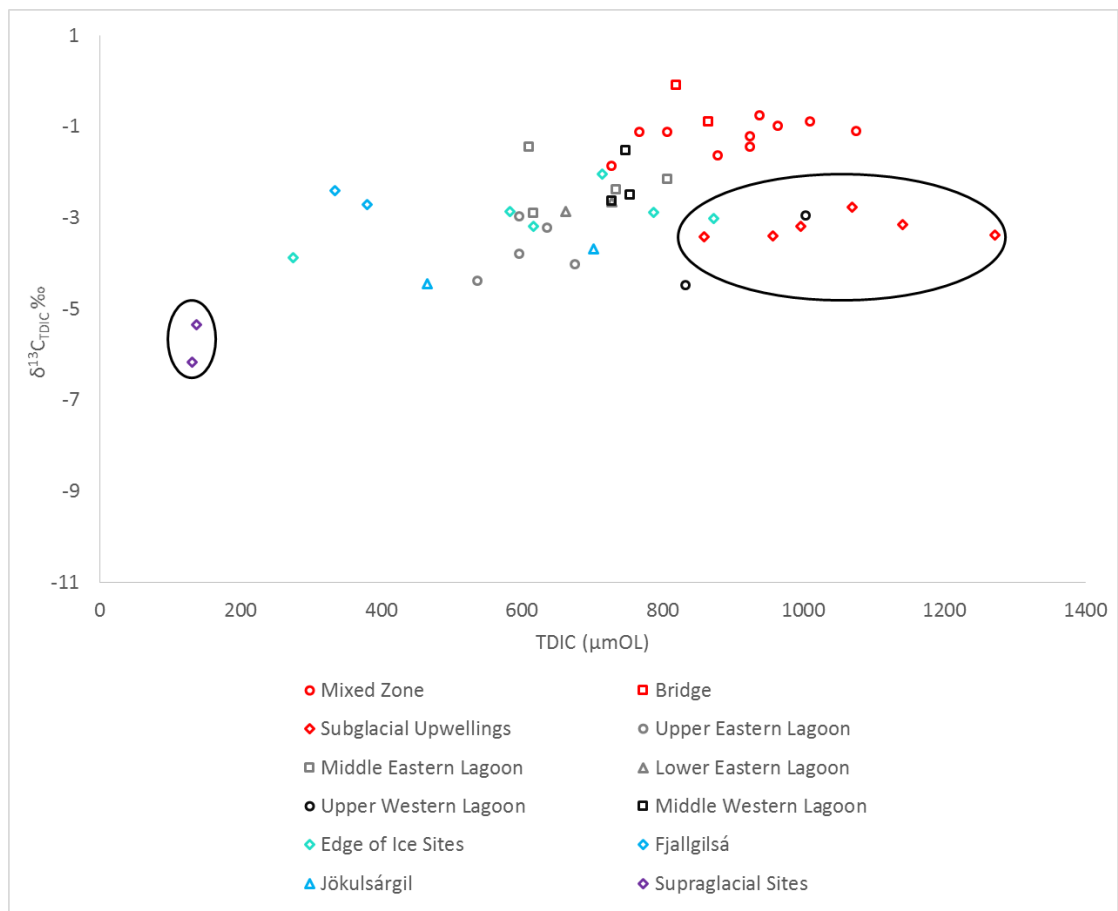
Figure 5.12: Bi-plot of $\delta^{13}C_{TDIC}$ and TDIC concentration during Spring 2014

Subglacial upwelling waters are within the black oval

Similarly, during Summer 2013 a split was observed between high and low TDIC concentrations, accompanied by isotopic enrichment downstream. $\delta^{13}C_{TDIC}$ signatures exhibited greater fluctuations than Spring, with a large variability in supraglacial samples. Upper Eastern Lagoon meltwaters demonstrated $\delta^{13}C_{TDIC}$ and TDIC concentrations similar to those observed in supraglacial waters, reflecting a heightened importance of these sources during periods of extensive surface run off.
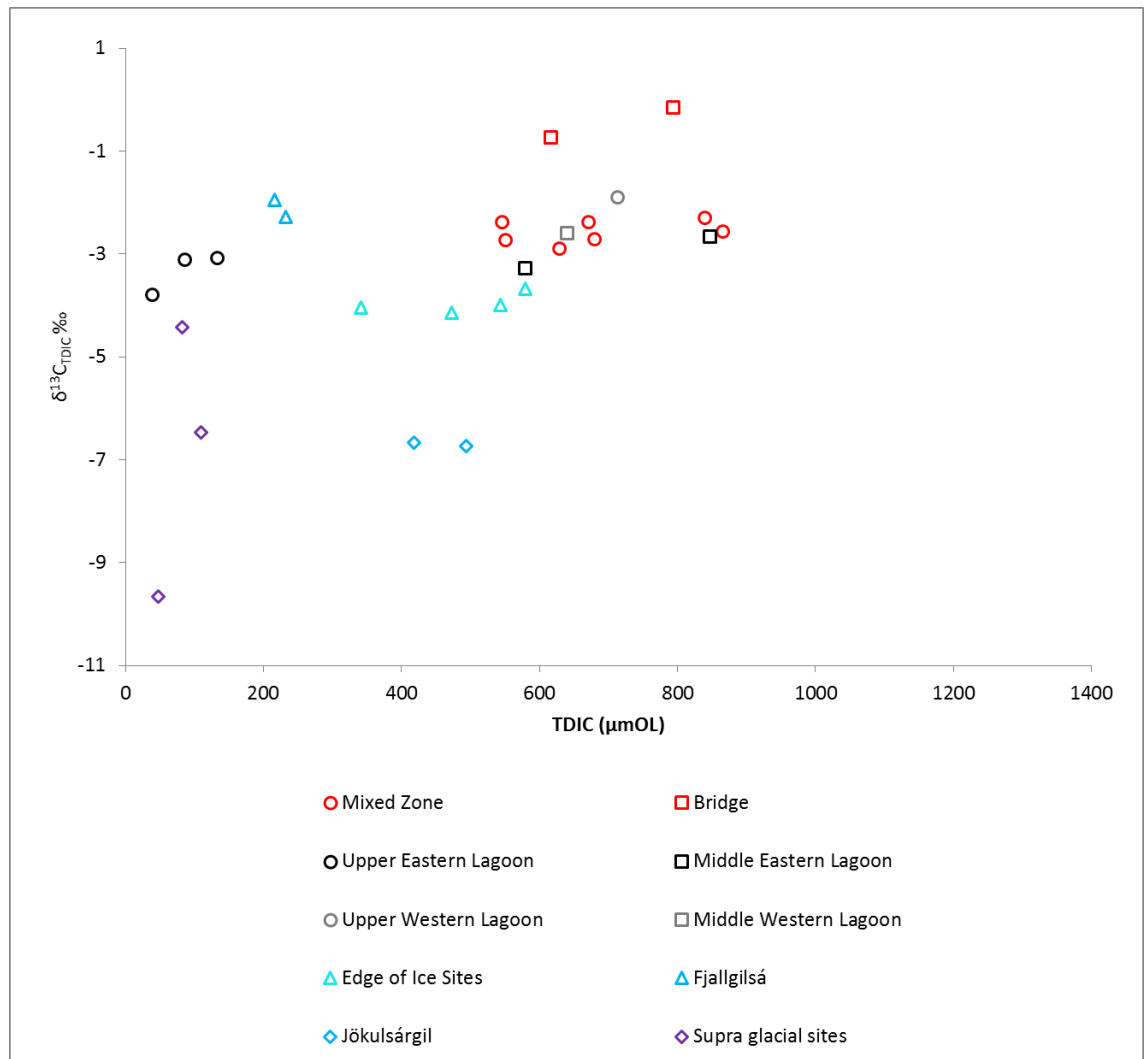
Figure 5.13: Bi-plot of $\delta^{13}C_{TDIC}$ and TDIC concentration during Summer 2013

The broad range of isotopic values within the proglacial lagoon encompassed those discharging from the subglacial upwelling and those sourced from Jökulsárgil.

However, supraglacial $\delta^{13}C_{TDIC}$ values was outside the range of those in the lagoon, indicating this source of TDIC to be of minimal impact upon lagoon signatures. There was progressive enrichment of $\delta^{13}C_{TDIC}$ signatures as meltwaters were conveyed through the catchment between lagoon and Bridge sampling sites.
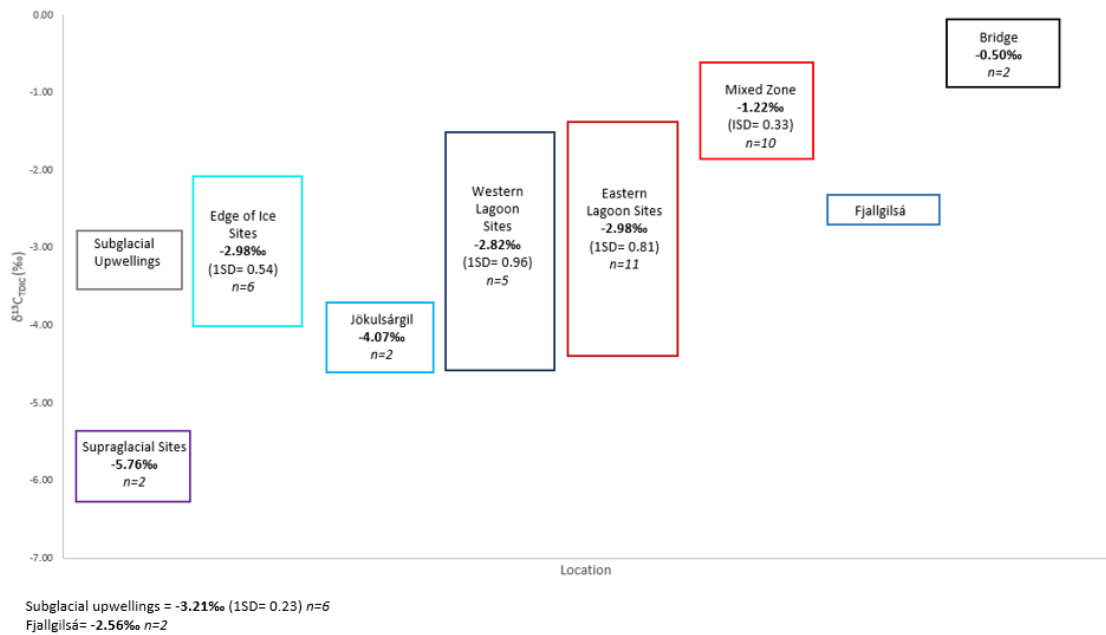
Figure 5.14: Changes in $\delta^{13}C_{DIC}$ (‰) across the Sólheimajökull proglacial foreland during Spring 2014

During Summer, supraglacial sites exhibited a far larger range of $\delta^{13}C_{TDIC}$ values, but remained isotopically distinct from lagoon waters. The range of proglacial lagoon values reflected an East/West split between isotopic signatures with heaviest $\delta^{13}C_{TDIC}$ values found at Western sites. Additionally, lighter Eastern Lagoon sites displayed similarities to Edge of Ice Sites. Values found at the Mixed Zone represented a mix of East and West lagoon values. Significant downstream enrichment was apparent at the Bridge sampling site consistent with the spring season. Rivers of non-glacial origin appear to have limited influence upon downstream $\delta^{13}C_{TDIC}$ values.

Edge of Ice Sites= **-3.96‰** (1SD= 0.17) *n=4*
Fjallgilsá= **-2.12‰** *n=2*
Jökulsárgil= **-6.70‰** *n=2*
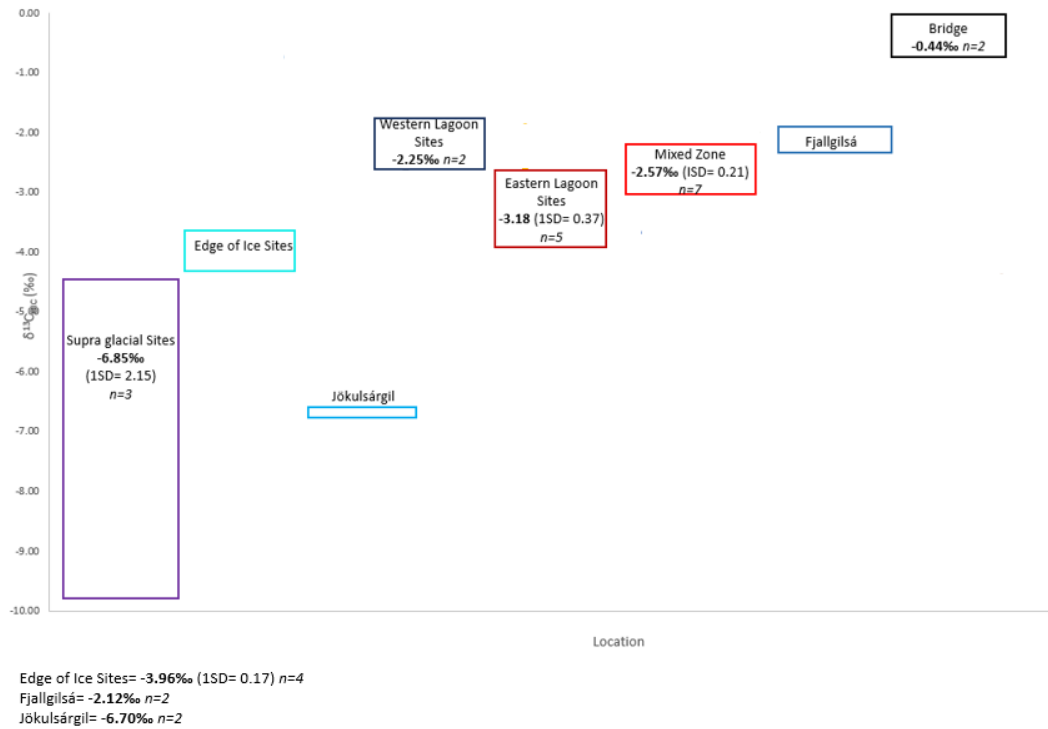
Figure 5.15: Changes in $\delta^{13}C_{DIC}$ (‰) across the Sólheimajökull proglacial foreland
during Summer 2013

5.5.2. Summary of $\delta^{13}C_{TDIC}$ investigation of Sólheimajökull proglacial waters

1. $\delta^{13}C_{TDIC}$ analysis of Sólheimajökull meltwaters support signatures which lie within the range of carbon isotope values measured within hydrothermal calcites found across the Sólheimajökull proglacial forefield. Geochemical and isotopic evidence is therefore consistent with hydrothermal calcites being a key source of TDIC at Sólheimajökull.

2. Low TDIC abundance in supraglacial waters and isotopic values enriched in ^{12}C generate little impact on $\delta^{13}C_{TDIC}$ signatures in bulk proglacial meltwaters, but likely originate from kinetic fractionation during the early stages of calcite dissolution, and/or dissolution of atmospheric CO_2 in supraglacial waters.

3. $\delta^{13}C_{TDIC}$ enrichments are evident downstream with heaviest values observed at the Bridge despite little change in TDIC concentration, likely a result of

isotopic equilibrium being approached during carbonate dissolution or pCO$_2$ change.

5.6. Discussion of TDIC sources at Sólheimajökull

5.6.1. Identifying potential sources of TDIC to Sólheimajökull proglacial meltwaters

High TDIC concentrations dominate the solute load of meltwaters at Sólheimajökull. This is not uncommon in Iceland, where rivers drain areas of geologically young and easily weathered volcanic rocks (Flaathen et al., 2009). The geology of Southern Iceland is dominated by basalts and acidic volcanic rocks providing siliceous mineral inputs of major ions, as well as acting as a potential rock source of TDIC (Carswell, 1983; Gislasson et al., 1996; Flaathen et al., 2009). However, basaltic minerals are not the only source of TDIC to glacial meltwaters. Hydrothermal calcite inclusions within basaltic bedrock, and in some cases almost pure hydrothermal calcite rocks are common in Iceland. These are formed by hydrothermal alteration of basaltic flows within large volcanic centres such as the Katla geothermal system which resides beneath Sólheimajökull (Kristjánsson, 2012). Due to high solubility and fast dissolution rates, leaching of disseminated calcite can provide an important TDIC source (Brown, 2002; Nowak and Hodson, 2013). Even at trace amounts, hydrothermal calcite inclusions can dominate water chemistry, for example at Fjallsjökull, Vatnajökull, where calcite dissolution provides much of the bulk solute load, despite abundance below 3% in the subglacial host rock (Georg et al., 2007).

Despite limited reporting of carbonates in the Sólheimajökull region, consideration of geochemical and isotopic evidence points towards a hydrothermal calcite TDIC source. This is supported by high ratios of Ca^{2+}: Si and Ca^{2+}: Mg^{2+} indicating elevated acquisition of Ca^{2+} which cannot be accounted for by weathering of primary basaltic minerals. Mobilities and abundances of Ca^{2+} and Si during basaltic mineral weathering are similar therefore, weathering of a purely basaltic mineral component at Sólheimajökull can be expected to yield constant riverine Ca^{2+}: Si concentrations

with a ratio of 1, or potentially less for silica rich basalts. High Ca^{2+}: Si molar ratios predominantly above 2 in Spring demonstrate a non basalt mineral contribution of Ca^{2+}. Furthermore, during the summer season, Ca^{2+}:Mg^{2+} molar ratios in meltwaters from Sólheimajökull frequently exceed expected ratios obtained from leaching of pure basalt (0.9 – 3) (Georg et al., 2007). Basaltic minerals such as Plagioclase and Olivine are rich in both Ca^{2+} and Mg^{2+} which have been shown to weather congruently (Georg et al., 2007) therefore, elevated molar ratios again reflect increased acquisition of Ca^{2+}. Given that this is not matched by increases in Mg^{2+} once again this cannot be accounted for by a basaltic primary mineral source.

Potential sources of additional Ca^{2+} in riverine run off could be linked to atmospheric deposition or sourced from trace amounts of hydrothermal calcite within the subglacial realm (Georg et al., 2007; White, 1999). An atmospheric Ca^{2+} source is unlikely to account for the concentrations observed in the glacial meltwaters, therefore hydrothermal calcites, which are typically enriched in Ca^{2+} relative to Mg^{2+} and Si geochemically represent the most likely contributor. This is not unheard of in glacial settings with hydrothermal calcite contributions observed as the source of increased Ca^{2+}: Mg^{2+} ratios at Kangelussuaq, Greenland (Wimpenny et al., 2010). This is further supported by estimation of carbonate and silicate sources using equations from Hodson et al (2000). These indicate that large amounts of proglacial bulk meltwater TDIC (typically around 75%) are shown to originate from carbonates- likely subglacial hydrothermal calcites. This is an essential component of carbon dynamics at Sólheimajökull. Hydrothermal calcites are magmatic in origin, meaning that dissolution of these minerals can ultimately supply mantle derived TDIC to the atmosphere (Weise et al., 2008; Jacobson et al., 2015).

However, despite Ca^{2+}:Si and Ca^{2+}: Mg^{2+} ratios being indicative of a hydrothermal calcite source, molar ratios of Ca^{2+}: Na^+ fall within the range (0.2 to 3.9) quoted for rivers draining basaltic terrain(Dessert et al., 2003). Most meltwater sources at Sólheimajökull support Ca^{2+}: Na^+ ratios <1 indicative of silicate mineral weathering.

Elevated Na^+ concentrations thereby appear to be masking this additional source of Ca^{2+} and the Ca^{2+}: Na^+ ratio is not a true end member signal, but a mixture of element sources. Previous evidence has pointed towards geothermal fluids as a source of Na^+ in the Sólheimajökull system (Lawler et al., 1996). Given that geothermal fluids contain large quantities of Na^+ in relation to Ca^{2+} (Georg et al., 2007) low molar ratios could reflect an additional supply of solutes and potentially some TDIC from subglacial geothermal systems. Streams of external catchment origin do not have any geothermal or hydrothermal calcite input and this is clearly reflected through a pure silicate weathering geochemical signal in all ion ratios studied.

Isotopic ratios further support a hydrothermal calcite source of TDIC. $\delta^{13}C_{TDIC}$ isotopic values observed in Sólheimajökull proglacial meltwaters closely align to those found in hydrothermal calcites collected from the Sólheimajökull proglacial forefield (-7.61‰ to +3.35‰). The most feasible scenario is a combination of TDIC sources, dominated by hydrothermal calcite contributions within weatherable basaltic bedrocks. This is in keeping with previous Ca^{2+} isotopic geochemistry of Icelandic waters which has identified mixing of both basaltic mineral and hydrothermal calcite sources (Jacobson et al., 2015). The relative contribution of each of these sources is likely a function of weathering rates governed by rock water contact times and hydrological configuration, further complicated by geothermal inputs which offer the potential to drive a unique subglacial weathering regime.

5.7.2. Identifying weathering Pathways of TDIC Supply

Classical drainage theories outline associations between dominant hydraulic configuration and prevailing weathering mechanism. Conventional systems demonstrate a dominance of weathering by SO-CD processes during winter and early spring when the subglacial hydraulic network is restricted to a distributed cavity system. These cavities are isolated from the atmosphere, allowing little ingress of atmospheric CO_2 and usually promoting weathering via SO-CD pathways with protons sourced from sulphide oxidation and above atmospheric pCO_2 values

(Brown, 2002; Wadham et al., 1996). Seasonal evolution of the subglacial drainage network to a discrete channelized system well connected to the atmosphere encourages the dominance of carbonation reaction mechanisms for driving TDIC supply. pCO_2 values reflect this connectivity to the atmosphere, with values expected to be in equilibrium with or lower than atmospheric pCO_2.

However, geochemical evidence from Sólheimajökull proglacial meltwaters is at odds with traditional drainage theories and thus presents a unique TDIC source and supply scenario. The winter subglacial system is partially connected to the atmosphere and locally sourced, whereas the summer system expands head wards and supports an anoxic regime fuelled by geothermal fluid inputs (Wynn et al., 2015). TDIC source attribution suggests approximately 70% of inorganic carbon is sourced from hydrothermal calcite dissolution with the remaining 30 % gained from silicate weathering. SO-CD does not serve as a proton source to fuel these weathering mechanisms and the low oxygen redox status of the waters suggests CO_2 is not being supplied from the atmosphere. Connectivity to geothermal systems can attempt to reconcile these discrepancies with subglacial CO_2 supplied by volcanic/geothermal activity in the Mýrdalsjökull basin potentially acting as proton source for weathering via carbonation as well as a feasible supply of total dissolved carbonate (Brown, 2002). The Katla subglacial volcanic system is sensitive to pressure changes associated with seasonal unloading of the snow pack and subsequent stress readjustments. This results in a well-documented volcanic history characterised by increased summer volcanism (Albino et al., 2010). Expansion of the summer arborescent drainage system allows access to these areas of increased geothermal activity, as previously recognised by high pCO_2 anoxic waters containing geothermally derived products, such as H_2S, SO_4^-, pH and total dissolved carbonate (Lawler et al. 1996; Brown, 2002; Wynn et al., 2015). Enhanced supply of geothermal protons drives vigorous weathering across large areas of the glacier bed, further enhancing pCO_2 levels and maintaining high rates of TDIC supply. Complimentary isotopic analysis and geochemical evidence supports a hydrothermal calcite source with potential overlap with $\delta^{13}C_{TDIC}$ signatures observed in Icelandic geothermal

fluids (Kjartansdóttir, 2015). Therefore based upon this, TDIC is likely predominantly sourced from hydrothermal accessory calcite contained within basalts at Sólheimajökull, with potential for secondary geothermal inputs.

Weathering of TDIC sources is not solely constrained to the subglacial realm. Downstream isotopic enrichment of $\delta^{13}C_{TDIC}$ in the Jökulsa á Sólheimasandi river system provides evidence of proglacial riverine weathering and evolution of TDIC characteristics. During Spring and Summer average isotopic values of TDIC recorded at the Bridge monitoring site are enriched compared to the rest of the catchment, whilst there is no change in downstream concentration. This downstream enrichment in TDIC isotopes is likely associated with isotopic equilibrium being approached during carbonate dissolution of suspended sediments, and hyporheic exchange (Skidmore et al., 2004). This places $\delta^{13}C_{TDIC}$ values close to those associated with weathering of catchment hydrothermal calcites. Similar $\delta^{13}C_{TDIC}$ isotopic values between Spring and Summer suggest this is a process that happens across seasons, regardless of subglacial hydrology, weathering mechanism or potential geothermal inputs. Ultimately, TDIC leaving the catchment is not representative of processes occurring subglacially. As the majority of past geochemical analysis of bulk meltwater output is recorded at the Bridge site (e.g. Lawler et al., 1996; Sigvaldasson, 1963), it is questionable how accurately this portrays carbon dynamics within the subglacial environment. Basalt mineral weathering, and particularly the dissolution of hydrothermal calcites is essential to the global carbon cycle (Jacobson et al., 2015). In Iceland magma is considered to be the only CO_2 source in geothermal systems and therefore weathering of basalt acts as a mechanism by which mantle derived CO_2 can interact with the atmosphere (Weise et al., 2008). This means that meltwaters in the Sólheimajökull proglacial system have the potential to act as a previously unrecognised mantle derived carbon source to the atmosphere.

5.8. Overall summary of TDIC findings

1.   Major ion chemistry accompanied by $\delta^{13}C_{TDIC}$ isotopic signatures indicates the potential for subglacial TDIC to be sourced from basaltic primary mineral

components as well as disseminated hydrothermal calcites supplied via carbonation mechanisms. This is supported by equations adapted from Hodson et al (2000) showing a large (around 75%) component of TDIC in proglacial bulk meltwaters is derived from carbonates, with the remainder from silicates- likely subglacial hydrothermal calcites contained within basalt.

2. Discrepancies arise between traditional theories associated with seasonal hydrology and findings at Sólheimajökull. Typically SO-CD mechanisms should dominate early season distributed drainage networks, where contact with the atmosphere is limited. Carbonation reactions should prevail in the well oxygenated discrete channelized system associated with summertime drainage configuration. Major ion chemistry at Sólheimajökull reveals a reverse trend.

3. Proglacial pCO_2 values are above atmospheric equilibrium during both seasons. Values are particularly high during summer. This suggests large quantities of free protons in the subglacial realm. This raises issues as to the proton source for carbonation, as potentially this could indicate a non-atmospheric source of CO_2.

4. TDIC source and supply at Sólheimajökull is much more complex than simple rock/mineral weathering. Subglacial geothermal activity also influences TDIC dynamics. Cyclical 'sweeping out' of the geothermal zone has been identified during summer and interactions between hydrology and geothermal proton sources could drive carbonation supply pathways and increase pCO_2.

5. $\delta^{13}C_{TDIC}$ signatures also demonstrate downstream evolution of carbonates, providing a bulk $\delta^{13}C_{TDIC}$ signature at the Bridge monitoring site that does not necessarily reflect the true TDIC dynamics existing beneath the glacier.

6. In conclusion, TDIC is reliant upon weathering of hydrothermal calcites with contributions from primary silicate minerals, both contained within the basalt bedrock of the catchment. A unique weathering regime prevails, driven by a subglacial geothermal proton supply.

6. Provenance and Fate of Dissolved Organic Carbon within the Sólheimajökull System

6.1. Introduction to dissolved organic carbon and the glacial ecosystem

Glacial environments have been shown to support viable microbial ecosystems. This ranges from supraglacial communities existing in cryoconite holes and within the snowpack, to subglacial communities adapted to survive in both oxic and anoxic areas across the glacier bed (Tranter et al., 2005; Stibal et al., 2010). Previous studies have provided evidence of viable methanogens in basal sediments of Antarctica, the Canadian Arctic and Greenland, inferring the presence of a suitable organic carbon substrate to enable methane production (Boyd et al., 2010; Wadham et al., 2008). This subglacial organic carbon (OC) can be sourced from the supraglacial and subglacial environment. Supraglacial carbon originates from a variety of inputs including in situ production in cryoconite holes, aeolian dust deposition and surface in wash from glacier margins. If hydraulic connectivity allows, supraglacial organic carbon can be transported as Dissolved Organic Carbon (DOC) or Particulate Organic Carbon (POC) via moulins and crevasses to the subglacial drainage system where it can be a notable source of organic carbon for subglacial microbial metabolism. In addition to supraglacial organic carbon, the subglacial realm acquires carbon from in situ microbial metabolism, and overridden soils, ancient vegetation and bedrock via a process known as the glacial burial hypothesis (Barker et al., 2006; Lafrenière and Sharp, 2004; Zeng, 2003).

Carbon sequestered in the subglacial realm can be transformed and released to proglacial waters (Singer et al., 2012). Microbes play a vital role in the transformation of glacial organic carbon through mechanisms of production and consumption (Dubnick et al., 2010). Processes such as methanogenesis utilise organic carbon providing a potential source of methane and carbon dioxide to the atmosphere. Additionally carbon dioxide generated is a source of acidity for weathering which will affect solute budgets (Barker et al., 2006).

Ultimately glacial drainage dictates transport of DOC from supraglacial and subglacial sources to the proglacial environment. Recycling of ancient carbon within the subglacial microbial community can export organic carbon which has a unique glacial signature, distinct from terrestrial riverine export (Bhatia, 2013). Typically concentrations of DOC are low, usually less than 2ppm, however even in low amounts this could have implications for downstream microbial life (Barker et al., 2009; Singer et al., 2011). Dissolved organic matter and in particular DOC is an important component of carbon cycling and energy budgets in stream and lake ecosystems, as well as supplying a source of organic carbon to the oceans (Smart et al., 1976). However, in spite of the importance of this organic contribution, investigation of DOC dynamics from glaciated terrain is lacking.

Concentrations and stable isotope analysis of DOC can provide valuable information on the origin, transfer and transformation of organic matter within glacial systems (Federherr et al., 2014). Abundance of DOC can provide information on glacier carbon release, although to fully constrain DOC cycling in a glacial environment including provenance, fate and bioavailability of glacial organic carbon pools additional analytical techniques to parameterise organic matter are necessary (Wynn et al., unpublished; Bhatia et al., 2010). Concentration of DOC and its fluorescent properties can bridge the gap between DOC export, and OC sources (Lafrenière and Sharp, 2004). This chapter aims to identify and attempt to parameterise organic carbon sources at Sólheimajökull via DOC concentrations, isotopic characteristics and fluorescent properties. Given that chapters 4 and 5 have indicated low subglacial redox conditions at Sólheimajökull, identification of organic matter is a vital precursor for exploring potential methanogenesis under anoxic conditions.

6.2. Results: DOC concentrations across the Sólheimajökull proglacial area

The Sólheimajökull proglacial area receives DOC from both glacial and extra glacial sources. The catchment itself is 71% glacierized, meaning a large proportion of DOC is glacially derived from supraglacial and subglacial water routing. In addition to this,

riverine inputs of external catchment origin (Jökulsárgil and Fjallgilsá) also contribute to DOC dynamics in the Sólheimajökull proglacial area. Concentration data from DOC sources during Summer 2013 is presented in table 6.1. Subglacial upwelling waters were not directly sampled during this period as summertime expansion of the subglacial drainage system results in injection of waters below the lake surface. Extensive summer melt resulted in large volumes of water on the glacier surface. Therefore, supraglacial waters were partitioned into free flowing efficient surface channels and stagnant water pools. Furthermore, summer rainfall events resulted in localised overland flows delivering DOC from the proglacial forefield. Such flows were identified on both eastern and western margins, however DOC data reported was applicable to a western overland surface flow. Overland inputs presented the highest DOC concentrations at 0.91mg/L. Lowest DOC source abundances were found in Jökulsárgil and Fjallgilsá which demonstrated concentrations of 0.65mg/L and 0.64mg/L respectively.

Site	Average Dissolved Organic Carbon (DOC) mg/L
Mixed Zone	0.73 (0.15) Min= 0.49 Max= 0.92 *n=4*
Bridge	0.53 (-) Min= 0.50 Max=0.55 *n=2*
Eastern Lagoon Sites	
Upper Eastern Lagoon	0.59 (-) Min= 0.49 Max= 0.68 *n=2*
Middle Eastern Lagoon	0.64 (-) Min= -0.40 Max= -0.87 *n=2*
Lower Eastern Lagoon	0.64 (-) 5 *n=1*
Western Lagoon Sites	
Upper Western Lagoon	0.66 (-) *n=1*
Middle Western Lagoon	0.67 *n=1*
Edge of Ice Sites	
Edge of Ice Site 3	0.62 (-) *n=1*
Supraglacial Sites	
Free Flowing Supraglacial Site	0.75 (-) *n=1*
Stagnant Supraglacial Sites	0.68 (-) Min= 0.65 Max= 0.72 *n=2*
External Inputs	
Fjallgilsá	0.64 (-) Min= 0.63 Max=0.72 *n=2*
Jökulsárgil	0.65 (-) Min= 0.58 Max= 0.71 *n=2*
Overland Input	0.91 (-) *n=1*

Table 6.1: DOC concentration data for Summer 2013

Standard deviations are in brackets

DOC distribution in Sólheimajökull bulk meltwaters during Summer 2013 is presented in figure 6.1 (DOC distribution map). Average DOC concentrations ranged from

0.53mg/L at the Bridge outlet to 0.73 (1SD= 0.19) at the Mixed Zone, reflecting low differentiation between sampling locations. Localised low DOC concentrations were observed at the Upper Eastern Lagoon site in close proximity to the glacier margin with average values of 0.59mg/L (1SD= 0.19). Low DOC concentrations prevailed across the proglacial lagoon with a limited range of DOC abundance observed at Sólheimajökull.
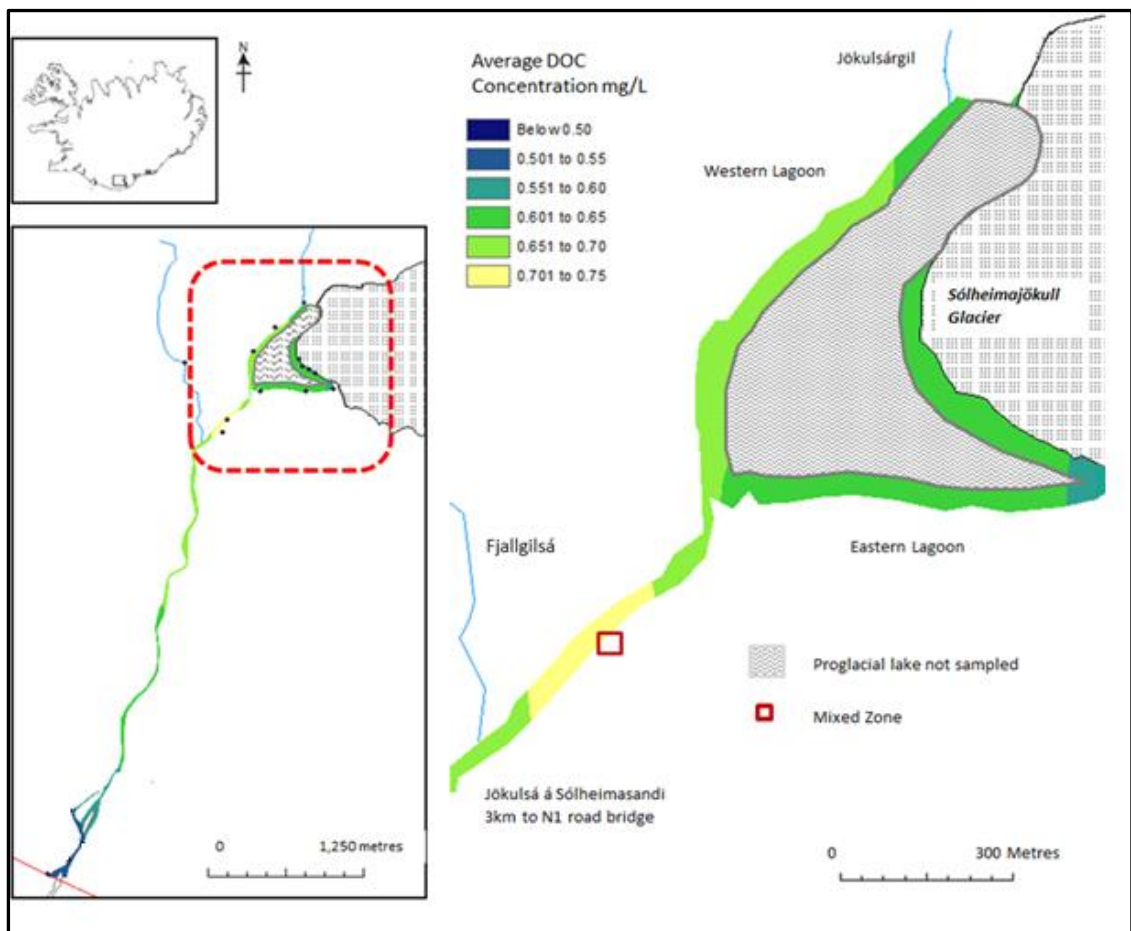
Figure 6.1. DOC distribution across the Sólheimajökull proglacial lagoon Summer 2013

Low DOC concentrations such as those demonstrated in Summer 2013 bulk meltwaters at Sólheimajökull are not uncommon in glaciated catchments.

Comparison of average Sólheimajökull bulk meltwater DOC concentrations to other glacial locations are presented in table 6.2. Sub 1ppm concentrations evident at Sólheimajökull are in keeping with DOC abundances observed across the Gulf of Alaska and glacier fed Alpine Lakes. The 0.53mg/L and 0.73mg/L range of values observed in Sólheimajökull proglacial meltwaters closely aligns to values found in the Mendenhall and Sheridan glacierized catchments where DOC abundances were 0.7 and 0.6mg/L respectively (Hood et al., 2009). Furthermore, Sólheimajökull DOC abundance across the proglacial area is high in comparison to Alpine glacier fed lakes at 0.39mg/L (Sommaruga et al., 1999). This reinforces that DOC in glacial environments is low with litte range.

Study	Location	Dissolved Organic Carbon (mg/L)
Lafrenière and Sharp (2004)	Glacial Stream	0.35 (0.15) *n=17*
Sommaruga et al (1999) Study of 57 Alpine mountain lakes	Glacier Fed Lakes	0.39
Hood et al (2009) Gulf of Alaska Drainage Basin incorporating 11 coastal watersheds	Mendenhall Catchment 55% glacier cover Sheridan Catchment 64% glacier cover	0.7 0.6

Table 6.2: DOC concentrations at Sólheimajökull in comparison to other glacial Locations

6.3. $\delta^{13}C_{DOC}$ isotopes across the Sólheimajökull proglacial area

Table 6.3 highlights $\delta^{13}C_{DOC}$ values across the Sólheimajökull proglacial area. Within this tight isotopic range, there was evidence of small variations between proglacial waters. Overland waters exhibited amongst the heaviest isotopic values at -10.89‰. Jökulsárgil and Fjallgilsá displayed lighter isotopic signatures with values of -11.52‰ and -11.47‰ respectively. Across the proglacial area $\delta^{13}C_{DOC}$ values ranged from -10.89‰ at the Lower Eastern Lagoon to -11.72‰ at the Middle Western Lagoon. Two isotopic trends became apparent. Firstly, there was an east/west division in $\delta^{13}C_{DOC}$ signature, with lighter isotopic values prevailing along the western lagoon margin and heavier values along the east. Superimposed onto this was a transition towards heavier $\delta^{13}C_{DOC}$ isotopic signatures with increasing distance from the glacier along the eastern lagoon margin. This places $\delta^{13}C_{DOC}$ isotopes at Sólheimajökull within the isotopic range exhibited by C4 photosynthetic pathways (-16 to -10‰ according to O'leary and Osmond, 1980). In contrast, $\delta^{13}C$ analysis of proglacial sediments indicated a C3 carbon source with a range of -29.75‰ to -24.65‰ (Data reported in Appendix 5). Suspended sediments found in Spring upwelling waters and at Edge of Ice site 3 during Summer, exhibited a far more enriched $\delta^{13}C$ signature of -13.68‰ and -6.2‰, closer to that of DOC found in Sólheimajökull proglacial waters.

Site	Average δ^{13}C DOC ‰ 1 Standard Deviation (1SD) in parentheses
Mixed Zone	**-11.40** (0.15) Min = -11.55 Max= -11.16 *n=4*
Bridge	**-10.91** (...) Min=-10.98 Max= -10.83 *n=2*
Eastern Lagoon Sites	
Upper Eastern Lagoon	**-11.47** (...) Min= -11.83 Max= -11.11 *n=2*
Middle Eastern Lagoon	**-10.97** (...) Min= -11.10 Max= -10.85 *n=2*
Lower Eastern Lagoon	**-10.89** (...) *n=1*
Western Lagoon Sites	
Upper Western Lagoon	**-11.17** (...) *n=1*
Middle Western Lagoon	**-11.72** (...) *n=1*
Edge of Ice Sites	
Edge of Ice Site	**-11.70** (...) *n=1*
Supraglacial Sites	
Free Flowing Supraglacial Site	**-11.37** (...) *n=1*
Stagnant Supraglacial Sites	**-11.36** (...) Min= -11.38 Max= -11.35 *n=2*
External Inputs	
Fjallgilsá	**-11.47** (...) Min= -11.53 Max= -11.40 *n=2*
Jökulsárgil	**-11.52** (...) Min= -11.59 Max= -11.45 *n=2*
Overland Input	**-10.89** (...) *n=1*

Table 6.3: Average δ^{13}C_{DOC} isotopic signatures across the Sólheimajökull proglacial area Summer 2013

Relationships between $\delta^{13}C_{DOC}$ and DOC abundance are presented in figure 6.2. The main cluster of data fell within the red oval, demonstrating a weak negative linear trend represented by an R^2 value of 0.31. In this instance, the lowest DOC abundances corresponded to heavier $\delta^{13}C_{DOC}$ signatures. As DOC concentration increased, $\delta^{13}C_{DOC}$ isotopes transitioned towards lighter values. Within this main cluster of data, rivers of external catchment origin grouped together, as do supraglacial samples shown by the blue envelope. Large shifts in DOC abundance and isotopic signature were observed at the Mixed Zone, representing the variable inputs from all other upstream sources.
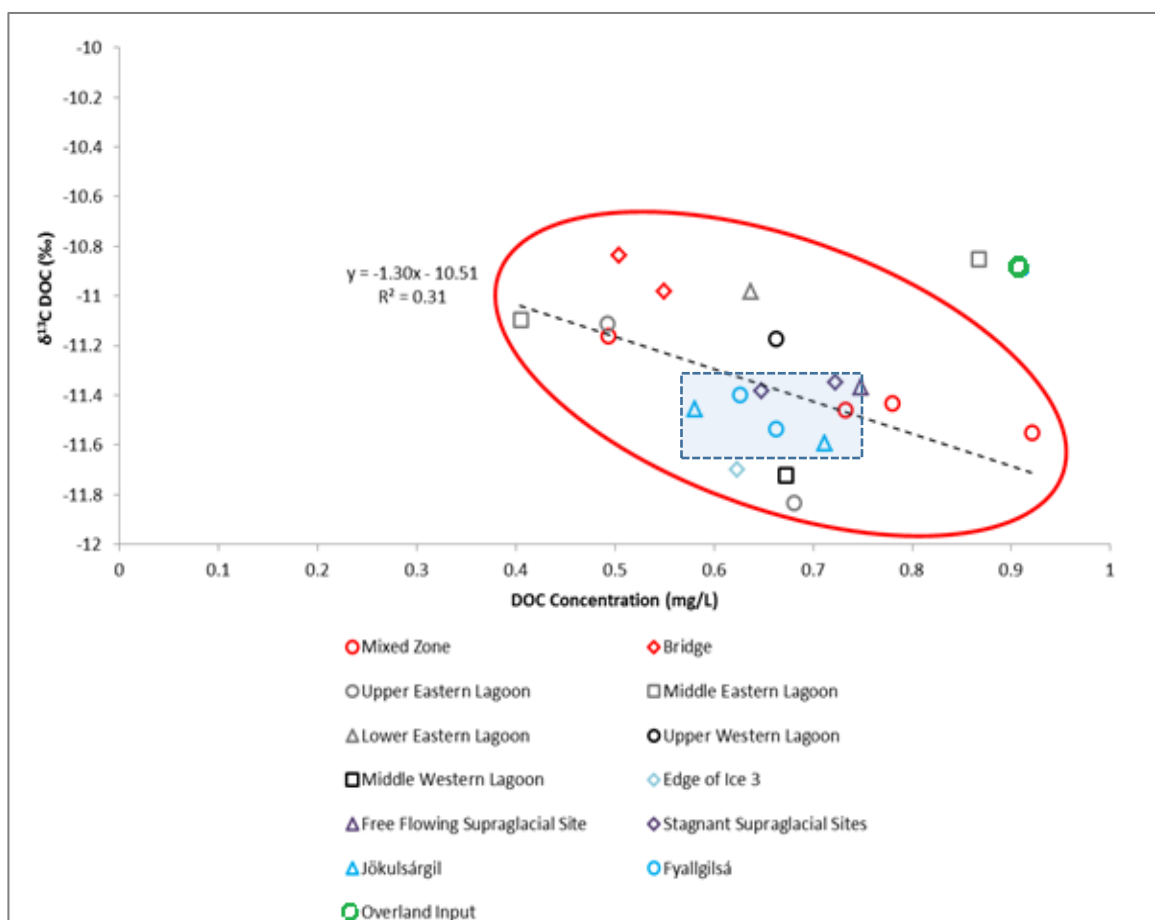
Figure 6.2. Bi-plot of $\delta^{13}C_{DOC}$ isotopic signature and DOC concentration for Summer 2013

6.4. Discussion of DOC concentrations and isotopic signatures at Sólheimajökull

DOC abundance at Sólheimajökull demonstrates sub 1ppm DOC concentrations, with notable clustering of supraglacial and external catchment sites. However, low concentrations observed at Sólheimajökull are not uncommon in other glacierized catchments. The presence of a glacier within a watershed alters DOC abundance dynamics with a negative relationship between glacier coverage and DOC concentration observed (Hood et al., 2009). The Mendenhall and Sheridan catchments which are 55 and 64% glacierized demonstrate DOC concentrations of 0.70 and 0.64mg/L respectively (Hood et al., 2009). This is comparable to average Sólheimajökull proglacial water DOC concentrations which range from 0.73 (1SD= 0.19) to 0.53mg/L (1SD=0.21) from a catchment which is 71 % glacierized.

δ^{13}C isotopes of DOC can provide additional information on OC sources and supply across the proglacial area. Plant derived organic carbon can be termed C3 or C4, dependent upon photosynthetic pathway (O'Leary and Osmond, 1980). Typically, C3 plants display average δ^{13}C values of -28.1‰ with a range of -20 to -37‰ whilst C4 plants average around -13.5‰ with typical ranges of -16 to -10‰ (O'Leary and Osmond, 1980). $\delta^{13}C_{DOC}$ signatures from Sólheimajökull are firmly placed within the isotopic boundaries of C4 plant derived organic matter sources. However, Iceland is dominated by C3 vegetation and carbon isotopes found within proglacial sediments corroborate this. Sediments obtained from subglacial upwelling water during Spring 2014 demonstrate δ^{13}C values of -13.68‰ indicating that the sediments from beneath the glacier are also enriched in δ^{13}C organic matter, and likely represent the source of the DOC.

Investigation of DOC abundance and isotopic characteristics during Summer 2013 offer insight into DOC distribution and delivery at Sólheimajökull. DOC abundances and $\delta^{13}C_{DOC}$ values exhibit a tight range. Partitioning between heavy and light $\delta^{13}C_{DOC}$ values and corresponding low/higher concentrations of DOC exists suggesting possible mixing between heavy and light isotopic end member components.

However, data is limited to the Summer 2013 season only and the absence of a sampled subglacial end member means true parameterisation of DOC sources at Sólheimajökull is restricted. The next stage is to investigate the fluorescent properties of DOC to help elucidate potential sources and linkages to hydraulic connectivity over summer and spring seasons.

6.5. Initial summary of DOC concentration and isotopic findings

1.   Summer DOC concentrations range from 0.91mg/L to 0.53mg/L. Supraglacial and external catchment waters display similar DOC concentrations with proglacial waters on the whole encompassing lower DOC values.

2. $\delta^{13}C_{DOC}$ values range from -10.89 to -11.72‰, suggestive of a C4 plant origin. Contemporary proglacial sediments contain organic matter of C3 origin, although sediments transferred from beneath the glacier suspended in the subglacial waters are much heavier in isotopic composition and likely represent a large proportion of the organic matter in subglacial discharge.

3.   A negative relationship between DOC concentration and $\delta^{13}C_{DOC}$ signature exists suggestive of a two-component end member mixing between isotopically heavy and light sources of DOC.

6.6. Fluorescence properties of bulk meltwaters at Sólheimajökull

The fluorescent properties of Humic and Fulvic-like fractions of DOC in proglacial meltwaters can help build on existing understanding of DOC dynamics and offer greater insight into the ultimate source of organic matter. DOC is dominated by humic acid and fulvic-like substances which comprise 50 to 70% of the total fluorescing DOC concentration (Hood et al., 2003; Lafrenière and Sharp, 2004). The fluorescent properties of humic and fulvic-like fractions can be used to elucidate organic matter provenance and fate across the proglacial environment. Fluorescence

of organic compounds is a type of luminescence caused by irradiation of fluorescing species (fluorophores). When fluorophores transition from an excited to a lower energy state the relaxing molecules provide fluorescence characteristics related to the molecular structure of the DOC within the sample (Barker et al., 2006). The variable dominance of humic and fulvic acids thereby affects the fluorescence of DOC in glacial waters (Smart et al., 1976).

Fulvic Emission peaks can be used to identify microbial and terrestrial sources of fulvic-like materials. Shorter (lower) wavelengths are indicative of fulvic materials from microbial biopolymers and longer (higher) wavelengths are associated with terrestrial sources (Barker et al., 2006). However, distinguishing DOC source using fulvic emission peak is often complicated by issues of microbial degradation and structural changes, which have the potential to alter fluorescent properties of this fraction. Humic-like organic matter is generally considered to be more recalcitrant, yet still diagnostic of source, enabling its use in characterising glacial organic matter sources (Wynn et al., unpublished). The relationship between humic-like fluorescence intensity and DOC abundance can be displayed in terms of humic-like fluorescence intensity per mg C. It is thought that approaching fluorescence analysis using this biomarker can elucidate between the age and source of organic matter (Wynn et al., unpublished). Recalcitrant, old organic carbon released from weathering of bedrock and suspended sediment exhibits lower humic-like fluorescence intensity per mg C, whilst young, labile organic carbon from microbial/ necromass sources displays greater fluorescence intensity. It is the division between these two carbon pools that constitutes traditional glacial DOC concepts.

6.8. Results: humic-like fluorescence per mg C of bulk meltwaters at Sólheimajökull

Fluorescence of glacial waters was conducted following methods outlined in chapter 3.5.3. Average humic-like fluorescence per mg C is displayed in table 6.4. Average values ranged from 26.62 (1SD= 4.77) in supraglacial sites to 89.12 (n=1) at the Bridge. Variability was shown across the proglacial lagoon where Eastern lagoon sites

demonstrated high average fluorescence per mg C values of 75.01 (1SD= 14.85) compared to lower average values of 41.36 (n=1) found at Western sites. The Edge of Ice site exhibited the lowest average humic-like fluorescence per mg C at 35.15 in glacial meltwater samples, inferring localised influence of supraglacial run off. Waters of external catchment origin displayed similar humic-like fluorescence per mg C with averages of 32.57 (n=1) and 31.50 (n=1) for Jökulsárgil and Fjallgilsá respectively.

Sampling Location	Average humic-like fluorescence per mg C 1 Standard Deviation (1SD) is in parentheses
Mixed Zone	**87.10** *(12.88)* Min= 31.12 Max=206.33 *n=4*
Bridge	**89.12** *(…)* Min= 73.81 Max= 104.44 *n=2*
Eastern Lagoon	**75.01** *(14.85)* Min= 69.01 Max= 95.87 *n=4*
Western Lagoon	**41.36** *(…)* Min= 25.86 Max= 56.87 *n=2*
Edge of Ice Sites	**35.15** *(…) n=1*
Supraglacial Sites	**26.62** *(4.77)* Min= 21.02 Max= 32.66 *n=3*
Jökulsárgil	**32.57** *(…)* Min= 30.29 Max= 34.85 *n=2*
Fjallgilsá	**31.50** *(…)* Min= 25.91 Max= 37.08 *n=2*
Overland Flows	**68.77** *(…) n=1*

Table 6.4: Average humic-like fluorescence per mg C for Summer 2013

The Humic-like fluorescence intensity per mg C is plotted against Dissolved Organic carbon data for 2013 in figure 6.3. Glacial meltwaters mainly clustered within the red oval represented by an R^2 value of 0.41 (including the outlying Western Lagoon and the Edge of Ice sites, but excluding the outlined Mixed Zone site). Known DOC sources were identified and represented by blue and green envelopes. Supraglacial and waters of external source origin (Jökulsárgil and Fjallgilsá) which clustered within the blue envelope displayed low humic fluorescence intensity per mg C indicative of an older more recalcitrant carbon source. In contrast, the overland input within the green envelope, displayed slightly higher humic fluorescence per mg C indicating a younger more labile carbon source. In order to achieve the negative linear trend observed there must be a three way source mixing with an additional low DOC source with elevated humic-like fluorescence per mg C. Based upon previously identified water sources to Sólheimajökull this is thought to be waters of subglacial origin. This would infer a young, labile subglacial carbon source. Proximity to DOC source clearly imparted an influence on DOC abundance and fluorescent properties with one Western Lagoon site showing similarity to DOC from Jökulsárgil and the Edge of Ice Site plotting amongst the identified supraglacial source envelope.
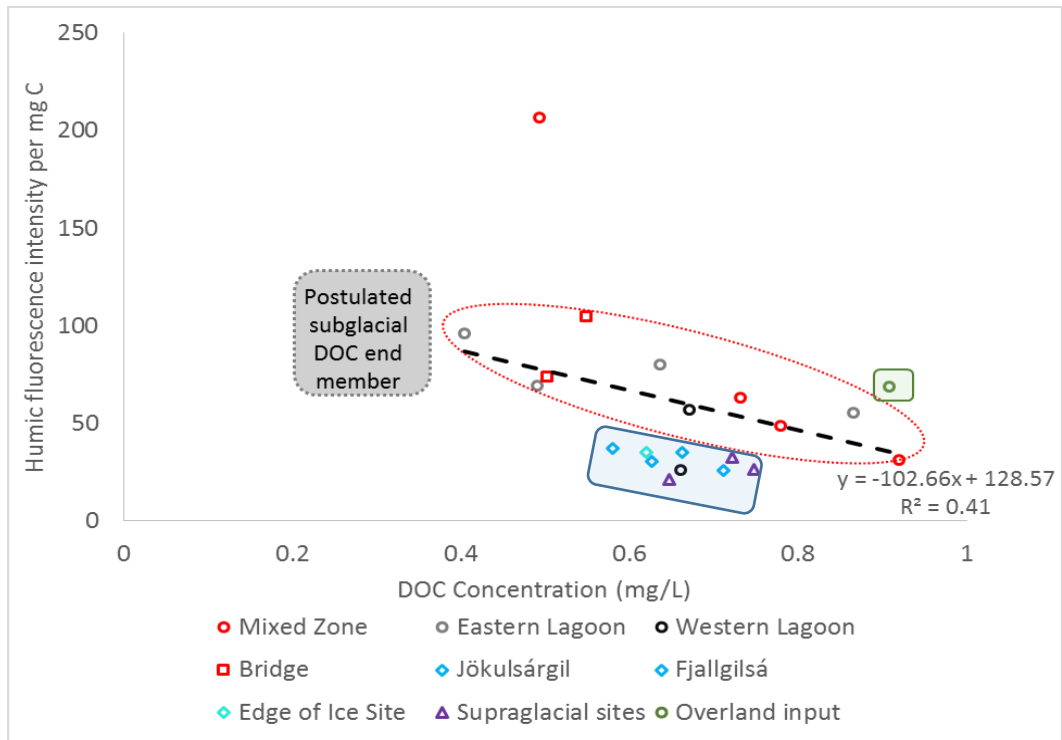
Figure 6.3: Bi-plot of humic-like fluorescence per mg C against DOC concentration for Summer 2013

Analysis of relationships between $\delta^{13}C$ of DOC and humic-like fluorescence per mg C are presented in figure 6.4. The majority of proglacial meltwater samples ploted along a positive linear trajectory with an R^2 value of 0.39 (with exception of the Mixed Zone outlier which is excluded). Isotopic mixing was evident between lighter isotopic values with low humic fluorescence intensity per mg C demonstrated in supraglacial and external catchment waters and heavier isotopic signatures in overland flows with increased humic fluorescence intensity per mg C. Overland inputs can be discounted as having a large influence on isotopic composition and fluorescence per mg C due to their limited discharge and ephemeral nature. This leaves a high humic-like fluorescence per mg C end member of approximately -11‰, which could be of summer subglacial origin. However, in the absence of this subglacial end member and Spring season data, only crude assumptions of DOC source contribution can be made.
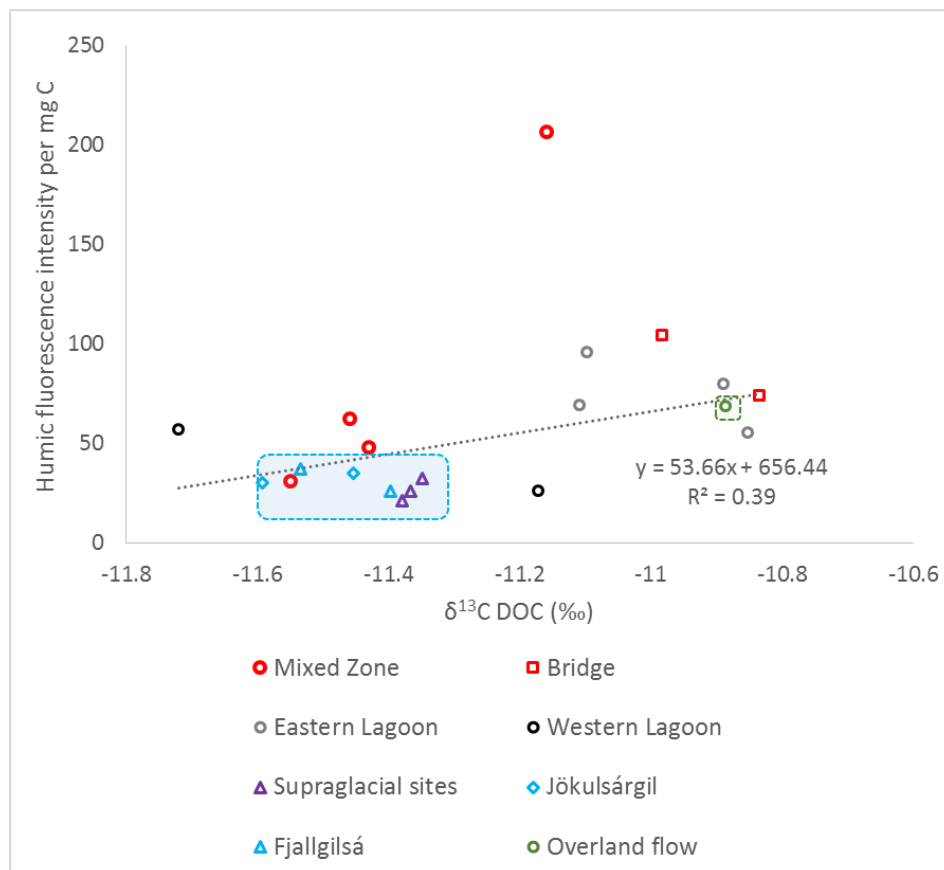
Figure 6.4: Bi-plot of humic-like fluorescence per mg C against $\delta^{13}C_{DOC}$ for Summer 2013

6.9. Discussion of humic-like fluorescence per mg C of bulk meltwaters at Sólheimajökull

Discernible seasonal disparities in the fluorescence properties of DOC are not uncommon in glacial catchments. On a seasonal basis evolution of subglacial drainage dynamics, changes in supraglacial melt rates and differences in discharge are likely factors contributing to variability of fluorescence characteristics, linked to mobilisation and transfer of dissolved organic matter from different pools (Barker et al., 2009). Current models of glacial carbon dynamics outline two major pools of DOC to the hydrological system: supraglacial and subglacial. Firstly, supraglacial carbon pools are traditionally regarded as a source of predominantly young organic carbon, derived from fixation of CO_2 during photosynthesis and necromass existing within the supraglacial biome. This can be directly transferred to proglacial meltwaters via

direct supraglacial run off, or where seasonal hydraulic coupling allows it be transferred to the bed (Tranter et al., 2005). Once entering the subglacial realm supraglacially sourced waters engage with older more recalcitrant carbon pools from underlying bedrock and glacially overridden soils providing a mixed meltwater DOC (Wynn et al., unpublished). This has been shown to be in operation at an Arctic Glacier (Midtre Lovenbreen; Wynn et al. unpublished) where division exists between supraglacial samples with greater fluorescence intensity and samples taken from subglacial/ proglacial riverine environments with organic matter content of lower fluorescence intensity.

This traditional concept of young supraglacial carbon pools and hydraulic coupling liberating carbon from older, more recalcitrant subglacial carbon sources largely hinges on three main assumptions: 1) that the ultimate source of glacial meltwater is of supraglacial origin, 2) that there is seasonal snowpack cover supporting supraglacial microbial life and 3) that bedrock/glacially overridden carbon are the dominant sources of subglacial DOC. This classical interpretation of organic carbon cycling largely overlooks Icelandic glaciers, where basal melting from geothermal heat sources and hydraulic connectivity to geothermal zones interacts with hydrochemistry, coupled with continual low level ablation preventing the persistence of a surficial snowpack. At Sólheimajökull during Summer 2013, a reversal in DOC dynamics is evident. Here, humic-like fluorescence intensity per mg C reveals an older, more recalcitrant supraglacial DOC origin and the potential for a younger, subglacial DOC component with greater fluorescence intensity. This is likely a consequence of a unique hydraulic configuration supporting reverse redox conditions. The low descent of the Sólheimajökull glacier tongue combined with a mild maritime climate supports continual low level ablation. This strips the glacier snout of snow cover, revealing large areas of dead ice, and inhibiting young carbon production via microbial ecosystem functioning. This is particularly notable during the summer when sampling was undertaken. Exposure of large debris cones consisting of volcanic ash and bedrock dust liberated by onshore winds from the large proglacial forefield ensure a large amount of crustally derived material is

157

available for weathering. Supraglacial waters also bear close similarities to Jökulsárgil and Fjallgilsá, in terms of DOC abundance, isotopes and fluorescent properties, indicating a common DOC source. It is therefore likely a bedrock component dominates the release of a recalcitrant DOC from the supraglacial environment.

Bi-plots of humic-like fluorescence per mg C and DOC abundance (mg/L) reveal a missing high fluorescence low mg/L concentration source. In accordance with previous knowledge of water sources across the Sólheimajökull catchment (as outlined in Chapter 4) this is postulated to be a subglacial DOC source. It is believed that reverse redox conditions facilitated by summertime hydraulic connectivity to geothermal zones provides a precursor for microbial activity, such as methanogenesis under low redox conditions. Such anoxic conditions are in keeping with findings at John Evans Glacier, where release of DOC from sub oxic linked cavity drainage also exhibited a strongly microbial signature (Barker et al., 2006). Therefore, fluorescence signatures during the Sólheimajökull summer drainage configuration are likely linked to microbial processing of subglacial organic materials under reducing conditions at the glacier bed (Lafrenière and Sharp, 2004; Barker et al., 2006; Bhatia et al., 2010).

Overall it can be determined that DOC is evident in low amounts at Sólheimajökull, comparable to DOC concentrations quoted for other glacial catchments. In terms of humic-like fluorescence per mg C a reverse model of organic carbon cycling is presented, largely influenced by unique hydrological conditions at Sólheimajökull and reverse seasonal redox status. However on the basis of incomplete evidence, only limited conclusions on the provenance and fate of DOC in Sólheimajökull bulk meltwaters can be made.

6.11. Summary of humic-like fluorescence per mg C analysis

1. DOC evident across the Sólheimajökull catchment displays varying humic fluorescence per mg C.

2. Comparison against DOC abundance suggests an unidentified end member component not acknowledged through the data obtained. Based on the negative linear relationship displayed this must be a low concentration DOC source with high humic-like fluorescence intensity per mg C.

3. Previous knowledge of water sources across the Sólheimajökull catchment suggest this missing end member to be a subglacial DOC origin.

4. With this in mind, meltwaters at Sólheimajökull could suggest a summertime reversal in traditional glacial organic carbon models, with older more recalcitrant organic carbon found in supraglacial waters and younger, more labile organic carbon in the subglacial realm.

5. This is likely governed by unique modes of glacial hydrology operating at Sólheimajökull. Most notably anoxia fuelled by head ward expansion of subglacial drainage into geothermal zones during summer allows subglacial microbial activity under low redox conditions. This is accompanied by continual low level ablation inhibiting supraglacial ecosystem functioning, and an abundance of crustally derived surface material determining a recalcitrant surface input of low fluorescence per mg DOC.

6.12. Overall Summary of DOC dynamics at Sólheimajökull

1. DOC is evident in low amounts at Sólheimajökull, with all sites demonstrating sub-1ppm DOC abundance. Supraglacial and external catchment waters exhibit higher DOC concentrations, whilst DOC (mg/L) in proglacial lagoon samples is reduced, inferring a low DOC end member component which cannot be identified through the data obtained. Comparison of humic-like fluorescence per mg C and DOC concentration further supports this additional

source. Based on previous investigation it is thought that subglacial waters are likely to constitute a low DOC end member.

2. If this is correct, then Sólheimajökull demonstrates a unique mode of DOC cycling with surficial inputs dominated by old, recalcitrant carbon contrasted with young, labile subglacial carbon, a reversal of traditional concepts of glacial carbon dynamics. This is likely linked to exclusive hydraulic configuration and reverse redox conditions in the subglacial realm, where summertime connectivity to geothermal zones provides ideal conditions for low redox microbial functioning. Ultimately, when combined with potential labile organic carbon substrates, it is feasible to consider this a location conducive to methanogenesis.

3. Attempts to parameterise the source and supply of this DOC have been made however, in the absence of Spring concentration and isotope data estimates of annual characteristics of DOC are tentative.

7. Methane in Sólheimajökull meltwaters

7.1. Introduction

Methane is an inorganic constituent of the glacier carbon cycle. Within the natural environment methane is generated by biological and geothermal processes. Active methanogens have been found to inhabit alpine subglacial sediments (Boyd et al., 2010). However, tangible data surrounding in situ methane release from contemporary ice margins is lacking. Icelandic glaciers offer the ideal situation to study mechanisms of methane formation, as they overlie both organic rich sediments and active volcanic zones providing opportunity for methanogenesis via bacterial and geologic means. Sólheimajökull is an outlet glacier from the Mýrdalsjökull Icecap which is situated over the Katla Volcanic system. Previous discharge chemistry has indicated the influence of geothermal activity in the subglacial drainage system (Lawler et al., 1996), signifying the potential for geogenic methane production. Overlying ice then acts as a cryospheric cap, incubating methane from the atmosphere. The long-term presence and stability of this overlying cap plays a key role in regulating the release of methane for past, present and future climatic scenarios. This chapter will identify the presence of methane discharging from the subglacial environment, and use stable isotopes to attribute pathways of formation. The significance of this source is discussed in the context of global glacier distribution.

7.2. Results: Aqueous methane in Sólheimajökull bulk meltwaters

7.2.1. Methane concentration distribution across the proglacial area

Methane concentrations were obtained through methods outlined in sections 3.47 and 3.55. Understanding the distribution of methane concentrations across the proglacial area is essential to identify areas of methane production/supply within the Sólheimajökull system. Methane concentration was not evenly distributed across the proglacial area. Instead, concentration was dependent upon location and seasonality

as well as additional factors such as oxidation and diffusion. Water within the Sólheimajökull catchment comes from three main origins: Supraglacial run off, subglacial drainage and sites of external catchment origin (Jökulsárgil and Fjallgilsá). Initial Summer 2013 sampling established key locations where methane in water was monitored, these included the three main water supplies to Sólheimajökull outlined above and key locations around the proglacial lagoon, the edge of the glacier and the Jökulsa á Sólheimasandi. Subsequent extensive sampling during Spring 2014 provided further monitoring of these sites and additional locations to provide concentration data from 39 sites across the Sólheimajökull catchment. These are displayed in figures 7.1 and 7.2 (aqueous methane distribution maps below).

Supraglacial waters demonstrated negligible amounts of methane irrespective of season or location on the glacier. During Spring, concentrations ranged from 0.60ppm to 0.89ppm with an average of 0.70ppm (1SD= 0.14). Concentrations were also low during Summer ranging from 0.28ppm to 0.34ppm. Similarly, sites of external catchment origin also displayed amongst the lowest methane concentrations. Jökulsárgil waters displayed average methane values of 0.61ppm (1SD= 0.04) and 0.34ppm (n=2) for Spring and Summer respectively. Similarly, Fjallgilsá waters displayed comparable methane concentrations of 0.61ppm (1SD= 0.02) and 0.28ppm (n=2) for Spring and Summer. Given that these are open channel systems, operating under oxic conditions it is not surprising methane concentrations were low, and therefore these can be discredited as potential methane sources. Subglacial waters provided the only significant supply of methane entering the proglacial lake. During Spring 2014, water was found to be emanating from two locations on the ice frontal margins of Sólheimajökull. Methane concentrations for these upwellings ranged from 28.14ppm to 46.05ppm and 26.06 to 48.37ppm for Upwellings 1 and 2 respectively. From this it can be said that methane originated in the subglacial realm.

During Spring, low average methane concentrations prevailed across many areas of the proglacial lagoon, where the majority of sites displayed average values below 5ppm, however, methane concentrations across the proglacial lagoon during Spring were not homogeneous. Instead spatial analysis (figure 7.1) identified a division between Eastern and Western Sampling Sites, whereby highest methane concentrations occurred at western lagoon sites whilst lower concentrations occurred on the east. Proximity to water source clearly influenced the dispersal of methane at this time. Most notably, the Upper Western Lagoon site had an average methane concentration of 12.10ppm (n=2) whilst, low average methane concentrations of 1.02ppm (1SD= 0.27) were found at the upper eastern lagoon in close proximity to areas of supraglacial run off. Lowest average values of 0.60ppm (1SD= 0.03) were found at western site O, which is an area of water in close proximity to where Jökulsárgil joins the lagoon separated from the main lagoon by a gravel spit.

Average CH₄ Concentration in Jökulsárgil

0.61ppm (1SD= 0.04) Min= 0.58 Max= 0.67 *n=3*

Average CH₄ Concentrations in Subglacial Upwellings

Sub glacial upwelling 1	39.36ppm (1SD= 7.98) Min= 28.14 Max=46.05 *n=3*	
Sub glacial upwelling 2	38.83ppm (1SD= 9.39) Min= 26.06 Max= 48.37 *n=3*	

Average CH₄ Concentration in Supraglacial waters

0.70ppm (1SD= 0.14) Min= 0.60 Max= 0.89 *n=3*

Average CH₄ Concentrations at Eastern Lagoon Sites

A. Upper Eastern Lagoon	1.02ppm (1SD= 0.27) Min= 0.63 Max= 1.54 *n=8*
D. Middle Eastern Lagoon	3.23ppm (1SD=1.14) Min= 1.86 Max= 4.96 *n=4*
G. Lower Eastern Lagoon	4.81ppm (1SD= 3.02) Min= 2.02 Max= 9.33 *n=4*

Average CH₄ Concentration at the Mixed Zone

2.21ppm (1SD= 1.00) Min= 1.04 Max= 4.34 *n=15*

Average CH₄ Concentrations at Western Lagoon Sites

P. Upper Western Lagoon	12.10ppm (-) Min= 5.78 Max= 18.43 *n=2*
R. Middle Western Lagoon	5.62ppm (1SD= 3.89) Min= 2.53 Max= 11.10 *n=3*

Sólheimajökull Glacier

Edge of Ice Sites

Proglacial lake not sampled

Sand and Gravel Banks

Mixed Zone

Jökulsá á Sólheimasandi
3km to N1 road bridge

Average CH₄ Concentration in Fjallgilsá

0.61ppm (0.02) Min= 0.59 Max= 0.63 *n=3*

Average CH₄ Concentration at the Bridge

2.30ppm (1SD= 2.37) Min= 0.72 Max= 6.92 *n=6*

Average Methane Concentration (ppm)

0.00 to 5.00
5.01 to 10.00
10.01 to 15.00
15.01 to 20.00
20.01 to 25.00
25.01 to 30.00
30.01 to 35.00
35.01 to 40.00

300 Metres

0

Figure 7.1: Map of methane concentration distribution across the Sólheimajökull

proglacial area, Spring 2014

Label on Map	Average Methane Concentration (ppm) 1 standard deviation (1SD) is in parentheses
Eastern Lagoon	
b	1.03 (0.24) Min= 0.84 Max= 1.36 n=3
c	2.06 (0.70) Min= 0.97 Max= 2.93 n=3
e	5.47 (2.54) Min= 1.93 Max= 8.50 n=4
f	2.36 (1.41) Min= 0.96 Max= 4.69 n=4
h	4.35 (2.08) Min= 1.41 Max= 5.95 n=3
i	3.46 (1.56) Min= 1.56 Max= 5.39 n=3
j	4.01 (…) n=1
Western Lagoon	
o	0.60 (0.03) Min= 0.57 Max= 0.63 n=3
q	4.17 (2.17) Min= 1.14 Max= 6.10 n=3
s	4.26 (…) n=1
Jökulsá River	
k	2.13 (1.63) Min= 0.94 Max= 4.94 n=4
l	3.19 (…) n=1
m	3.88 (…) n=1
t	5.71 (2.64) Min= 3.83 Max= 9.45 n=3
Edge of Ice Samples	
1	2.99 (1.46) Min= 1.04 Max= 4.55 n=4
2	3.09 (0.90) Min= 2.30 Max= 4.54 n=4
5	2.22 (1.45) Min= 0.82 Max= 4.21 n=4
7	1.10 (0.46) Min= 0.74 Max= 1.75 n=3

Table 7.1: Additional average methane concentrations to support Spring sampling sites displayed in figure 7.1

Higher methane concentrations prevailed across the proglacial lagoon during Summer 2013. Direct seasonal comparison, showed a 15 fold increase in average Summer methane concentrations at the Mixed Zone in comparison to Spring 2014. Notable localised methane hotspots existed at various locations, including the Mixed Zone where methane concentrations reached as high as 46.26ppm. Subglacial upwelling water was not apparent at this time of year, although likely emerged from beneath the lake water level as indicated by high concentrations of methane (39.41ppm) at the Edge of Ice site 4. Additional localised high methane concentrations were also evident at the middle and lower eastern lagoon and eastern site K, downstream of the Mixed Zone. Areas of high methane concentrations were comparable to Spring subglacial samples. Low proglacial lagoon methane concentrations were associated with inputs of supraglacial run off at the Upper Eastern Lagoon with an average concentration of 7.34ppm (1SD= 3.41) and Edge of Ice site 6 with a measured concentration of 7.73ppm. Additionally, downstream decreases in methane concentration were evident with comparatively lower values recorded at the Bridge site.

Average CH₄ Concentration in Jökulsárgil

0.34ppm (-) Min= 0.27 Max= 0.42 n=2

Average CH₄ Concentration in Supraglacial waters

0.31ppm (-) Min= 0.28 Max= 0.34 n=2

Average CH₄ Concentrations at Edge of Ice Sites

Edge of Ice1	15.93ppm (-) n=1
Edge of Ice3	11.21ppm (-) n=1
Edge of Ice4	39.41ppm (-) n=1
Edge of Ice6	7.73ppm (-) n=1

Average CH₄ Concentrations at Eastern Lagoon Sites

A. Upper Eastern Lagoon	7.34 (1SD=3.41) Min=1.78 Max=11.41 n=5
D. Middle Eastern Lagoon	31.74 (1SD=7.72) Min=20.18 Max=40.37 n=4
G. Lower Eastern Lagoon	31.74 (1SD=7.72) Min=20.18 Max=40.37 n=4

Average CH₄ Concentration at the Mixed Zone

33.72ppm (1SD=12.21) Min= 13.24 Max=46.26 n=8

Average CH₄ Concentration in the Eastern River (k)

38.74ppm (-) n=1

Average CH₄ Concentrations at Western Lagoon Sites

| P. Upper Western Lagoon | 25.80ppm (-) n=1 |
| R. Middle Western Lagoon | 28.39ppm (-) n=1 |

Sólheimajökull Glacier

Jökulsárgil

Proglacial lake not sampled

Sand and Gravel Banks

Mixed Zone

Fjallgilsá

Average Methane Concentration (ppm)

0.00 to 5.00
5.01 to 10.00
10.01 to 15.00
15.01 to 20.00
20.01 to 25.00
25.01 to 30.00
30.01 to 35.00
35.01 to 40.00

Average CH₄ Concentration in Fjallgilsá

0.28ppm (-) Min= 0.26 Max= 0.30 n=2

Average CH₄ Concentration at the Bridge

9.45ppm (-) Min= 8.63 Max=10.27 n=2

N

300 Metres

0

Figure 7.2: Map of methane concentration distribution across the Sólheimajökull proglacial area, Summer 2013.

7.3.2. Addressing the time series of aqueous methane in Sólheimajökull bulk meltwaters

Mixed Zone and Bridge sampling locations are representative of bulk outflow in the Jökulsa á Sólheimasandi, and consequently samples measured here represent water from all identified proglacial sources. Methane delivery from external and supraglacial waters was low, therefore methane must be associated with water supplied from the subglacial system. Subglacial inputs to the lake varied on a seasonal and inter seasonal time scale. Time series of methane concentrations from these sites were plotted to identify injection of subglacially sourced methane (Figure 7.3).

During Spring Mixed Zone and Bridge locations showed low average methane concentrations of 2.14ppm (1SD= 1.01) and 2.30ppm (1SD= 2.37) respectively. From DOY 128 onwards there were notable increases in methane concentrations at the Mixed Zone, reaching peak values of 4.34ppm on DOY 133. Similarly, increased methane concentrations were also observed at the Bridge with peak values of 6.92ppm also evident on DOY 133.
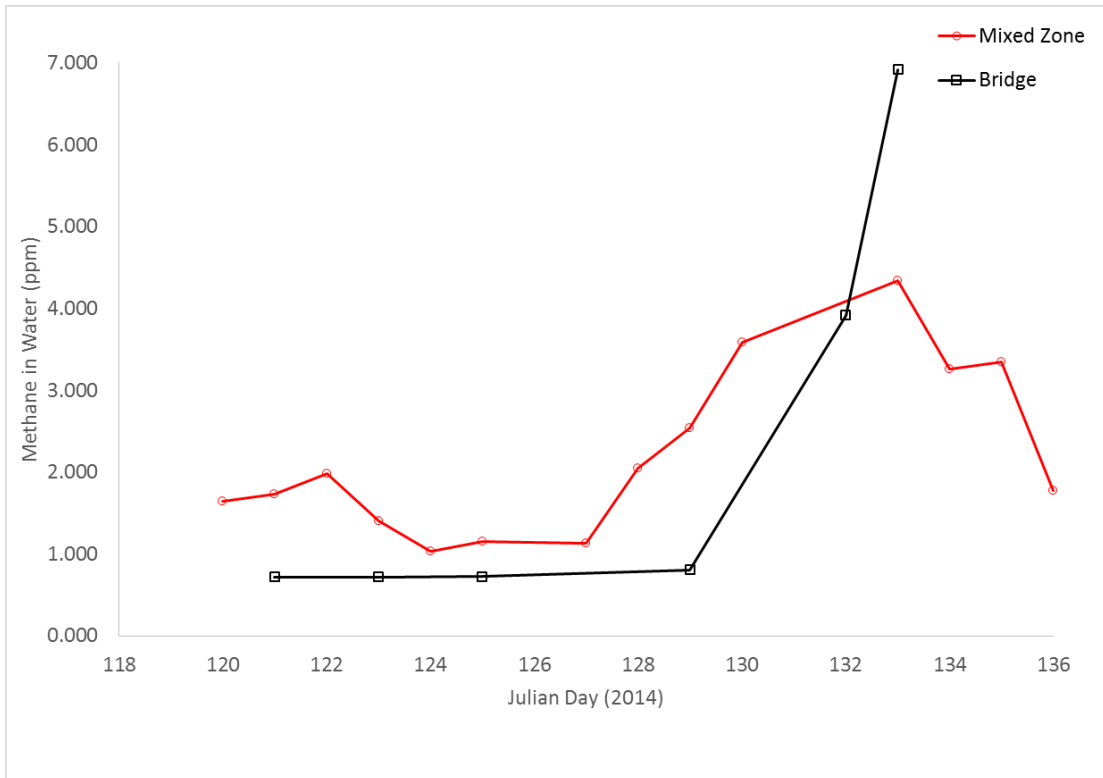
Figure 7.3: Time series data of daily methane concentrations at the Mixed Zone and

Bridge during Spring 2014

This transition to higher methane concentrations coincided with release of subglacial waters (as shown in figure 7.4), providing a high concentration source of methane to the proglacial area. Subglacial methane values increased from the onset of the upwellings' opening, with peak values of 46.05ppm and 48.37ppm on DOY 130 for upwellings 1 and 2 respectively. Once the subglacial portal had been fully established methane supply remained elevated for the rest of the study period.
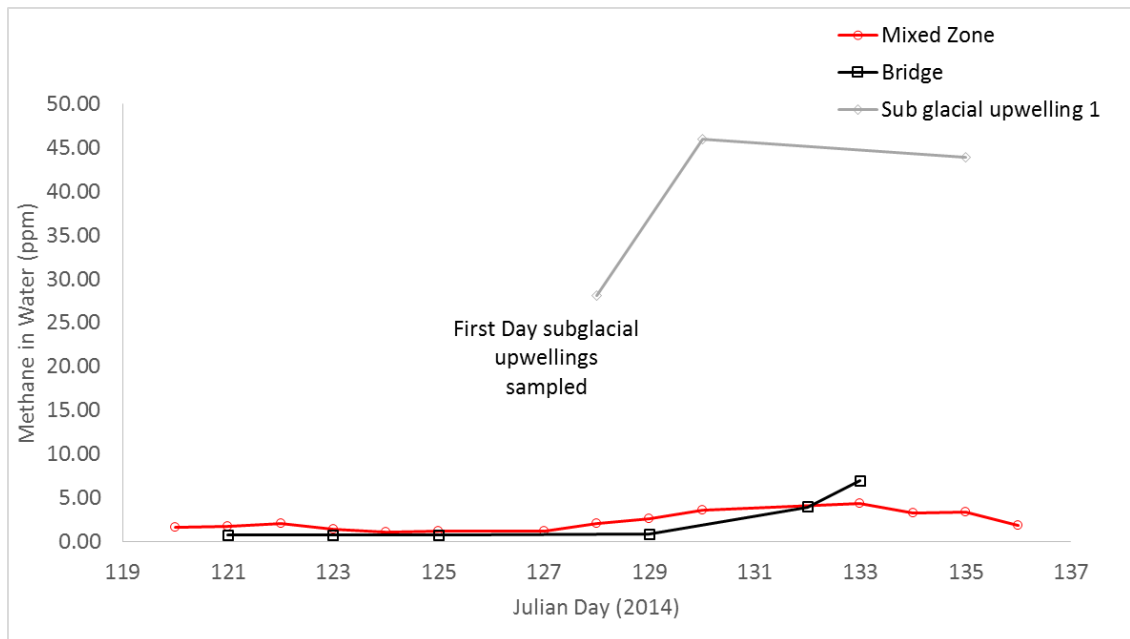
Figure 7.4: Time series data of daily methane concentrations at the Mixed Zone and Bridge, alongside concentrations from subglacial waters

7.3.3 Using δ^{13}C / δD isotopes to identify methane sources

Analysis of methane concentrations identified spatial and seasonal trends in methane distribution across the proglacial area. Whilst this can provide information on potential methane sources e.g. subglacial upwellings, and associated dispersal patterns, the actual origin of methane cannot be established through concentration data alone. Stable Isotopes of Carbon and Hydrogen (as obtained through methods outlined in section 3.56) provide natural tracers of methane formation mechanisms and subsequent chemical and physical fate in the proglacial system. There are two possible origins of natural methane within the Sólheimajökull system: near surface microbial gas produced by methanogens present within subglacial substrates and geogenic methane supplied by the Katla subglacial volcanic system. Each production pathway offers a unique isotopic fingerprint. In Geogenic methane generation higher temperatures associated with hydrocarbon production lead to values of δ^{13}C CH$_4$= ~ -50 to -20 ‰ and δD CH$_4$= ~ -275 to -100‰ (Whiticar et al., 1986). Microbially

170

produced gases are enriched in ^{12}C and ^{1}H with δ^{13}C CH$_4$ around -50 to -60 ‰ and δD CH$_4$ around -250 to -380‰. If fractionation does not occur due to methane oxidation (methanotrophy), stable isotopes should be able to distinguish between methane of a biogenic or geogenic origin.

Extensive monitoring during Spring established a range of isotopic signatures across the proglacial area which are presented in figure 7.5 (δ^{13}C CH$_4$ and δD plot). A strong linear correlation existed between the two isotopes (R^2 value=0.80). Lightest δ^{13}C / δD CH$_4$ values were associated with water emanating from subglacial sources with δ^{13}C CH$_4$ values ranging from -59.54 to -59.88‰ and δD CH$_4$ values ranging from -322.6 to -324.3‰. This placed subglacial methane within the realm of bacterial methane formation. Western Lagoon sampling sites also displayed light δ^{13}C / δD CH$_4$ values compared to other proglacial lagoon locations. Heaviest δ^{13}C / δD CH$_4$ values were found at the Edge of Ice site 2 (δ^{13}C CH$_4$ = -7.63 and δD = 161.1 ‰), which were well beyond the bounds of microbial or geogenic methane sources. Most proglacial lagoon sites plotted between these two values. Sites of External Catchment Origin represented an additional source in the Sólheimajökull proglacial system, plotting off the main linear trend with average values of -45.2 and -108.8‰ for δ^{13}C CH$_4$ and δD CH$_4$ respectively. Whilst these sites offer an external input of water to the Sólheimajökull system, isotopic influence was limited due to the very low concentrations present in these streams.
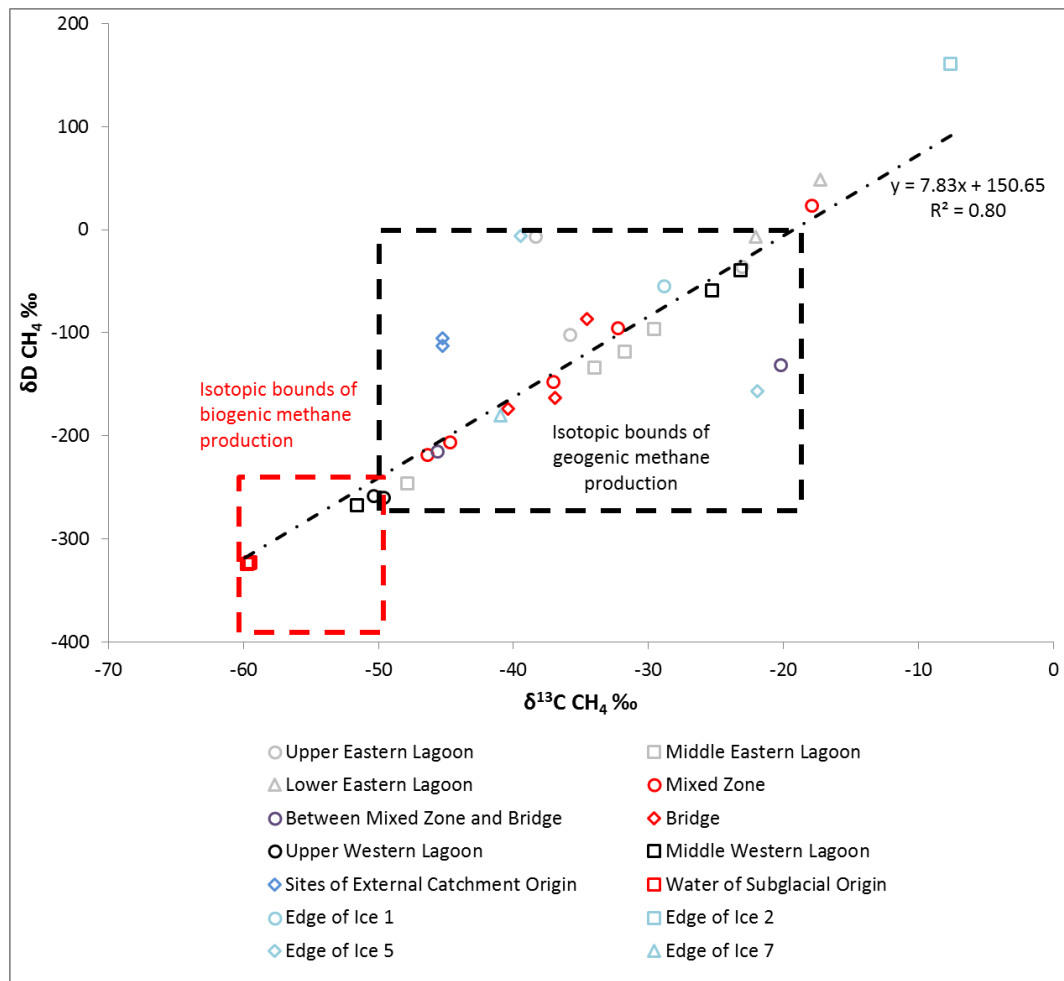
Figure 7.5: Bi-plot of $\delta^{13}C$ CH$_4$ and δD CH$_4$ isotopes compared to biogenic and geogenic source signatures

Mixed Zone values exhibitted a large isotopic range between $\delta^{13}C$ CH$_4$ = -17.93 and -46.38‰ and δD values between -22.9 and -218.2‰ plotting largely beyond the isotopic realm of a microbial methane source. Further investigation of Mixed Zone time series data of daily isotopic signatures reflected a temporal shift towards lighter $\delta^{13}C$ CH$_4$ and δD isotopic values, which coincided with the opening of subglacial upwellings.
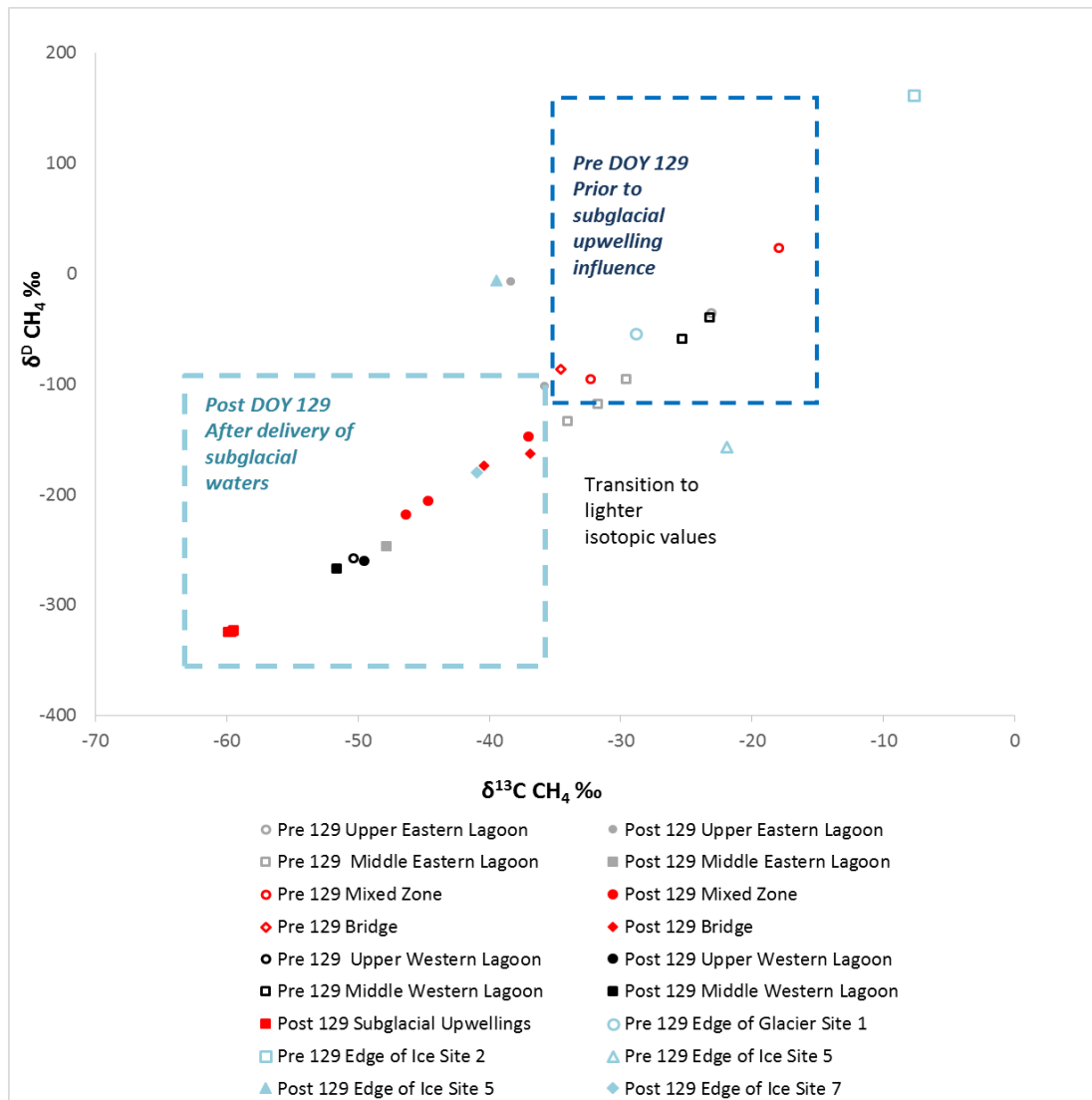
Figure 7.6: Bi-plot of $\delta^{13}C\,CH_4$ and $\delta D\,CH_4$ isotopes pre/post injection of subglacial waters

Establishment of subglacial upwellings was thought to have triggered a transition to lighter isotopic signatures at the Mixed Zone, with an evident split between pre and post upwelling isotopes. Upon further analysis of isotopic signatures across the proglacial area, it became clear that this temporal partitioning was also evident across the majority of proglacial lagoon sites. Pre upwelling, $\delta^{13}C\,CH_4$ isotopic values outlined in the darker blue box, plotedt between -7.63‰ and -34‰ whilst after this, values transitioned towards a lighter signature which ranged from -35.58 to -59.81‰. $\delta D\,CH_4$ values also demonstrated a similar trend, with all pre upwelling

values above -156.9‰. Conversely, post upwelling values plotted below this (with the exception of the Edge of Ice Site 5 and 2 Upper Eastern Lagoon Sites).

7.4.4 Seasonal isotopic trends- comparison to Summer 2013 data

Methane isotopic values for Summer 2013 are compared to the Spring 2014 season in Table 7.2. Data for both pre and post emergence of the 2014 subglacial drainage are presented. Summer season signatures were consistently isotopically enriched in ^{12}C compared to those from the Spring season and were most closely aligned with those waters present after the opening of the subglacial portal around DOY 129.

Site	Spring 2014 pre subglacial upwelling	Spring 2014 post subglacial upwelling	Summer 2013
Mixed Zone	**-23.72** (4.52) n=8	**-41.01** (4.57) n=5	**-49.92** (7.31) n=8
Upper Eastern Lagoon	**-22.94** (9.95) n=4	**-37.10** (...) n=2	**-51.36** (2.55) n=4
Middle Eastern Lagoon	**-31.77** (2.22) n=3	**-47.84** (...) n=1	**-49.53** (10.70) n=4
Eastern Site K (River)	**-30.54** (...) n=2	**-44.36** (...) n=1	**-58.61** (...) n=1
Bridge	**-34.41** (...) n=1	**-38.65** (...) n=2	**-49.55** (...) n=2
Upper Western Lagoon	**-50.32** (...) n=1	**-49.57** (...) n=1	**-56.45** (...) n=1
Middle Western Lagoon	**-24.24** (...) n=1	**-51.61** (...) n=1	**-56.76** (...) n=1
Edge of Ice Site 1	**-28.81** (...) n=1	Not sampled	**-56.53** (...) n=1
Subglacial upwellings	Not Sampled	**-59.66** (0.15) n=4	Not Sampled

Table 7.2: Seasonal comparison of δ^{13}C CH$_4$ isotopes (‰)

Standard deviations are in parenthesis

7.4.5. Relationships between concentration and isotopic Signature

The relationship between methane concentrations and isotopes (Figure 7.7) depicted an asymptotic relationship during Spring 2014. High concentration, isotopically light methane which emanated from the subglacial upwelling formed one end member of the plot, whilst sites enriched in ^{13}C clustered at much lower concentrations. The proglacial lagoon demonstrated a clear division between Eastern and Western Isotopic Values. δ^{13}C CH$_4$ values on the Eastern Edge of the Lagoon showed low concentrations and relatively heavy isotopic signatures, whilst those on the Western Lagoon had much higher concentrations and a lighter isotopic composition. Sites of external catchment origin (Jökulsárgil and Fjallgilsá) demonstrated slightly different methane characteristics with lowest CH$_4$ concentrations (0.58ppm and 0.59ppm) and mid-range isotopic signatures at around -45‰. Despite different source origins, the consistency in methane concentrations and δ^{13}C CH$_4$ isotopic signatures in Fjallgilsá and Jökulsárgil was striking. From this it could be inferred that these parameters are typical of non-glacial streams in the Sólheimajökull catchment, further demonstrating the distinct methane dynamics displayed in subglacial waters.
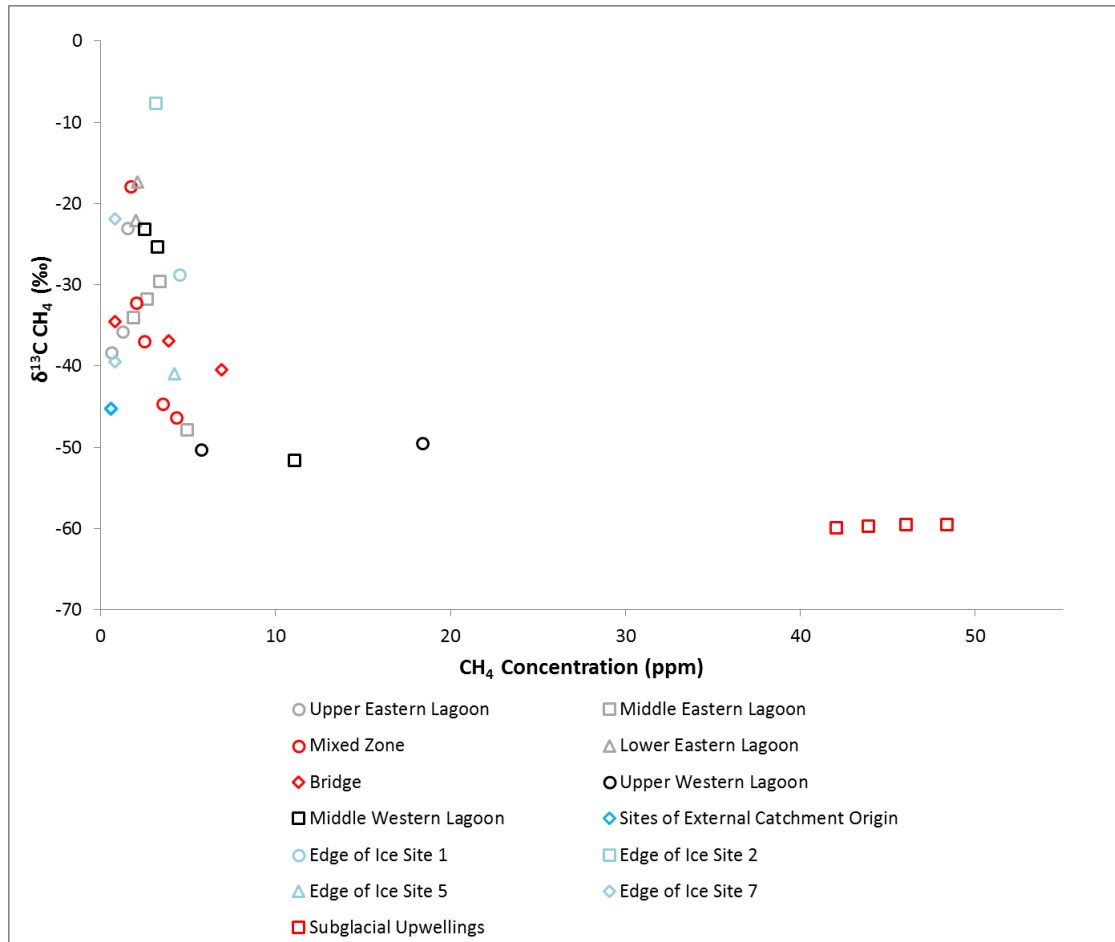
Figure 7.7: Bi-plot of $\delta^{13}C$ CH$_4$ isotopic signature and CH$_4$ concentration for Spring 2014

Comparison of Spring and Summer $\delta^{13}C$ values and methane concentrations reflected distinct seasonality across the proglacial area. The Summer system was swamped by waters containing high concentrations of isotopically light methane. The majority of Summer data plotted below -45‰ and above concentrations of 5ppm, with no distinct relation between isotopic signature and concentration apparent.
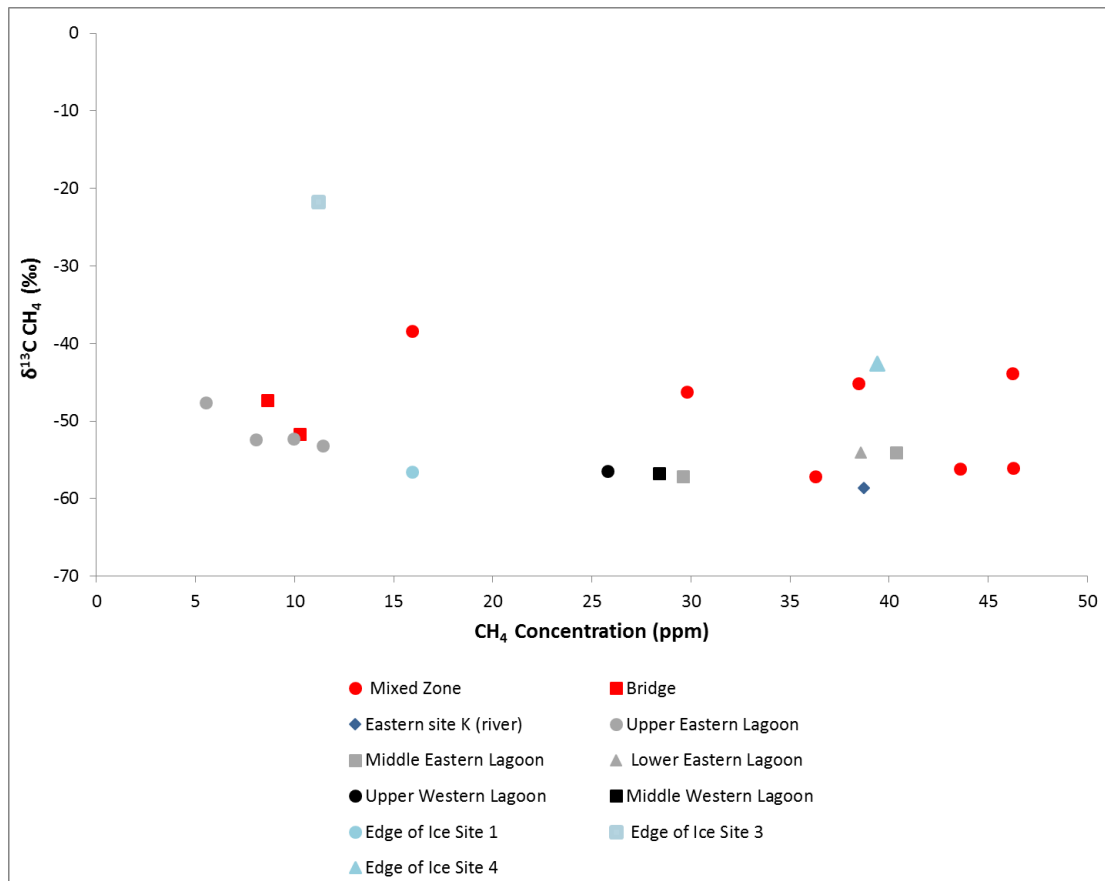
Figure 7.8: Bi-plot of $\delta^{13}C$ CH_4 isotopic signature and CH_4 concentration for Summer 2013

7.4.6. Determining the flux of methane exiting the glacial catchment

To place the release of methane from Sólheimajökull into the context of an emissions inventory, attempts were made to calculate an annual flux based on meltwater discharge and concentrations contained within the bulk meltwater channel. Such a calculation was difficult to achieve accurately due to poor constraints on the meltwater discharge at this site, limited temporal variability in aqueous methane concentration measurements and poor constraints on the rate of methane outgassing between the point of emergence at subglacial upwelling to the point of measurement at the Mixed Zone sampling site. Based on this an approach to calculate a range of methane fluxes using minimum and maximum discharges and

methane concentrations was employed. Sólheimajökull exhibited moderate discharges all year round as shown in figure 7.9. Yearly (January 2013-December 2014) differences in average monthly water stage was 66.7cm and 73cm for 2013 and 2014 respectively. Previous studies state that winter discharges for October to April average around 10 $m^3 s^{-1}$ (Lawler et al., 2003). This is corroborated by individual discharge measurements of 10 $m^3 s^{-1}$ observed on 30th November 1988 (Lawler et al., 1992). The majority of discharge occurs in the summer months with typical summer melt season flows ranging from 20 to 30 $m^3 s^{-1}$ (Lawler et al., 2003). Peak run off occurs in late July with peak flows around DOY 200, however discharge peaks of 90 $m^3 s^{-1}$ have been observed in early August (Lawler et al., 2003; Lawler et al., 1992). Bankful discharges are around 100 $m^3 s^{-1}$ occupying a channel width of about 25m and depth of 2.5m (Lawler et al., 2003; Lawler et al., 1996; Lawler et al., 1991).
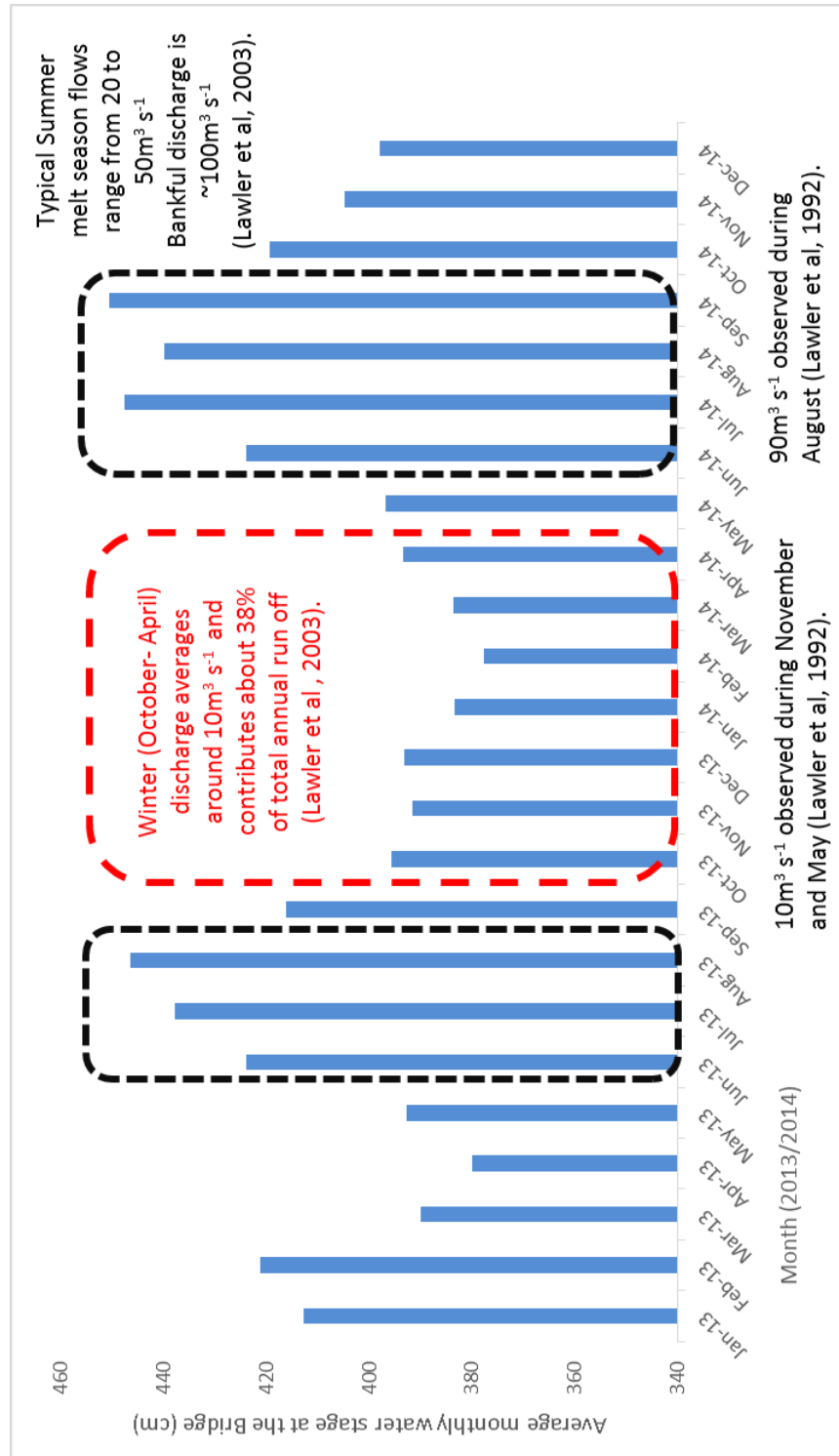
Figure 7.9: Average monthly water stage from January 2013 to December 2014 alongside previously known water discharge parameters

Methane concentrations peaked in waters exiting the subglacial drainage system which was active between April to September. Prior to the subglacial drainage system opening, methane was still apparent in the meltwaters, albeit at lower concentrations. The Mixed Zone was taken to be representative of bulk meltwaters exiting the proglacial lagoon, therefore Mixed Zone waters prior to subglacial upwelling injection were thought to represent wintertime drainage conditions. Therefore, concentrations from the Mixed Zone prior to DOY 129, an average value of 1.44ppm (1SD=0.33) were used to estimate wintertime methane flux.

Calculations based on an average discharge of 10 m^3 s^{-1} from October to April and an average methane concentration of 1.44ppm render a winterime methane flux of 264 tonnes (as outlined in appendix 7) based on the following equation:

$$Flux\ estimation\ 1st\ October\ to\ 30th\ April$$

$$1st\ October - 30th\ April\ =\ 212\ days$$

$$Seconds\ in\ a\ day\ =\ 86400$$

$$Seconds\ over\ winter\ period$$
$$=\ seconds\ in\ a\ day\ \times\ number\ of\ days\ in\ the\ winter\ period$$

$$m^3\ over\ winter\ period$$
$$=\ seconds\ over\ winter\ period\ \times discharge\ at\ 10 cumecs$$

$$Litres\ over\ winter\ period\ =\ m^3\ over\ winter\ period\ \times\ 1000$$

$$Methane\ (mg) over\ winter\ period =\ 1.44\ \times\ litres\ over\ winter\ period$$

$$(where\ 1.44\ is\ the\ average\ ppm\ value\ at\ the\ Mixed\ Zone\ prior\ to\ the\ addition\ of$$

$$subglacial\ upwelling\ waters).$$

$$\textit{Conversion to tonnes over the winter period}$$
$$= \textit{methane in mg} \div 1000000000$$

Using a lower discharge estimate of 20 m^3 s^{-1} (equation A) and an average discharge of 50 m^3 s^{-1} from May to Sept (equation B) alongside average summertime methane concentrations of 33.72ppm from the Mixed Zone produces a summertime methane flux ranging from 8915 to 22288 tonnes based on the following equation:

$$\textit{Seconds over summer period}$$
$$= \textit{seconds in a day} \times \textit{number of days in the summer period}$$

$$m^3 \textit{ over summer period} = \textit{seconds over summer period} \times \textit{discharge}$$

$$\textit{Litres over summer period} = m^3 \textit{ over summer period} \times 1000$$

$$\textit{Methane (mg)over summer period} = 33.72 \times \textit{litres over summer period}$$

$$(\textit{where } 33.72 \textit{ is the average summertime ppm value at the Mixed Zone}$$

$$\textit{Conversion to tonnes over the summer period}$$
$$= \textit{methane in mg} \div 1000000000$$

$$\textbf{\textit{Total tonnes annually}}$$
$$= \textbf{\textit{estimated summer period tonnes}}$$
$$+ \textbf{\textit{estimated winter period tonnes}}$$

7.3. Discussion

7.3.1. Sources of methane as indicated by isotopic evidence

Subglacial waters have been shown to deliver large quantities of methane to the proglacial area. Isotopic investigation of potential methane sources using $\delta^{13}C$ CH_4 and δD CH_4 isotopes obtained from Spring samples indicated that proglacial isotopic signatures encompassed both biogenic and geogenic ranges. There is the possbility that both origins were actively supplying methane to the subglacial drainage system, or that isotopic shifts away from the biogenic end member could be due to fractionation. Potential methane generation mechanisms and oxidation fate of methane within Sólheimajökull proglacial waters will there be explored below.

7.3.1.1. Biogenic Methane Sources

Water emanating from subglacial sources during Spring 2014 contributes one isotopic end member to the $\delta^{13}C/D$ CH_4 mixing plot. As identified in figure 7.5, these subglacial upwellings had an isotopic signature associated with methane of a microbial origin, with average $\delta^{13}C$ CH_4 values of -59.7‰ (1SD= 0.15) and an average δD of -323.7‰ (1SD= 0.65). Microbial methane can be further partitioned by methane production pathway. Two primary metabolic pathways for bacterial methanogenesis have been identified: reduction of carbon dioxide (CO_2+ $8H^+$ +$8e^-$ $\rightarrow$ CH_4 +$2H_2O$) and fermentation of acetate (conversion of methyl groups to CH_4 represented by: $CH_3COOH \rightarrow CH_4$ +CO_2) both with differing isotopic signals (Whiticar, 1999; Whiticar et al. 1986). In this instance the $\delta^{13}C$ CH_4 /δD isotopic values associated with the sub-glacial upwellings fall into the range of methanogenesis via the acetate fermentation pathway mediated by acetoclastic methanogens ($\delta^{13}C$ values -60to -50‰ and δD -400 to-250‰). In terrestrial and freshwater environments the acetoclastic reaction accounts for 70% of methane production compared to 30% generated via the CO_2 reduction pathway (McCalley et al., 2014; Valentine et al., 2004).

Acetoclastic production pathways involve microbial transformation of organic monomers into fatty acid compounds, facilitated by homoacetogenic bacteria. This precursory stage of methane production generates the necessary carbon and energy sources to drive methanogenic fermentation processes. The combination of high aqueous methane concentrations and an isotopic signature indicative of bacterial intervention in subglacial upwelling waters, suggests enhanced methane production mediated by synergy between homoacetogenic bacteria and methanogens in the anoxic Sólheimajökull subglacial realm. Whilst the subglacial upwellings deliver methane which is of biogenic origin, many sites display isotopic signatures which fall beyond the microbial isotopic range. Such isotopic enrichment likely reflects the process of methane oxidation (methanotrophy) under aerobic conditions and associated fractionation along the trajectory depicted in figure 7.6.

7.3.1.2. Potential geogenic methane sources

Given the dominance of a microbial methane source emanating from beneath the glacier in the subglacial meltwaters, it would seem appropriate to suggest that the heavy methane isotopes found within the proglacial meltwater area are associated with fractionation during methanotrophic methane oxidation. However, geogenic sources of methane support an isotopic signature which overlaps with a methanotrophic source (Figure 7.5). Interactions between the Katla subglacial volcanic system and meltwater in the proglacial area are not uncommon at Sólheimajökull. The Jökulsa á Sólheimasandi has been previously shown to convey geothermally derived ions and has been assigned the local name Fulilaekur (foul smelling river) linked to the sulphurous odour emitted, mostly during Summer (Lawler et al., 1996). Similar Sulphurous smells are also released at Kverkjökull Stream, Northern Vatnajökull and Skafta Meltwater River North West Vatnajökull and linked to meltwater exchange with areas of geothermal activity (Fenn and Ashwell, 1985; Lawler et al., 1996). The nature of subglacial volcanism at Sólheimajökull offers the unique situation whereby methane of geogenic origin cannot be conclusively ruled out.

7.3.2. Hydraulic configuration as a driving factor of methane source

Synchronicity between subglacial water delivery and increases in microbial methane concentration show hydrology to be a major contributing factor to methane dynamics at Sólheimajökull. However, prevalence of high concentrations of microbial methane during the late Spring 2014 and Summer 2013 periods is at odds with classical glacier hydrology concepts. Traditionally, during the accumulation season low meltwater fluxes to the glacier bed promotes distributed drainage in a linked cavity network or saturation and slow fow through subglacial sediments. Isolation from the atmosphere promotes widespread anoxia allowing chemical reduction of nitrates (Wynn et al., 2007; Ansari et al., 2014), sulphates (Wadham et al., 2004) and the potential for methane formation by bacterial means (Skidmore et al., 2000). 'Normal' ablation season subglacial drainage would result in oxidizing conditions, as oxic meltwaters flood the subglacial system forcing channelization and transfer of waters in partially filled conduits under variable pressure. Conditions at Sólheimajökull do not conform to these traditional drainage concepts. Low methane concentrations prior to the delivery of subglacial waters, and high summertime methane concentrations during the prevalence of summertime anoxic conditions (Wynn et al., 2015) suggest a reversal of classical redox conditions. Bulk meltwater characteristics, TDIC concentrations and solute flux indicate a three stage seasonal development of the drainage at Sólheimajökull. This expansion and contraction of the subglacial hydraulic network will be explored as a potential driver of methane dynamics.

Bulk meltwaters continually exit the proglacial lagoon via Jökulsa á Sólheimasandi implying year round drainage. The descent of the Sólheimajökull glacier tongue to low elevations combined with the mild maritime climate favours year round surface melt on the lower reaches of the glacier, supporting the maintenance of a localised channelized drainage configuration well connected to the atmosphere. This system will convey relatively low volumes of meltwater sourced from both low elevation surface melt and from subglacial cavity seepage continuously throughout the winter. Low methane concentrations exhibited during early Spring, are likely supplied from

cavity seepage into the localised channel system and oxidized by methanotrophic microbial assemblages which are thriving in the well aerated channel margins (Dieser et al., 2014). Such methanotrophy accounts for enriched $\delta^{13}C_{CH4}$ signatures prevalent prior to subglacial upwelling opening.

As the subglacial portal opens, large quantities of microbial methane are delivered from anoxic areas of the bed. This extensive injection of subglacial water with a light isotopic signature, mixes with existing proglacial lagoon water, overwhelming previous isotopic signatures and imparting a widespread transition to lighter isotopes. Once the subglacial drainage system has been established, expansion occurs throughout the summer. Late Spring isotopic signatures are comparable to Summer $\delta^{13}C$ CH_4 isotopes indicating a prevalent source of microbial methane across these two seasons. In addition, high concentrations of methane overwhelm the proglacial area during Summer. Light isotopic methane signatures with little evidence of oxidation during the late spring and Summer, are in keeping with findings linked to low sulphur redox conditions during Summer seasons (Wynn et al., 2015) suggesting dominance of widespread anoxia. Two potential processes are driving Summertime anoxia: drainage of water stored in linked cavities or release of reduced gases from geothermal zones which generate anoxic meltwaters by utilising any dissolved oxygen content.

Initial Spring expansion of the drainage system could lead to incorporation of anoxic methane rich waters from isolated linked cavities that have persisted during partial winter shut down. Anoxia could then be maintained by widespread constant purging of anoxic areas of sediment and pockets of water across the glacier bed in line with subglacial drainage expansion (Wynn et al., 2006). However, this would require large scale continual linked cavity drainage to maintain widespread basal anoxia. Alternatively, release of reduced gases from geothermal zones offer another solution to summertime anoxia. Expansion of the subglacial drainage system head wards likely intersects the Katla geothermal zone at the time of year when seismic activity

and geothermal processes are at their peak. Two areas of seismic activity have been identified beneath the Mýrdalsjökull ice cap: one in the South East and another in the South West not far from Sólheimajökull (Lawler et al., 1996). Seismic activity is highly seasonal in South West Mýrdalsjökull, with activity peaking during July-October (Lawler et al., 1996; Guðmundsson et al., 1994; Einarsson and Brandsdóttir, 2000), frequently associated with surface melt and seasonal unloading of the snowpack. Low summertime overburden pressures from snowpack unloading (3-9m of snowpack melting leads to an estimated seasonal unloading of 0.003MPa (Einarrsson and Brandsdóttir, 2000) have been deemed sufficient to trigger seismic and geothermal activity (Pagli and Sigmundssen, 2008), coinciding with drainage system expansion. Since Sólheimajökull is a temperate based glacier, meltwater is able to percolate into the crust below via faults, dykes and fissures, reaching areas of geothermal activity (Lawler et al., 1996; Einarrsson and Brandsdóttir, 2000) providing the opportunity for reduced geothermal gases to utilise any dissolved oxygen content in meltwaters and transport these constituents towards the glacier snout under conditions of anoxia. This cyclic 'sweeping out' of the geothermal zone has been previously recorded in meltwater discharge from Sólheimajökull and hydrochemical perturbations associated with this process recur each summer, providing pulses of chemically enriched subglacial water (Lawler et al., 1996). Supply of water from geothermal areas would promote widespread anoxia across the subglacial area, even where channelized drainage prevails. This summer season anoxia enables the continued production of biogenic methane and transport from beneath the ice mass.

Anoxia driven by geothermal zones could also be accompanied by geogenic methane release, accounting for enriched isotopic signatures across the proglacial lagoon. However, methane isotopic signatures of subglacial waters remain firmly in the biogenic range, likely precluding this possibility. The only way to distinguish between the biogenic and geogenic sources in a definitive fashion, would be to analyse the clumped isotopic composition of methane, addressing ^{13}C-^{2}H bonding structures which vary in abundance according to temperature.

7.3.3. Methane flux comparisons

Flux estimations have provided annual methane fluxes of between 9,179 and 22,551 tonnes of CH_4 based upon summer discharges of 20 and 50 m^3 s^{-1} respectively. Potential annual methane flux from Sólheimajökull is high, exceeding conservative estimates of 10,000 tonnes per year for total european geothermal and volcanic systems (Etiope et al., 2007). In comparison total annual methane flux for Grimsvotn, Krafla and Askja volcanoes in Iceland equates to 440 tonnes of CH_4 yr^{-1}. The estimated total of methane emissions from all parameterised Icelandic geothermal systems is approximately 1,300 tonnes CH_4 yr^{-1} (Etiope et al., 2007). If Sólheimajökull methane flux estimations prove to be accurate, the lower methane emission estimate from Sólheimajökull alone is ten times that of Icelandic total geothermal methane emission. This clearly highlights the importance of subglacial microbial methanogenesis, and that under such unqiue conditions, brought about by hrdraulic configuration and geothermal connectivity, glaciers offer an ideal scenario to generate and release large quantities of methane to the atmosphere.

7.4. Summary

1. There are two possible origins of natural methane within the Sólheimajökull Proglacial system: bacterial and geogenic.
2. Subglacial waters measured during Spring 2014 contain high average concentrations of bacterial methane produced via the acetate fermentation pathway (average of 0.574 (1 SD = 0.128 ppm).
3. Isotopic data from the proglacial area indicates that opening of the subglacial upwellings is crucial in the supply of bacterial methane and once established becomes a dominant source of methane to the proglacial system. Summer $\delta^{13}C$ CH_4 isotopes support methane from a bacterial source indicating expansion of subglacial upwellings in line with development of seasonal channelised drainage.

4. Methane isotopes from subglacial upwellings show little oxidation pointing towards widespread anoxia across the subglacial realm.

5. Seasonal release of reduced gases from geothermal areas drives widespread anoxia in a channelised drainage system as supported by the work of Lawler et al. (1996) and Wynn et al. (2015).

6. δ^{13}C / δD CH$_4$ plots indicate oxidation of methane within the Proglacial Lake with relatively heavy isotopic signatures observed in early Spring. Since hydro chemical evidence cannot provide support for a distinct geogenic end member it is most likely that the relationship between δ^{13}C and δD is a methanotrophy fractionation trajectory of a dominant subglacial bacterial source.

7. Methane flux estimates range from 9179 to 22,551 tonnes of CH$_4$ based upon Summer discharges of 20 and 50 m^3 s^{-1} respectively. Lower estimates are in excess of total postulated Icelandic geothermal emissions.

8. Assessing Methane Dynamics in Sólheimajökull proglacial and subglacial substrates

8.1. Introduction

Current research identifies discharge of methane from beneath Sólheimajökull. This is characterised by low methane concentrations in early Spring and a transition to higher concentrations of bacterially sourced methane concurrent with delivery of subglacial waters. Maximum methane concentrations of 48.37ppm measured in subglacial upwellings are accompanied by methane isotopic signatures of -59.54 to -59.88‰ and -322.6 to -324.3‰ for $\delta^{13}C$ CH$_4$ and δD CH$_4$ respectively. This indicates high concentrations of bacterial methane originating in anoxic areas of the Sólheimajökull subglacial realm. After discharging from beneath the glacier, methane interaction with the atmosphere is regulated by the coeval processes of methanogenesis and methanotrophy. Aqueous methane represents one aspect of methane dynamics at Sólheimajökull. Subglacial and proglacial sediments offer additional constraints on methane sources and sinks within the catchment. This thesis will now present in situ static chamber analysis of methane dynamics across the Sólheimajökull proglacial forefield, alongside in vitro incubation of basal sediments, in order to elucidate areas of methanogenesis and methanotrophy.

8.2. Employment of in situ static chambers to monitor Sólheimajökull proglacial methane dynamics

Proglacial methane dynamics were monitored in situ during Summer 2013 and Spring 2014 using static chamber methods outlined in sections 3.6.2, in an attempt to elucidate whether the Sólheimajökull proglacial forefield is an area of net methanogenesis or net methanotrophy. In some cases, glacier forefields have been demonstrated to switch from a zone of net methane production to one of net methane consumption in the wake of ice recession (Barcena et al., 2010). The glacial foreland is therefore generally accepted to be an area of importance to the methane

biogeochemical cycle, although precise dynamics depend upon site specific conditions.

8.2.1. Results from static chamber analysis

Figure 8.1 provides examples of methane dynamics observed through in situ static chamber analysis, during Summer 2013 and Spring 2014. Little variation in methane concentration was observed over the given time periods, a pattern applicable to all static chamber observations. Whilst Spring proglacial sediments exhibited higher methane concentrations ~7ppm, again little variation in overall headspace was observed. Longer term employment of the static chamber method during Spring 2014 (figure8.2) also reflected that methane variability was low even over extended time periods.
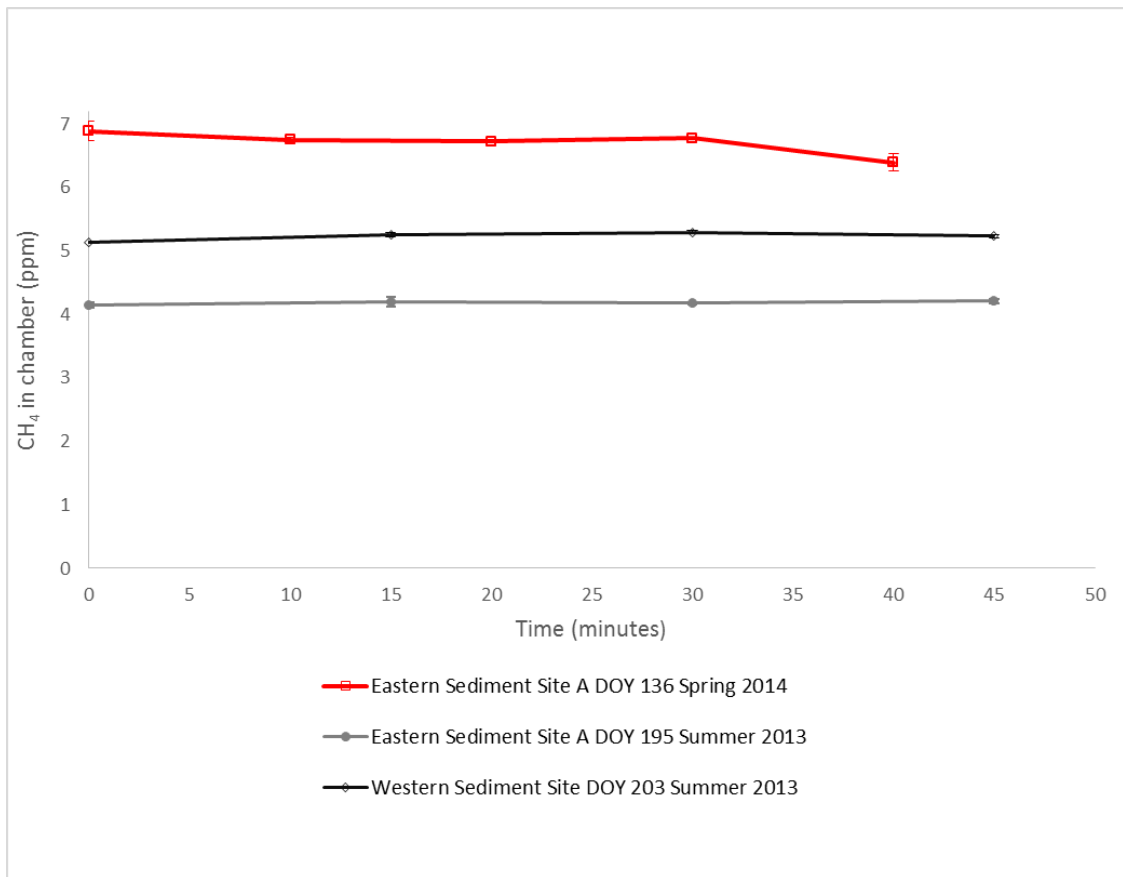
Figure 8.1: Methane headspace concentrations for static chamber analysis during Spring 2014 and Summer 2013 at selected Eastern and Western sites.

Methane in chamber headspace value is an average taken from the deployment of three static chambers at each site. The standard deviation between these three chambers, portrayed as vertical error bars is often too small to distinguish.
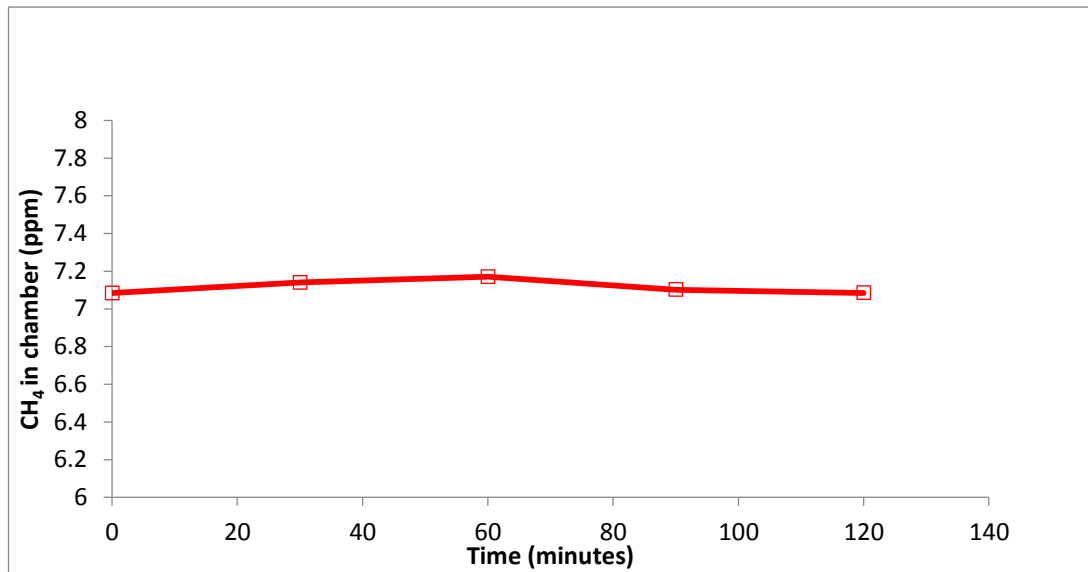
Figure 8.2.: Methane headspace concentrations for static chamber analysis at the long term eastern sediment site, DOY 136, Spring 2014

Data from all static chamber measurements for Summer 2013 (additional data can be found in appendix 6) was converted into fluxes and presented in table 8.1. Negative fluxes represented methane consumption, whilst positive fluxes represented methane production. Again, in keeping with time series data of methane change fluxes were small. During summer, the most negative flux was observed close to the glacier at Eastern Sediment Site A, whilst the highest flux was at Eastern Sediment Site D, perhaps inferring a slight change in methane dynamics with proximity to the glacier. However, on the whole fluxes during summer were extremely low and there was no reliable evidence to suggest that the sediments in the proglacial area contribute to the methane cycling. Based upon this the sole source of methane to the meltwater streams emanated from the subglacial upwelling.

Site	Average change in methane concentration over 45 minutes (ppm)	Methane flux per hour (ppm)
Eastern Sediment Site A	-0.084 (0.254) Min=-0.442 Max=0.109 *n=3*	-0.112
Eastern Sediment Site B	-0.012 (0.290) Min=-0.308 Max=0.466 *n=3*	-0.016
Eastern Sediment Site C	0.012 (0.290) Min=-0.308 Max=0.466 *n=8*	0.016
Eastern Sediment Site D	0.168 (0.204) Min=0.012 Max=0.584 *n=5*	0.224
Eastern Sediment Site E	-0.030 (0.048) Min=-0.113 Max=0.023 *n=6*	-0.040
Eastern Sediment Site F	0.089 (0.286) Min=-0.163 Max=0.692 *n=6*	0.119
Western Sediment Site	0.113 (…) Min=0.106 Max=0.120 *n=2*	0.139

Table 8.1.: Average methane fluxes calculated from time of closure for static chamber analysis during Summer 2013

8.2.2. Summary of static chamber analyses

1. Static chamber analysis demonstrated little variation in methane headspace concentrations.

2. Methane flux across the proglacial forefield was minimal, perhaps there was some suggestion of methanotrophy in sediments closest to the glacier where net methane flux is negative, however values were too low to decipher any dominant trend.

3. Unlike many proglacial forefields which become net sources or sinks of methane, sediments at Sólheimajökull do not show any notable participation in methane cycling.

8.3. In vitro experiments to determine Sólheimajökull subglacial sediment methane dynamics

Subglacial sediments were extracted from crevasse thrust planes along the Sólheimajökull glacier snout in accordance with methods outlined by Kaštovská et al. (2005) and explained in section 3.6.1. It is believed that these sediments have been transferred from the bed of the glacier to the surface as thrusts play an important role in the recycling of basal debris (Hambrey, 1994). Thrust faults, or shear planes are the product of strong compression in the ice, potentially where ice slows at the snout or encounters a basal object. Two types of sediment were visually identified during Spring 2014- light brown and grey. XRD analysis has shown almost identical chemical composition of these sediments, therefore colour was thought to represent iron oxidation state. The light grey sediment would be typically associated with Fe^{2+} under anoxic conditions and oxidized Fe^{3+} prevalent within the brown sediment.

Following range-finder experiments (outlined in section 3.6.5.1.), a suite of incubations at optimised conditions were undertaken to investigate rates of methane production and consumption in each sediment type (for main methodology please refer to section 3.6.5).

8.3.1. Results from Methanogenesis Incubations

Average Methane concentrations determined via replicates of gas measurements from headspaces of Wheatons A, B and C alongside a controlled experiment were as follows:

Time Since Closure (Days)	Wheaton A Average Methane Concentration in ppm (Standard deviation)	Wheaton B Average Methane Concentration in ppm (Standard deviation)	Wheaton C Average Methane Concentration in ppm (Standard deviation)	Control Experiment Average Methane Concentration in ppm (Standard deviation)
0	0.000 (0.00) *n=3*	0.000 (0.00) *n=3*	0.000 (0.00) *n=3*	0.000 (0.00) n=3
7	0.405 (0.25) *n=3*	0.421 (-) *n=2*	0.215 (-) *n=2*	0.000 (0.00) *n=3*
14	0.931 (-) *n=2*	0.470 (-) n=1	0.631 (-) *n=2*	0.122 (-) *n=2*
21	0.626 (0.04) *n=3*	0.484 (-) *n=2*	0.606 (0.04) *n=3*	0.150 (0.03) *n=3*
35	1.202 (-) *n=2*	1.030 (0.10) *n=3*	1.000 (0.09) *n=3*	0.054 (0.09) *n=3*
49	1.700 (0.33) *n=3*	1.176 (0.09) *n=3*	1.580 (0.18) *n=3*	0.016 (-) *n=2*

Table 8.2: Average methane concentrations in headspaces for all methanogenesis incubation experiments

1 standard deviation (1SD) is in parentheses.

Final methane ppm corrected against control		
Wheaton A	Wheaton B	Wheaton C
1.684	1.160	1.564

Table 8.3: Final methane concentrations corrected against the control experiment

All Wheatons containing Fe^{2+} enriched (grey) sediment demonstrated the production of methane over a 49 day period, with final headspace concentrations of 1.70ppm, 1.18ppm and 1.58ppm recorded during the incubation period for Wheatons A, B and C respectively (figure 8.4). Methanogenesis was first detected 7 days after closure and continued to be produced throughout the incubation period. In contrast, methane concentrations in the control sample remained low ranging from 0 to 0.15ppm indicating that methane detected in Wheatons containing sediment was linked to microbial activity.
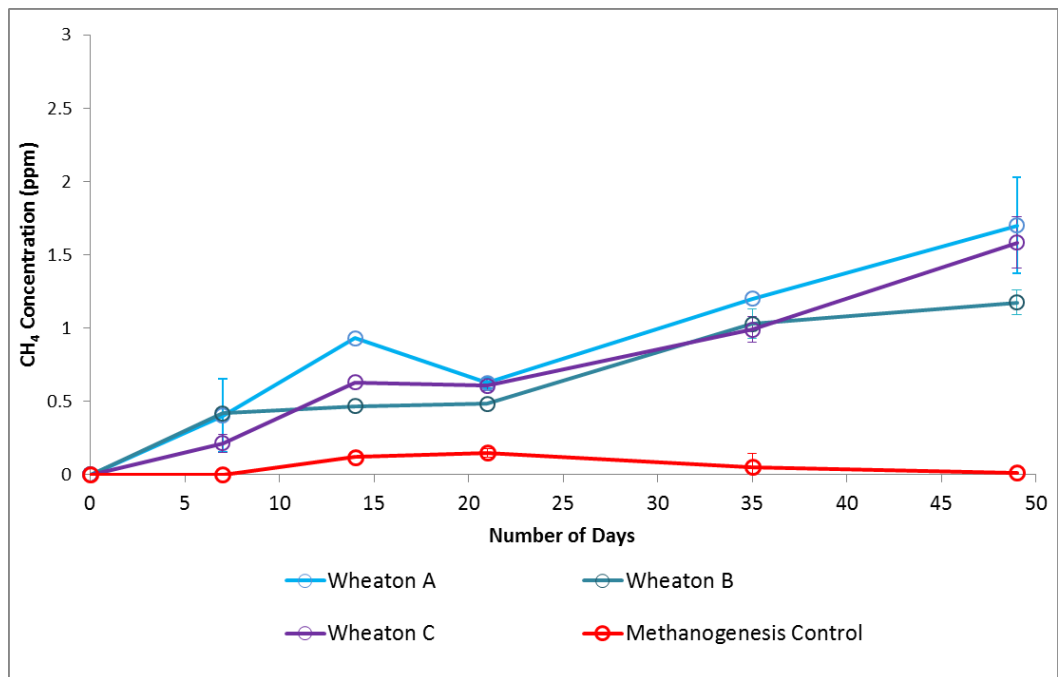
Figure 8.4: Time series of methane concentrations in Wheatons A, B and C alongside the control experiment

Methane concentration was converted into methane produced per gram of dry weight incubation sediment, per hour. This was then compared to other incubation studies. Investigation of moisture content revealed a ~32% loss of mass during drying, therefore sediment dry weight is calculated as ~68% of the original wet weight.

Wheaton	Sediment in Wheaton Wet Weight (g)	Sediment in Wheaton Dry Weight (g)
A	10.01	6.81
B	9.95	6.77
C	9.99	6.79

Table 8.4: Dry weights of sediments used in methanogenesis incubations

Wheaton	Total methane produced over sample period corrected against control (ppm)	Dry Weight Sediment	CH_4 per g per hr (ppm)	CH_4 per g per hr (Femtomoles)
A	**1.684**	6.81	0.0002	2.1×10^8
B	**1.160**	6.77	0.0001	1.4×10^8
C	**1.564**	6.79	0.0002	1.9×10^8
Average (1SD)	1.469 (0.22)	6.79 (0.02)	0.0002 (>0)	1.8×10^8

Table 8.5: Methane produced per g of dry weight Fe^{2+} enriched (grey) sediment per hour

8.3.2. Discussion of findings from methanogenesis experiments

Methanogens are fermentative archaea bacteria that metabolize organic matter under selective environmental conditions (Whiticar, 1999). Microbial methanogenesis accounts for 90% of atmospheric methane (Boyd et al., 2010). However, methanogenic activity in the subglacial realm is an important, but largely overlooked component of the global carbon cycle (Boyd et al., 2010; Wadham et al., 2008). Incubations of Subglacial Sediment A demonstrate replicable methanogenesis over a 49 day period, indicating active methanogens beneath Sólheimajökull. This is in line with other studies which have identified viable methanogens in basal sediments of Antarctica, the Canadian Arctic and Greenland (Boyd et al., 2010; Wadham et al., 2008).

Slow initial production rates observed in the incubations and low overall methane headspace concentrations, are by no means indicative of a sluggish or small scale methanogenic community. Slow methane production in the initial stages of incubation are characteristic of methane production pathway and adjustment of microbes to ambient conditions from a state of dormancy (Sudimoto and Wada, 1993; Stibal et al., 2012). Incubations of subglacial sediments from the Canadian High Arctic, Antarctic and Greenland demonstrate long lag periods of up to 200 days before significant amounts of CH_4 are observed (Stibal et al., 2012). Additionally, low initial methane production has been demonstrated elsewhere, with incubation of Japanese paddy soils exhibiting low methane concentrations during the first several days of incubation. This was succeeded by rapid methane production and attributed to precursor reactions such as acetate formation (Sudimoto and Wada, 1993).

Scaled up calculations of methanogenesis per gram of dry weight sediment per hour reveals the true methanogenic potential of Sólheimajökull subglacial sediments, with values of 1.8×10^8 (as indicated in table 8.6.). Previous incubation studies have highlighted elevated rates of methanogenesis in the Canadian Arctic and Antarctic sediments with rates of 10^2-10^3 fmol CH_4 g^{-1} h^{-1} and 10^3-10^4 fmol CH_4 g^{-1} h^{-1}

respectively (Wadham et al., 2012). This is contrasted with lower methanogenesis production values of 9-93 fmol CH_4 g^{-1} h^{-1} and 9-51 fmol CH_4 g^{-1} h^{-1} demonstrated in Greenland sediments and at Robertson Glacier, Canada (Boyd et al., 2010; Wadham et al., 2012). Ultimately this suggests the subglacial environment at Sólheimajökull contains sediments which are capable of producing methane at rates which surpass those found in other subglacial environments.

Sediment	Study	Fmol Methane per gram of dry weight sediment per hour
Sólheimajökull Fe^{2+} enriched sediment (grey)	This study	Average of 1.8×10^8
Robertson Glacier Canada	Boyd et al. (2010)	9- 51
Greenland	Boyd et al. (2010)	9- 93
Antarctic Sediments	Wadham et al. (2012)	10^3- 10^4
Canadian Arctic Sediments	Wadham et al. (2012)	10^2-10^3

Table 8.6: Comparison of methane production rates found in Sólheimajökull subglacial Fe^{2+} enriched (grey) to other studies

Elevated methanogenesis rates (calculations of fmol CH_4 g^{-1} h^{-1}) at Sólheimajökull are likely due to a combination of favourable conditions. These include a combination of widespread anoxia; organic carbon substrate, from overridden sediments and nutrient recharge supplied by presence of water at the pressure melting point (Stibal et al., 2012). Anoxia prevails across the subglacial realm during late spring and throughout summer, facilitated by linkages between subglacial drainage and areas of geothermal activity (Wynn et al., 2015). This creates a unique situation whereby

summertime anoxia coincides with peak water flows through the subglacial system. As nutrient recharge from meltwaters is an important factor in methanogenesis, the rare combination of these two factors could explain exceptional methane production rates in Sólheimajökull subglacial sediments. Furthermore, geothermal heat sources at Sólheimajökull create an exclusive situation which could favour enhanced methanogenesis. Optimum methane production rates from Arctic wetland sediments were shown to be around 30°C (Blake et al., 2015). Elevation above extremely low temperatures at the glacier bed could be enhancing methanogenic potential at Sólheimajökull. Finally, organic carbon has been shown to exist in proglacial meltwaters as DOC. The combination of these factors, some of which are unique to Sólheimajökull can vindicate high scaled up methanogenesis rates observed.

8.4. Investigation of Potential Methanotrophy in Sólheimajökull Subglacial Sediments

Methane flux to the atmosphere is not solely a function of methanogenesis. Instead methanotrophy also regulates methane dynamics. As incubations have revealed active methanogens operating within Sólheimajökull subglacial sediments, it can be expected that viable methanotrophic communities also exist. Range finder experiments (Appendix 4) of the Fe^{3+} enriched (brown) subglacial sediment indicated methane consumption within enriched headspaces. Further testing of rates of methanotrophy (as outlined in section 3.6.5.3.) and isotopic fractionation can provide insight into the fate of methane in the oxic zone. This will support $\delta^{13}C/D$ field data which are thought to indicate oxidation of bacterially sourced methane (as identified in figure 7.5 Chapter 7.3.3).

8.4.1. Results: methane headspace concentrations during methanotrophy experiments

Average Methane concentrations determined via replicates of gas measurements from headspaces of Wheatons One, Two and Three alongside a controlled experiment were as follows:

Average Methane Concentrations in ppm (1SD)				
Time since closure (hours)	Wheaton One	Wheaton Two	Wheaton Three	Control Experiment
0	145.35 (-) *n=2*	147.56 (-) *n=2*	150.53 (2.38) *n=3*	150.40 (5.24) *n=3*
1.5	147.10 (4.90) *n=3*	148.25 (1.31) *n=3*	156.88 (-) *n=2*	150.28 (-) *n=2*
4	150.19 (-) *n=2*	149.35 (1.21) *n=3*	155.78 (-) *n=2*	156.53 (-) *n=2*
24	139.22 (1.72) *n=3*	143.46 (1.06) *n=3*	142.68 (-) *n=2*	156.15 (2.50) *n=3*
48	120.72 (1.04) *n=3*	119.25 (-) *n=2*	119.73 (0.62) *n=3*	148.78 (-) *n=2*
72	94.27 (-) *n=2*	99.62 (6.99) *n=3*	96.27 (1.77) *n=3*	139.30 (5.62) *n=3*
95	76.19 (-) *n=2*	76.10 (1.26) *n=3*	84.14 (2.91) *n=3*	137.35 (3.55) *n=3*
167	37.41 (-) *n=2*	39.32 (0.73) *n=3*	40.27 (0.45) *n=3*	123.77 (-) *n=2*

Table 8.7: Presentation of average methane concentrations during methanotrophy experiments

This was then presented as a change in methane concentration based upon comparison to methane headspace at initial closure as follows:

Change in methane concentration (ppm)				
Time since closure (hours)	Wheaton One	Wheaton Two	Wheaton Three	Control Experiment
0	0	0	0	0
1.5	1.74	0.7	6.35	-0.12
4	4.84	1.79	5.25	6.13
24	-6.13	-4.09	-7.84	5.74
48	-24.63	-28.31	-30.8	-1.62
72	-51.08	-47.94	-52.25	-11.1
95	-69.16	-71.45	-66.39	-13.05
167	-107.94	-108.24	-110.26	-26.63

Table 8.8: Change in methane headspace concentrations from closure

When corrected against methane depletion in the control headspace this rendered total average consumption values of 81.31ppm, 81.61ppm and 83.63ppm for Wheatons one, two and three respectively.

	Wheaton One	Wheaton Two	Wheaton Three	Control Experiment
Methane Headspace Reduction (ppm)	107.94	108.24	110.26	26.63
Corrected against control experiment	81.31	81.61	83.63	

Table 8.9: Presentation of average methane concentrations during methanotrophy experiments corrected against the control experiment

Incubations of Fe^{3+} enriched (brown) subglacial sediment demonstrated methane consumption which was replicated across all three Wheatons. Initial average methane consumption (figure 8.5) exhibited a period of stabilisation within the first four hours of closure. This was followed by decline in headspace concentrations from 24 hours onwards. Once methanotrophy had commenced, consumption continued at a steady rate across all three Wheatons as indicated by headspace reductions (table 8.8). Control values displayed a differing behaviour, demonstrating trends observed in Wheatons One, Two and Three were representative of methanotrophic activity.
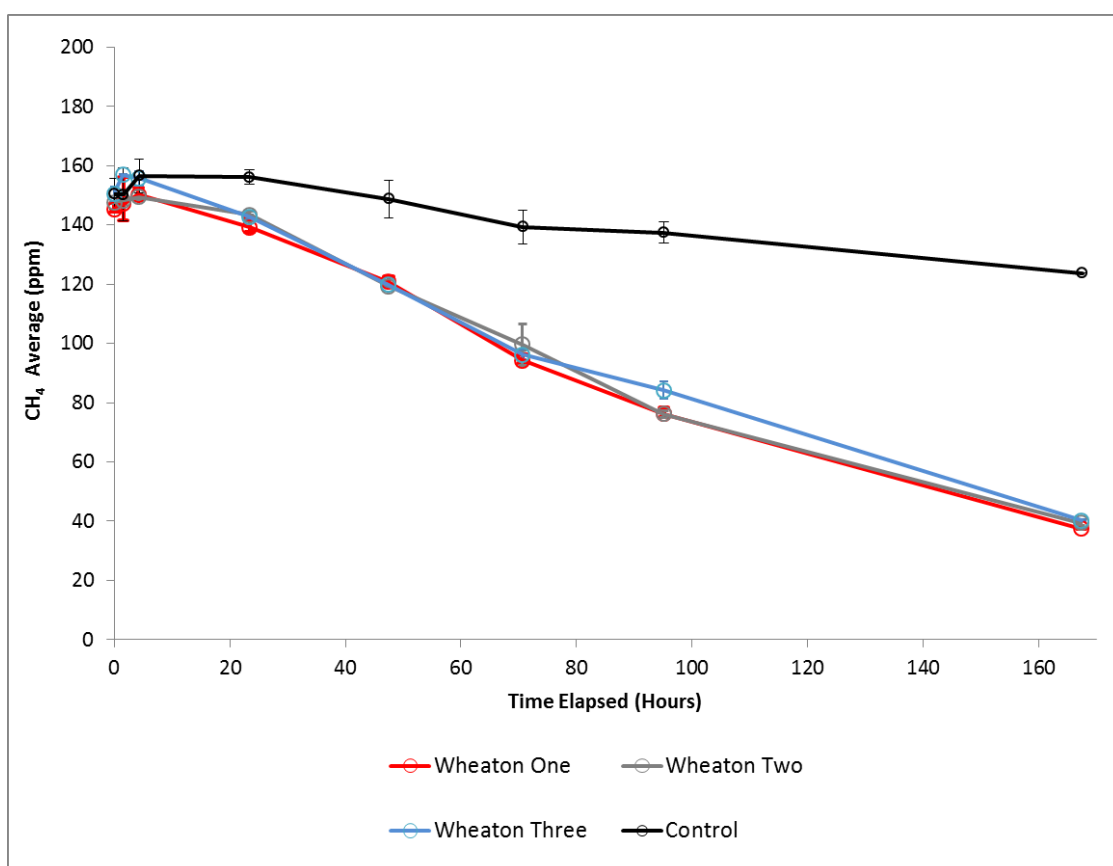
Figure 8.5: Time series of methane consumption in Wheatons one, two and three alongside the control experiment

Average percentage of methane headspace consumed corrected against changes in the control experiment headspace is displayed in figure 8.6. Consumption began within 24 hours with around 5% of methane consumed in this early period. At the

end of the 167 hour study period an average of 55% (1SD=0.26) of the methane headspace had been consumed.
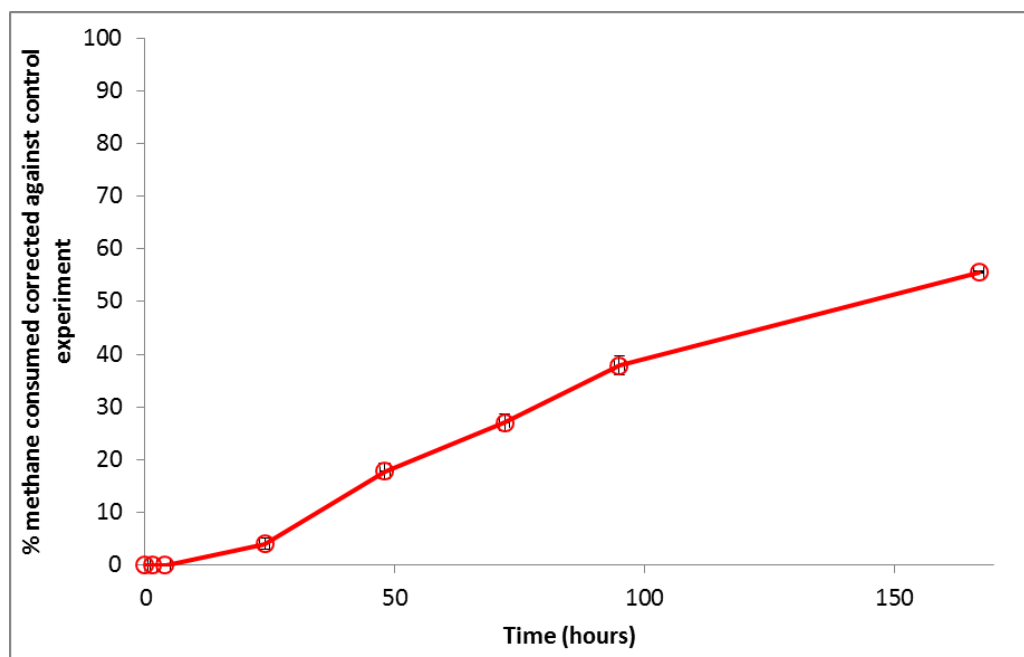
Figure 8.6: Time series of average methane consumption across all three Wheatons corrected against the control experiment

Methane concentration was converted into methane consumed per gram of dry weight incubation sediment, per hour. This was then compared to other incubation studies. Investigation of moisture content revealed a ~36% loss of mass during drying, therefore sediment dry weight is calculated as ~64% of the original wet weight, as follows:

Wheaton	Sediment in Wheaton Wet Weight (g)	Sediment in Wheaton Dry Weight (g)
One	5.01	3.21
Two	4.97	3.18
Three	4.99	3.21

Table 8.10: Dry weights of Fe^{3+} enriched (brown) subglacial sediment used in methanotrophy incubations

Methane consumption per gram of Fe^{3+} enriched (brown) subglacial sediment per hour can then be calculated as follows:

Wheaton	Total methane consumed over sample period corrected against control (ppm)	Dry Weight Sediment	CH_4 per g per hr (ppm)	CH_4 per g per hr (Femtomoles)
One	81.31	3.21	0.1517	9.5×10^9
Two	81.61	3.18	0.1537	9.6×10^9
Three	83.63	3.21	0.1560	9.8×10^9
Average (1SD)	**82.18 (1.26)**	**3.20 (0.01)**	**0.154 (0.002)**	**9.61×10^9**

Table 8.11: Methane consumed per gram of dry weight Fe^{3+} enriched (brown) subglacial sediment per hour

8.4.2. Results: isotopic fractionation as a result of methanotrophy

Oxidation of methane by methanotrophic bacteria has the capacity to alter the isotopic composition of the residual methane. During methanogenic consumption, the light isotope ^{12}C is selectively oxidised more rapidly than the heavier isotope ^{13}C leaving a residual CH_4 signal enriched in the heavier isotope. The resulting isotopic signal is often very similar to that of CH_4 produced by geogenic means (Coleman et al. 1981; Cicerone and Oremland, 1988; Whiticar, 1999).

Isotopes of $\delta^{13}C$ CH_4 (Wheatons One and Three) and δD CH_4 (Wheaton Two) were tested to analyse for fractionation as methanotrophy progresses. A positive relationship between $\delta^{13}C$ CH_4 value and time elapsed was evident, whereby as the incubation progresses, $\delta^{13}C$ CH_4 in the remaining headspace displayed a transition to

heavier values. Final δ^{13}C CH$_4$ values of -13.63‰ and -13.66‰ were observed for Wheatons One and Three representing increases of 29.57‰ and 29.49‰ over the incubation period.

Time since closure (hours)	Wheaton One δ^{13}C	Wheaton Three δ^{13}C	Average δ^{13}C Value Wheatons One and Three *n=2*
0	-43.20	-43.10	-43.15
1.5	n/a	n/a	n/a
4	-42.77	-42.95	-42.86
24	-40.63	-40.64	-40.64
48	-36.72	-37.22	-36.97
72	-33.28	-34.07	-33.68
95	-29.26	-29.20	-29.23
167	-13.63	-13.68	-13.66

Table 8.12: Average δ^{13}C values of Wheatons One and Three

Progression towards heavier isotopic signatures with time elapsed was also observed in δD values from Wheaton Two. Initially light δD values of -163.3‰ were recorded at the start of the sampling period. As incubation time progressed there was a transition towards heavier values with a final δD signature of 100.3‰, representing a 263.0‰ increase.

Time since closure (hours)	Wheaton Two δD
0	-163.28
4	-164.86
24	-148.76
48	-123.19
72	-94.45
95	-52.94
167	+100.27

Table 8.13: Observed δD values for Wheaton Two

Presentation of time series δ^{13}C CH$_4$ and δD isotopic signatures further demonstrated this transition towards heavier isotopes was a function of time. This evolution of the δ^{13}C signal was not observed in the control sample, suggesting the δ^{13}C and δD CH$_4$ isotopic signatures were driven by processes occurring in the active subglacial sediments.
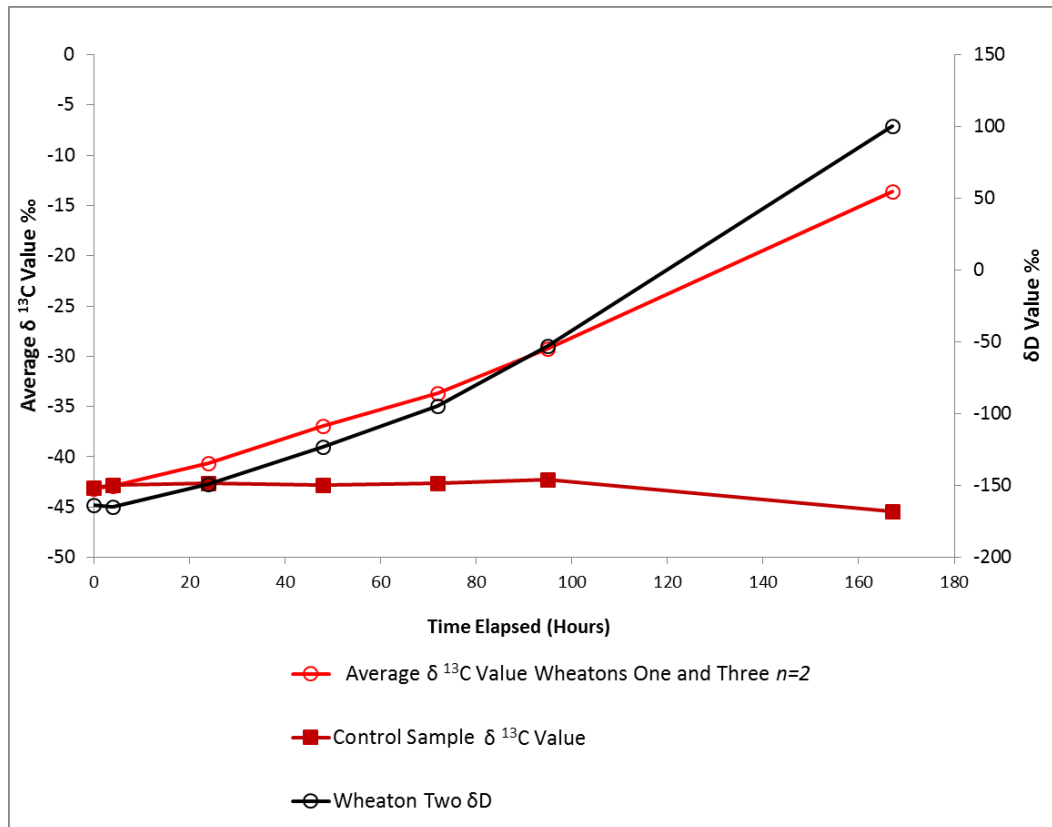
Figure 8.7: Time series of average δ^{13}C and actual δD CH$_4$ isotopic enrichment during methanotrophy incubations

A Bi-plot of δ^{13}C CH$_4$ and δD values indicated a sympathetic change in δ^{13}C and δD values driven by methanotrophic activity in Sólheimajökull subglacial sediments. The fractionation trajectory displayed during incubation of the Fe^{3+} enriched (brown) subglacial (R^2 value of 0.99 and gradient of 9.00) was comparable to that demonstrated by incubation of methanotrophic communities by Coleman et al. (1981). In this instance, for every 10‰ change in δ^{13}C CH$_4$ there was an

accompanying fractionation of 85‰ evident in δD CH$_4$ signatures, which equated to a linear fractionation gradient of 8.5 (Coleman et al., 1981).
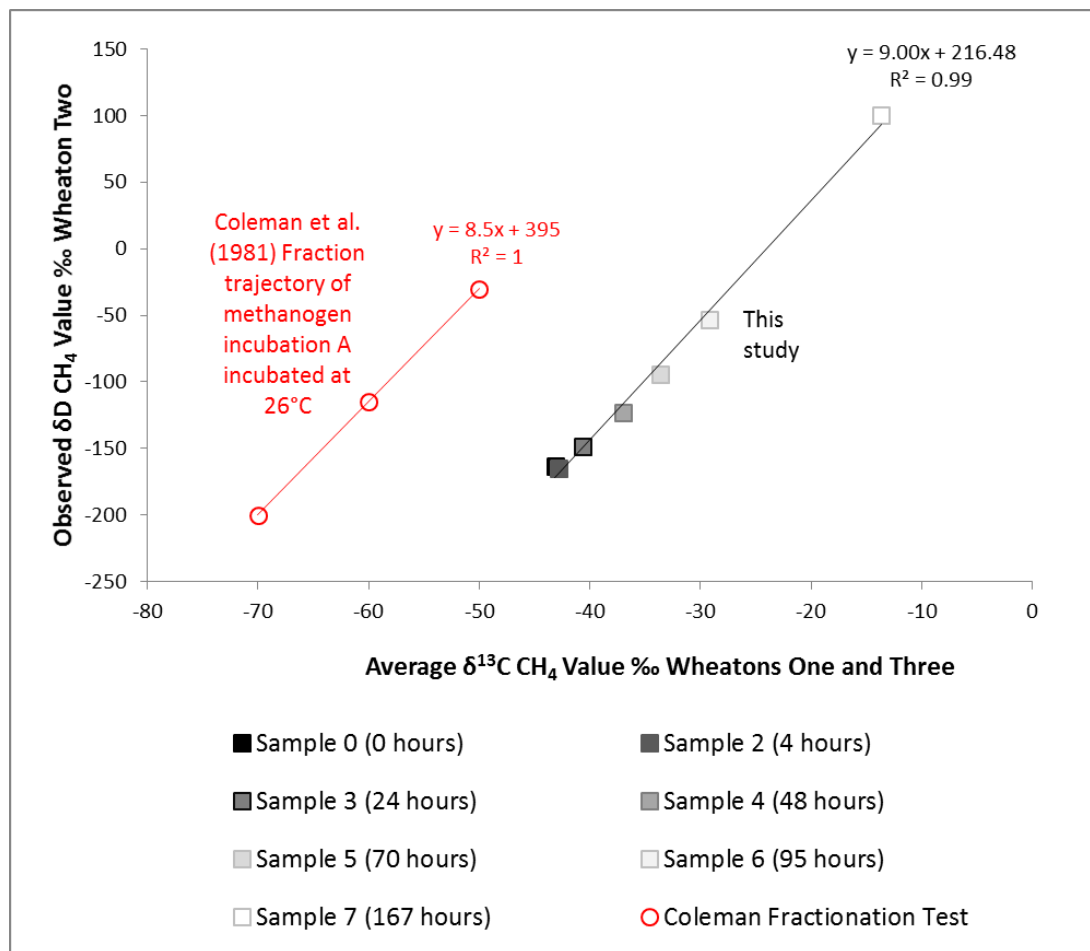
Figure 8.8: Fractionation trajectory of δ^{13}C and δD CH$_4$ signatures during incubation of Sólheimajökull subglacial sediment B compared to fractionation quoted by Coleman et al. (1981)

Evidence of microbial isotopic fractionation demonstrated during incubation experiments provided linkages to isotopic variance observed in proglacial waters. The enrichment gradient of Sólheimajökull proglacial waters was shown to be 8.67 ($R^2 = 0.99$). This was in keeping with previous fractionation displayed by Coleman et al. (1981) and from incubation of Sólheimajökull Fe^{3+} enriched (brown) subglacial sediment where relative change in δ^{13}C and δD CH$_4$ values resulted in gradients of 8.5 and 9.00 respectively. As demonstrated in figure 8.9, both aqueous methane and

methanotrophy in sediment incubations encompassed isotopic signatures typically associated with geogenic methane before reaching final isotopic values beyond the realm of either methane source. This further supported the idea that methane at Sólheimajökull is of a biogenic origin which fractionated during proglacial methanotrophy, rather than a mixing of biogenic and geogenic sources.
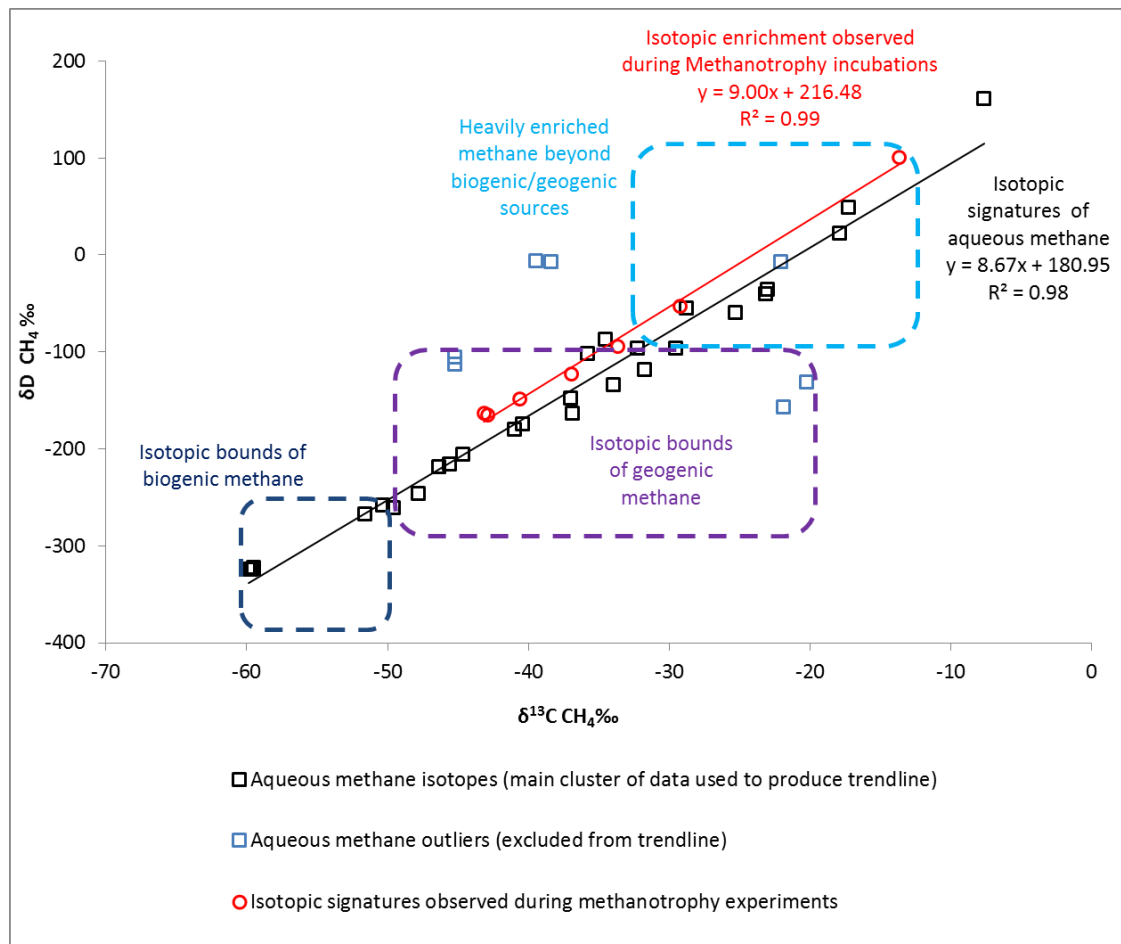
Figure 8.9: Bi-plot of $\delta^{13}C$ and δD CH_4 signatures observed in methanotrophy incubations and proglacial aqueous methane

8.5. Discussion of methanotrophy observed during subglacial sediment incubations

Coeval processes of methanogenesis and methanotrophy govern the net flux of methane to the atmosphere. Methane oxidising bacteria (methanotrophs) are widespread, occurring in both freshwater and marine environments, acting as a 'methane filter' reducing methane release to the atmosphere (Berestovskaya et al., 2002). Globally, methanotrophs represent a net sink of CH_4 by consuming approximately 20 to 60Tg of CH_4 per year (Barcena et al., 2011; Coleman et al. 1981). At Sólheimajökull, incubation of subglacial sediments has demonstrated a rate of methane consumption in excess of production (10^8fmol CH_4 g^{-1} h^{-1} for methanogenesis compared to 10^9fmol CH_4 g^{-1} h^{-1} for methanotrophy). Accelerated consumption in Sólheimajökull sediments exceeds other environmental studies, for example, Chan and Parkin (2001) quote highest rates of 10^6fmol CH_4 g^{-1} hr^{-1} for Iowa agricultural soils. This indicates that methanotrophs are not only viable in Sólheimajökull subglacial sediments, but also offer the potential for rapid, largescale methane consumption. However, the relative importance of methane production and consumption at Sólheimajökull is dependent upon access to each type of subglacial sediment and access to the prevailing conditions necessary to drive each microbial reaction.

Incubation of methanotrophic microbes has also demonstrated the potential to achieve isotopic signatures enriched in ^{13}C and D beyond the envelope of expected values from a biogenic or geogenic source. Methanotrophs preferentially incorporate lighter isotopes into cellular biomass leaving a residual gas that is sympathetically enriched in [13]C /D (Elvert et al., 1999; Chanton, 2005). Therefore, if a microbially produced methane migrated to an oxic environment and was subjected to partial oxidation by methanotrophs then the residual gas could have a carbon isotopic signature similar to methane of geogenic origin (Coleman et al., 1981). Field observations of aqueous methane concentrations indicate large quantities of bacterially produced methane exiting the subglacial system, which is thought to fractionate along an oxidation trajectory. Incubation of Fe^{3+} enriched brown subglacial sediment supports this with $\delta^{13}C$ and δD values demonstrating a positive

fractionation trajectory in line with other methanotrophy experiments (Coleman et al., 1981). In addition, lab based oxidation experiments account for heavy isotopic signatures (greater than $\delta^{13}C$ = -20‰ and δD= -50‰) observed in proglacial waters with final isotopic signatures displayed during lab incubations reaching $\delta^{13}C$= -13.66‰ and δD= +100.27‰. This provides evidence that methanotrophic activity is active within the field environment and further suggests the methane isotopic signatures which plot away from a biogenic source to be associated with methanotrophy rather than geogenic sources.

The interconnected relationship between methanogenesis and methanotrophy has a fundamental role in methane dynamics within the Sólheimajökull system. However, aqueous methane concentrations found in Sólheimajökull bulk meltwaters exhibit great seasonality, inferring periodic changes in the variable rates of methanogenesis and methanotrophy. Seasonal hydraulic configuration and connectivity to geothermal hotspots determines the relative functioning of methanogenesis and methanotrophy. Prevalence of summer seasonal anoxia drives methanogenesis and supresses methanotrophy, resulting in large scale transport of bacterial methane to the proglacial zone. Conversely during Spring low methane concentrations prevail. Here, methanogenesis is restricted to localised pockets of anoxia, within the linked cavity network. Once these areas of methane production drain into the continual channelized drainage system beneath the lower reaches of the glacier snout, methane is rapidly oxidised (Dieser et al., 2014) resulting in the transfer of low quantities of methane, with an enriched $\delta^{13}C/\delta D_{CH4}$ signature. This fully demonstrates how redox conditions are essential in the maintenance and delivery of methane to the proglacial zone.

Once waters transfer to the proglacial lagoon they are subjected to oxic conditions and methanotrophy processes dominate. Waters which are closest to subglacial inputs for example the Upper Western Lagoon site which demonstrated a microbial isotopic signature across Spring and Summer seasons experience little oxidation.

Conversely, waters which are most distal from subglacial bacterial inputs (e.g. Upper Eastern Lagoon Sites) experience the greatest oxidation of methane as they have dwelled in the proglacial area the longest. This provides evidence for active aqueous methane cycling with production under anoxic subglacial conditions and consumption in oxic proglacial settings.

8.5. Summary

1. Subglacial sediments collected from crevasse thrust planes at Sólheimajökull demonstratde replicable evidence for methanogenesis and methanotrophy.

2. Methanogenesis was observed over a 49 day period in Fe^{2+} enriched (grey) subglacial sediment.

3. Methanogenesis supported a production rate of 10^8 fmol CH_4 g^{-1} h^{-1}. This demonstrated elevated levels of methanogenesis compared to other published incubation experiments.

4. Subglacial methanogenesis can therefore account for the microbial methane signature observed in Sólheimajökull subglacial waters.

5. Rapid methanotrophy is observed in Fe^{3+} enriched (brown) subglacial sediment, with 70-90% of the methane headspace consumed within 167 hours.

6. Methanotrophy supported a consumption rate of 10^9 fmol CH_4 g^{-1} hr^{-1}, which was rapid compared to other published methanotrophy incubations.

7. Methanotrophs caused a sympathetic enrichment of $\delta^{13}C$/ δD CH_4 isotopic signatures. This proceeded at a fractionation trajectory defined by a gradient of 9.0 in lab incubations, close to a trajectory of 8.5 observed by Coleman et al. (1981).

8. An observed aqueous methane fractionation gradient of 8.7 indicates the likelihood that methane in bulk meltwaters was of microbial origin and subjected to extensive oxidation, as opposed to a mixing between microbial and geogenic sources.

9. Processes of methanogenesis and methanotrophy occured in Sólheimajökull subglacial sediments. Methanotrophic rates observed in Fe^{3+} enriched brown subglacial sediment exceed production rates from Fe^{2+} enriched grey subglacial sediment. This could suggest that methanotrophy should be the dominant process. However, rates of methanogenesis and methanotrophy are governed by the distribution of sediments, redox state and hydraulic configuration.

10. In addition to this, hydraulic configuration and geothermal linkages are pivotal in determining the relative contribution of each process. Extensive summertime drainage and connectivity to geothermal hot spots promotes widespread anoxia, which supports extensive methanogenesis and inhibits methanotrophy in the subglacial realm. This provides evidence of a unique methane cycling system at Sólheimajökull.

9. Summary and suggestions for further research

This study has presented the first comprehensive parameterisation of carbon dynamics at a glaciated catchment fuelled by subglacial volcanic activity. Field and laboratory investigations have indicated that subglacial hydraulic configuration and geothermal activity impart a unique signature on carbon cycle dynamics, providing notable distinction from non-volcanic glaciated catchments.

9.1. Overall synthesis of carbon dynamics at Sólheimajökull

Glacier-volcano interactions have resulted in the distinctive subglacial geology evident at Sólheimajökull. Acidic and basaltic rocks have been shown to dominate the Sólheimajökull area (Carswell, 1983). The Katla volcanic system produces basaltic tephras which provide a readily weathered basaltic TDIC source beneath the glacier. Inorganic geochemical parameters including increased TDIC levels also infer an additional TDIC source originating from hydrothermal calcites deposited as an accessory component within the basalts. Ultimately, the combination of subglacial volcanism and glaciology set the geologic template for a unique mode of carbon cycling. Where suitable hydrological and physical conditions prevail, subglacial weathering can act as a release mechanism and vector by which mantle derived TDIC is released to the atmosphere.

Glacier hydraulics and subglacial volcanism have shown a unique coeval relationship leading to the identification of exclusive Winter/early Spring and Summer season configurations. The conceptual model shown in figure 9.1 (adapted from Wynn et al., 2015) highlights the relationship between hydrological evolution, subglacial volcanism and carbon dynamics. Building upon findings from Wynn et al. (2015) this study proposes inverse subglacial redox conditions at Sólheimajökull, as a result of subglacial volcanism, with this unique situation facilitating distinctive carbon dynamics.

During Winter/early Spring (prior to the injection of subglacial upwelling water) a dual hydrological configuration exists. Continual low level ablation promotes year round subglacial drainage, likely as a discrete channelized system restricted to the lower reaches of the glacier snout. Conversely a distributed linked cavity system persists under the remainder of the glacier where surface melt is not sufficient to promote channelized drainage (i.e. above the snow line). Water discharging from the subglacial environment during this early season configuration comprises an overwhelming component which has been sourced at low elevation and transported through a permanently established channelized system under atmospheric conditions. Leakage from the distributed system is minimal and carbon species representative of low redox status (for example methane) are rapidly oxidised upon entering the channelized system. These cavities facilitate temporary storage of water with increased rock: water contact times, promoting great TDIC acquisition. Isolation from the atmosphere alongside ion S ratio analyses indicative of weathering via carbonation of carbonates and silicates, suggests weathering driven by geothermally sourced protons. Additionally, where anoxia prevails, localised methane production is possible. However, where cavities are drained by small channels, meltwaters are transferred into the oxic channelized system beneath the glacier snout. Here, changes in redox conditions likely promote rapid methanotrophy of subglacial methane (Dieser et al., 2014) resulting in heavy $^{13}C_{CH4}$ isotopic signatures observed during early Spring. Winter/early Spring carbon dynamics are therefore dominated by TDIC acquisition from subglacial weathering under atmospheric conditions, alongside low concentrations of partially oxidised methane.

Summer season carbon and hydraulic modes are dominated by unique inverse redox conditions. Periodic increases in basal water pressure and head ward expansion of channelized drainage allows connectivity with areas of subglacial geothermal activity beneath Mýrdalsjökull resulting in the discharge of confined geothermal waters charged with reduced gases (Wynn et al., 2015). These waters swamp the subglacial drainage system, forcing widespread anoxia before ultimately upwelling at the

glacier snout. Inorganic carbon dynamics rely heavily upon this unique seasonal quirk, with subglacially sourced CO_2 (likely from geothermal fluids) a major proton source for weathering, accounting for elevated TDIC concentrations during summer. DOC characteristics are also influenced by summertime anoxia. The presence of subglacial organic carbon alongside widespread summertime anoxia facilitates microbial functioning under low redox conditions, as indicated by the seasonal release of methane rich subglacial waters. Methane discharged from the subglacial system has an isotopic signature indicative of a bacterial (acetoclastic) source subject to little oxidation. In this instance low redox conditions are pivotal for preserving methane via inhibition of methanotrophic activity. Hydrology then acts as a vector to allow delivery of methane to the proglacial zone, where it then rapidly engages with the atmosphere.
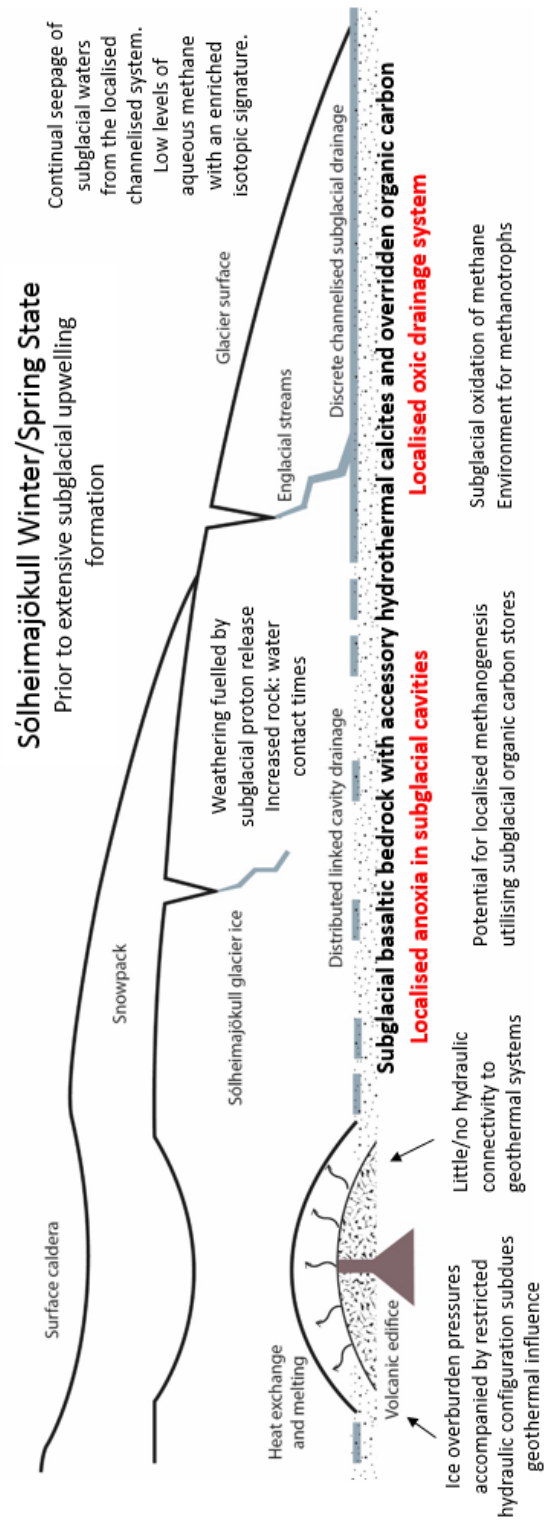
Figure 9.1: Schematic of Winter/Spring hydraulic configuration alongside redox status and carbon dynamics

Adapted from Wynn et al. (2015)
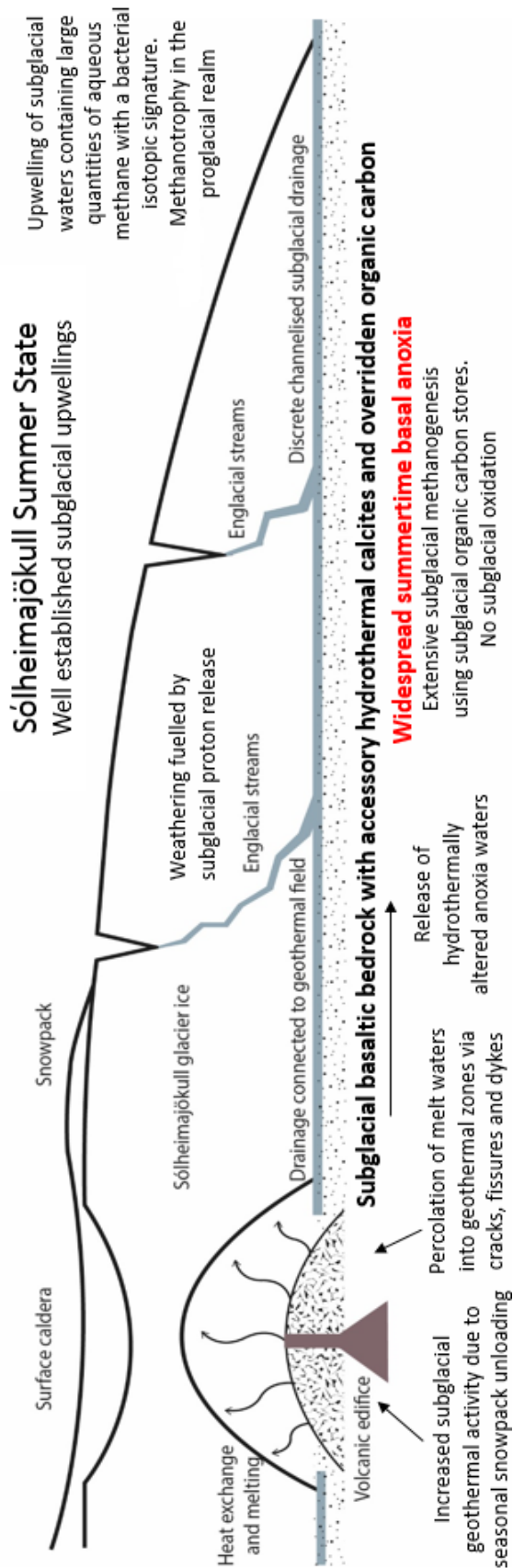
Figure 9.2: Schematic of Summer hydraulic configuration alongside redox status and carbon dynamics

Adapted from Wynn et al. (2015)

The seasonal modes of organic and inorganic carbon dynamics at Sólheimajökull have been outlined. Redox status determined by hydraulic connectivity to geothermal zones exerts a major influence on carbon within the Sólheimajökull system and provides the necessary conditions for methane production. As high latitude warming continues, increases in surficial melt, reductions in ice overburden pressures facilitating enhanced volcanism and extension of summer season drainage, results in the potential for adaptions in glacial carbon dynamics at Sólheimajökull and increased methane release. It is therefore essential to understand the broader significance of the unique modes of carbon cycling observed in this study.

9.2. Broader significance of carbon dynamics at Sólheimajökull

These unique findings observed at Sólheimajökull provide valuable contributions to furthering understanding of glaciology and carbon cycling, particularly in areas such as Iceland, where glaciers and volcanoes co-exist. However, implications of findings extend beyond this study, encompassing the wider dynamics of basalt weathering, repercussions of subglacial methane release and conflicts of classical drainage theories.

Unique findings linked to basalt weathering impart a wider significance for the global carbon cycle. Basalt represents only 5% of the crustal rocks exposed at the Earth's surface (Jacobson et al., 2015) yet accounts for large quantities of the Earth's subsurface. This is particularly notable in Iceland where basalt compromises 80-85% of the bedrock (Gislason et al., 1996) but also applicable to Hawaii (Ziegler et al., 2005) and other volcanic Islands (Louvat and Allègre, 1997).

Basalt weathering (and the weathering of Ca bearing minerals in basalt) is regarded to have a disproportionately large effect on the long term carbon cycle, acting as a sink for atmospheric CO_2 (Jacobson, et al., 2015; Georg et al., 2007). However, this is based on the assumption that protons used for weathering originate through the

drawdown of atmospheric CO_2. At Sólheimajökull, carbonation of basalt silicates and hydrothermal calcites contained within as accessory minerals uses protons sourced from subglacial CO_2 emissions in the absence of any atmospheric CO2 drawdown. This allows basaltic weathering in this location to act as a vector by which mantle derived CO_2 is liberated from the bedrock and delivered by subglacial hydrology to the proglacial environment where it has the potential to exchange with the atmosphere. Many other areas in Iceland exhibit similar glacier-volcano interactions, including other outlet glaciers of Mýrdalsjökull (Kötlujökull and Entlujökull) Vatnajökull (Grimsvotn) and most famously Eyjafjallajökull, where carbonation of silicates and hydrothermal calcites via protons sourced from a mantle origin could also proceed in a similar manner. Beyond this Iceland offers the potential to act as an analogue for other locations where glacio-volcanism is present such as Western Antarctica and areas of historical glacio-volcanism in Canada.

This study has also provided the first in situ evidence of extensive subglacial methane formation and release, which is essential in order to parameterise future methane inventories. Tentative annual methane flux estimations place potential emission from the Sólheimajökull catchment at 9179 and 22,551 tonnes based on Summer discharges of $20m^3s^{-1}$ and $50m^3s^{-1}$ respectively. These estimates indicate that significant methane flux could derive from the Sólheimajökull catchment, exceeding total Icelandic geothermal emissions, which have been quantified as 1,300 tonnes per year (Etiope et al., 2007). If this is a process occuring across Iceland, or beyond, then reconsideration of methane inventories is essential, particularly in light of climate induced glacial recession.

Finally, this study has highlighted the importance of understanding redox dynamics in glaciers and shown how subglacial volcanism has the potential to alter classical biogeochemical theories. Previously, redox was only thought to be lowered to reduced status when water was stored for long periods of time (for example cavity drainage). Whilst this provoked geochemical interest linked to weathering

mechanisms and postulation of microbial significance, traditional water storage redox conditions have limited impact on nutrient dynamics. Instead inverse conditions fuelled by geothermal/ hydraulic connectivity exhibited during this study, holds huge implication for nutrient dynamics and volatile release. Unique modes of carbon and nutrient cycling have large ramifications for further work linked to the cryosphere. Furthermore, volatile release and the geochemical signature this imparts on subglacial meltwaters is a vital method of monitoring subglacial volcanic activity and potentially predicting imminent eruptions and/or outwash floods. Better understanding of hydrochemical dynamics in light of redox conditions can offer increased accuracy in volcanic prediction and sheds light on a new aspect of the glacial ecosystem.

9.3. Suggestions for further research

This study has highlighted that unique carbon cycling exists at Sólheimajökull. One of the pivotal and most exciting findings is the discharge of methane from the subglacial realm. However in order to fully elucidate methane dynamics with the scope to extend the study beyond Sólheimajökull, further process-based investigation into the age, origin and release mechanisms of methane in this environment is necessary. Whilst conclusions can be made based upon the findings of this study, this is based on a limited set of Spring season isotopes to help provenence methane to source, with the absence of δD_{CH4} for the summer season. Furthermore, data has been collected over short field seasons, under conditions of spatially restricted sampling and limited laboratory investigations. In light of this, future research should incorporate extensive determination of aqueous methane concentrations over prolonged campaigns, including autumn and winter sampling to capture changes in subglacial drainage. This can be undertaken at established sampling sites, but should also include consideration of methods to sample the proglacial lake interior.

Further methods to expand the understanding of methane dynamics at Sólheimajökull should include further stable isotopes and clumped isotope analysis

to distinguish between microbial/ geogenic methane. Clumped isotopes of methane are especially important as they can reveal formation temperature and therefore differentiate between methane origin. This can be supported by use of noble gases (He-Xe) to elucidate between supraglacial and subglacial sources of meltwaters aswell as indicate the strength of the geothermal field beneath the glacier.

In situ methane analysis needs to be supplemented with extensive in vitro analysis with additional incubation experiments across a range of temperatures and headspace conditions, for differing sediment types. This could be supplemented with characterisation of methane production via RNA assays and carbon 14 dating to parameterise the nature of microbial methane production.

Beyond methane focussed research, there are two main areas in which further research is necessary: DOC analysis and riverine discharge measurements. DOC investigation has been limited to concentration, isotopic and fluorescence properties of Summer season samples. In order to fully parameterise DOC characteristics further research is necessary, incorporating extensive sampling over a variety of seasons. Furthermore, discharge measurements of waters from Jökulsárgil, Fjallgilsá and the Jökulsá á Sólheimasandi are necessary in order to estimate subglacial meltwater contributions and calculate accurate methane, TDIC, DOC and ionic fluxes based on observed discharge measurements.

9.4. Summary

This study offers the first attempt to parameterise cryospheric carbon cycling at an Icelandic glacier subject to intense subglacial geothermal activity. Research has highlighted an exclusive subglacial situation of reverse redox arising from hydraulic connectivity to geothermal zones as highlighted in hypothesis 2 (Chapter 1.2). This facilitates unique modes of carbon/ methane cycling with potential implications for subglacial meltwaters to be vectors of carbon release to the atmosphere. Firstly,

subglacial volcanism has a profound impact upon inorganic carbon chemistry via supply of protons for weathering of hydrothermally altered basalts, releasing mantle derived TDIC (hypothesis 1). In addition, low concentrations of dissolved organic carbon are present within Sólheimajökull bulk meltwaters, which when combined with unique reverse redox induced by geothermal activity, facilitates a biological community of methanogens and methanotrophs (hypothesis 3). In conclusion, this study reveals that a unique mode of carbon cycling exists at Sólheimajökull, heavily influenced by the subglacial active volcanic system.

Bibliography

Agustsdottir, A. M. and Brantley, S. L., 1994, Volatile Fluxes Integrated Over Four Decades at Grimsvotn Volcano, Iceland, Journal of Geophysical Research 99 (5) pp9505-9522.

Aiken, G. R., Spencer, R. G. M., Striegl, R. G., Schuster, P. F. and Raymond, P. A., 2014, Influences of Glacier Melt and Permafrost Thaw on the Age of Dissolved Organic Carbon in the Yukon River Basin, Global Biogeochemical Cycles, 28(5), 525-537.

Albino, F., Pinel, V., Sigmundsson, F., 2010, Influence of surface load variations on eruption likelihood: application to two Icelandic subglacial volcanoes, Grímsvötn and Katla. Geophysical Journal International, 181, 1510–1524.

Allègre, C.J., 2008, Isotope Geology, Cambridge University Press, Cambridge, UK.

Anderson, R. S., Anderson, S. P., Macgregor, K. R., Waddington, E. D., O'neel, S., Riihimaki, C. A. and Loso, M. G., 2004, Strong Feedbacks between Hydrology and Sliding of a Small Alpine Glacier. Journal of Geophysical Research-Earth Surface, 109.

Anderson, S.P., Drever, J.I. and Humphrey, N.F., 1997, Chemical weathering in glacial environments, Geology, 25, 399-402.

Anderson, S.P., Drever, J.I., Frost, C.D. and Holden, P., 2000, Chemical weathering of a retreating glacier, Geochimica et Cosmochimica Acta, 64, 1173-1189.

Anderson, S.P., Drever, J.I., Frost, C.D. and Holden, P., 2000, Chemical weathering in the foreland of a retreating glacier. Geochimica et Cosmochimica Acta, 64(7), pp.1173-1189.

Anesio, A M and Laybourn-Parry, J., 2012, Glaciers and Ice Sheets as a Biome, Trends in Ecology and Evolution 27 (4) pp219-225.

Anesio, A M; Hodson, A J; Fritz, A; Psenner, R and Sattler, B., 2009, High Microbial Activity on Glaciers: Importance to the Global Carbon Cycle, Global Change Biology.

Anesio, A.M. and Laybourn-Parry, J., 2012, Glaciers and ice sheets as a biome. Trends in Ecology and Evolution, 27(4), pp.219-225.

Anesio, A.M., Hodson, A.J., Fritz, A., Psenner, R. and Sattler, B., 2009, High microbial activity on glaciers: importance to the global carbon cycle. Global Change Biology, 15(4), pp.955-960.

Anesio, A.M., Sattler, B., Foreman, C., Telling, J., Hodson, A., Tranter, M. and Psenner, R., 2010, Carbon fluxes through bacterial communities on glacier surfaces. Annals of Glaciology, 51(56), pp.32-40.

Archer, D., Winguth, A., Lea, D. and Mahowald, N., 2000, What caused the glacial/interglacial atmospheric pCO2 cycles? Reviews of Geophysics,38(2), pp.159-189.

Arnalds, O., 2008, Soils of Iceland, Jökull, 58, pp.409-421.

Arnason, B., 1977, Hydrothermal systems in Iceland traced by deuterium. Geothermics 5, 125–151.

Bagshaw, E.A., Tranter, M., Fountain, A.G., Welch, K.A., Basagic, H. and Lyons, W.B., 2007, Biogeochemical evolution of cryoconite holes on Canada glacier, Taylor Valley, Antarctica. Journal of Geophysical Research: Biogeosciences, 112(G4).

Bárcena, T. G., Finster, K. W., and Yde, J. C., 2011, Spatial Patterns of Soil Development, Methane Oxidation, and Methanotrophic Diversity along a Receding Glacier Forefield, Southeast Greenland, Arctic, Antarctic, and Alpine Research, v. 43, p. 178-188.

Barker, J.D., Sharp, M.J., Fitzsimons, S.J. and Turner, R.J., 2006, Abundance and dynamics of dissolved organic carbon in glacier systems, Arctic, Antarctic, and Alpine Research, 38, 2, 163-172.

Barker, J.F. and Fritz, P., 1981, Carbon isotope fractionation during microbial methane oxidation. Nature, 293(5830), pp.289-291.

Barnett, M.J., Pawlett, M., Wadham, J.L., Jackson, M. and Cullen, D.C., 2010, In-Field Assessment of Subglacial Microbial Populations: A Multi-Technique Approach. Megan Barnett, p.95.

Berestovskaya, Y.Y., Rusanov, I.I., Vasil'eva, L.V. and Pimenov, N.V., 2005, The processes of methane production and oxidation in the soils of the Russian Arctic tundra. Microbiology, 74(2), pp.221-229.

Berestovskaya, Y.Y., Vasil'eva, L.V., Chestnykh, O.V. and Zavarzin, G.A., 2002, Methanotrophs of the psychrophilic microbial community of the Russian arctic tundra. Microbiology, 71(4), pp.460-466.

Bhatia, M. P., Das, S. B., Kujawinski, E. B., Henderson, P., Burke, A. and Charette, M. A., 2011, Seasonal Evolution of Water Contributions to Discharge from a Greenland Outlet Glacier: Insight from a New Isotope-Mixing Model. Journal of Glaciology, 57(205), 929-941.

Bhatia, M. P., Das, S. B., Xu, L., Charette, M. A., Wadham, J. L. and Kujawinski, E. B., 2013, Organic Carbon Export from the Greenland Ice Sheet. Geochimica Et Cosmochimica Acta, 109, 329-344.

Bhatia, M.P., Das, S.B., Longnecker, K., Charette, M.A. and Kujawinski, E.B., 2010, Molecular characterization of dissolved organic matter associated with the Greenland ice sheet. Geochimica et Cosmochimica Acta, 74(13), pp.3768-3784.

Bingham, R. G., Nienow, P. W., Sharp, M. J. and Boon, S., 2005, Subglacial Drainage Processes at a High Arctic Polythermal Valley Glacier. Journal of Glaciology, 51(172), 15-24.

Bingham, R. G., Nienow, P. W., Sharp, M. J. and Copland, L., 2006, Hydrology and Dynamics of a Polythermal (Mostly Cold) High Arctic Glacier. Earth Surface Processes and Landforms, 31(12), 1463-1479.

Björnsson, H. and Pálsson, F., 2008, Icelandic glaciers. Jökull, 58, pp.365-386.

Björnsson, H., Pálsson, F. and Guðmundsson, M.T., 2000, Surface and bedrock topography of the Mýrdalsjökull ice cap, Iceland: the Katla caldera, eruption sites and routes of jökulhlaups, Jökull 49, 29-46.

Björnsson, H., Pálsson, F., Sigurdsson, O. and Flowers, G. E., 2003, Surges of Glaciers in Iceland. In: RAYMOND, C. F. (ed.) Annals of Glaciology, Vol 36.

Blair, N.E. and Carter, W.D., 1992, The carbon isotope biogeochemistry of acetate from a methanogenic marine sediment. Geochimica et Cosmochimica Acta, 56(3), pp.1247-1258.

Blair, N.E., Martens, C.S. and Des Marais, D.J., 1987, Natural abundances of carbon isotopes in acetate from a coastal marine sediment. Science,236(4797), pp.66-68.

Blake, D. R., Smith, T. W., Chen, T. Y., Whipple, W. J., and Rowland, F. S., 1994, Effects of biomass burning on summertime nonmethane hydrocarbon concentrations in the Canadian wetlands. Journal of Geophysical Research: Atmospheres, 99(D1), 1699-1719.

Body, E S; Lange, R K, Mitchell, A C, Havig, J, R; Hamilton, T L; Lafreniere, M J; Shock, E L, Peters, J W and Skidmore, M., 2011, Diversity, Abundance and Potential Activity of Nitrifying and Nitrate-Reducing Microbial Assemblages in a Subglacial Ecosystem, Applied Environmental Microbiology 77 (14).

Bottrell, S.H., Tranter, M., 2002, Sulphide oxidation under partly anoxic conditions at the bed of Haut Glacier D'Arolla, Switzerland. Hydrological Process. 16 (5), 959–993.

Boyd, E. S., Skidmore, M., Mitchell, A. C., Bakermands, C. and Peters, J. W., 2010, 'Methanogenesis in Subglacial Sediments' Environmental Microbiology Reports 2 (5) pp685-692.

Brock, B. W., Willis, I. C., Sharp, M. J. and Arnold, N. S., 2000, Modelling Seasonal and Spatial Variations in the Surface Energy Balance of Haut Glacier D'arolla, Switzerland, In: STEFFEN, K. (ed.) Annals of Glaciology, Vol 31.

Brook, E.J, Sowers, T, Orchardo, J., 1996, Rapid Variations in Atmospheric Methane Concentration During the Past 110,000 Years, Science vol 273 pp1087-1091

Brook, E.J., Harder, S., Severinghaus, J., Steig E.J., and Sucher, C.M., 2000, On the Origin and Timing of Rapid Changes in Atmospheric Methane During the Last Glacial Period, Global Biogeochemical Cycles vol14 (2) pp559-572.

Brown, G. H., 2002, Glacier Meltwater Hydrochemistry. Applied Geochemistry, 17(7), 855-883.

Brown, G. H., Sharp, M. J., Tranter, M., Gurnell, A. M. and Nienow, P. W., 1994, Impact of Post-Mixing Chemical-Reactions on the Major Ion Chemistry of Bulk Meltwaters Draining the Haut Glacier Darolla, Valais, Switzerland. Hydrological Processes, 8(5), 465-480.

Brown, G.H., Hubbard, B. and Seagren, A.G., 2001, Kinetics of solute acquisition from the dissolution of suspended sediment in subglacial channels, Hydrol. Process., 15, 3487-3497.

Brown, G.H., Tranter, M. and Sharp, M.J., 1996, Experimental investigations of the weathering of suspended sediment by Alpine glacial meltwater, Hydrological Processes, 10, 579-597.

Brunet, F., Gaiero, D., Probst, J.L., Depetris, P.J., Gauthier Lafaye, F. and Stille, P., 2005, δ^{13}C tracing of dissolved inorganic carbon sources in Patagonian rivers (Argentina), Hydrological Processes, 19(17), pp.3321-3344.

Cameron K.A., Hodson A.J. and Osborn A.M., 2012, Structure and diversity of bacterial, eukaryotic and archaeal communities in glacial cryoconite holes from the Arctic and the Antarctic. FEMS Microbiology Ecology 82, 254–267.

Campen, R.K., Sowers, T., and Alley, R.B., 2003, Evidence of microbial consortia metabolizing within a low-latitude mountain glacier: Geology, v. 31, p. 231–234.

Cao, M. and Woodward, F. I., 1998, Dynamic Responses of Terrestrial Ecosystem Carbon Cycling to Global Climate Change. Nature, 393(6682), 249-252.

Carswell, D.A., 1983, The volcanic rocks of the Sólheimajökull area, Southern Iceland, Jökull, 33, 61 – 71.

Chan, A.S.K. and Parkin, T.B., 2001, Methane oxidation and production activity in soils from natural and agricultural ecosystems. Journal of Environmental Quality, 30(6), pp.1896-1903.

Chanton, J. P., 2005, The effect of gas transport on the isotope signature of methane in wetlands. Organic Geochemistry, *36*(5), 753-768.

Chesler, A. Evidence of subglacial methane gas emission from Sólheimajökull Iceland (unpublished masters thesis).

Cicerone, R.J. and Oremland, R.S., 1988, Biogeochemical aspects of atmospheric methane. Global biogeochemical cycles, 2(4), pp.299-327.

Coleman, D.D., Risatti, J.B. and Schoell, M., 1981, Fractionation of carbon and hydrogen isotopes by methane-oxidizing bacteria. Geochimica et Cosmochimica Acta, 45(7), pp.1033-1037.

Collins, D. N., 1978, Hydrology of an Alpine glacier as indicated by the chemical composition of meltwater. Zeitschr(ft fiir Gletscherkunde und Glazialgeologie 13, 219- 238.

Collins, D. N., 1977, Hydrology of an Alpine Glacier as Indicated by Chemical Composition of Meltwater. Transactions-American Geophysical Union, 58(9), 901-901.

Cox, P. M., Betts, R. A., Jones, C. D., Spall, S. A. and Totterdell, I. J., 2000, Acceleration of Global Warming Due to Carbon-Cycle Feedbacks in a Coupled Climate Model. Nature, 408(6809), 184-187.

Crochet, P., 2013, Sensitivity of Icelandic River Basins to Recent Climate Variations. Jökull, 63, 71-90.

Crompton, J.W., Flowers, G.E., Kirste, D., Hagedorn, B. and Sharp, M.J., 2015. Clay mineral precipitation and low silica in glacier meltwaters explored through reaction-path modelling. *Journal of Glaciology*, *61*(230), pp.1061-1078.

Cumberland, S.A. and Baker, A., 2007, The freshwater dissolved organic matter fluorescence–total organic carbon relationship, Hydrological Processes, 21(16), pp.2093-2099.

Dansgaard, W., 1964, Stable isotopes in precipitation, Tellus, 16, 4, 436-468.

Daval, D., Martinez, I., Corvisier, J., Findling, N., Goffé, B., & Guyot, F., 2009, Carbonation of Ca-bearing silicates, the case of wollastonite: experimental investigations and kinetic modelling. *Chemical Geology*, *265*(1), pp.63-78.

Dessert, C., Dupré, B., Gaillardet, J., François, L.M. and Allegrè, C.J., 2003, Basalt weathering laws and the impact of basalt weathering on the global carbon cycle, Chemical Geology, 202(3), pp.257-273.

Dieser, M., Broemsen, E. L., Cameron, K. A., King, G. M., Achberger, A., Choquette, K. and Christner, B. C., 2014, Molecular and biogeochemical evidence for methane cycling beneath the western margin of the Greenland Ice Sheet. *The ISME journal*, *8*(11), pp.2305-2316.

Dubnick, A., Barker, J., Sharp, M., Wadham, J., Lis, G., Telling, J., Fitzsimons, S. and Jackson, M., 2010, Characterization of dissolved organic matter (DOM) from glacial environments using total fluorescence spectroscopy and parallel factor analysis. Annals of Glaciology, 51(56), pp.111-122.

Dugmore, A.J. and Sugden, D.E., 1991, Do the anomalous fluctuations of Sólheimajökull reflect ice-divide migration? Boreas, 20, 105-113.

Dunfield, P., Knowles, R., Dumont, R., and Moore, T.R., 1993, Methane Production and Consumption in Temperate and Subarctic Peat Soils: Response to Temperature and pH: Soil, Biology, and Biochemistry, v. 25, p. 321-326.

Einarsson, T. and Albertsson, K.J., 1988, The glacial history of Iceland during the past three million years: Philosophical Transactions of the Royal Society, London, B. 318, p. 637-644.

Einarsson, M. Á., 1984, Climate of Iceland. In: van Loon, H., ed., Climates of the Oceans, Elsevier, Amsterdam, 673–697.

Einarsson, P. and Brandsdóttir, B., 2000, Earthquakes in the Mýrdalsjökull area, Iceland, 1978 – 1985: Seasonal correlation and connection with volcanoes, Jökull, 49, 59-74.

Einarsson, T. and Albertson, K.J., 1988, The glacial history of Iceland during the past 3 million years. Philos. Trans. R. Soc. London, Ser. B, 318: 637-644.

Elvert, M., Suess, E. and Whiticar, M.J., 1999, Anaerobic methane oxidation associated with marine gas hydrates: superlight C-isotopes from saturated and unsaturated C20 and C25 irregular isoprenoids. Naturwissenschaften, 86(6), pp.295-300.

Escudey, M., Förster, J.E. and Galindo, G., 2004, Relevance of organic matter in some chemical and physical characteristics of volcanic ash-derived soils. Communications in Soil science and plant analysis, 35(5-6), pp.781-797.

Etiope, G., Fridriksson, T., Italiano, F., Winiwarter, W., and Theloke, J., 2007, Natural emissions of methane from geothermal and volcanic sources in Europe Journal of Volcanology and Geothermal Research, v. 165, p. 76-86.

Etiope, G. and Klusman, R.W., 2002, Geologic emissions of methane to the atmosphere. Chemosphere, 49(8), pp.777-789.

Etiope, G. and Milkov, A.V., 2004, A new estimate of global methane flux from onshore and shallow submarine mud volcanoes to the atmosphere. Environmental Geology, 46(8), pp.997-1002.

Etiope, G., 2009, Natural emissions of methane from geological seepage in Europe. Atmospheric Environment, 43(7), pp.1430-1443.

Etiope, G. and Sherwood Lollar, B., 2013. Abiotic methane on Earth. *Reviews of Geophysics*, *51*(2), pp.276-299.

Fairchild, I. J., Bradby, L., Sharp, M. and Tison, J.-L., 1994, Hydrochemistry of carbonate terrains in alpine glacial settings. Earth Surface Processes and Landforms 19, 33-54.

Fairchild, I. J., Killawee, J. A., Sharp, M. J., Spiro, B., Hubbard, B., Lorrain, R. D. and Tison, J. L., 1999, Solute Generation and Transfer from a Chemically Reactive Alpine

Glacial-Proglacial System. Earth Surface Processes and Landforms, 24(13), 1189-1211.

Falkowski, P., Scholes, R. J., Boyle, E., Canadell, J., Canfield, D., Elser, J., Gruber, N., Hibbard, K., Hogberg, P., Linder, S., Mackenzie, F. T., Moore, B., Pedersen, T., Rosenthal, Y., Seitzinger, S., Smetacek, V. and Steffen, W., 2000, The Global Carbon Cycle: A Test of Our Knowledge of Earth as a System. Science, 290(5490), 291-296.

Federherr, E., Cerli, C., Kirkels, F.M.S.A., Kalbitz, K., Kupka, H.J., Dunsbach, R., Lange, L. and Schmidt, T.C., 2014, A novel high-temperature combustion based system for stable isotope analysis of dissolved organic carbon in aqueous samples. I: development and validation, Rapid Communications in Mass Spectrometry, 28(23), pp.2559-2573.

Fellman, J. B., Nagorski, S., Pyare, S., Vermilyea, A. W., Scott, D. and Hood, E., 2014, Stream Temperature Response to Variable Glacier Coverage in Coastal Watersheds of Southeast Alaska. Hydrological Processes, 28(4), 2062-2073.

Fellman, J.B., Hood, E. and Spencer, R.G., 2010, Fluorescence spectroscopy opens new windows into dissolved organic matter dynamics in freshwater ecosystems: A review. Limnology and Oceanography, 55(6), pp.2452-2462.

Fellman, J.B., Hood, E., Edwards, R.T. and D'Amore, D.V., 2009, Changes in the concentration, biodegradability, and fluorescent properties of dissolved organic matter during stormflows in coastal temperate watersheds. Journal of Geophysical Research: Biogeosciences, 114(G1).

Fenn, C. and ASHWELL, I., 1985, Some observations on the characteristics of the drainage system of Kverkjökull, Central Iceland. Jökull, (35), pp.79-82.

Flaathen, T.K. and Gislason, S.R., 2007, The groundwater beneath Hekla Volcano, Iceland: A natural analogue for CO_2 sequestration. Geochimica et Cosmochimica Acta, 71, p.A283.

Flaathen, T.K., Gíslason, S.R., 2007, The effect of volcanic eruptions on the chemistry of surface waters: the 1991 and 2000 eruptions of Mt. Hekla, Iceland. Journal of Volcanology and Geothermal Research 164 (4), 293–316.

Flowers, G. E., 2015, Modelling Water Flow under Glaciers and Ice Sheets. Proceedings of the Royal Society a-Mathematical Physical and Engineering Sciences, 471(2176).

Flowers, G. E., Marshall, S. J., Bjornsson, H. and Clarke, G. K. C., 2005, Sensitivity of Vatnajökull Ice Cap Hydrology and Dynamics to Climate Warming over the Next 2 Centuries. Journal of Geophysical Research-Earth Surface, 110(F2).

Flowers, G.E., Björnsson, H., Pálsson, F., 2003, New insights into the subglacial and periglacial hydrology of Vatnajökull, Iceland, from a distributed physical model. Journal of Glaciology 49 (165), 257–270.

Foght, J., Aislabie, J., Turner, S., Brown, C.E., Ryburn, J., Saul, D.J. and Lawson, W., 2004, Culturable bacteria in subglacial sediments and ice from two southern hemisphere glaciers. Microbial Ecology, 47(4), pp.329-340.

Fountain A.G., Tranter M., Nylen T.H., Lewis K.J. and Mueller D.R., 2004, Evolution of cryoconite holes and their contribution to meltwater runoff from glaciers in the McMurdo Dry Valleys, Antarctica. Journal of Glaciology 50, 35–45.

Fountain, A. G. and Walder, J. S., 1998, Water Flow through Temperate Glaciers. Reviews of Geophysics, 36(3), 299-328.

Fountain, A. G., 1992, Subglacial Water-Flow Inferred from Stream Measurements at South Cascade Glacier, Washington, USA. Journal of Glaciology, 38(128), 51-64.

Fountain, A. G., 1996, Effect of Snow and Firn Hydrology on the Physical and Chemical Characteristics of Glacial Runoff. Hydrological Processes, 10(4), 509-521.

Fountain, A. G., Levy, J. S., Gooseff, M. N. and Van Horn, D., 2014, The Mcmurdo Dry Valleys: A Landscape on the Threshold of Change. Geomorphology, 225, 25-35.

Fountain, A.G., Walder, J., 1998, Water flow through temperate glaciers. Reviews of Geophysics, 36, 299–328.

Friis, B., 2011, Late Holocene glacial history of Sólheimajökull, southern Iceland.

Fung, I., John, J., Lerner, J., Matthews, E., Prather, M., Steele, L.P. and Fraser, P.J., 1991, Three Dimensional Model Synthesis of the Global Methane Cycle, Journal of Geophysical Research vol 96 pp13,033-13,065

Gaidos, E. and Marion, G., 2003, Geological and Geochemical Legacy of a Cold Early Mars. Journal of Geophysical Research-Planets, 108(E6).

Galeczka, I., Oelkers, E.H. and Gíslason, S.R., 2014, The chemistry and element fluxes of the July 2011 Múlakvísl and Kaldakvísl glacial floods, Icelandic Journal of Volcanology and Geothermal Research, 273, 41–57.

Georg, R.B., Reynolds, B.C., West, A.J., Burton, K.W. and Halliday, A.N., 2007, Silicon isotope variations accompanying basalt weathering in Iceland, Earth and Planetary Science Letters, 261(3), pp.476-490.

Gerlach, T. M., Doukas, M. P., Mcgee, K. A. and Kessler, R., 2000, Airborne Detection of Diffuse Carbon Dioxide Emissions at Mammoth Mountain (Vol 26, Pg 3661, 1999). Geophysical Research Letters, 27(5), U3-U3.

Gíslason, G. M., Ólafsson, J. S. and Adalsteinsson, H., 2000, Life in Glacial and Alpine Rivers in Central Iceland in Relation to Physical and Chemical Parameters. Nordic Hydrology, 31(4-5), 411-422.

Gíslason, S.R., Snorrason, A., Kristmannsdóttir, H., Sveinbjörnsdóttir, Á.E., Torsander, P., Ólafsson, J., Castet, S., Dupré, B., 2002, Effects of volcanic eruptions on the CO$_2$

content of the atmosphere and the oceans: the 1996 eruption and flood within the Vatnajökull Glacier, Iceland, Chemical Geology, 190, 181–205.

Gorham, E., 1991, Northern Peatlands: Role in the Carbon Cycle and Probable Responses to Climatic Warming. Ecological applications, 1(2), 182-195.

Griselin, M., Marlin, C., Dever, L., Moreau, L., 1994, Hydrology and geochemistry of the Loven East glacier, Spitsbergen. In: Griselin, M. (Ed.), Actes du 3e symposium international Cavités glaciers et cryokarst en regions polaires et de haute montagne, Chamonix-France. Annales lit.

Gristwood, R. Establishing the source of the CO_2 in the meltwaters of the Sólheimajökull valley, southern Iceland: a warning of an imminent eruption from Katla, or an indicator of normal background meltwater geochemistry? (unpublished masters thesis).

Guan, M., Wright, N.G., Sleigh, P.A. and Carrivick, J.L., 2015, Assessment of hydro-morphodynamic modelling and geomorphological impacts of a sediment-charged jökulhlaup, at Sólheimajökull, Iceland. Journal of Hydrology, 530, pp.336-349.

Guðmundsson H.J., 1997, A review of the Holocene environmental history of Iceland: Quaternary Science Reviews, v. 16, p. 81-92.

Guðmundsson, M.T., Hoganadóttir, P., Kristinsson, A.B., Gudbjornsson, S., 2007, Geothermal activity in the subglacial Katla caldera, Iceland, 1999–2005, studied with radar altimetry. Annals of Glaciology, 45, 66–72.

Guðmundsson, M.T., Hoganadottir, Þ., Kristinsson, A.B. and Gudbjornsson, S., 2007, Geothermal activity in the subglacial Katla caldera, Iceland, 1999 – 2005, studied with radar altimetry, Annals of Glaciology, 45, 66-72.

Guðmundsson, M.T., Larsen, G., Höskuldsson, Á., Gylfason, Á.G., 2008, Volcanic hazards in Iceland. Jökull 58, 251–268.

Guicharnaud, R., Arnalds, O. and Paton, G.I., 2010, Short term changes of microbial processes in Icelandic soils to increasing temperatures. Biogeosciences, 7(2), pp.671-682.

Gulley, J. D., Benn, D. I., Mueller, D. and Luckman, A., 2009, A Cut-and-Closure Origin for Englacial Conduits in Uncrevassed Regions of Polythermal Glaciers. Journal of Glaciology, 55(189), 66-80.

Hambrey, M.J., 1994, Glacial environments. UBC Press.

Hambrey, M.J, 1974, Oxygen Isotope Studies at Charles Rabots Bre, Okstindan, Northern Norway. *Geografiska Annaler. Series A, Physical Geography, 56*(3/4), pp.147-158.

Hamilton, T.L., Peters, J.W., Skidmore, M.L. and Boyd, E.S., 2013. Molecular evidence for an active endogenous microbiome beneath glacial ice. *The ISME journal*, *7*(7), pp.1402-1412.

He, R., Wooller, M.J., Pohlman, J.W., Catranis, C., Quensen, J., Tiedje, J.M. and Leigh, M.B., 2012, Identification of functionally active aerobic methanotrophs in sediments from an arctic lake using stable isotope probing. Environmental microbiology, 14(6), pp.1403-1419. B

He, R., Wooller, M.J., Pohlman, J.W., Quensen, J., Tiedje, J.M. and Leigh, M.B., 2012, Shifts in identity and activity of methanotrophs in Arctic lake sediments in response to temperature changes. Applied and environmental microbiology, 78(13), pp.4715-4723. A

Heinze, C., Maier-Reimer, E. and Winn, K., 1991, Glacial pCO2 reduction by the world ocean: Experiments with the Hamburg carbon cycle model. Paleoceanography, 6(4), pp.395-430.

Hock, R., 2005, Glacier Melt: A Review of Processes and Their Modelling. Progress in Physical Geography, 29(3), 362-391.

Hodgkins, R., 1997, Glacier hydrology in Svalbard, Norwegian high arctic. Quaternary Science Reviews, 16(9), pp.957-973.

Hodgkins, R., Tranter, M. and Dowdeswell, J.A., 1998. The hydrochemistry of runoff from a 'cold-based' glacier in the High Artic (Scott Turnerbreen, Svalbard). *Hydrological Processes*, *12*, pp.87-103.

Hodson A., Anesio A.M., Ng F., Watson R., Quirk J., Irvine-Fynn T., Dye A., Clark C., McCloy P., Kohler J. and Sattler B., 2007, A glacier respires: quantifying the distribution and respiration CO2 flux of cryoconite across an entire Arctic supraglacial ecosystem, Journal of Geophysical Research—Biogeosciences 112

Hodson, A., Anesio, A.M., Tranter, M., Fountain, A., Osborn, M., Priscu, J., Laybourn-Parry, J. and Sattler, B., 2008, Glacial ecosystems. Ecological monographs, 78(1), pp.41-67.

Hodson, A., Tranter, M. and Vatne, G., 2000, Contemporary Rates of Chemical Denudation and Atmospheric Co2 Sequestration in Glacier Basins: An Arctic Perspective. Earth Surface Processes and Landforms, 25(13), 1447-1471.

Hodson, A., Tranter, M., Gurnell, A., Clark, M. and Hagen, J. O., 2002, The Hydrochemistry of Bayelva, a High Arctic Proglacial Stream in Svalbard. Journal of Hydrology, 257(1-4), 91-114.

Hodson, A.J., Mumford, P.N., Kohler, J. and Wynn, P.M., 2005, The High Arctic glacial ecosystem: new insights from nutrient budgets, Biogeochemistry, 72, 233 – 256.

Hoffman, M. and Price, S. 2014. Feedbacks between Coupled Subglacial Hydrology and Glacier Dynamics. Journal of Geophysical Research-Earth Surface, 119(3), 414-436.

Hoham, R.W. and Duval, B., 2001, Microbial ecology of snow and freshwater ice with emphasis on snow algae. Snow ecology: an interdisciplinary examination of snow-covered ecosystems, Cambridge University Press, Cambridge, pp.168-228.

Hood, E., Battin, T.J., Fellman, J., O'Neel, S. and Spencer, R.G., 2015, Storage and release of organic carbon from glaciers and ice sheets, Nature Geoscience, 8(2), pp.91-96.

Hood, E., Battin, T.J., Fellman, J., O'Neel, S. and Spencer, R.G., 2015, Storage and release of organic carbon from glaciers and ice sheets. Nature Geoscience, 8(2), pp.91-96.

Hood, E., Fellman, J., Spencer, R.G., Hernes, P.J., Edwards, R., D'Amore, D. and Scott, D., 2009, Glaciers as a source of ancient and labile organic matter to the marine environment, Nature, 462(7276), pp.1044-1047.

Hood, E., McKnight, D.M. and Williams, M.W., 2003, Sources and chemical character of dissolved organic carbon across an alpine/subalpine ecotone, Green Lakes Valley, Colorado Front Range, United States. Water Resources Research, 39(7).

Hood, E; Fellman, J; Spencer, R G M, Hernes, P J, Edwards, R, D'Amore, D and Scott, D. 2009, 'Glaciers as a source of Ancient and Labile Organic Matter to the Marine Environment' Nature 462

Hooke, R. LeB., 1984, On the role of mechanical energy in maintaining subglacial water conduits at atmospheric pressure. Journal of Glaciology 30, 180-187.

Hubbard, B. and Nienow, P., 1997, Alpine Subglacial Hydrology. Quaternary Science Reviews, 16(9), 939-955.

Indermühle, A., Stocker, T., Joos, F., Fischer, H., Smith, H., Wahlen, M., Deck, B., Mastroianni, D., Tschumi, J. and Blunier, T., 1999, Holocene Carbon-Cycle Dynamics Based on Co2 Trapped in Ice at Taylor Dome, Antarctica. Nature, 398(6723), 121-126.

Ingólfsson, Ó., Norðdahl, H. and Schomacker, A., 2010, Deglaciation and Holocene glacial history of Iceland, Developments in Quaternary Science, 13, 51-68.

IPCC, Fourth Assessment Report, 2007, Contribution of Working Groups I, II and III to the Fourth Assessment Report of the Intergovernmental Panel on Climate Change Core Writing Team, Pachauri, R.K. and Reisinger, A. (Eds.) IPCC, Geneva, Switzerland. pp 104

IPCC, 2013, Climate Change 2013: The Physical Science Basis. Contribution of Working Group I to the Fifth Assessment Report of the Intergovernmental Panel on Climate Change [Stocker, T.F., D. Qin, G.-K. Plattner, M. Tignor, S.K. Allen, J.

Boschung, A. Nauels, Y. Xia, V. Bex and P.M. Midgley (eds.)]. Cambridge University Press, Cambridge, United Kingdom and New York, NY, USA, 1535

Jacobson, A.D., Andrews, M.G., Lehn, G.O. and Holmden, C., 2015, Silicate versus carbonate weathering in Iceland: New insights from Ca isotopes. Earth and Planetary Science Letters, 416, pp.132-142.

Jóhannesson, T., Aðalgeirsdóttir, G., Björnsson, H., Crochet, P., Elíasson, E. B., Guðmundsson, S., Jónsdóttir, J. F., Ólafsson, H., Pálsson, F., Rögnvaldsson, Ó., Sigurðsson, O., Snorrason, A., Sveinsson, Ó. G. Bl. and. Thorsteinsson, Th., 2007, Effect of climate change on hydrology and hydro-resources in Iceland. Final report of the VO-project, OS-2007/011.

Joos, F., Sarmiento, J. and Siegenthaler, U., 1991, Estimates of the Effect of Southern Ocean Iron Fertilization on Atmospheric CO_2 Concentrations.

Karakashev, D., Batstone, D.J., Trably, E. and Angelidaki, I., 2006, Acetate oxidation is the dominant methanogenic pathway from acetate in the absence of Methanosaetaceae, Applied and environmental microbiology, 72(7), pp.5138-5141.

Kaštovská K., Stibal M., Sabacka M., Cerna B., Santruckova H. and Elster J., 2007, Microbial community structure and ecology of subglacial sediments in two polythermal Svalbard glaciers characterized by epifluorescence microscopy and PLFA. Polar Biology 30, 277–287.

Kaštovská, K., Elster, J., Stibal, M. and Šantrůčková, H., 2005, Microbial assemblages in soil microbial succession after glacial retreat in Svalbard (High Arctic). Microbial Ecology, 50(3), pp.396-407.

Kirkels, F.M.S.A., Cerli, C., Federherr, E., Gao, J. and Kalbitz, K., 2014, A novel high-temperature combustion based system for stable isotope analysis of dissolved organic carbon in aqueous samples. II: optimization and assessment of analytical performance. Rapid Communications in Mass Spectrometry, 28(23), pp.2574-2586.

Knight, P. G., Waller, R. I., Patterson, C. J., Jones, A. P. and Robinson, Z. P., 2000, Glacier Advance, Ice-Marginal Lakes and Routing of Meltwater and Sediment: Russell Glacier, Greenland. Journal of Glaciology, 46(154), 423-426.

Knight, P.G., 1999, Glaciers Stanley Thornes: UK.

Krawczyk, W.E., Lefauconnier, B. and Pettersson, L.E., 2003, Chemical denudation rates in the Bayelva catchment, Svalbard, in the fall of 2000, Physics and Chemistry of the Earth, Parts A/B/C, 28(28), pp.1257-1271.

Kristiansen, S. M., Yde, J. C., Barcena, T. G., Jakobsen, B. H., Olsen, J. and Knudsen, N. T., 2013, Geochemistry of Groundwater in Front of a Warm-Based Glacier in Southeast Greenland. Geografiska Annaler Series a-Physical Geography, 95A (2), 97-108.

Kristjánsson, L., 2012, Iceland spar and its legacy in science. History of Geo- and Space Sciences, 3(1), pp.117-126.

Kristmannsdóttir, H. and Ármannsson, H., 1996, Chemical monitoring of Icelandic geothermal fields during production, Geothermics, 25(3), pp.349-364.

Kristmannsdóttir, H., Gíslason, S., Haraldsson, H., Hauksdóttir, S., Gunnarsson, A., 2002, Seasonal variation in the chemistry of glacial-fed rivers in Iceland. In: Snorrason, A., Finnsdóttir, H.P., Moss, M. (Eds.), The Extremes of the Extremes: Extraordinary Floods. Proceedings of a Reykjavik Symposium, IAHS Publ no. 271, pp. 223–229.

Kroeger, K.F., Di Primio, R. and Horsfield, B., 2011, Atmospheric methane from organic carbon mobilization in sedimentary basins—The sleeping giant? Earth-Science Reviews, 107(3), pp.423-442.

Krüger, J., 1988, Glacial geomorphological research at Mýrdalsjökull, Iceland, 1977–86. I: the northern margin, Geografisk Tidsskrift-Danish Journal of Geography, 88(1), pp.68-77.

Kvenvolden K.A., 1988, Methane Hydrate – A Major Resevoir of Carbon in the Shallow Geosphere? Chemical Geology, v. 71, p. 41-51.

La Frenierre, J. and Mark, B. G., 2014, A Review of Methods for Estimating the Contribution of Glacial Meltwater to Total Watershed Discharge. Progress in Physical Geography, 38(2), 173-200.

Lamb, H. H., Tranter, M., Brown, G. H., Hubbard, B. P., Sharp, M. J., Gordon, S., Smart, C. C., Willis, I. C. and Nielsen, M. K., 1995, The composition of subglacial meltwaters sampled from boreholes at the Haut Glacier d'Arolla, Switzerland. 1AHS/IUGG XXI General Assembly, July 2-14, 1995, Boulder, Colorado, USA. International Association of Hydrological Sciences Publication 228, 395-403.

Lang, S.Q., Butterfield, D.A., Schulte, M., Kelley, D.S. and Lilley, M.D., 2010, Elevated concentrations of formate, acetate and dissolved organic carbon found at the Lost City hydrothermal field, Geochimica et Cosmochimica Acta, 74(3), pp.941-952.

Larsen, G. 2010. Katla: tephrochronology and eruption history, in A. Schmacker, J. Kruger, K.H. Kjaer (Eds.) 2010, The Mýrdalsjökull ice cap, Iceland (13 ed.), Elsevier, Amsterdam.

Lawler, D., 1991, Sediment and Solute Yield from the Jökulsá á Sólheimasandi Glacierized River Basin, Southern Iceland. Environmental Change in Iceland: Past and Present, 7, 303-332.

Lawler, D. M., 1991, Sediment and solute yield from the Jökulsá á Sólheimasandi glacierized river basin, southern Iceland, in Maizels, J. K. and Caseldine, C. (Eds) (1991) Environmental change in Iceland: past and present, Kluwer, Dordrecht, 303-332.

Lawler, D. M., 1994, Recent Changes in Rates of Suspended Sediment Transport in the Jökulsa á Sólheimasandi Glacial River, Southern Iceland.

Lawler, D. M., Bjornsson, H. and Dolan, M., 1996, Impact of Subglacial Geothermal Activity on Meltwater Quality in the Jökulsa á Sólheimasandi System, Southern Iceland, Hydrological Processes, 10(4), 557-577.

Lawler, D. M., Mcgregor, G. R. and Phillips, I. D., 2003, Influence of Atmospheric Circulation Changes and Regional Climate Variability on River Flow and Suspended Sediment Fluxes in Southern Iceland, Hydrological Processes, 17(16), 3195-3223.

Lawler, D.M., Björnsson, H. and Dolan, M., 1996, Impact of subglacial geothermal activity on meltwater quality in the Jökulsa a Sólheimasandi system, Southern Iceland, Hydrological Processes, 10, 557 – 578.

Lawler, D.M., Dolan, M., Tomasson, H. and Zophoniasson, S., 1992, Temporal variability of suspended sediment flux from a subarctic glacial river, southern Iceland, Erosion and sediment transport monitoring programmes in river basins (Proceedings of the Oslo Symposium, August 1992) IAHS Publication no. 210.

Le Heron, D. P. and Etienne, J. L., 2005, A Complex Subglacial Clastic Dyke Swarm, Sólheimajökull, Southern Iceland. Sedimentary Geology, 181(1-2), 25-37.

Levy, A., Robinson, Z., Krause, S., Waller, R. and Weatherill, J., 2015, Long-Term Variability of Proglacial Groundwater-Fed Hydrological Systems in an Area of Glacier Retreat, Skeioararsandur, Iceland, Earth Surface Processes and Landforms, 40(7), 981-994.

Liptay, K., Chanton, J., Czepiel, P. and Mosher, B., 1998, Use of stable isotopes to determine methane oxidation in landfill cover soils. Journal of Geophysical Research: Atmospheres, 103(D7), pp.8243-8250.

Lliboutry, L.L., 1968, General theory of subglacial cavitation and sliding of temperate glaciers. J. Glaciol. 7, 21–58.

Long, D., 1992, Devensian Late-glacial Gas Escape in the Central North Sea, Continental Shelf Research vol 12 (10) pp1097-1110

Macdonald, G. J., 1990, The Role of Methane Clathrates in Past and Future Climates Climatic Change 16 pp247-281

Macias, F. and Arbestain, M. C., 2010, Soil Carbon Sequestration in a Changing Global Environment. Mitigation and Adaptation Strategies for Global Change, 15(6), 511-529.

Mackenzie, F. T. and Lerman, A., 2006, Brief Overview of Carbon on Earth. Topics in Geobiology, 25, 1-22.

Mackintosh, A. N., Dugmore, A. J. and Hubbard, A. L., 2002, Holocene Climatic Changes in Iceland: Evidence from Modelling Glacier Length Fluctuations at Sólheimajökull, Quaternary International, 91, 39-52.

Mackintosh, A.N., Dugmore, A.J. and Hubbard, A.L., 2002, Holocene climatic changes in Iceland: evidence from modelling glacier length fluctuations at Sólheimajökull, Quaternary International, 91, 39-52.

Mair, D., Nienow, P., Sharp, M. J., Wohlleben, T. and Willis, I., 2002, Influence of Subglacial Drainage System Evolution on Glacier Surface Motion: Haut Glacier D'arolla, Switzerland. Journal of Geophysical Research-Solid Earth, 107(B8).

Martin, J. H., Gordon, R. M. and Fitzwater, S. E., 1990, Iron in Antarctic Waters.

McCalley, C.K., Woodcroft, B.J., Hodgkins, S.B., Wehr, R.A., Kim, E.H., Mondav, R., Crill, P.M., Chanton, J.P., Rich, V.I., Tyson, G.W. and Saleska, S.R., 2014, Methane dynamics regulated by microbial community response to permafrost thaw. Nature, 514(7523), pp.478-481.

McKnight, D.M., Boyer, E.W., Westerhoff, P.K., Doran, P.T., Kulbe, T. and Andersen, D.T., 2001, Spectrofluorometric characterization of dissolved organic matter for indication of precursor organic material and aromaticity. Limnology and Oceanography, 46(1), pp.38-48

Meire, L., Søgaard, D.H., Mortensen, J., Meysman, F.J.R., Soetaert, K., Arendt, K.E., Juul-Pedersen, T., Blicher, M.E. and Rysgaard, S., 2015, Glacial meltwater and primary production are drivers of strong CO2 uptake in fjord and coastal waters adjacent to the Greenland Ice Sheet, Biogeosciences, 12(8), pp.2347-2363.

Melillo, J., Steudler, P., Aber, J., Newkirk, K., Lux, H., Bowles, F., Catricala, C., Magill, A., Ahrens, T. and Morrisseau, S., 2002, Soil Warming and Carbon-Cycle Feedbacks to the Climate System, Science, 298(5601), 2173-2176.

Mitchell, A. C. and Brown, G. H., 2007, Diurnal Hydrological - Physicochemical Controls and Sampling Methods for Minor and Trace Elements in an Alpine Glacial Hydrological System, Journal of Hydrology, 332(1-2), 123-143.

Mitchell, A. C., Brown, G. H. and Fuge, R., 2006, Minor and Trace Elements as Indicators of Solute Provenance and Flow Routing in a Subglacial Hydrological System, Hydrological Processes, 20(4), 877-897.

Mitchell, A., Brown, G. H. and Fuge, R., 2001, Minor and Trace Element Export from a Glacierized Alpine Headwater Catchment (Haut Glacier D'arolla, Switzerland) Hydrological Processes, 15(18), 3499-3524.

Mitchell, A.C. and Brown, G.H., 2008, Modelling geochemical and biogeochemical reactions in subglacial environments, Arctic, Antarctic, and Alpine Research, 40(3), pp.531-547.

Müller, T., Bleiss, W., Martin, C.D., Rogaschewski, S. and Fuhr, G., 1998, Snow algae from northwest Svalbard: their identification, distribution, pigment and nutrient content, Polar Biology, 20(1), pp.14-32.

Naghibi, H., Dec, S.F. and Gill, S.J., 1986, Heat of solution of methane in water from 0 to 50°C, The Journal of Physical Chemistry, 90(19), pp.4621-4623.

Niemann, H., Fischer, D., Graffe, D., Knittel, K., Montiel, A., Heilmayer, O., Nöthen, K., Pape, T., Kasten, S., Bohrmann, G. and Boetius, A., 2009, Biogeochemistry of a low-activity cold seep in the Larsen B area, western Weddell Sea, Antarctica, Biogeosciences, 6(11), pp.2383-2395.

Nienow, P., Sharp, M. and Willis, I., 1998, Seasonal Changes in the Morphology of the Subglacial Drainage System, Haut Glacier D'arolla, Switzerland, Earth Surface Processes and Landforms, 23(9), 825-843.

Nisbet, E.G., 2012, Have Sudden Large Releases of Methane from Geological Reservoirs Occurred since the Last Glacial Maximum, and Could Such Releases Occur Again? Philosophical Transactions of the Royal Society London 360 pp581-607

Nowak, A. and Hodson, A., 2013, Hydrological Response of a High-Arctic Catchment to Changing Climate over the Past 35 Years: A Case Study of Bayelva Watershed, Svalbard, Polar Research, 32.

Nye, J., 1973, Water at the bed of the glacier, Association Internationale d'Hydrologie Scientifique Commission de Nieges et Glaces, Symposium on the hydrology of glaciers, Cambridge, 7-13 September 1969. International Association of Hydrological Sciences Publication 95, 189-194.

O'Leary, M.H. and Osmond, C.B., 1980, Diffusional contribution to carbon isotope fractionation during dark CO_2 fixation in CAM plants, Plant physiology, 66(5), pp.931-934.

Oliva, P., Viers, J. and Dupré, B., 2003, Chemical weathering in granitic environments, Chemical Geology, 202(3), pp.225-256.

Oremland, R.S., 1988, Biogeochemistry of methanogenic bacteria, Biology of anaerobic microorganisms, pp.641-705.

Pagli, C. and Sigmundsson, F., 2008, Will present day glacier retreat increase volcanic activity? Stress induced by recent glacier retreat and its effect on magmatism at the Vatnajökull ice cap, Iceland, Geophysical Research Letters, 35(9).

Pagli, C., Sigmundsson, F., 2008, Will present day glacier retreat increase volcanic activity? Stress induced by recent glacier retreat and its effect on magmatism at the Vatnajökull ice cap, Iceland. Geophysical Research Letters, 35 (Art. No L09304).

Pellicciotti, F., Carenzo, M., Bordoy, R. and Stoffel, M., 2014, Changes in Glaciers in the Swiss Alps and Impact on Basin Hydrology: Current State of the Art and Future Research, Science of the Total Environment, 493, 1152-1170.

Post, W. M., Peng, T.-H., Emanuel, W. R., King, A. W., Dale, V. H. and Deangelis, D. L., 1990, The Global Carbon Cycle, American scientist, 78(4), 310-326.

Prentice, I., Farquhar, G., Fasham, M., Goulden, M., Heimann, M., Kheshi, H., Quere, L., Scholes, R., Wallace, D. and Archer, D., 2001, The Carbon Cycle and Atmospheric Carbon Dioxide, in Houghton, J.T., Ding, Y., Griggs, D.J., Noguer, M., Linden, PJVD., Dai X., Maskell, K. and Johnson C.A. (eds), Climate Change 2001: The Scientific Basis. Cambridge University Press, pp. 183 - 237.

Prinzhofer, A. and Pernaton, E., 1997. Isotopically light methane in natural gas: bacterial imprint or diffusive fractionation?. *Chemical Geology*, *142*(3), pp.193-200.

Raiswell, R. and Thomas, A.G., 1984, Solute acquisition in glacial meltwaters. I: Fjallsjökull (South-East Iceland): bulk meltwaters with closed-system characteristics, Journal of Glaciology, 30(104), pp.35-43.

Raiswell, R., 1984. Chemical models of solute acquisition in glacial melt waters. *Journal of Glaciology*, *30*(104), pp.49-57.

Reynolds, R.C. and Johnson, N.M., 1972, Chemical weathering in the temperate glacial environment of the Northern Cascade Mountains. Geochimica et Cosmochimica Acta, 36(5), pp.537-554.

Rothlisberger, H., 1972, Water pressure in intra- and subglacial channels. Journal of Glaciology 11, pp 177-204.

Russell, A. J., Roberts, M. J., Fay, H., Marren, P. M., Cassidy, N. J., Tweed, F. S. and Harris, T., 2006, Icelandic Jökulhlaup Impacts: Implications for Ice-Sheet Hydrology, Sediment Transfer and Geomorphology, Geomorphology, 75(1-2), 33-64.

Russell, A. J., Tweed, F. S., Knudsen, O., Roberts, M. J., Harris, T. D. and Marren, P. M., 2002, Impact of the July 1999 Jokulhlaup on the Proximal River Jökulsa á Sólheimasandi, Mýrdalsjökull Glacier, Southern Iceland. In: SNORRASON, A., FINNSDOTTIR, H. P. and MOSS, M. E. (eds.) Extremes of the Extremes: Extraordinary Floods.

Russell, A. J., Tweed, F. S., Roberts, M. J., Harris, T. D., Gudmundsson, M. T., Knudsen, O. and Marren, P. M., 2010, An Unusual Jokulhlaup Resulting from Subglacial Volcanism, Sólheimajökull, Iceland, Quaternary Science Reviews, 29(11-12), 1363-1381.

Sander, R., 2015, Compilation of Henry's law constants (version 4.0) for water as solvent, Atmospheric Chemistry and Physics, 15(8) pp4399-4981

Säwström, C., Mumford, P., Marshall, W., Hodson, A. and Laybourn-Parry, J., 2002, The microbial communities and primary productivity of cryoconite holes in an Arctic glacier (Svalbard 79 N), Polar Biology, 25(8), pp.591-596.

Schlesinger, W. H. and Andrews, J. A., 2000, Soil Respiration and the Global Carbon Cycle, Biogeochemistry, 48(1), 7-20.

Schoell, M. 1988 (Ed) Multiple Origins of Methane in the Earth. Chemical Geology 71 pp265

Schomacker, A., Benediktsson, I. O., Ingolfsson, O., Friis, B., Korsgaard, N. J., Kjaer, K. H. and Keiding, J. K., 2012, Late Holocene and Modern Glacier Changes in the Marginal Zone of Sólheimajökull, South Iceland, Jökull, 62, 111-130.

Schomacker, A., Kjær, K.H. and Krügers, J., 2010, Subglacial environments, sediments and landforms at the margins of Mýrdalsjökull, Developments in Quaternary Science, 13, 127-144.

Schlosser, E., 1999, Effects of seasonal variability of accumulation on yearly mean delta-O-18 values in Antarctic snow, Journal of Glaciology, 45, 463.

Segers, R., 1998, Methane production and methane consumption: a review of processes underlying wetland methane fluxes. Biogeochemistry, 41(1), pp.23-51.

Sharp, M., Parkes, J., Cragg, B., Fairchild, I.J., Lamb, H. and Tranter, M., 1999, Widespread bacterial populations at glacier beds and their relationship to rock weathering and carbon cycling, Geology, 27, 2, 107-110.

Sharp, M., Parkes, J., Cragg, B., Fairchild, I.J., Lamb, H. and Tranter, M., 1999, Widespread bacterial populations at glacier beds and their relationship to rock weathering and carbon cycling. Geology, 27(2), pp.107-110.

Shreve, R. L., 1972, Movement of water in glaciers. Journal of Glaciology 11, 205-214.

Siegenthaler, U., Stocker, T. F., Monnin, E., Lüthi, D., Schwander, J., Stauffer, B., Raynaud, D., Barnola, J.-M., Fischer, H. and Masson-Delmotte, V., 2005, Stable Carbon Cycle–Climate Relationship During the Late Pleistocene, Science, 310(5752), 1313-1317.

Sigvaldason, G.E., 1963, Influence of geothermal activity on the chemistry of three glacier rivers in southern Iceland, Jökull, 13, 125-128.

Singer, G A., Fasching, C., Wilhelm, L., Niggemann, J., Steier, P., Dittmar, T. and Battin, T. J., 2012, Biogeochemically Diverse Organic Matter in Alpine Glaciers and its Downstream Fate, Letters Nature Geoscience 5 PP710-714

Skidmore, M. L. and Sharp, M. J., 1999, Drainage System Behaviour of a High-Arctic Polythermal Glacier, In: KLEMAN, J. (ed.) Annals of Glaciology.

Skidmore, M. L., Foght, J. M. and Sharp, M. J., 2000, Microbial Life beaneath a High Arctic Glacier, Applied and Environmental Microbiology 66 (8) pp3124-3220

Skidmore, M., Sharp, M. and Tranter, M., 2004, Kinetic isotopic fractionation during carbonate dissolution in laboratory experiments: implications for detection of microbial CO_2 signatures using δ^{13}C-DIC, Geochimica et Cosmochimica Acta, 68, 21, 4309 – 4317.

Smart, P.L., Finlayson, B.L., Rylands, W.D. and Ball, C.M., 1976, The relation of fluorescence to dissolved organic carbon in surface waters, Water Research, 10(9), pp.805-811.

Sommaruga, R., Psenner, R., Schafferer, E., Koinig, K.A. and Sommaruga-Wögrath, S., 1999, Dissolved organic carbon concentration and phytoplankton biomass in high-mountain lakes of the Austrian Alps: Potential effect of climatic warming on UV underwater attenuation, Arctic, Antarctic, and Alpine Research, pp.247-253.

Srikanta Dani, K, G., Mader, H. M., Wolff, E. W. and Wadham, J. L., 2012, Modelling the Liquid-water Vein System Within Polar Ice Sheets as a Potential Microbial Habitat, Earth and Planetary Science Letter 333-334 pp238-249

Staines, K. E. H. and Carrivick, J. L., 2015, Geomorphological Impact and Morphodynamic Effects on Flow Conveyance of the 1999 Jökulhlaup at Sólheimajökull, Iceland, Earth Surface Processes and Landforms, 40(10), pp.1401-1416.

Staines, K. E. H., Carrivick, J. L., Tweed, F. S., Evans, A. J., Russell, A. J., Johannesson, T. and Roberts, M., 2015, A Multi-Dimensional Analysis of Pro-Glacial Landscape Change at Sólheimajökull, Southern Iceland, Earth Surface Processes and Landforms, 40(6), pp.809-822.

Sebacher, D. I., Harriss, R. C., & Bartlett, K. B., 1983, Methane flux across the air-water interface: Air velocity effects. *Tellus B*, *35*(2), pp.103-109.

Stefánsson, A. and Gíslason, S.R., 2001, Chemical weathering of basalts, Southwest Iceland: effect of rock crystallinity and secondary minerals on chemical fluxes to the ocean, American Journal of Science, 301(6), pp.513-556.

Stibal M., Tranter M., Benning L.G. and Řehák J., 2008, Microbial primary production on an Arctic glacier is insignificant in comparison with allochthonous organic carbon input, Environmental Microbiology 10, pp.2172–2178.

Stibal, M., Schostag, M., Cameron, K. A., Hansen, L. H., Chandler, D. M., Wadham, J. L. and Jacobsen, C. S., 2015, Different Bulk and Active Bacterial Communities in Cryoconite from the Margin and Interior of the Greenland Ice Sheet, Environmental Microbiology Reports, 7(2), pp.293-300.

Stibal, M., Tranter, M., Benning, L. G. and Rehak, J., 2008, Microbial Primary Production on an Arctic Glacier Is Insignificant in Comparison with Allochthonous Organic Carbon Input, Environmental Microbiology, 10(8), 2172-2178.

Stibal, M., Hasan, F., Wadham, J. L., Sharp, M. J. and Anesio, A M., 2012, Prokaryotic Diversity in Sediments Beneath two Polar Glaciers with Contrasting Organic Carbon Substrates, Extremophiles 16 pp.255-265

Stichler, W. and Schotterer, U., 2000, From Accumulation to Discharge: Modification of Stable Isotopes During Glacial and Post-Glacial Processes, Hydrological Processes, 14(8), pp.1423-1438.

Stolper, D. A., Lawson, M., Davis, C. L., Ferreira, A. A., Santos Neto, E. V., Ellis, G. S., Lewan, M. D., Martini, A. M., Tang, Y., Schoell, M., Sessions, A. L. and Eiler, J. M., 2014, Formation Temperatures of Thermogenic and Biogenic Methane, Science, 344(6191), 1500-1503.

Stoops, G., Gérard, M. and Arnalds, O., 2008, A micromorphological study of Andosol genesis in Iceland, In New Trends in Soil Micromorphology (pp. 67-89). Springer Berlin Heidelberg.

Sugimoto, A. and Wada, E., 1993, Carbon isotopic composition of bacterial methane in a soil incubation experiment: Contributions of acetate and CO_2H_2, Geochimica et Cosmochimica Acta, 57(16), pp.4015-4027.

Takeuchi, N., Kohshima, S. and Seko, K., 2001, Structure, formation, and darkening process of albedo-reducing material (cryoconite) on a Himalayan glacier: a granular algal mat growing on the glacier, Arctic Antarctic and Alpine Research 33, pp.115–122.

Telling, J., Boyd, E.S., Bone, N., Jones, E.L., Tranter, M., MacFarlane, J.W., Martin, P.G., Wadham, J.L., Lamarche-Gagnon, G., Skidmore, M.L. and Hamilton, T.L., 2015, Rock comminution as a source of hydrogen for subglacial ecosystems, Nature Geoscience, 8(11), pp.851-855.

Tepe, N., and Bau, M., 2014, Importance of nanoparticles and colloids from volcanic ash for riverine transport of trace elements to the ocean: evidence from glacial-fed rivers after the 2010 eruption of Eyjafjallajökull volcano, Iceland. Science of the Total Environment, *488*, 243-251.

Theakstone, W. H., 1988, Temporal variations of isotopic composition of glacier river water during summer: observations at Austre Okstindbreen, Okstindan, Norway, Journal of Glaciology 34, pp.309-317.

The Icelandic Meteorological Office. Delivery of data from the Hydrological database, no. 2015-05-06/02.

Thompson, C. Identifying the drivers of glacier melt in Southern Iceland (unpublished masters thesis).

Thordarson, T. and Larsen, G., 2007, Volcanism in Iceland in historical time: Volcano types, eruption styles and eruptive history, Journal of Geodynamics, 43, 118 – 152.

Tranter, M., 1991, Controls on the composition of snowmelt. In Seasonal Snowpacks; Processes of Compositional Change, eds. T. D. Davies, M. Tranter and H. G. Jones, pp. 241-271. Springer, Berlin.

Tranter, M., Brown, G. H., Hodson, A. J. and Gurnell, A. M., 1996, Hydrochemistry as an Indicator of Subglacial Drainage System Structure: A Comparison of Alpine and Sub-Polar Environments, Hydrological Processes, 10(4), pp.541-556.

Tranter, M., Brown, G., Raiswell, R., Sharp, M. and Gurnell, A., 1993, A conceptual model of solute acquisition by Alpine glacial meltwaters, Journal of Glaciology, 39, 133, pp.573-581.

Tranter, M., Brown, G.H., Hodson, A.J. and Gurnell, A.M. (1996) Hydrochemistry as an indicator of subglacial drainage system structure: a comparison of alpine and sub-polar environments, Hydrological Processes, 10, 541 – 556.

Tranter, M., Huybrechts, P., Munhoven, G., Sharp, M.J., Brown, G.H., Jones, I.W., Hodson, A.J., Hodgkins, R. and Wadham, J.L., 2002. Direct effect of ice sheets on terrestrial bicarbonate, sulphate and base cation fluxes during the last glacial cycle: minimal impact on atmospheric CO_2 concentrations. Chemical Geology, 190(1), pp.33-44.

Tranter, M., Sharp, M.J., Brown, G.H., Willis, I.C., Hubbard, B.P., Nielsen, M.K., Smart, C.C., Gordon, S., Tulley, M. and Lamb, H.R. (1997) Variability in the chemical composition of in situ subglacial meltwaters, Hydrological Processes, 11, 59 – 77.

Tranter, M., Sharp, M.J., Brown, G.H., Willis, I.C., Hubbard, B.P., Nielson, M.K., Smart, C.C., Gordon, S., Tulley, M., Lamb, H.R., 1997. Variability in the chemical composition of in situ subglacial meltwaters. Hydrol. Process. 11, 59–77.

Tranter, M., Sharp, M.J., Lamb, H.R., Brown, G.H., Hubbard, B.P. and Willis, I.C., 2002. Geochemical weathering at the bed of Haut Glacier d'Arolla, Switzerland—a new model. Hydrological Processes, 16(5), pp.959-993.

Tranter, M., Skidmore, M. and Wadham, J., 2005. Hydrological controls on microbial communities in subglacial environments. Hydrological Processes,19(4), pp.995-998.

Tuffen, H., 2010, How will melting of ice affect volcanic hazards in the twenty-first century? Philosophical Transactions of the Royal Society of London A: Mathematical, Physical and Engineering Sciences, 368(1919), pp.2535-2558.

Tyler, S.C., Crill, P.M. and Brailsford, G.W., 1994. 13C12C Fractionation of methane during oxidation in a temperate forested soil. Geochimica et Cosmochimica Acta, 58(6), pp.1625-1633.

United States Geological Survey, 1994, Resources on Isotopes, URL: http://wwwrcamnl.wr.usgs.gov/isoig/period/h_iig.html [04/09/2016]

Valentine, D.L., Chidthaisong, A., Rice, A., Reeburgh, W.S. and Tyler, S.C., 2004, Carbon and hydrogen isotope fractionation by moderately thermophilic methanogens, Geochimica et Cosmochimica Acta, 68(7), pp.1571-1590

Vincent, W. F., 2010, Commentary: Microbial Ecosystem Responses to Rapid Climate Change in the Arctic, The ISME Journal 4 pp.1089-1091

von Strandmann, P.A.P., Burton, K.W., James, R.H., van Calsteren, P., Gislason, S.R. and Sigfússon, B., 2008, The influence of weathering processes on riverine magnesium isotopes in a basaltic terrain, Earth and Planetary Science Letters, 276(1), pp.187-197.

Wadham J.L., Tranter M., Tulaczyk S., and Sharp M., 2008, Subglacial methanogenesis: A potential climatic amplifier? Global Biogeochemical Cycles, v. 22, GB2021.

Wadham, J. L., Arndt, S., Tulaczyk, S., Stibal, M., Tranter, M., Telling, J., Lis, G. P., Lawson, E., Ridgewell, A., Dubnick, A., Sharp, M, J., Anesio, A. M. and Butler, C. E. H., 2012, Potential Methane Reservoirs Beneath Antarctica, Nature 488 pp.633-637

Wadham, J.L., Tranter, M., Tulaczyk, S. and Sharp, M., 2008, Subglacial methanogenesis: a potential climatic amplifier? Global Biogeochemical Cycles, 22(2).

Wadham, J. L., Hodson, A. J., Tranter, M. and Dowdeswell, J. A., 1998, The Hydrochemistry of Meltwaters Draining a Polythermal-Based, High Arctic Glacier, South Svalbard: I. The Ablation Season, Hydrological Processes, 12(12), pp.1825-1849.

Wadham, J. L., Tranter, M. and Dowdeswell, J. A., 2000, Hydrochemistry of Meltwaters Draining a Polythermal-Based, High-Arctic Glacier, South Svalbard: Ii. Winter and Early Spring, Hydrological Processes, 14(10), pp.1767-1786.

Wadham, J. L., Tranter, M., Hodson, A. J., Hodgkins, R., Bottrell, S., Cooper, R. and Raiswell, R., 2010, Hydro-Biogeochemical Coupling beneath a Large Polythermal Arctic Glacier: Implications for Subice Sheet Biogeochemistry. Journal of Geophysical Research-Earth Surface, 115.

Wake, C.P., 1989, Glaciochemical investigations as a tool for determining the spatial and seasonal variation of snow accumulation in the central Karakoram, northern Pakistan, Annals of Glaciology, 13, pp.279-284.

Wang, Y. and Wooller, M.J., 2006, The stable isotopic (C and N) composition of modern plants and lichens from northern Iceland: with ecological and paleo environmental implications, Jökull, 56, pp.27-38.

Weertman, J., 1972, General theory of water flow at the base of a glacier or ice sheet, Reviews Geophysics and Space Physics 10(1), pp.287-333.

Wegener, G., Niemann, H., Elvert, M., Hinrichs, K.U. and Boetius, A., 2008, Assimilation of methane and inorganic carbon by microbial communities mediating the anaerobic oxidation of methane, Environmental Microbiology,10(9), pp.2287-2298.

Weitemeyer, K.A. and Buffet, B.A., 2006, Accumulation and release of methane from clathrates below the Laurentide and Cordilleran ice sheets, Global and Planetary Change, v. 53, pp.176-187.

White, A.F., Bullen, T.D., Vivit, D.V., Schulz, M.S. and Clow, D.W., 1999, The role of disseminated calcite in the chemical weathering of granitoid rocks, Geochimica et Cosmochimica Acta, 63(13), pp.1939-1953.

Whiticar, M.J., Faber, E. and Schoell, M., 1986. Biogenic methane formation in marine and freshwater environments: CO_2 reduction vs. acetate fermentation—isotope evidence. *Geochimica et Cosmochimica Acta*, *50*(5), pp.693-709.

Whiticar M. J., 1999, Carbon and hydrogen isotopes systematics of bacterial formation and oxidation of methane, Chemical Geology, v. 161, pp.291-314.

Wiese, F., Fridriksson, T. and Ármannsson, H., 2008, CO_2 fixation by calcite in high-temperature geothermal systems in Iceland, Report from the Iceland Geosurvey (Ísor), Ísor-2008/003, Reykjavik.

Wimpenny, J., Gíslason, S.R., James, R.H., Gannoun, A., Von Strandmann, P.A.P. and Burton, K.W., 2010, The behaviour of Li and Mg isotopes during primary phase dissolution and secondary mineral formation in basalt, Geochimica et Cosmochimica Acta, 74(18), pp.5259-5279.

Wynn, P. M., Morrell, D. J., Tuffen, H., Barker, P., Tweed, F. S. and Burns, R., 2015, Seasonal Release of Anoxic Geothermal Meltwater from the Katla Volcanic System at Sólheimajökull, Iceland, Chemical Geology, 396, pp.228-238.

Wynn, P.M., Hodson, A. and Heaton, T., 2006, Chemical and isotopic switching within the subglacial environment of a High Arctic glacier, Biogeochemistry, 78, pp.173-193.

Wynn, P.M., Hodson, A.J., Heaton, T.H.E., Chenery, S., 2007, Nitrate production beneath a High Arctic Glacier, Chemical Geology, 244, pp.88–102.

Wynn, P. M., Baker, A. and Hodson, A.J., unpublished, Characterisation of organic matter in glacial meltwaters by fluorescence spectroscopy.

Yde, J. C., Hodson, A. J., Solovjanova, I., Steffensen, J. P., Nørnberg, P., Heinemeier, J., & Olsen, J., 2012, Chemical and isotopic characteristics of a glacier-derived naled in front of Austre Grønfjordbreen, Svalbard, Polar Research, *31*.

Yoshimura, Y., Kohshima, S. and Ohtani, S., 1997, A community of snow algae on a Himalayan glacier: change of algal biomass and community structure with altitude, Arctic and Alpine Research, pp.126-137.

Zeng, N., 2003, Glacial-interglacial atmospheric CO_2 change—The glacial burial hypothesis, Advances in Atmospheric Sciences, 20(5), pp.677-693.

Ziegler, K., Chadwick, O. A., Brzezinski, M. A., & Kelly, E. F., 2005, Natural variations of δ 30 Si ratios during progressive basalt weathering, Hawaiian Islands. *Geochimica et Cosmochimica Acta*, *69*(19), pp.4597-4610.

Zimov, S. A., Schuur, E. A. G. and Chapin III, F S., 2006, Permafrost and the Global Carbon Budget, Science 312.

Appendix

Appendix 1. Basic meltwater geochemical parameters averaged by individual sampling sites for Spring 2014 and Summer 2013

Site	Electrical Conductivity (EC) µS/cm	pH	Temperature (°C)	$\delta^{18}O$	δD
			Spring 2014		
Mixed Zone	134 (14.42) Min=108 Max=153 n=18	7.31 (0.38) Min=6.89 Max=8.51 n=18	2.83 (1.43) Min=1.50 Max=5.60 n=17	-9.34 (0.38) Min=-9.99 Max=-8.72 n=18	-65.44 (2.66) Min=-67.91 Max=-56.79 n=14
Bridge	126 (11.46) Min=106 Max=138 n=7	7.57 (0.11) Min=7.44 Max=7.70 n=7	3.43 (0.78) Min=2.80 Max=4.30 n=6	-8.99 (0.29) Min=-.933 Max=-8.63 n=7	-65.00 (1.58) Min=-67.00 Max=-62.30 n=6
Subglacial Upwelling 1	145 (16.50) Min=124 Max=164 n=3	6.71 (0.29) Min=6.30 Max=6.98 n=3	0.00 (0.08) Min=-0.10 Max=0.10 n=3	-9.69 (0.23) Min=-9.92 Max=-9.38 n=3	-68.60 (0.79) Min=-69.4 Max=-67.8 n=2
Subglacial Upwelling 2	145 (17.99) Min=122 Max=166 n=3	6.61 (0.19) Min=6.36 Max=6.83 n=3	-0.07 (0.05) Min=-0.1 Max=0 n=3	-9.47 (0.11) Min=-9.58 Max=-9.36 n=3	-69.44 (1.44) Min=-71.31 Max=-67.81 n=3
Upper Eastern Lagoon	78 (15.55) Min=53 Max=109 n=11	7.92 (0.32) Min=7.48 Max=8.55 n=11	0.76 (0.60) Min=0.2 Max=2.1 n=11	-8.72 (0.42) Min=-9.43 Max=-8.17 n=9	-61.80 (1.71) Min=-63.52 Max=-57.52 n=10
Middle Eastern Lagoon	112 (17.07) Min=86 Mx=133 n=5	7.43 (0.24) Min=7.14 Max=7.78 n=5	1.9 (0.69) Min=0.7 Max=2.6 n=5	-8.78 (0.26) Min=-9.17 Max=-8.17 n=4	-64.44(0.49) Min=-64.90 Max=-63.64 n=4
Lower Eastern Lagoon	124 (24.05) Min=104 Max=165 n=4	6.67 (0.50) Min=5.84 Max=7.18 n=4	1.3 (0.15) Min=1.1 Max=1.5 n=4	-9.15 (-) Min=-9.46 Max=-8.74 n=2	-63.87 (-) Min=-67.67 Max=60.07 n=2
Upper Western Lagoon	137 (19.94) Min=110 Max=157 n=3	7.23 (0.34) Min=6.89 Max=7.70 n=3	3.9 (1.62) Min=2.3 Max=6.1 n=3	-9.70 (0.66) Min=-10.63 Max=-9.14 n=3	-66.40 (0.41) Min=-66.70 Max=-65.83 n=3
Middle Western Lagoon	139 (10.34) Min=125 Max=150 n=3	7.13 (0.09) Min=7.03 Max=7.25 n=3	2.77 (0.82) Min=1.80 Max=3.8 n=3	-9.35 (0.35) Min=-9.68 Max=-8.87 n=3	-66.85 (0.94) Min=-67.98 Max=65.69 n=3
Edge of Ice 1	137 (-) Min=133 Max=141 n=2	6.83 (-) Min=6.35 Max=7.31 n=2	1.85 (-) Min=1.3 Max=2.4 n=2	-8.89 (-) Min=-8.92 Max=-8.84 n=2	-65.20 (-) Min=-66.11 Max=64.29 n=2
Edge of Ice 2	121 (-) Min=118 Max=124 n=2	7.64 (-) Min=7.06 Max=8.22 n=2	0.8 (-) Min=0.5 Max=1.1 n=2	-9.14 (-) n=1	-63.70 (-) n=1
Edge of Ice 3			Not Sampled		
Edge of Ice 4			Not Sampled		
Edge of Ice 5	105 (-) n=1	7.5 (-) n=1	0.1 (-) n=1	-9.12 (-) n=1	-66.02 (-) n=1
Edge of Ice 6	93 (47.85) Min=33 Max=150 n=2	7.18 (0.18) Min=6.98 Max=7.42 n=3	0.43 (0.17) Min=0.20 Max=0.60 n=3	-8.85 (0.09) Min=-8.97 Max=-8.76 n=3	-63.17 (1.72) Min=-65.20 Max=-61.00 n=3
Fjallgilsá	74 (6.68) Min=67 Max=83 n=3	7.26 (0.48) Min=6.68 Max=7.86 n=3	3.8 (0.85) Min=3.2 Max=5.00 n=3	-9.30 (0.08) Min=-9.40 Max=-9.22 n=3	-65.43 (-) Min=-66.57 Max=64.29 n=2
Jökulsárgil	106 (8.29) Min=97 Max=117 n=3	7.91 (0.13) Min=7.74 Max=8.05 n=3	4.17 (0.76) Min=3.40 Max=5.20 n=3	-9.31 (0.00) Min=-9.31 Max=-9.31 n=3	-66.05 (1.28) Min=-67.63 Max=-64.49 n=3
Spring Supraglacial Site 1	1 (-) n=1	7.8 (-) n=1	0.1 (-) n=1	-9.59 (-) n=1	-64.06 (-) n=1
Spring Supraglacial Site 2	4 (-) n=1	7.22 (-) n=1	4.2 (-) n=1	-8.93 (-) n=1	
Sring Supraglacial Site 3	11 (-) n=1	6.03 (-) n=1	0 (-) n=1	-8.44 (-) n=1	-54.76 (-) n=1

Site	Electrical Conductivity (EC) µS/cm	pH	Temperature (°C)	δ¹⁸O	δD
			Summer 2013		
Mixed Zone	106 (17.05) Min=80 Max=135 n=13	6.52 (0.16) Min=6.32 Max=6.85 n=13	1.19 (0.31) Min=0.70 Max=2.00 n=13	-9.30 (0.08) Min=-9.40 Max=-9.22 n=12	-65.43 (1.14) Min=-66.57 Max=-64.29 n=11
Bridge	96 (11.27) Min=85 Max=114 n=4	7.57 (0.11) Min=7.44 Max=7.7 n=7	2.55 (0.56) Min=1.9 Max=3.2 n=4	-9.15 (0.29) Min=-9.64 Max=-8.88 n=4	-68.71 (0.44) Min=-69.33 Max=-68.35 n=3
Subglacial Upwelling 1			Not Sampled		
Subglacial Upwelling 2					
Upper Eastern Lagoon	35 (16.25) Min=14 Max=58 n=7	6.97 (0.23) Min=6.65 Max=7.40 n=7	1.26 (0.30) Min=0.7 Max=1.6 n=7	-8.46 (-) Min=-8.62 Max=-8.30 n=2	-64.76 (1.86) Min=-67.46 Max=-62.39 n=4
Middle Eastern Lagoon	110 (16.12) Min=81 Max=129 n=5	6.97 (0.23) Min=6.65 Max=7.4 n=5	2.42 (1.26) Min=1.00 Max=4.40 n=5	-8.93 (0.37) Min=-9.32 Max=-8.44 n=3	-67.20 (2.86) Min=-70.22 Max=-63.36 n=3
Lower Eastern Lagoon	198 (-) n=1	96 (-) n=1	0.9 (-) n=1	6.28 (-) n=1	-8.80 (-) n=1
Upper Western Lagoon	108 (-) Min=97 Max=118 n=2	6.82 (-) Min=6.51 Max=7.13 n=2	5 (-) Min=2.8 Max=7.2 n=2	-9.00 (-) Min=-9.47 Max=-8.53 n=2	-70.63 (-) Min=-73.93 Max=-67.32 n=2
Middle Western Lagoon	122 (-) n=1	2.30 (-) n=1	6.60 (-) n=1	-10.36 (-) n=1	-73.23 (-) n=1
Edge of Ice 1	90 (-) n=1	6.92 (-) n=1	1.80 (-) n=1	-8.86 (-) n=1	-67.81 (-) n=1
Edge of Ice 2			Not Sampled		
Edge of Ice 3	93 (-) n=1	6.21 (-) n=1	1.00 (-) n=1	-9.56 (-) n=1	-70.06 (-) n=1
Edge of Ice 4	50 (-) n=1	7.15 (-) n=1	1 (-) n=1	-8.71 (-) n=1	-64.08 (-) n=1
Edge of Ice 5			Not Sampled		
Edge of Ice 6	36 (-) n=1	6.59 (-) n=1	1.8 (-) n=1	-7.60 (-) n=1	-59.35 (-) n=1
Fjallgilsá	42 (-) Min=38 Max=45 n=2	7.41 (-) Min=7.20 Max=7.62 n=2	4.95 (-) Min=4.1 Max=5.8 n=2	-8.77 (-) Min=-9.31 Max=-8.23 n=2	-64.26 (-) Min=-67.88 Max=-60.65 n=2
Jökulsárgil	66 (-) Min=52 Max=79 n=2	7.75 (-) Min=7.67 Max=7.82 n=2	3.75 (-) Min=3.20 Max=4.3 n=2	-8.76 (-) Min=-8.77 Max=-8.75 n=2	-68.08 (-) Min=-69.42 Max=-66.74 n=2
Free Flowing Supraglacial Water	6 (-) n=1	0.1 (-) n=1	7.27 (-) n=1	-8.37 (-) n=1	
Stagnant Supraglacial Water	22 (-) n=1	0.5 (-) n=1	6.87 (-) n=1	-8.65 (-) n=1	-63.63 (-) n=1

Appendix 2. Bulk meltwater average cation and anion abundances for Spring 2014 and Summer 2013

Spring 2014 (standard deviations are in parentheses)

Site	Ca^{2+}	K^+	Mg^{2+}	Na^+	Si	F^-	Cl^-	SO_4^{2-}	NO_3^-	TDIC
Mixed Zone	190.38 (10.18) n=14	29.98 (2.58) n=14	94.50 (7.50) n=14	561.32 (51.36) n=14	113.57 (11.64) n=14	14.79 (1.74) n=14	150.70 (17.97) n=14	19.49 (1.84) n=14	0.64 (0.48) n=14	892.06 (107.08) n=14
Bridge	242.43 (46.00) n=6	29.50 (3.39) n=6	95.41 (4.78) n=6	543.43 (35.13) n=6	122.02 (14.61) n=6	12.77 (2.68) n=6	168.36 (24.79) n=6	14.99 (1.77) n=6	0.47 (0.32) n=6	863.15 (30.66) n=6
Subglacial Upwellings	223.60 (16.84) n=6	30.93 (2.01) n=6	105.79 (14.60) n=6	581.49 (56.04) n=6	108.85 (14.32) n=6	10.43 (5.21) n=6	155.63 (13.47) n=6	16.54 (1.99) n=6	0.56 (0.72) n=6	1048.89 (145.47) n=6
Edge of Ice Sites	162.43 (37.02) n=7	23.69 (9.31) n=7	71.16 (29.06) n=7	434.48 (166.55) n=7	88.25 (36.83) n=7	11.50 (3.07) n=7	119.44 (48.95) n=7	13.23 (5.43) n=7	0.28 (0.32) n=7	665.86 (145.47) n=7
Upper Eastern Lagoon	151.03 (32.24) n=10	18.26 (3.99) n=10	52.84 (14.52) n=10	393.62 (73.17) n=10	80.07 (15.84) n=10	11.51 (1.83) n=10	106.42 (26.91) n=10	13.42 (3.87) n=10	0.18 (0.12) n=10	545.42 (115.21) n=10
Middle Eastern Lagoon	236.82 (38.57) n=4	23.21 (3.10) n=4	76.45 (10.97) n=4	505.63 (64.40) n=4	100.85 (10.97) n=4	12.43 (1.43) n=4	134.66 (28.29) n=4	14.75 (2.17) n=4	0.23 (0.17) n=4	691.61 (95.53) n=4
Lower Eastern Lagoon	251.83 (...) n=2	23.80 (...) n=2	80.68 (...) n=2	487.28 (...) n=2	99.22 (...) n=2	11.50 (...) n=2	123.39 (...) n=2	14.48 (...) n=2	0.20 (...) n=2	694.89 (...) n=2
Upper Western Lagoon	297.99 (55.08) n=3	28.97 (4.25) n=3	99.41 (13.95) n=3	570.97 (90.11) n=3	114.20 (20.49) n=3	13.81 (2.02) n=3	158.06 (26.14) n=3	16.65 (2.28) n=3	0.52 (0.18) n=3	834.742 (167.18) n=3
Middle Western Lagoon	302.77 (28.95) n=3	28.50 (3.50) n=3	101.83 (7.87) n=3	569.16 (71.94) n=3	116.31 (12.49) n=3	10.75 (1.67) n=3	162.37 (16.67) n=3	14.65 (2.23) n=3	0.11 (0.11) n=3	742.96 (13.65) n=3
Fjallgilsá	86.71 (8.71) n=3	23.76 (3.25) n=3	88.32 (12.18) n=3	325.23 (29.25) n=3	120.24 (15.62) n=3	8.87 (0.19) n=3	205.73 (10.47) n=3	9.44 (0.59) n=3	0.012 (0.02) n=3	386.78 (56.01) n=3
Jökulsárgil	140.96 (11.77) n=3	31.18 (2.58) n=3	98.19 (8.87) n=3	535.42 (40.55) n=3	110.41 (7.29) n=3	13.63 (0.44) n=3	195.35 (18.82) n=3	10.58 (2.17) n=3	0.65 (0.76) n=3	622.78 (136.25) n=3
Supraglacial Sites	34.46 (...) n=2	1.99 (...) n=2	6.07 (...) n=2	16.72 (...) n=2	1.08 (...) n=2	5.51 (...) n=2	10.62 (...) n=2	1.73 (...) n=2	0.02 (...) n=2	134.39 (...) n=2

Summer 2013 (standard deviations are in parentheses)

Site	Ca^{2+}	K^+	Mg^{2+}	Na^+	Si	F^-	Cl^-	SO_4^{2-}	NO_3^-	TDIC
Mixed Zone	243.90 (23.42) n=12	26.46 (5.06) n=12	71.54 (5.48) n=12	424.23 (84.88) n=12	146.95 (25.06) n=12	6.78 (1.09) n=12	74.46 (19.71) n=12	56.88 (35.51) n=12	0.12 (0.26) n=12	642.52 (108.11) n=12
Bridge	207.34 (20.99) n=4	26.48 (4.51) n=4	65.12 (7.42) n=4	420.78 (84.07) n=4	148.67 (27.97) n=4	4.97 (0.64) n=4	72.42 (9.90) n=4	29.76 (3.59) n=4	0.05 (0.00) n=4	627.47 (101.05) n=4
Subglacial Upwellings	Not Sampled									
Edge of Ice Sites	188.71 (43.44) n=4	17.31 (4.18) n=4	52.60 (11.57) n=4	296.36 (68.75) n=4	101.27 (23.78) n=4	4.68 (0.71) n=4	54.43 (14.68) n=4	29.43 (5.19) n=4	0.02 (0.03) n=4	484.64 (90.94) n=4
Upper Eastern Lagoon	95. 59 (53.74) n=5	7.60 (6.08) n=5	35.90 (33.15) n=5	110.60 (72.39) n=5	68.51 (58.58) n=5	1.07 (1.17) n=5	47.05 (29.57) n=5	28.75 (22.03) n=5	0.16 (0.25) n=5	197.30 (171.73) n=5
Middle Eastern Lagoon	297.94 (52.96) n=4	28.29 (4.43) n=4	82.25 (11.46) n=4	454.87 (69.77) n=4	154.27 (18.39) n=4	10.22 (2.41) n=4	117.61 (66.36) n=4	122.37 (79.11) n=4	0.13 (0.21) n=4	627.94 (132.49) n=4
Lower Eastern Lagoon	192.48 (...) n=1	24.98 (...) n=1	58.48 (...) n=1	422.99 (...) n=1	142.96 (...) n=1	6.32 (...) n=1	105.58 (...) n=1	47.98 (...) n=1	0.05 (...) n=1	555.60 (...) n=1
Upper Western Lagoon	255.77 (...) n=2	26.39 (...) n=2	78.39 (...) n=2	403.67 (...) n=2	132.17 (...) n=2	6.55 (...) n=2	78.51 (...) n=2	45.59 (...) n=2	0.00 (...) n=2	648.05 (...) n=2
Middle Western Lagoon	285.43 (...) n=1	30.17 (...) n=1	86.89 (...) n=1	457.51 (...) n=1	149.20 (...) n=1	2.29 (...) n=1	78.00 (...) n=1	154.62 (...) n=1	0.00 (...) n=1	639.76 (...) n=1
Fjallgilsá	54.19 (...) n=2	13.90 (...) n=2	49.63 (...) n=2	182.25 (...) n=2	122.60 (...) n=2	4.57 (...) n=2	74.23 (...) n=2	21.07 (...) n=2	0.00 (...) n=2	224.25 (...) n=2
Jökulsárgil	119. 68 (...) n=2	23.23 (...) n=2	61.06 (...) n=2	326.72 (...) n=2	104.35 (...) n=2	5.27 (...) n=2	74.65 (...) n=2	13.66 (...) n=2	0.03 (...) n=2	455.95 (...) n=2
Supraglacial Sites	26.28 (14.08) n=4	0.91 (0.87) n=4	9.96 (8.12) n=4	11.72 (4.98) n=4	18.42 (10.93) n=4	0.85 (1.47) n=4	2.37 (1.30) n=4	2.69 (2.10) n=4	0.22 (0.12) n=4	70.42 (27.14) n=4

Appendix 3. Relevant ionic abundances used for calculation of %TDIC from carbonates and silicates

Site		TDIC meq/L	Si meq/L	1.58*Si meq/L	(1.58*Si)+Ca+Mg	Average TDIC-(1.58*Si)+Ca+Mg	%TDIC from Silicates	%TDIC from Carbonates
	Spring							
Mixed Zone		0.90 (0.10) Min= 0.73 Max= 1.08 n=13	0.11 (0.01) Min= 0.10 Max= 0.13 n=13	0.18 (0.02) Min= 0.15 Max= 0.21 n=13	0.75 (0.05) Min= 0.66 Max= 0.83 n=13	0.15 (0.08) Min= 0.00 Max= 0.27 n=13	23.92 (1.24) Min= 21.62 Max= 25.21 n=13	76.08 (1.24) Min= 74.79 Max= 78.38 n=13
Bridge		0.86 (0.03) Min= 0.82 Max=0.90 n=6	0.12 (0.01) Min= 0.10 Max= 0.14 n=6	0.19 (0.02) Min= 0.15 Max= 0.21 n=6	0.87 (0.07) Min= 0.78 Max= 0.95 n=6	-0.01 (0.08) Min= -0.10 Max= 0.09 n=6	22.43 (3.76) Min= 17.43 Max= 27.45 n=6	77.57 (3.76) Min=72.55 Max= 82.57 n=6
Subglacial Upwellings		1.05 (0.13) Min= 0.86 Max= 1.27 n=6	0.11 (0.01) Min=0.09 Max=0.12 n=6	0.17 (0.02) Min= 0.14 Max= 0.20 n=6	0.83 (0.05) Min= 0.76 Max= 0.88 n=6	0.22 (0.10) Min= 0.10 Max= 0.41 n=6	20.80 (2.83) Min= 16.20 Max= 22.87 n=6	79.20 (2.83) Min= 77.13 Max= 83.80 n=6
Edge of Ice Sites		0.67 (0.19) Min= 0.28 Max= 0.87 n=7	0.09 (0.03) Min= 0.03 Max=0.13 n=7	0.14 (0.05) Min= 0.05 Max= 0.20 n=7	0.61 (0.18) Min=0.31 Max= 0.80 n=7	0.06 (0.05) Min= -0.03 Max= 0.12 n=7	22.13 (3.15) Min= 15.36 Max= 24.95 n=7	77.87 (3.15) Min= 75.04 Max= 84.64 n=7
Eastern Lagoon		0.60 (0.11) Min= 0.35 Max= 0.81 n=16	0.09 (0.02) Min= 0.06 Max= 0.11 n=16	0.13 (0.03) Min= 0.09 Max= 0.18 n=16	0.63 (0.16) Min= 0.35 Max=0.91 n=16	-0.03 (0.10) Min= -0.17 Max= 0.23 n=16	22.37 (2.33) Min= 18.28 Max= 26.41 n=16	77.63 (2.33) Min= 73.59 Max= 81.72 n=16
Western Lagoon		0.79 (0.11) Min= 0.67 Max= 1.00 n=6	0.12 (0.01) Min= 0.10 Max= 0.13 n=6	0.18 (0.02) Min= 0.15 Max= 0.22 n=6	0.98 (0.11) Min= 0.79 Max= 1.11 n=6	-0.32 (0.34) Min= -1.06 Max= -0.11 n=6	18.51 (0.87) Min= 16.89 Max= 19.40 n=6	81.49 (0.87) Min= 80.60 Max= 83.11 n=6
Fjallgilsá		0.39 (0.05) Min= 0.33 Max= 0.45 n=3	0.12 (0.01) Min=0.11 Max= 0.14 n=3	0.19 (0.02) 0.16 Max= 0.21 n=3	0.54 (0.05) Min= 0.48 Max= 0.61 n=3	-0.15 (0.01) Min= -0.17 Max= 0.15 n=3	35.16 (0.24) Min= 34.82 Max= 35.36 n=3	64.84 (0.24) Min= 64.64 Max= 65.17 n=3
Jökulsárgil		0.62 (0.11) Min=0.45 Max= 0.70 n=3	0.11 (0.01) Min= 0.10 Max= 0.19 n=3	0.17 (0.01) Min= 0.16 Max= 0.19 n=3	0.65 (0.04) Min=0.61 Max= 0.71 n=3	-0.03 (0.08) Min= -0.14 Max= 0.06 n=3	26.75 (0.34) Min= 26.27 Max= 27.03 n=3	73.25 (0.34) Min= 72.97 Max= 73.73 n=3
Supraglacial sites		0.13 (-) Min= 0.14 Max= 0.13 n=2	0.00 (-) Min=0.00 Max= 0.00 n=2	0.00 (-) Min= 0.00 Max= 0.00 n=2	0.08 (-) Min= 0.05 Max= 0.12 n=2	0.05 (-) Min= 0.02 Max= 0.08 n=2	1.46 (-) Min= 0 Max= 2.93 n=2	98.53 (-) Min= 97.07 Max= 100 n=2

	Summer						
Site	TDIC meq/L	Si meq/L	1.58*Si meq/L	(1.58*Si)+Ca+Mg	Average TDIC-(1.58*Si)+Ca+Mg	%TDIC from Silicates	%TDIC from Carbonates
Mixed Zone	0.64 (0.11) Min= 0.54 Max= 0.87 n=12	0.15 (0.03) Min= 0.12 Max= 0.20 n=12	0.23 (0.04) Min= 0.18 Max= 0.31 n=12	0.86 (0.09) Min= 0.73 Max= 1.01 n=12	-0.22 (0.06) Min= -0.31 Max= -0.13 n=12	26.79 (2.69) Min= 21.88 Max= 30.70 n=12	73.21 (2.69) Min= 69.30 Max= 78.12 n=12
Bridge	0.62 (0.10) Min= 0.53 Max= 0.78 n=4	0.15 (0.03) Min= 0.13 Max= 0.19 n=4	0.24 (0.04) Min= 0.20 Max= 0.31 n=4	0.78 (0.10) Min= 0.70 Max= 0.94 n=4	-0.15 (0.03) Min= -0.17 Max= -0.13 n=4	29.93 (2.36) Min= 26.85 Max= 32.50 n=4	70.07 (2.36) Min= 67.51 Max= 73.15 n=4
Subglacial Upwellings	Not Sampled						
Edge of Ice Sites	0.49 (0.09) Min= 0.34 Max= 0.58 n=4	0.10 (0.02) Min= 0.07 Max= 0.14 n=4	0.16 (0.04) Min= 0.19 Max= 0.22 n=4	0.64 (0.13) Min= 0.44 Max= 0.78 n=4	-0.16 (0.05) Min= -0.23 Max= -0.10 n=4	25.15 (4.00) Min= 18.94 Max= 29.87 n=4	74.85 (3.96) Min= 70.13 Max= 81.06 n=4
Eastern Lagoon	0.41 (0.26) Min= 0.04 Max= 0.81 n=10	0.11 (0.06) Min= 0.02 Max= 0.18 n=10	0.17 (0.10) Min= 0.04 Max= 0.30 n=10	0.66 (0.37) Min= 0.17 Max= 1.20 n=10	-0.26 (0.18) Min= -0.71 Max= -0.08 n=10	26.49 (3.88) Min= 19.96 Max= 33.00 n=10	73.51 (3.88) Min= 67.00 Max= 80.04 n=10
Western Lagoon	0.65 (0.05) Min= 0.58 Max= 0.71 n=3	0.14 (0.01) Min= 0.12 Max= 0.15 n=3	0.22 (0.02) Min= 0.19 Max= 0.24 n=3	0.91 (0.08) Min= 0.81 Max= 0.98 n=3	-0.27 (0.05) Min= -0.34 Max= -0.22 n=3	23.86 (0.40) Min= 23.30 Max= 24.24 n=3	76.14 (0.40) Min= 75.76 Max= 76.70 n=3
Fjallgilsá	0.22 (-) Min= 0.22 Max= 0.23 n=2	0.12 (-) Min= 0.12 Max= 0.13 n=2	0.19 (-) Min= 0.19 Max= 0.20 n=2	0.40 (-) Min= 0.38 Max= 0.42 n=2	-0.18 (-) Min= -0.19 Max= -0.16 n=2	48.29 (-) Min= 47.80 Max= 48.80 n=2	51.71 (-) Min= 52.20 Max= 51.20 n=2
Jökulsárgil	0.46 (-) Min= 0.42 Max= 0.49 n=2	0.10 (-) Min= 0.09 Max= 0.12 n=2	0.17 (-) Min= 0.14 Max= 0.19 n=2	0.53 (-) Min= 0.46 Max= 0.60 n=2	-0.07 (-) Min= 0.09 Max= -0.05 n=2	32.80 (-) Min= 29.50 Max= 31.13 n=2	68.87 (-) Min= 67.2 Max= 70.5 n=2
Supraglacial sites	0.07 (0.03) Min= 0.04 Max= 0.11 n=4	0.02 (0.01) Min= 0.01 Max= 0.03 n=4	0.03 (0.02) Min= 0.01 Max= 0.05 n=4	0.10 (0.06) Min= 0.04 Max= 0.19 n=4	-0.03 (0.03) Min= -0.08 Max= 0.01 n=4	28.38 (4.32) Min= 2.22 Max= 34.38 n=4	71.62 (4.32) Min= 65.63 Max= 77.78 n=4

Appendix 4. Incubation range finder experiments

Headspace concentrations of preliminary range finder experiments conducted May 2014 at Lancaster University. Experiments were set up using methods outlined in chapter 3.5.5.1. Incubation temperature was set at 15°C, using a slurry of substrate and deionised water.

<u>Enriched methane headspace</u>
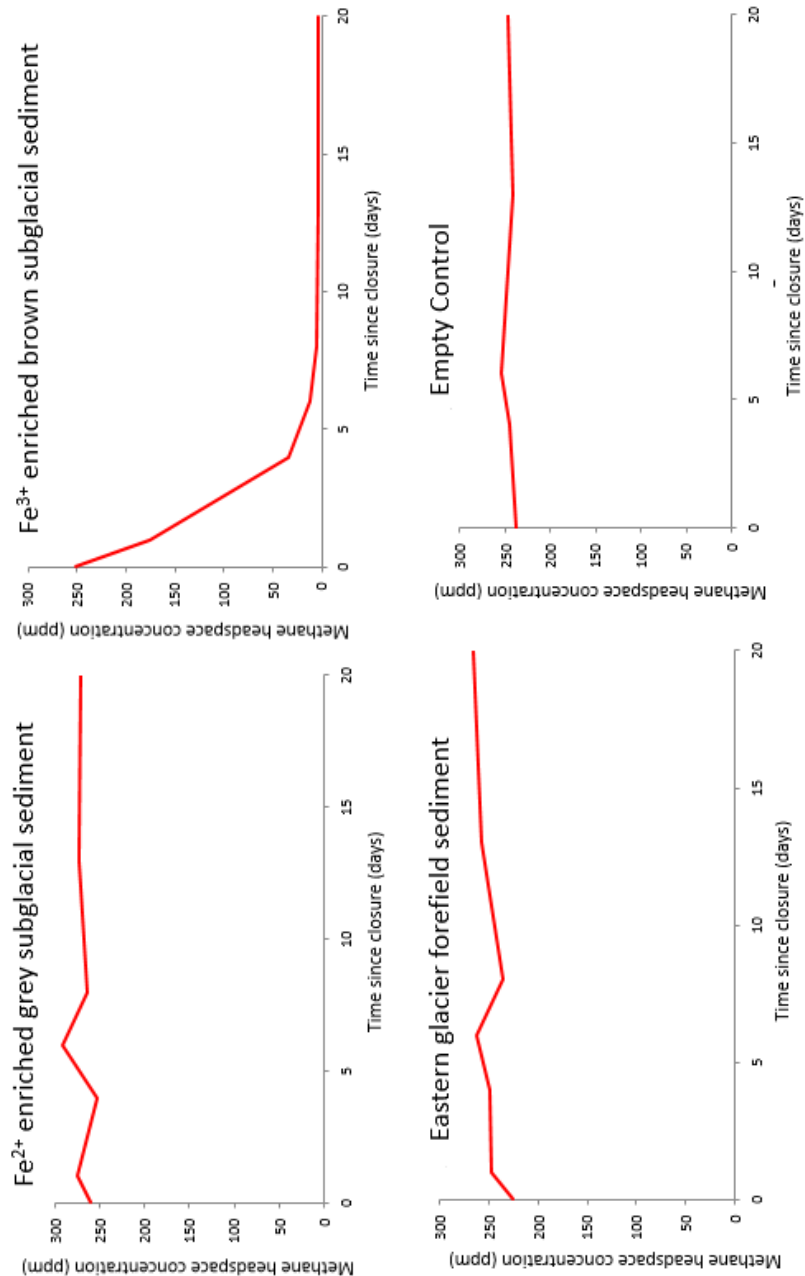
Compressed Air Headspace

Fe³⁺ enriched brown subglacial sediment

Fe²⁺ enriched grey subglacial sediment

Empty Control

Eastern glacier forefield sediment
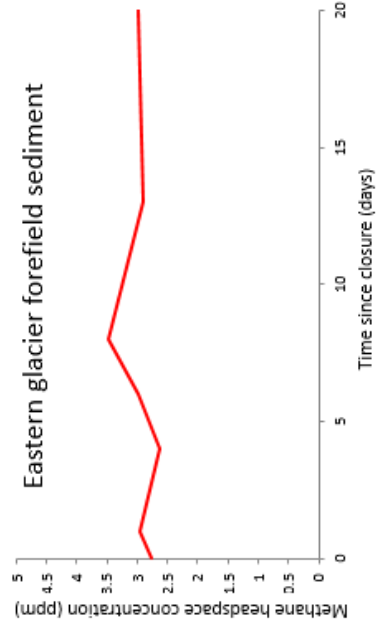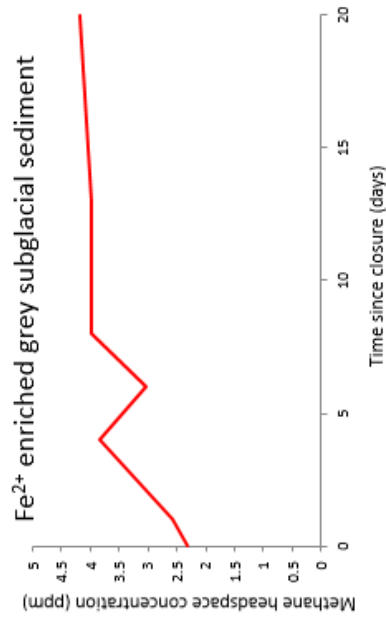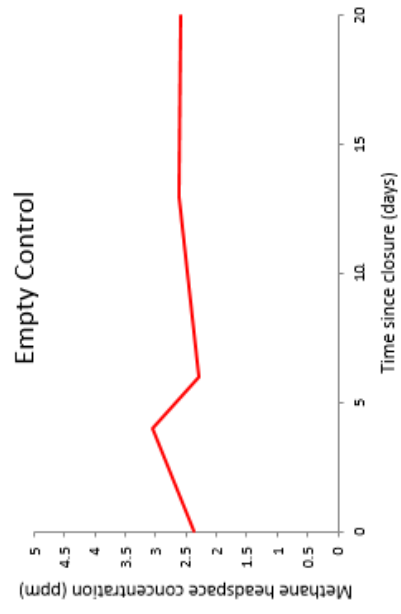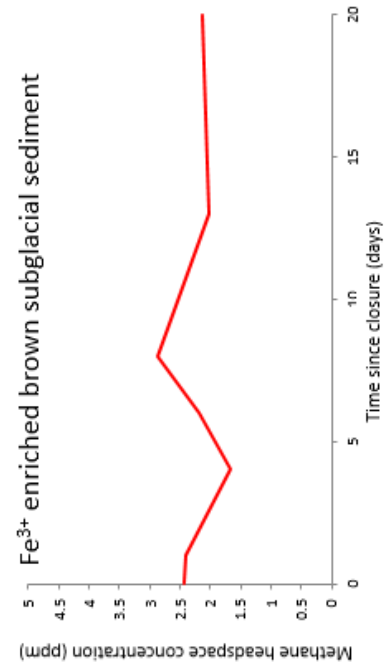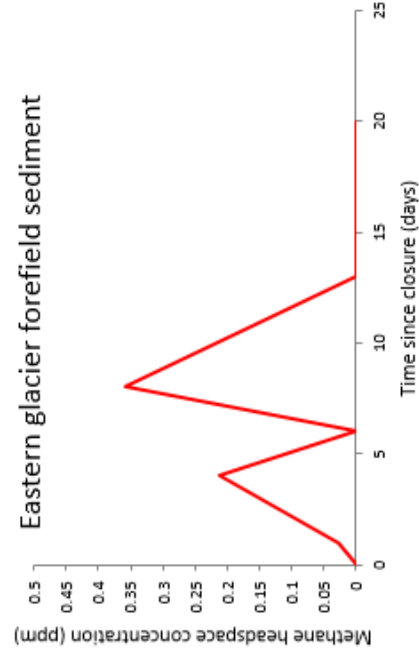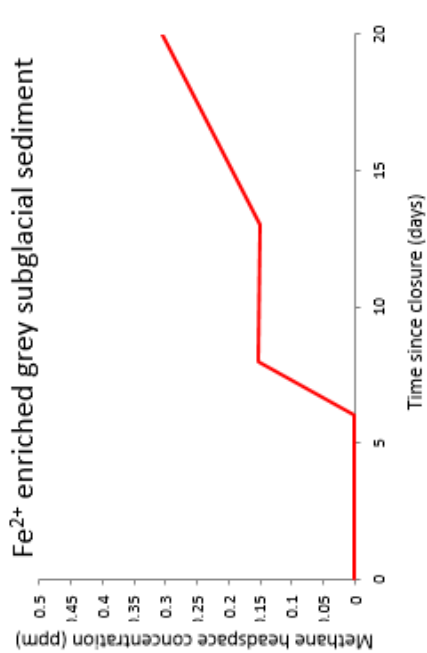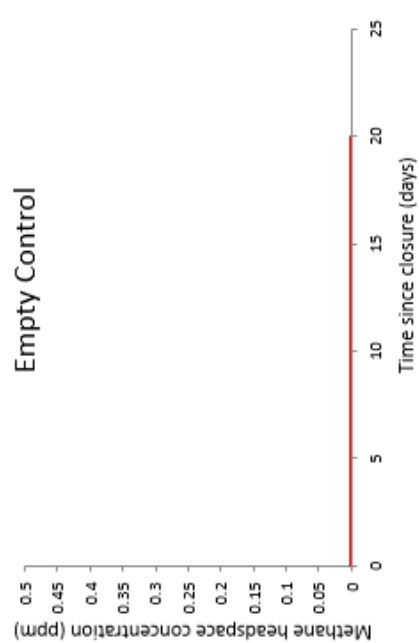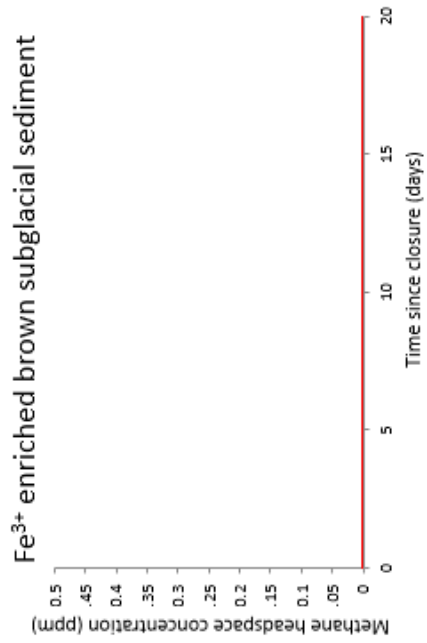
Appendix 5. Presentation of proglacial sediment δ^{13}C isotopic signatures

Average δ^{13}C isotopic signatures of proglacial sediments collected during Summer 2013. 1 standard deviation is in parenthesis.

Sediment	Average δ^{13}C (‰)
Eastern proglacial sediments	**-26.85** (1.19) Min= -29.75 Max= -24.78 *n=32*
Western proglacial sediments	**-26.32** (1.24) Min= -28.21 Max= -25.022 *n=4*
Supraglacial clay	**-27.65** (0.69) Min= -28.65 Max= -26.68 *n=5*
Supraglacial ash	**-27.09** (-) Min= -27.57 Max= -26.61 *n=2*

Appendix 6. Average methane flux from proglacial sediment static chambers

	Average Methane Flux in ppm (standard deviation) *n*			
Site	**Flux after 15 Minutes**	**Flux after 30 Minutes**	**Flux after 45 Minutes**	**Total Average Flux**
Eastern Sediment Site A	-0.084 (0.193) Min=-0.357 Max=0.053 *n=3*	-0.092 (0.153) Min= -0.308 Max=0.020 *n=3*	-0.084 (0.254) Min=-0.442 Max=0.109 *n=3*	-0.087 (0.204) Min=-0.442 Max=0.109
Eastern Sediment Site B	-0.090 (0.121) Min=-0.261 Max=0.002) *n=3*	0.147 (0.327) Min=-0.338 Max=0.801 *n=3*	-0.012 (0.290) Min=-0.308 Max=0.466 *n=3*	-0.049 (0.081) Min=-0.261 Max=0.011
Eastern Sediment Site C	0.048 (0.237) Min=-0.338 Max=0.579 *n=8*	0.147 (0.327) Min= -0.338 Max= 0.801 *n=7*	0.012 (0.290) Min=-0.308 Max=0.466 *n=8*	0.057 (0.293) Min=-0.338 Max=0.801
Eastern Sediment Site D	0.050 (0.133) Min=-0.104 Max=0.286 *n=5*	0.050 (0.133) Min=-0.104 Max=0.286 *n=5*	0.168 (0.204) Min=0.012 Max=0.584 *n=5*	0.113 (0.170) Min=-0.118 Max=0.584
Eastern Sediment Site E	-0.053 (0.060) Min=-0.166 Max=0.017 *n=6*	-0.004 (0.059) Min=-0.099 Max=0.088 *n=6*	-0.030 (0.048) Min=-0.113 Max=0.023 *n=6*	-0.029 (0.059) Min=-0.166 Max=0.088
Eastern Sediment Site F	0.319 (0.650) Min=-0.003 Max=1.769 *n=6*	0.126 (0.429) Min=-0.133 Max=1.077 *n=6*	0.089 (0.286) Min=-0.163 Max=0.692 *n=6*	0.178 (0.489) Min=-0.163 Max=1.769
Western Sediment Site	0.085 (0.049) Min=0.019 Max=0.138 *n=3*	0.117 (0.076) Min=0.015 Max=0.200 *n=3*	0.113 (-) Min=0.106 Max=0.120 *n=2*	0.104 (0.058) Min=0.015 Max=0.200

Appendix 7: Rough Calculations of Aqueous Methane Flux

Flux estimation $\mathbf{1}$*st October to April* $\mathbf{30}$*th*

$$1st\ October\ -\ 30th\ April\ =\ 212\ days$$

$$Seconds\ in\ a\ day\ =\ 86400$$

$$Seconds\ over\ winter\ period\ =\ 86400\ \times\ 212\ days\ =\ 18316800$$

$$m^3\ over\ winter\ period\ =\ 18316800\ \times discharge\ at\ 10 cumecs\ =\ 183168000$$

$$Litres\ over\ winter\ period\ =\ 183168000\ \times\ 1000\ =\ 183168000000$$

Flux estimation $\mathbf{1}$*st May to September* $\mathbf{30}$*th*

$$1st\ May\ -\ 30th\ September\ =\ 153\ days$$

$$Seconds\ in\ a\ day\ =\ 86400$$

$$Seconds\ over\ summer\ period\ =\ 86400\ \times\ 153\ days\ =\ 13219200$$

Based on an average Mixed Zone methane measurement of 33.72ppm

Discharge at 20cumecs *Equation A*

m^3 over summer period= 13219200 x 20

$= 264384000$

Litres over summer period= m^3 x 1000

$= 264384000000$

Methane (mg) = 33.72 x 264384000000

Discharge at 50cumecs *Equation B*

m^3 over summer period= 13219200 x 50

$= 660960000$

Litres over summer period= m^3 x 1000

$=660960000000$

Methane (mg) = 33.72 x 660960000000

$$= 8.91 \times 10^{12} \qquad\qquad = 2.23 \times 10^{13}$$

Tonnes= $8.91 \times 10^{12} \div 1000000000$ Tonnes= $2.22 \times 10^{13} \div 1000000000$

= 8915.03 Summer methane at   **=22287.57 Summer methane at**

20cumecs   **50cumecs**

Equation C   *Equation D*

Add winter methane flux of 263.76   Add winter methane flux of 263.76

Total annual methane flux = 9178.79   **Total annual methane flux = 22551.33**

tonnes   **tonnes**